The University Of Sheffield.

Development of novel neurotherapeutics using the zebrafish model of amyotrophic lateral sclerosis

Olfat Qais Abduljabbar

Thesis submitted for the degree of Doctor of Philosophy (PhD)

Faculty of Medicine, Dentistry, and Health

Department of Neuroscience (SITraN)

Supervisors:

Dr. Tennore M Ramesh

Dr. Jonathan D Wood

Dr. Alexander McGown

April 2020

Acknowledgments

My foremost thanks and undying gratitude go to the omnipresent GOD, for providing me the strength to perform this work.

I would like to thank The Ministry of Higher Education and Scientific Research-Iraq and the Iraqi cultural attaché for giving this me the opportunity and financial support to do a Ph.D. abroad.

I would also like to give special thanks to my supervisors Dr. Tennore M Ramesh, Dr. Jonathan D Wood, and Dr. Alexander McGown, who have supported and guided me throughout the research. I will never forget benefitting from their wealth of experience.

I would like to thank all SITraN staff and students who always made my Ph.D. life enjoyable.

My appreciation and utmost gratitude to my beloved family (mother, sister, and brother), who helped me to survive during my Ph.D. They always advised me to face any challenge during my Ph.D. study and to make it a new explore experience.

Finally, I would like to dedicate this work to the memory of my father, who suffered and died from Alzheimer's and Parkinson's disease.

Abstract

Amyotrophic Lateral Sclerosis (ALS) is a fatal adult-onset neurodegenerative disease. Mutations of the *C9ORF72* and *SOD1* genes are the commonest causative genes of ALS. Riluzole and recently, edaravone, are the modest approved ALS treatment. This identifies an urgent need for effective disease modulation, mainly to block the earliest pathophysiological events. Zebrafish characteristics that are suited for high-throughput analysis, creating an ideal *in vivo* model that could bridge high-throughput drug screens to advanced pre-clinical and clinical trials.

The mutant *sod1*G93Ros10 model, and the *C9orf72* (C9) sense $(G4C2)_{45}$ and anti-sense $(C4G2)_{39}$ hexanucleotide expansion transgenic zebrafish models were utilised to perform this work. These ALS *in vivo* models demonstrated early neuronal pathology in the form of activation of cellular stress that was measured using an *hsp70*::DsRed transgene (fluorescent stress readout). The *sod1*G93Ros10 zebrafish shows ALS pathophysiological phenotypes, i.e. motor neuron loss, neuromuscular defects, swimming endurance reduction, muscle atrophy, and premature death, while the C9 zebrafish, in addition, shows RNA foci and dipeptide repeat protein (DPR) proteinopathy.

Based on the fluorescence readout, a high-throughput drug screen of 4494 of an ion channel modulator compound library designed by LifeArc was performed. Utilising high-throughput liquid handling and imaging systems identified novel compounds with drug-like dose-response profiles. The screen revealed one novel compound MRT00201527 that showed efficacy in reducing neuronal stress in the *sod1*G93R zebrafish model and also a reduction of DPR expression levels in the C9 transgenic zebrafish model of ALS.

In conclusion, the sod1 and C9 zebrafish models have robust disease phenotypes which facilitated a novel *in vivo* high-throughput LifeArc ion channel screen based on *hsp70*::DsRed. It identified novel DPR modulating compounds. This sheds light on the potential of ion channel modulating therapy in ALS drug discovery and the potential impact of high-throughput drug screening in ALS zebrafish models for rapidly identifying pre-clinical lead.

Table of contents

List of figures

List of tables

CHAPTER 1

1- Introduction

1.1 Amyotrophic lateral sclerosis (ALS)

ALS is a motor neuron disease with spinal motor and bulbar symptoms associated with dysphagia, dyspnea, cognitive impairment, abnormal behaviour, muscular weakness and atrophy (Hardiman et al., 2017; Merrilees et al., 2010). It is a fatal neurodegenerative disease in which the survival is, on average, 3-5 years from the onset of symptoms. ALS is observed as a progressive degeneration of the corticospinal tract and the loss of upper and lower motor neurons, which leads to progressive muscle atrophy, paralysis, and consequently death from respiratory failure (Kiernan et al., 2011). Men have a higher incidence rate (3.0) than women (2.4) per 100,000 European people (Logroscino et al., 2010).

As a result of devasting motor neuron degeneration, and poor understanding of the cellular pathophysiological mechanisms of ALS, no effective ALS therapy exists and riluzole treatment only modestly prolongs survival by 3-4 months. Riluzole is known to act on reducing excitotoxicity (Bensimon, 1994), but its exact cellular mechanism is still unknown. Recently, edaravone an anti-oxidant drug was approved for ALS and is thought to act by the modulation of oxidative stress (Rothstein, 2017). This demonstrates that more understanding of the cellular and molecular pathophysiology is required in drug discovery for ALS.

1-2 Genetics of ALS

Sporadic amyotrophic lateral sclerosis (sALS) accounts for 90-95% of all cases, and familial amyotrophic lateral sclerosis (fALS) accounts for the remaining 5-10% (Al-Chalabi et al., 2012). Numerous genes have been identified and linked to ALS pathogenesis such as *superoxide dismutase 1* (*SOD1*), *Chromosome 9 open reading frame 72* (*C9ORF72*), *Transactivating response element DNA binding protein-43* (*TDP-43*), *Fused in Sarcoma* (*FUS*), *Optineurin* (*OPTN*), *Sequestosome-1* (*SQSTM-1* or p62) and many

others (for review see (Al-Chalabi et al., 2012; Peters et al., 2015)). While fALS cases are inherited, some mutations have also been identified in sporadic ALS patients. In addition to the main causal genes identified in ALS patients with fALS, other rare genes and modifiers of ALS have been identified. Table (1-1) shows a list of genetic mutations and modifiers identified in ALS. This list is not exhaustive, and more are being identified. However, the key aspect of these findings is that most of the identified mutations are very rare, and only a couple of cases exist for some of the mutations identified. Thus, ALS is a complex disease with multiple causes and may be more accurately described as a polygenetic disease with important environmental factors impacting on the manifestation of the disease.

Table 1-1: Mutated and modifier genes identified in ALS. Adapted from (Al-Chalabi et al., 2012; Mathis et al., 2019; Peters et al., 2015; Taylor et al., 2016).

ALS inheritance mode	Genes	locus	Encoded proteins	Functions	fALS%	sALS%	References
AD AR(rare)	SOD1(Superoxide dismutase)	21q22.11	SOD1 protein	Antioxidant enzyme	20-25%	2%	(Rosen et al., 1993)
AD	C9ORF72	9q21.2	C9ORF72	Regulation of RNA transcription, pre-mRNA splicing, and membrane traffic via Rab GTPase family	40-50%	6-10%	(DeJesus-Hernandez et al., 2011; Renton et al., 2011)
AD	TDP-43 (TARDBP(TAR DNA-binding protein 43)	1p36.22	TDP-43 protein	RNA metabolism	4-5%	<1%	(Kabashi et al., 2009; Neumann et al., 2006; Sreedharan et al., 2008)
AD	FUS/TLS (Fused in sarcoma/ translated in liposarcoma)	16p11.2	FUS protein	RNA metabolism	4-5%	<1%	(Kwiatkowski, 2009; Vance et al., 2009)
AD	OPTN	10p15-p14	Optineurin	Autophagy & regulator of NF-kB signalling	2-4%	<1%	(Maruyama et al., 2010)

Modifier gene	ATXN2	12q24	Ataxin-2	RNA translation & endocytosis	1-2%		(Elden et al., 2010)
AD	VCP	9p13.3	Valosin-containing protein	Degradation of the protein & membrane fusion	1-2%	<1%	(Johnson et al., 2010)
AD	CHMP2B	3p11.2	CHMP2B	Vesicle trafficking	<1%		(Parkinson et al., 2006)
AD	TUBA4A	2q35	Tubulin α4A	Major proteins in microtubules	<1%	<1%	(Smith et al., 2014)
AD	hnRNPA1	12q13.1	hnRNPA1	RNA metabolism	<1	<1%	(Liu et al., 2016a)
AD	VAPB	20q13.33	VAPB	Regulation of vesicle transport	<1		(Nishimura et al., 2004)
AD	SQSTM1 (sequestosome-1)	5q35.3	SQSTM1 or p62 or	Autophagy, immunity function, regulation of NF-kB signalling pathway, & UPS	<1		(Teyssou et al., 2013)
AD	DCTN1	2P13.1	Dynactin	Axonal transport	<1	<1%	(Puls et al., 2003)
X-linked (XL)	UBQLN2 2	Xp11.21	Ubiquilin-2	UPS	<1	<1%	(Deng et al., 2011)

AD	CHCHD10	22q11.23	Coiled-coil-helix-coiled-coil-helix domain containing 10	Mitochondrial protein may play role in oxidative phosphorylation	<1%	<1%	(Bannwarth et al., 2014)
AD	TBK1	12q14.1	TANK-binding kinase 1	Autophagy and inflammation regulator			(Freischmidt et al., 2015)
AD	MATR3	5q31.2	Matrin 3	RNA metabolism	<1%	<1%	(Johnson et al., 2014)
Modifier gene	KIFAP3	1q24.2	Kinesin associated protein-3	Axonal transport			(Landers et al., 2009)
Modifier gene	SMN	5q13	Germin1	Biogenesis regulator of snRNPs			(review (Peters et al., 2015)

AD: autosomal dominant, AR: autosomal recessive, UPS: ubiquitin-proteasome system, CHMP2B: charged multivesicular body protein 2B; hnRNPA1: heterogeneous nuclear ribonucleoprotein A1, VAPB: vesicle-associated membrane protein B, snRNPs: small nuclear ribonucleoprotein

Detailed below are some of the most well studied common genes involved in ALS.

1-2-1- Superoxide dismutase1 (SOD1)

The *superoxide dismutase 1* (*SOD1*) gene was the first causative gene of ALS identified. *SOD1* mutation was identified and found at chromosome position 21q22.1 in 1993 (Rosen et al., 1993). SOD1 is a Cu/Zn containing anti-oxidant enzyme and is located in the cytoplasm, nucleus, and intermembrane space of the mitochondria. It is a homodimer protein of 153 amino acids with copper and zinc metal-binding sites. It plays the catalytic role of detoxifying superoxide ($O_2^{\cdot-}$/radical species) by converting it into hydrogen peroxide (H_2O_2) and oxygen (O_2) (Valentine and Hart, 2003)

1-2-1-1 *SOD1* mutations

More than 180 mutations of the *SOD1* gene have been identified and cause approximately 25% of fALS and 2% of sALS and fALS together (Al-Chalabi et al., 2012). Mutations span all over the protein sequence, and most are inherited in a dominant fashion. However, some mutations exhibit recessive inheritance, e.g. asparagine to serine at codon 86 (N86S) (Hayward et al., 1998). The most commonly found mutations are A4V, D90A, and G93A. The mutation at position 93 (glycine to alanine; G93A) is the most investigated mutation and the mutation at position 4 (alanine to valine; A4V) is the common mutation in USA population, while the mutation at position 90 (aspartic acid to alanine; D90A), was the first discovered mutation in the SOD1 gene (for review see (Pansarasa et al., 2018)). These mutations result in ALS regardless of whether the protein has or lacks SOD1 enzyme activity (Turner and Talbot, 2008). For example, the G37R mutation at residue 37 of the SOD1 peptide sequence has been shown to cause vacuolation of dendrites, axons, and perikarya with widespread mitochondrial defects and ALS phenotype with elevated SOD1 activity (Wong et al., 1995). Other SOD1 mutations that show no change or loss of the enzyme activity such as SOD1G93A and G85R also cause ALS and show aggregation of mutant SOD1 (Deng et al., 2006; Gurney et al., 1994; Matsumoto et al., 2005). As both loss of activity and gain of activity lead to ALS pathology, it seems likely

that a dominant gain of function mechanism leads to the toxicity seen with SOD1 mutations. However, a recent report suggests that it could be a combination of a loss of function and gain of toxicity that co-operatively causes ALS pathology (Saccon et al., 2013) through oxidative stress and misfolded SOD1 protein.

1-2-1-2 Cellular toxicity of SOD1 mutations

SOD1 mutations affect a variety of cellular toxicity pathways such as oxidative stress, where reactive oxygen species (ROS) could cause toxicity (Mattiazzi et al., 2002), protein aggregation (Matsumoto et al., 2005), mitochondrial defects (Cacabelos et al., 2016), mitochondria-endoplasmic reticulum (ER) associated membrane defects (Giovanni Manfredi and Hibiki Kawamata, 2016), axonal defects (Kaur et al., 2016) and others. It was recently shown that the elevation of ROS induced stress allowed the re-localisation of SOD1 into the nucleus and induced transcription of anti-oxidant genes to protect from DNA damage in yeast (Tsang et al., 2014). Such a transcriptional role in ALS has not been well studied, and it is still unknown whether the different SOD1 mutations affect this nuclear function.

1-2-1-3 Therapeutic approaches specific to SOD1

The cellular pathogenesis of SOD1 mutations in ALS has been targeted by performing preclinical testing of potential future therapies utilising antisense knockdown. Therapies that have been successfully tested in the SOD1G93A mouse model include antisense oligonucleotides (ASO) and small interference RNA (siRNA) to reduce mutant SOD1 expression (Smith et al., 2006; van Zundert and Brown, 2017). Another study that utilised intracerebroventricular and intravenous injection of adeno-associated virus AAV10-U7-hSOD1 in the SOD1G93A mouse showed weight gain, delay of the disease onset and progression, extended lifespan and maintained innervation of the neuromuscular junction (Biferi et al., 2017).

A small molecule drug treatment targeted to reduce misfolded SOD1 involves stabilisation of mutant SOD1 and reduced oxidative stress using metal compounds that can metallate mutant SOD1. Metal complex therapeutic

agents such as Copper(II) diacetyl-di(N4-methylthiosemicarbazone) or copper ATSM have been tested with good results (Hilton et al., 2017). These agents improved locomotor function and lifespan in the SOD1G37R mouse model and increased SOD1 enzyme activity in the spinal cord of the SOD1G93A treated mice (Hilton et al., 2017; McAllum et al., 2015). Despite this, the genetic reduction of SOD1 expression in transgenic SOD1 mouse models has shown the most dramatic effect on enhancing survival (Ralph et al., 2005) and has now developed in to a clinical trial after initial safety testing showed no adverse reactions (Miller et al., 2013).

1-2-2- Hexanucleotide GGGGCC (G4C2) repeat expansion in *C9orf72*

A non-coding hexanucleotide GGGGCC (G4C2) repeat expansion in the *chromosome 9 open reading frame 72* (*C9orf72*) gene has been identified as the most common genetic factor causing ALS. It accounts for 40% of fALS cases and 6% of sALS (DeJesus-Hernandez et al., 2011; Renton et al., 2012). *C9orf72* is also has been identified as a pleiotropic gene as it is also linked to Alzheimer's disease, corticobasal degeneration, schizophrenia, frontotemporal dementia (FTD), and bipolar disorder (Cooper-Knock et al., 2014). How the expansion causes or increases the risk for this diverse variety of diseases is still unclear.

1-2-2-1 Hypotheses of *C9orf72* toxicity

The hypotheses of how *C9orf72* repeat expansions cause toxicity includes three cellular mechanisms. Firstly, haploinsufficiency of *C9orf72* gene expression is suggested to cause cellular toxicity in ALS patients due to methylation of the *C9orf72* locus and reduced *C9orf72* transcription (Dedeene et al., 2019; Saberi et al., 2018).

The second hypothesis of C9 toxicity is the formation of RNA foci due to the guanine and cytosine (GC) nucleotide rich hexanucleotide repeat expansion (HRE). This leads to an accumulation of RNA foci comprised of the repeat RNA in the nucleus and cytoplasm with sequestration of RNA binding proteins (DeJesus-Hernandez et al., 2011). A study in 2015 showed that RNA foci positive cells were widespread in most areas of human and $(G4C2)_{66}$ mouse

brain (Chew et al., 2015; DeJesus-Hernandez et al., 2011). It is clear that RNA foci can occur from both sense and antisense strands (DeJesus-Hernandez et al., 2011). One approach to reducing *C9orf72* neuropathology is by using antisense oligonucleotides (ASOs) (Jiang et al., 2016).

The third hypothesis of C9 toxicity is dipeptide repeat protein (DPR) production through repeat-associated non-ATG-initiated translation (RAN translation) of the HRE. Researchers have detected poly(glycine-proline) (GP), poly(glycine-alanine) (GA), and poly(glycine-arginine) (GR) from the sense strand and poly(proline-arginine) (PR), poly(proline-alanine) (PA), and poly(glycine-proline) (GP) polypeptides from the antisense strand (Ash et al., 2013; Mori et al., 2013)**.** The most abundant DPR inclusions are poly(GR), poly(PA), and poly(GA) in the hippocampus, neocortex, frontotemporal lobes and cerebellum (Mori et al., 2013). Also, it has been reported that the main cerebellar pathological form is poly(GR), while the pathology in the frontal cortex is mainly associated with poly(GA) (Gendron et al., 2015). It is also suggested that DPR inclusions are more abundant in the brain tissues than the spinal cord (Gomez-Deza et al., 2015).

Recently, it was reported that the function of proteins which regulate nucleocytoplasmic transport, such as RanGAP, is impaired in *C9orf72* expansion mediated toxicity and targeting this protein can rescue toxicity in *Drosophila* and motor neurons derived from C9 patient iPSCs (Freibaum et al., 2015; Zhang et al., 2015). Serine-arginine rich splicing factor 1 (SRSF1) is a nuclear export adaptor that is involved in the neurodegenerative process. Recently, a study showed SRSF1 is a novel neurotherapeutic target as its depletion reduced DPR production in C9 *Drosophila* and rescued the locomotor activity defects, and reduced nuclear export of repeat expansion containing RNA in patient neurons and induced astrocyte cell models (Hautbergue et al., 2017). EIF1A (Eukaryotic Initiation factor 1A) expression has also been shown to rescue RAN-mediated translation defects and decreased the neuronal toxicity induced by DPRs (GR-100 repeat) in a *Drosophila* C9 ALS model (Moens et al., 2019). Taken together, these

findings suggest that DPRs interact with multiple factors and ribosomal proteins, leading to multiple novel potential therapies to target C9 ALS toxicity.

1-2-3 RNA regulation genes in ALS/FTD

With the identification of *TARDBP* (encoding TDP-43) mutations in ALS/FTD, increasing focus was placed on identifying genes that modulate RNA metabolism. The identification of genes such as *FUS*, *MATR3*, and others in ALS patient populations demonstrated an increasing role for the dysfunction of RNA metabolism in ALS pathogenesis; see Table (1-1). More interestingly, many of the proteins involved in RNA metabolism were also shown to carry prion-like domains (PrLD), which are prone to misfolding and have increased aggregation propensity (Zhao et al., 2018). The classic examples of RNA binding proteins involved in ALS/FTD pathogenesis, TDP-43 and FUS, are discussed below.

1-2-3-1 Transactivating response element DNA-binding protein-43 (TDP-43)

The discovery of ubiquitinated TAR DNA-binding protein (TDP-43) in ALS/FTD pathological inclusions was the first discovery to draw attention to this gene (Neumann et al., 2006). TDP-43 was localised to ubiquitinated inclusions observed in most sporadic and familial ALS cases, indicating it to be a common player in ALS pathogenesis. The TDP-43 protein is usually predominantly nuclear but was observed in cytoplasmic glial and neuronal inclusions in fALS and sALS (Mackenzie et al., 2007; Neumann, 2009). TDP-43 inclusions were shown to be ubiquitinated in the hippocampus and motor cortex (Neumann et al., 2006). The inclusions were also shown to contain a truncated fragment of the *C*-terminus of TDP-43, which is phosphorylated, and importantly, the neurons with TDP-43 aggregates also show a profound loss of intra-nuclear TDP-43, suggesting that loss of nuclear TDP-43 may be the cause of toxicity. Loss of nuclear TDP-43 and/or TDP-43 aggregation caused motor neuron dysfunction and axonal growth abnormalities (Tripathi et al., 2014), and it has been shown to be involved in multiple pathological diseases, such as FTD, Alzheimer's disease, and Parkinson's disease(Chen-Plotkin et al., 2010). Moreover, TDP-43 cytoplasmic aggregates are almost universal in ALS, with the exception of *SOD1* and *FUS* mutation cases, and are seen in

association with *C9orf72* mutations (Chew et al., 2015; Dedeene et al., 2019). It should be noted that the *C*-terminus of TDP-43 contains a low complexity prion-like domain (PrLD) that is aggregate prone.

1-2-3-1-1 Mutations in TDP-43 gene and ALS/FTD:

After the discovery of TDP-43 positive inclusions in ALS (Forman et al., 2007; Neumann et al., 2006), patients with mutations in TDP-43 were identified (Sreedharan et al., 2008). Most of the mutations in TDP-43 patients are localised to the *C*-terminus in the prion-like domain region, suggesting a role of this domain in ALS pathogenesis (Zhao et al., 2018). In addition, some mutations in the RNA recognition motif (RRM) were also identified, suggesting a loss of function as a potential mechanism of disease pathogenesis. The deletion of the *C*-terminus and mutations in the RNA binding domain leads to cytotoxicity rather than cytoplasmic aggregation in some TDP-43 *in vivo* and *in vitro* models (Voigt et al., 2010; Wegorzewska et al., 2009). Mutations of TDP-43 affect RNA processing and gene expression (Casafont et al., 2009; Strong et al., 2007). Thus, the combination of aggregation-prone TDP-43 with PrLD, loss of nuclear TDP-43 and RRM mutations suggest that a combination of gain of function (TDP-43 aggregation) and loss of function may both be responsible for toxicity (Kabashi et al., 2009).

1-2-3-1-2 Drugs specifically targeting TDP-43 - effects on ALS pathology

Recently, some studies have reported possible drug therapies reducing cellular toxicity of TDP-43 proteinopathy. Hexachlorophene is a disinfectant that modulates wnt/beta-catenin signaling (Min et al., 2009). It showed a reduction of TDP-43 levels and also reductions in insoluble inclusion and TDP-43 pathology in N9 microglial cells (Narayan et al., 2015). Several active small compounds of diverse classes that act on a variety of biological targets such as ion channels, receptor moieties, and inflammatory modulation were identified in a screen to identify compounds that showed a decrease in stress granules (SGs), which are involved in cellular stress in ALS/FTD, in HEK293xT and motor neurons differentiated from a human-induced

pluripotent stem cells (MNs/hiPSC) (Fang et al., 2019). Another small molecule (rTRD01) that targeted the RRM domain showed modulation of TDP-43 interaction with *C9orf72* and improved larval turning in a *Drosophila* study (Francois-Moutal et al., 2019). These studies suggest the possibility that targeting multiple molecular pathways may be beneficial in rescuing TDP-43 mediated toxicity.

1-2-4 Other causative genes of ALS pathology

Other genes that each account for < 2% of fALS cases have been identified and are listed in Table (1-1). These include FUS and Ubiquilin.

1-2-4-1 Fused in sarcoma/ translated in liposarcoma (FUS/TLS)

FUS is an interesting protein with regard to ALS as it has many features similar to TDP-43, such as an RNA-binding domain and it also contains regions similar to the prion-like domain (PrLD) (King et al., 2012). Mutation in FUS, leading to ALS, were identified on chromosome 16 (Kwiatkowski, 2009; Vance et al., 2009). In FUS ALS patients, FUS was identified in cytoplasmic aggregates, indicating that the PrLD may be involved in disease pathogenesis. This cytoplasmic FUS pathology is similar to the aggregation phenotype of TDP-43. FUS mouse models show RNA dysregulation, motor neuron loss, and autophagy reduction (Ho and Ling, 2019). Many FUS *in vivo* models shows shortened lifespan, although they do not mimic all ALS phenotypes (for review see (Guerrero et al., 2016)). As FUS also plays an essential role in DNA damage repair, mutation of this gene indicates that therapeutic strategy to regulate DNA repair pathways may rescue neuronal loss (Wang and Hegde, 2019).

1-2-4-2 Protein clearance

Protein homeostasis is critical to neurons that do not divide and exist for decades of the life of a person. Protein inclusions are a hallmark feature of many neurodegenerative diseases, including ALS, ALS/FTD, and FTD, which span the spectrum of ALS and FTD. Therefore, it is not surprising that mutations in genes involved in protein clearance have been identified in a population of these patients. Genes such as *ubiquilin-2* (*UBQLN2*) (Deng et

al., 2011), *vasolin-containing protein* (*VCP*) (Johnson et al., 2010), *vesicle-associated membrane protein-associated protein B* (*VAPB*) (Nishimura et al., 2004), *optineurin* (*OPTN*) (Maruyama et al., 2010), *charged multivesicular body protein 2B* (*CHMP2B*) and *sequestosome-1* (*SQSTM1*) (Teyssou et al., 2013) were identified (for review see (Ling et al., 2013)). Interestingly, C9orf72 protein, which contains a DENN domain (Ugolino et al., 2016), and TBK-1 (Oakes et al., 2017) are also thought to be involved in protein clearance through autophagy pathways. Thus, a combination of proteasomal and autophagy degradation of damaged proteins is critical in ALS pathogenesis.

1-2-4-2-1 Ubiquilin 2 (UBQLN2)

ALS-associated mutations of *ubiquilin 2* (*UBQLN2*) were identified on chromosome X. It regulates the proteasome pathway, is involved in protein breakdown and is important in clearing misfolded proteins (Deng et al., 2012). Interestingly, UBQLN2 immunoreactive inclusions were observed in all types of sporadic and familial ALS cases tested and were present in fALS patients without TDP-43, FUS, or SOD1 mutations, and in patients carrying SOD1 mutations. Therefore, UBQLN2 positive inclusions were common to the diverse forms of ALS. The role of UBQLN2 in stress granule regulation, TDP-43 mislocalization, proteasomal degradation, and autophagy regulation, makes it a protein that spans many aspects involved in ALS pathogenesis (Renaud et al., 2019).

1-3 Cellular mechanisms of ALS relevant to the research project

Protein aggregation, oxidative stress, mitochondrial dysfunction, excitotoxicity, axonal transport, and non-neuronal defects are among the most prominent mechanisms implicated in the cellular pathology of ALS (Cozzolino et al., 2013; Ferrante et al., 1997; Parakh and Atkin, 2016). They have been investigated in various *in vivo* and *in vitro* ALS models to identify potential therapies. However, it is still unclear what the cascade of toxicity is and which are the primary and which are the subsequent downstream events involved in the onset and progression of ALS. Here I will focus on the key pathways relevant to the project.

1-3-1 Oxidative stress

Oxidative stress is one of the cellular pathologies that is actively involved in neurological disorders such as ALS, Alzheimer's, and Parkinson's disease. Oxidative stress has been shown in both sALS and fALS (Ferrante et al., 1997). The overproduction of reactive oxygen species (ROS) and reactive nitrogen species (NOS), along with imbalances in anti-oxidant enzymes, plays a vital role in oxidative stress. The interaction of these reactive species with other molecules can lead to mitochondrial oxidation, lipid, protein, post-transcriptional, and other cellular damage (for reviews see (Bozzo et al., 2017; Islam, 2017)).

Multiple exogenous and endogenous sources cause oxidative stress via ROS activation. The primary endogenous sources are mitochondrial defects in complex I and III (for review see (Bhat et al., 2015)). Also, reduced nicotinamide adenine dinucleotide phosphate oxidase (NADPH oxidase/NOX), which is a transmembrane bound oxidant enzyme family, has been implicated. It produces a higher level of ROS than other enzymes and causes oxidative stress in abnormal conditions. Recently, it became a target of a potential pre-clinical therapy for inhibition of oxidative stress via reduction of NOX and restoration of neuronal function in chronic and acute neurodegenerative disease, and compounds that modulate it such as apocynin and thioridazine have been identified (for reviews see (Barua et al., 2019; Seredenina et al., 2016).

Mitogen-activated protein kinases (MAPKs) are critical in cellular pathways that protect against ROS damage, with p38 kinase, extracellular signal-regulated kinases (ERK1/2), and c-Jun N-terminal kinase (JNK) all of interest. These kinases modulate antioxidant enzymes, such as heme oxygenase-1 (HO-1), which protect against ROS damage. A recent study identified fisetin, which is a natural antioxidant, as being neuroprotective through the activation of ERK in *in vivo* and *in vitro* SOD1 models, including hSOD1G85R *Drosophila*, hSOD1G93A NSC34 cells, and SOD1G93A mice. It was shown that fisetin extended survival, downregulated ROS, restored redox

homeostasis, reduced motor neurons death, and preserved the viability of hSOD1G93A-NSC34 cells (Wang et al., 2018).

SOD1 catalyses the conversion of the superoxide anion radical into hydrogen peroxide and molecular oxygen. Mutations in this gene lead to oxidative stress and ALS pathology (Barber and Shaw, 2010). However, the precise mechanism of motor neuron degeneration by oxidative stress is still unknown in SOD1 fALS. Therefore, one of the attractive therapies to attenuate oxidative stress caused by mutations in SOD1 is upregulation of Nrf2. Nrf2 is nuclear erythroid 2-related-factor 2 that interacts with the antioxidant response element (ARE) and drives expression of cytoprotective genes. Studies using the compound S[+]-apomorphine showed extended survival and preserved motor neurons by the induction of Nrf2 in T70I sod1 zebrafish and SOD1G93A mouse models (Da Costa et al., 2014; Mead et al., 2013). Edaravone has recently been approved as a neuroprotective treatment for ALS. However, the functional target is still unclear. Interestingly, a recent study showed that edaravone significantly alleviated the activation of an Nrf2 reporter for oxidative stress and showed a neuroprotective effect in the SOD1G93A mouse (Ohta et al., 2019). Therefore, it seems that multiple cellular pathways may potentially be a target for the alleviation of the oxidative stress involved in ALS pathology in the future.

1-3-2 mitochondrial defects

Mitochondrial defects have been highlighted as one of the major causes of cellular toxicity in ALS. Evidence of this is seen in the mutant SOD1 mice where homeostasis of Ca^{2+} in the mitochondria is altered, resulting in vacuolation. It was demonstrated that mitochondrial damage occurred before oxidative stress in SOD1G93A mice (Mattiazzi et al., 2002). Also, mitochondrial defects with muscle atrophy have been observed in the SOD1Q22R mouse (Corti et al., 2009). Dysfunction of mitochondria has been linked to other neurodegenerative diseases, such as Alzheimer's and Parkinson's disease.

The cellular toxicity pathways of mitochondrial dysfunction are still incompletely charaterised. Three potential sources of mitochondrial cytotoxicity in mutant SOD1 ALS models have been reported. The presence of mutated SOD1 in the intramembrane space of the mitochondria leads to oxidative stress by forming cytotoxic peroxynitrite. Importantly, peroxynitrite also reacts with mutated SOD1 to produce superoxide ($O_2^{\cdot -}$). Secondly, alterations of the electron transport chain (ETC) lead to the production of ($O_2^{\cdot -}$) and mitochondrial damage, which results in reduced energy (adenosine triphosphate/ATP levels). Thirdly, mitochondria may enhance programmed cell death (apoptosis) at the end stage of ALS (Dupuis et al., 2004). Therefore, a therapy that targets these mechanisms to handle the mitochondrial toxicity in ALS, such as creatine (Kliveny, 2006) or resveratrol (Song et al., 2014), may be beneficial. Resveratrol showed a reduction of motor neuron loss and prolonged survival in SOD1G93A mice through reduction in mitochondrial toxicity (Song et al., 2014).

1-3-3 Protein aggregation

Protein aggregation/inclusions are a hallmark pathology in motor neuron disease. More than 40 mutated genes are implicated in mis-folding of the encoded proteins, including SOD1, TDP-43 and FUS, in ALS patients. Therefore, this cellular pathology has been considered to be a potential neurotherapeutic target in a whole host of neurodegenerative diseases. However, it is still unknown precisely how these inclusions are created in ALS, and it raises the question of whether the aggregation drives the cellular toxicity or whether the aggregation is a consequence of toxic cellular events.

Recently, it has been reported that the accumulation of dipeptide repeat proteins (DPRs) from the non-ATG-initiated translation of the intronic region of the C9orf72 gene leads to cellular toxicity in ALS patients (Gendron et al., 2013; Mori et al., 2013b). However, DPR inclusions were absent in the motor neurons of the spinal cord with TDP-43 inclusions (Gomez-Deza et al., 2015). This suggests that DPRs may cause toxicity, but DPRs are not the only primary pathogenic factor in C9 ALS (Gomez-Deza et al., 2015).

The relationship between DPRs and TDP-43 in the pathology of *C9orf72* cases is still unclear. A study by McMillan and his colleagues discovered that hypermethylation of the *C9orf72* promoter may have a neuroprotective effect on the *C9orf72* gene expansion. They observed hypermethylation in the hippocampus, frontal cortex, and thalamus (areas that are protected from damage in the C9/ALS patients) (McMillan et al., 2015). It is possible that reduced *C9orf72* expression also consequently reduces DPR expression. Another study suggested that disruption of TDP-43 protein interaction with $(GGGGCC)_4$ could attenuate cellular toxicity and improve the strength of the neuromuscular junction in a *Drosophila* ALS fly model (Francois-Moutal et al., 2019). These studies suggest multiple potential avenues to develop neuroprotective therapies that target various aspects of *C9orf72* expansion mediated toxicity.

1-3-4 Excitotoxicity

Excitotoxicity is a neural death pathway mediated by excessive glutamate neurotransmitter at synapses, which is implicated in motor neuron death in ALS patients and has been shown to be important in *in vitro* and *in vivo* settings (Foran and Trotti, 2009). Glutamate excitotoxicity of spinal cord motor neurons involves Ca^{2+} permeable AMPA receptors and activation of astrocytes (for review see (Mahmoud et al., 2019)). Additionally, mitochondrial defects also contribute to excitotoxicity at the synapse due to excessive Ca^{2+} release from the mitochondria (Santa-Cruz et al., 2016). Riluzole is thought to modulate excitotoxicity and is one of the two drugs given for ALS in the UK.

The excitatory amino acid transporters (EAAT1/GLAST1 and EAAT2/GLT1), are glutamate transporters on astrocytes that are critical in the removal of excess glutamate at the synapse (Rose et al., 2018). The inhibition of glial EAAT2 neurotransmitter uptake leads to an overload of glutamate levels at the synapse and causes excitotoxicity (Sen et al., 2005; Van et al., 2000). This suggests the EAAT2 may be a cellular target in ALS therapy and upregulation of EAAT2 reduced extracellular glutamate toxicity, improved motor performance, and extended survival in the SOD1G93A mouse (Kong et al., 2014). Moreover, medications like lithium and valproate (VPA) that

modulate excitotoxicity were shown to be neuroprotective in *in vitro* cellular models, delaying onset of ALS symptoms and extending survival in the SOD1G93A mouse model (Feng et al., 2008). Despite these positive pre-clinical studies, clinical trials with ceftriaxone, a drug that upregulates EAAT2 transporter expression, failed in clinical trials. Therefore, the effect of anti-excitotoxic drugs and their efficacy in clinical trials is mixed, and the exact neuroprotective mechanism of riluzole is still unclear.

1-4 ALS experimental models

Numerous *in vivo* and *in vitro* ALS models have been generated for investigating ALS disease mechanisms, performing high throughput drug screens, and testing candidate neuroprotective agents that may proceed into clinical trials. These models are largely based on the genetic forms of disease introduced in section 1-2.

1-4-1 *In vitro* ALS models

Cellular models are critical for studying the genetic basis of neurodegenerative diseases and for performing high throughput studies utilising phenotypic drug screening. Fibroblasts derived from patients and motor neurons from a G93ASOD1 mouse model were used to screen 2000 drugs, identifying 44 hit compounds that activated the Nrf2-ARE antioxidant pathway. As a result, S[+]-apomorphine was identified as a potential drug to enhance antioxidant enzymes, reduce oxidative stress, and promote improved neuronal function (Mead et al., 2013). Previous work utilising NSC34 motor neurons expressing SOD1 mutations identified nine hit compounds with anti-oxidant activity from a library of 2000 drugs (Barber et al., 2009), leading to the identification of three possible neuroprotective agents.

Reprogramming of patient-derived cells such as fibroblasts allows study of human disease processes in a defined genetic background, allowing for personalised medicine. This is especially important for the study of sporadic forms of the disease. As 90% of the disease is sporadic, patient-derived cells are rapidly gaining importance in therapeutic development for ALS. Patient-derived cells are also important with regard to fALS. For example, iPSC-derived motor neurons from *C9orf72*, *SOD1*, *FUS*, and *TDP-43* patients were

used to demonstrate specific alteration in glutamate receptors properties and calcium gated channel expression (Bursch et al., 2019). These models could offer a better understanding of the role of glutamate excitotoxicity and calcium dynamics in ALS pathogenesis. While iPSC development technology provides robust *in vitro* models of different genetic backgrounds for studying ALS, there are some drawbacks with them due to the following factors: iPSC models show variability between individuals and often require multiple clones for experimentation; the protocols to reprogramme and differentiate into motor neurons are lengthy; additionally, the reprogramming process eliminates the aging phenotype, which is critical for normal disease development.

More recently, protocols for generating induced neural progenitor cells (iNPCs) have been developed (Hautbergue et al., 2017) and used to investigate ALS pathology. These protocols utilise somatic cells from patients, such as skin fibroblasts, adipocytes, and keratinocytes (Myszczynska and Ferraiuolo, 2016), and directly program them to iNPCs that can be differentiated into astrocytes (iAstrocytes) and neurons (iNeurons). This process is thought to retain aging properties better than iPSC generation and thus better reflect the human disease process (Rinaldi et al., 2017).

1-4-2 *In vivo* ALS models

1-4-2-1 Invertebrates ALS models

Invertebrate *in vivo* multi-cellular organism models offer a more complex system for investigating ALS pathology than cellular models. *Caenorhabditis elegans* and *Drosophila melanogaster* are amenable to large-scale genomic analysis. They offer a platform for identifying possible cellular toxicity targets for ALS and other neurodegenerative disorders. However, these models are relatively simple compared to the human body.

1-4-2-1-1 *Caenorhabditis elegans* (*C. elegans*)

C. elegans is a small nematode with a rapid reproductive cycle of 3.5 days and a three-week lifespan at 20°C. While the nervous system of *C. elegans* is composed of just 302 neurons, it still has 42% orthologous genes with humans (Li and Le, 2013). Different mutations of the *SOD1* gene along with

human wild type SOD1 were investigated in this model, such as A4V, G37R, and G93A (Oeda et al., 2001). The worms expressing mutant forms of SOD1 showed vulnerability to paraquat-induced oxidative stress compared to wild-type expressing worms and reduced degradation of the mutant SOD1 in the presence of oxidative stress (Oeda, 2001). Therefore, this study highlights that oxidative stress might contribute to the cellular toxicity and result in the aberrant aggregation of mutant SOD1. Moreover, *C.elegans* was used to identify Daf-2 insulin/insulin-like growth factor receptor as a suppressor of SOD1 toxicity that was shown to enhance the lifespan in SOD1G85R *C. elegans* when mutated, indicating that manipulation of this growth factor might be potentially neuroprotective in ALS (Boccitto et al., 2012).
Furthermore, A315T-TDP-43 *C*. *elegans* mediated toxicity has been used to validate 16 hits identified in a library of 75,000 compounds screened in a PC12 cellular model of TDP-43-induced stress aggregation. The compound LDN- 0130436 showed efficacy against TDP-43 toxicity and amelioration of locomotor deficits in the *C*. *elegans* model (Boyd et al., 2014). Therefore, this *in vivo* model identified a novel neuroprotective agent for further studies.

However, *C*. *elegans* is still an invertebrate model with a limited genome, reduced number of organs, and a different immune system than humans. Importantly, it has just 302 neurons and lacks the complex CNS architecture and supporting cells which are essential in mediating complex human behaviours.

1-4-2-1-2 *Drosophila melanogaster*

The second *in vivo* invertebrate organism model commonly used for screening approaches is *Drosophila melanogaster.* This model provides a platform for performing genetic manipulations with the ability to screen genome-wide for modifiers (Venken and Bellen, 2014). Moreover, phenotypes in flies can be rapidly identified since the life cycle takes only ten days to reach the adult stage. It is also low cost to maintain in the laboratory. The other essential point for the development of ALS therapy is that the nervous system of *Drosophila* is more complex than that of worms: the brain has neurons with glial cells and a blood-brain barrier. Additionally, it has a smaller genome (1.2

x 10^{8} base pairs) with fewer genes (14,000) compared to the human genome, which is 3.3 x 10^{9} base pairs with 20,000-25,000 genes. This smaller genome facilitates genome-wide genetic screening.

Drosophila shows cellular toxicity to the most common ALS genetic mutations, such as *SOD1*, *TDP-43*, and *C9orf72* (Baldwin et al., 2016; McGurk et al., 2015; Şxahin et al., 2017). Recently, a novel study involving SRSF1, a nuclear export adaptor, showed that inhibition of SRSF1 can alleviate cellular pathology in a *C9orf72 Drosophila* ALS model (Hautbergue et al., 2017). Genetic analysis using *Drosophila* was also instrumental in identifying a critical role in nuclear export and protein translation in *C9orf72* mediated toxicity (Boeynaems et al., 2016). Therefore, *Drosophila* allows a better understanding of the mechanisms underlying ALS pathology and is a good model to identify possible neuroprotective targets in the future.

However, the fly model still has several limitations. For example, the fly genome has around 75% human homologous genes, but the genes show considerable sequence variation from humans (Pandey and Nichols, 2011). Furthermore, the fly does not have the same receptors as mammals for some neurotransmitters. For instance, there are five classes of dopamine receptors in mammals, while there are just two in the fly. Additionally, there are six G protein-coupled serotonin receptors in mammals, while there are just three in the fly. Glutamate is the main excitatory neurotransmitter in the brain, while acetylcholine is the neurotransmitter at the neuronal muscular junctions (NMJ) in mammals, while the role of these neurotransmitters reverses in the fly (Pandey and Nichols, 2011).

1-4-2-2 Vertebrate *in vivo* ALS models

1-4-2-2-1 Rat and mouse *in vivo* ALS models

The most common vertebrate *in vivo* model used in ALS drug discovery is the mouse since it shows ALS-like phenotypes similar to human disease symptoms (Gurney et al., 1994). Different transgenic lines overexpressing mutated hSOD1 showed many features of human ALS pathology. The SOD1G85R mouse showed rapid disease progression and astrocyte inclusions with reduction of GLT-1 levels (Bruijn et al., 1997). SOD1G93A

transgenic mice showed hindlimb tremor, weakness and locomotor defects with distal synaptic and axonal degeneration at about three months(Gurney et al., 1994). Within one more month, fatal paralysis occurred from the loss of spinal motor neurons, which is accompanied by reactive gliosis. Additionally, fourteen transgenic mouse lines expressing human or murine SOD1, including mis-sense mutations, a truncation mutation, and mutations of the copper-binding showed ALS features (Ripps et al., 1995; Wong et al., 1995). However, transgenic SOD1G93A mice are the most commonly used model in ALS therapy development (Turner and Talbot, 2008). In addition to mutant SOD1 mice, various mutant TDP-43 mice show ALS phenotypes and pathology including the TDP-43 (A315T) transgenic line, which showed motor neurons loss, astrogliosis, microgliosis and paralysis (Wegorzewska et al., 2009). SOD1 mutations such as H46R and G93A have been expressed in rats. The rat models with the highest copy numbers are characterised by the death of motor neurons, astrogliosis and microgliosis. SOD1G93A rats showed vacuolation in the neuropil, while SOD1H46R rats showed protein aggregation with Lewy body-like inclusions in neurons and astrocytes (Nagai et al., 2001).

More recently, multiple transgenic *C9orf72* (C9) mouse models have been generated either using BAC clones derived from patient DNA or Adeno Associated Virus (AAV) integrated with the partial or full sequence of the human C9 gene for investigation of C9/ALS pathology (Jiang et al., 2016; Liu et al., 2016b; O'Rourke et al., 2015; Chew et al., 2015). These C9/ALS mouse models showed sense and anti-sense RNA foci, formation of DPRs and cellular toxicity to varying degrees. Ablation of C9orf72 protein in knockout mouse models showed de-regulation of autophagy and immune system dysfunction (Atanasio et al., 2016; Ugolino et al., 2016). The phenotypes observed in the transgenic models can be investigated for development of C9/ALS therapy.

To date, the SOD1G93A mice are the most studied *in vivo* ALS model and also the model where most of the potential neuroprotective therapies for ALS were investigated, prior to proceeding to clinical trials. For example, bexarotene (a retinoid X-receptor agonist), showed improvement in ALS

phenotypic indications, such as extended survival, delayed onset of disease, and reduced weight loss, with induced nuclear hypertrophy in the motor neurons of the spinal cord in the SOD1G93A mouse (Riancho et al., 2015). More recently, Genistein, which is an antioxidant and anti-inflammatory agent, was shown to improve motor neuron loss, delay the onset of disease, significantly extend survival (especially in males over females), and induce autophagy in the SOD1G93A mouse (Zhao et al., 2019). This discovery or validation step in pre-clinical models is a costly and valuable process to develop candidate compounds for clinical trials.

However, therapeutic efficacy problems have been raised in using the SOD1 mouse model because while many studies have identified a host of active compounds which are efficacious *in vivo* in mice, these compounds still failed in clinical trials (Aggarwal and Cudkowicz, 2008). This failure suggests that there are important limitations with the mouse models used in the studies. These limitations include the very high expression of the mutant SOD1 and metal-deficiency of SOD1G93A. Also, the differences in corticospinal anatomy, pharmacokinetics, and pharmacodynamics of rodents compared with humans (Turner and Talbot, 2008). Failures in clinical trials have also been attributed to poor study design, lack of proper quality controls, leading to lack of reproducibility in animal studies (Benatar; Scott et al., 2008). This highlights the need for better quality screens and new models in ALS research. However, mutant rodent models still offer an important platform to test disease hypotheses and therapeutics (Aggarwal and Cudkowicz, 2008; Turner and Talbot, 2008).

1-4-2-2-2 Zebrafish ALS *in vivo* models

Another *in vivo* model that has become the focus of many recent research studies is the zebrafish (*Danio rerio*). The zebrafish is a vertebrate *in vivo* model which shows functional genetic and physiological conservation with humans. It has a heart, kidney, liver, and the other organs which are not present or more complex than in worms and flies (Howe et al., 2013; MacRae and Peterson, 2015). Furthermore, it possesses homologous genes similar to those in humans, shows rapid *ex vivo* development with large number of

embryos produced, 3-4 months for sexual maturity, and neurogenesis starts around 10 hours post-fertilisation (hpf) (Kabashi et al., 2011), making it particularly well-suited to study brain development and model CNS disorders.
The zebrafish presents an amenable model for gene knockdown and transient expression studies. For example, neuromuscular junction (NMJ) defects and loss of motor neurons were seen following gene knockdown with antisense morpholino oligonucleotides (AMOs) against FUS (Armstrong and Drapeau, 2013) and C9orf72 (Ciura et al., 2013) orthologues. In addition, zinc finger nucleases (ZFN), transcription activator-like effector nuclease (TALEN) proteins, and clustered regularly interspaced short palindromic repeats-associated 9 (CRISPR/Cas9), have provided a new genome-editing toolbox in zebrafish for the generation of mutants linked to ALS for drug development.

Zebrafish *in vivo* models have become more commonly used for many neurodegenerative conditions (MacRae and Peterson, 2015), such as Parkinson's disease (Ren et al., 2016), Alzheimer's disease (Newman et al., 2014), and Charcot-Marie-Tooth (CMT) disease (Chapman et al., 2013). Moreover, the expression of mutant *sod1*G93R in zebrafish produces ALS-like symptoms and has been used to develop a novel drug screening assay (McGown et al., 2016; Ramesh et al., 2010). These *sod1* zebrafish show many of the hallmarks of the human disease, including NMJ defects, interneuron dysfunction, motor neuron loss, muscle weakness, and reduced survival.
Recently, C9 toxicity in zebrafish has been generated either by injections of repeat-containing RNA or expression of different lengths of DPRs (Swaminathan et al., 2018; Swinnen et al., 2018). A zebrafish *C9orf72* hexanucleotide expansion transgenic model, with the insertion of ATG driven interrupted $(G4C2)_{89}$ expression, showed DPR accumulation (GR, GP, and GA), motor neuron loss and swimming endurance defects at six months (Shaw, 2018). They also showed heat shock protein activation and neuronal stress at 5 dpf. Subsequently, pure C9 repeat models have been generated with sense strand $(G4C2)_{45}$ and anti-sense strand $(C4G2)_{39}$ expression in zebrafish without an ATG translation start codon. These fish show movement endurance defects at six months and a more significant reduction in

movement at one year compared to controls (A. McGown, University of Sheffield, unpublished data). Interestingly, they show DPR expression from both sense $(G4C2)_{45}$ and anti-sense $(C4G2)_{39}$ strands through RAN translation. They also show activation of the heat shock response via expression of *hsp70*::DsRed (a fluorescent neuronal stress reporter). This model may, therefore, be suitable for medium/high-throughput screens to identify therapies for *C9orf72*-mediated toxicity in the future. Taking these findings together, zebrafish models can be of significant value and contribute to drug discovery, target identification and other aspects of pharmacology through cellular toxicity and behavioral assays.

Drug screening is a critical step in the development of novel therapeutics for any disease. This involves testing large numbers of drugs and validating them using *in vitro* and *in vivo* models; see (Fig. 1-1). Zebrafish embryos offer an excellent model for medium to high-throughput screens since they yield a large number of transparent embryos, which can be investigated using microscopy, biochemical, and other fluorescence-based assays.

Zebrafish behavioral signatures are also suitable for medium to high-throughput pharmacological screening, an example being the discovery of anti-psychotic-like compounds using a behavioural battery assay (phenoBlast) (Bruni et al., 2016). Also, a high-throughput psychotropic screening study identified ether-a-go-go-related gene (ERG) potassium channels as a target for drugs regulating wakefulness by utilising an automated (rest/wake) behavioural assay (Rihel et al., 2010). Therefore, the zebrafish has demonstrated capability for investigating uncharacterized chemical compounds in behavioural screens and has excellent potential as a model to accelerate the discovery of novel molecules for pre-clinical trials.

Despite these facts, the zebrafish is still a relatively simple model organism compared to other models such as rodents and primates. They are less expensive to a house than rodents but incur more maintenance costs than worms or flies, have different brain structures than humans (e.g. no motor cortex), show widespread neurogenesis as adults, and do not have typical astrocytes. All these features are limitations of zebrafish models, which are

essential to recognise and understand when interpreting results. However, the zebrafish can be a robust model for the study of human neurodegenerative diseases and can serve as a bridge between *in vitro* and *in vivo* screening in drug discovery before proceeding to pre-clinical research in rodent models.

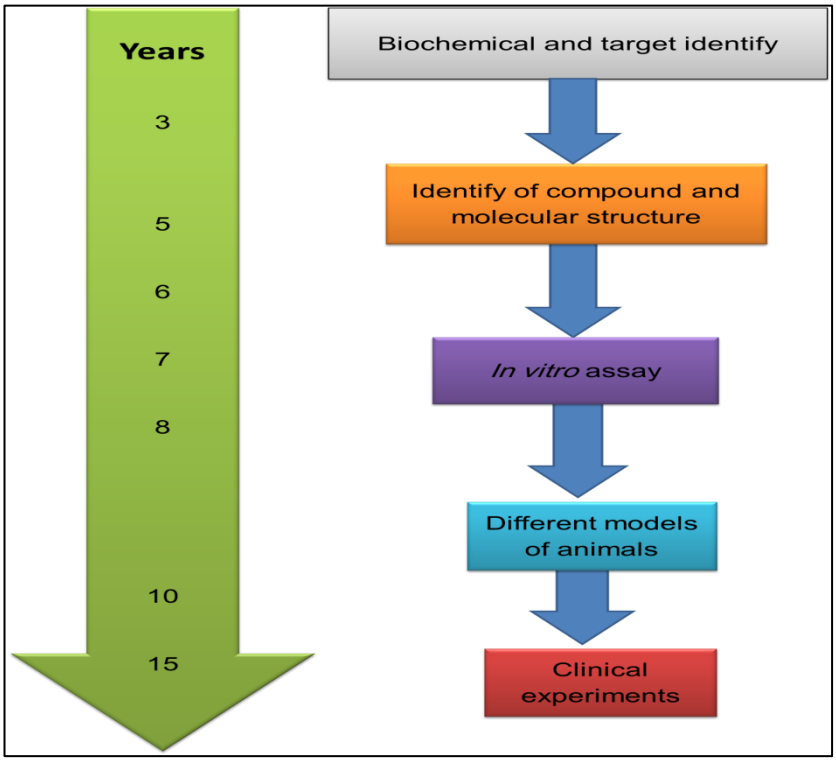

Figure 1-1: Diagram of the traditional drug screening process; adapted from (Bowman and Zon, 2010).

1-5 Implication of ion channels and neurotransmitter receptors in ALS pathology

1-5-1 Voltage-gated channels

1-5-1-1 Voltage-gated sodium (Na^+) channels

Voltage-gated sodium channels are pore-forming transmembrane proteins consisting of several subunits. The α subunit forms a pore with Na^+ ion selectivity and comprises four homologous domains (I-IV). These domains contain six α helical transmembrane segments (S1-S6) and a P-segment (nonhelical) between S5 and S6. These segments are connected by loops. The S4 segment is a voltage sensor responsible for initiating voltage-dependence of the channels due to the abundance of positively charged amino acids (Catterall, 2000).

Voltage-gated sodium (NaV) channels have an essential role in action potential firing and propagation of electrical signals in neurons, muscle and heart tissue. Neuronal cells have two types of Na^+ currents: transient Na^+ currents, a passive flow of Na^+ ions dependent on electrochemical gradients, and persistent Na^+ currents, which are a small fraction of total sodium current with slow inactivation, even with prolonged depolarization (for review see (Waszkielewicz et al., 2013)).

Voltage-gated sodium (NaV) channels are thought to be involved in the pathology of ALS. Increased persistent Na^+ ion currents have been shown in spinal and cortical motor neurons cultures from SOD1G93A transgenic mice (Kuo et al., 2005; Pieri et al., 2009), leading to hyperexcitability. Riluzole is the only approved drug for ALS and blocks the persistent flow of Na^+ ion current without any significant effect on fast Na^+ currents (Belluzzi and Urbani, 2000; Benedetti et al., 2016; Pieri et al., 2009).

1-5-1-2- Voltage-gated potassium (K^+) channels

Voltage-gated potassium channels (VGPC, K_v) are part of a superfamily of channels, including potassium-calcium activated, ligand-gated, inward-rectifying (K_{IR}), and two-pore (K_{TP}) channels. All of these are involved in neuronal excitation, electrical signaling, and ion homeostasis in the nervous system (Pischalnikova and Sokolova, 2009). These channels regulate the membrane action potential through repolarization.
Reduced delayed-rectifier potassium currents and increased persistent sodium currents lead to excitotoxicity, contributing to axonal hyperexcitability and motor neuron death in ALS (Wainger et al., 2014). Reduced delayed-rectifier potassium current amplitude has been shown in motor neurons derived from SOD1A4V ALS patients, which may induce hyperexcitability in motor neurons (Wainger et al., 2014). Retigabine is an anticonvulsant and approved to treat hyperexcitability disorders in humans (Corbin-Leftwich et al., 2016). This drug was identified as a specific activator of subthreshold Kv7 current in induced pluripotent stem cell (iPSC)-derived motor neurons and was shown to reverse electrophysiological defects in neurons derived from

SOD1A4V, C9ORF72, and FUS mutation patients. It has been proposed that it may block hyperexcitability in ALS (Wainger et al., 2014).

1-5-1-3 Voltage-gated calcium (Ca^{2+}) channels

Voltage-gated calcium (Ca^{+2}) channels are present in excitable cells. These channels open during the depolarisation of the membrane action potential, which in turn, initiates neurotransmitter release (Catterall, 2011). There are two families of these types of channels: High voltage-Activated (HVA) and Low Voltage-Activated (LVA). HVA channels include L-, N-, P-, Q- and R-type channels. These have a heterotrimeric structure of α, β, and α2δ subunits. LVA channels include the T-type channel, and consist of an α1 subunit monomer (Dolphin, 2018).

These channels are involved in ALS pathology by overloading Ca^{2+} levels, which leads to the excitotoxicity of axonal fibers (Van Den Bosch et al., 2006). Increased HVA Ca^{2+} currents are observed in the SOD1G93A motoneurons, but no changes are seen on LVA Ca^{2+} currents. The elevation of persistent Ca^{2+} currents could contribute to the early symptom of ALS pathology and therefore could be a drug target for therapy (Chang and Martin, 2016).

1-5-2 Glutamate receptors and excitotoxicity

Glutamate receptors (GluRs) are excitatory synaptic receptors and divide into two families: ionotropic GluRs (iGluRs) and metabotropic GluRs (mGluRs) (Zhu and Gouaux, 2016). They mediate neurotransmission in the membrane of most excitatory neuronal cells at synapses. Excitotoxicity is a cellular mechanism of neuronal death resulting in excessive stimulation of GluRs. The activation of GluRs can cause motor neuron death due to excessive influx of Na^{+} and Ca^{2+} and glutamate overload (Foran and Trotti, 2009). The excessive stimulation of GluRs may be caused by insufficient reuptake of glutamate, leading to an increase in synaptic glutamate concentration and cause the death of postsynaptic neurons (Van Den Bosch et al., 2006).

1-5-2-1 Metabotropic glutamate receptors (mGluRs)

Metabotropic glutamate receptors (mGluRs) are related to family C of the superfamily of G-protein-coupled receptors (GPCRs). The mGluRs are heterotrimeric, consisting of α, β, and γ subunits, and classify into three groups based on sequence similarity, signalling properties and pharmacology: the mGluR I group consists of mGluR1/mGluR5, the mGluR II group of mGluR2/mGluR3, and the mGluR III group of mGluR4 and mGluR6-8 (Niswender and Conn, 2010; Pin and Duvoisin, 1995).

Hyperactivation of group I mGluRs was shown in SOD1G93A transgenic mice due to release of excessive glutamate. Knockdown of mGluR1 delayed the onset of disease, extended survival, reduced astrocyte and microglial activation and decreased mGluR5 expression in the spinal cord of the SOD1G93A mouse, but it did not change glutamate transport or mRNA expression of antioxidant enzymes (Milanese et al., 2014). In addition, a recent study showed that the genetic ablation of mGluR5 in the SOD1G93A mouse improved motor neuron function, increased weight, and extended survival (Bonifacino et al., 2019). This suggests mGluRs are involved in ALS pathology, and inhibitors may constitue a novel therapy for the disease (Battaglia and Bruno, 2018).

1-5-2-2 Ionotropic glutamate receptors (iGluRs)

Ionotropic glutamate receptors (iGluRs) are responsible for neurotransmission and plasticity at excitatory synapses. The iGluRs are comprised of ligand-gated channel pores (Zhu and Gouaux, 2016) and are subdivided into three main families: N-methyl-D-aspartate (NMDA) receptors, α-amino-3-hydroxy-5-methyl-4-isoxazolepropionic acid (AMPA) receptors, and kainate receptors (Traynelis, 2010). Each family has a distinct function. AMPA receptors are responsible for depolarization of the membrane at the postsynaptic compartment. NMDA receptors contribute to synaptic plasticity due to slow inactivation. Kainate receptors participate in synaptic currents both pre-synaptically and post-synaptically (Zhu and Gouaux, 2016). However, NMDA receptors are permeable to Ca^{2+}, while AMPA receptors have variable Ca^{+2}

permeability as a result of the absence or presence of GluA2 subunits (Van Den Bosch et al., 2006).

Therapies for controlling excitotoxicity in motor neuron disease have been investigated in *in vivo* and *in vitro* models carrying SOD1 mutations, such as the SOD1G93A mouse and cell culture systems. SOD1G93A mice express altered AMPA receptor subunits and are more suceptible to kainate-induced excitotoxicity (Spalloni et al., 2004). Also, intraperitoneal injection of 12mer antisense peptide nucleic acid (PNA) against GluR3 in SOD1G93A mice gave extended lifespan, as well as reducing toxicity induced by AMPA receptor stimulation in NSC34 cells (Rembach et al., 2004). These studies suggest interference with GluR3 and AMPA receptors maybe a viable strategy for targeting excitotoxicity in ALS.

1-5-3 Ion channels in ALS

Muscle fasciculation although not predictive of ALS onset or progression is one of the most common feature in ALS clinical presentation. Ever since the identification of muscle fasciculations in ALS patients, an important role for ion channels that mediate axonal potential have been postulated. As axons are easy to evalaute in human ALS patients, one of the first studies on axonal ion-channel homeostatis suggested that fasciculations result from imbalance in sodium and possium ion channel function (Bostock et al., 1995). Another clinical observation that has geared study of ion channel is from the observation that antibodies against calcium ion channels were observed in some ALS patients and these antibodies were able to alter the function of ion channels in vitro suggested an auto-immune component to ALS (Smith et al., 1996). However glutamate excitotoxicity is considered a main feature in ALS as being an excitatory neurotransmitter with a wide variety of receptors such as NMDA, AMPA, Kainate and metabotrophic receptors has been widely implicated in ALS pathogenesis (Lau and Tymianski, 2010). These early studies lead to the discovery of Riluzole as a potential treatment for ALS (Wokke, 1996). However, its has been over 26 years since the first trial of riluzole in ALS (Bensimon, 1994) and the efficacy of riluzole in ALS is marginal at best.

Nevertheless the glutamate hypothesis is one of the best studied processes in ALS. Glutamate levels in the CSF of ALS patients is elevated although further research demonstrated that ony 40% of the patients display this (Tarasiuk et al., 2012). AMPA receptor is thought to be one of the major glutamate receptor involved in the cellular toxicity of ALS pathology. It is important to remember the many diverse receptors through which glutamate functions as a neurotransmitter. Thus, full exploration of these diverse mechanisms of glutamate is critical. Further a reduction in functional glutamate transporter EAAT2 or also referred to as GLT1 have been observed in ALS patients. The reduction in GLT1 is mediated by alteration in alternative splicing of the gene, thus effectively reducing GLT1 levels. GLT1 is expressed in astrocytes and mediates the clearance of glutamate from the synapse. However, ceftriaxone which enhanced GLT1 activity by modulating its aberrant splicing failed in clinical trial, thus its potential still unclear.

Aquaporins were also identified as a modulator of ALS through its role in regulating water and ion homeostasis (Zou et al., 2019). Aquaporin 4 expression was elevated in astrocytic end feet in ALS astrocytes and is thought to impact ion channels such as Kir4.1, thus dysregulating potassium ion homeostasis (Zou et al., 2019). Further aquaporin 4 was shown to modulate GLT1 expression thus together maintaining synaptic glutamate levels.

The high incidence of ALS parkinsonian disease named Guam ALS is thought to be mediated by neurotoxin from the Cycad nut and enriched in bats, which is consumed by humans in Guam (Chiu et al., 2011). BMAA, a toxin identified from the cycad nut is a neurotoxin, whose toxicity is mediated by glutamate excitotoxicty (Chiu et al., 2011).

Thus diverse processes appear to impact upon the role of ion channels in ALS pathogenesis. Our interest on ion channel derived from an unbiased screen of small molecule compounds that reduce neuronal stress in a *sod1*G93Ros10 zebrafish model of ALS. In a screen of over 1500 compounds, we obtained only two compounds that demonstrated a robust inhibition of neuronal stress in this model (Thesis (McGown, 2014). The two were riluzole and selamectin

Selamectin modulates neuronal stress via reducing glycinergic transmissions in transgenic zebrafish (Thesis (McGown, 2014)) and enhances high-throughput neuronal differentiation of pro-neurogenic mediated GABA receptor activity in pluripotent stem cells (PSCs) and also neurogenesis in the developed zebrafish brain (Sun et al., 2013).

Selamectin and ivermectin belong to a class of compounds named macrocyclic lactones. Ivermectin (Andries et al., 2007) inhibited the excitotoxicity of the ion channels, including AMPA receptors, extended lifespan of a SOD1G93A mouse. The other study has reported that antagonist perampanel showed motor neuron survival, ameliorate the motor dysfunction, and increase positive inclusion of focal TDP-43 in the ADAR2 mouse. This mouse exhibits a progressive ALS phenotype by a knockdown of the adenosine deaminase acting on RNA2 (catalyses RNA editing at the Q/R site of GluA2) (Akamatsu et al., 2016). These studies highlight the ion channel therapy would be the potential target for ALS in the future.

1-6 Heat shock proteins (HSPs)

Heat shock proteins are molecular chaperones families ubiquitously expressed proteins found in all organisms. It was first identified in a *Drosophila* in 1962 as a new RNA synthesized with increase in temperature (Ritossa, 1996).

HSPs are involved in refolding misfolded proteins. Various cellular stresses such as oxidative stress, heat, and disease conditions induce and activate HSPs to remodel misfolded protein to fold protein. Chaperone proteins bind with a wide range of substrate and proteins to build-up fold protein. It is composed of different forms in various tissue types. These chaperones are also specifically localized to the nucleus, cytoplasm, mitochondria, and endoplasmic reticulum to keep protein from misfolding. The HSPs families are classified based on molecular weight as HSP40, HSP60, HSP70, HSP90, HSP100 and smaller HSPs (Papsdorf and Richter, 2014).

Heat shock factor1 (HSF1) is a master regulator of the heat shock stress response in mammalian cells. It was recently demonstrated that dominant expression of HSF1 leads to a reduction of insoluble and hyper-phosphorylated TDP-43 and result in promoting cell survival (Chen et al., 2016). This activity was mediated through HSJ1a, a J domain containing heat shock protein. Recently, DPRs expression is associated with activation of HSPs that are regulated by HSF1 in C9ORF72-ALS/FTD patients (Mordes et al., 2018; Shaw, 2018). Also, it has reported that the up-regulation of HSF1 and highly hsps expression is associated with G4C2 repeat and poly-GR brain in Drosophila (Mordes et al., 2018).

Over-expression of HSPs are observed in many protein aggregation diseases such as Al-zaheimer's, Parkinson's, Huntington's, and prion diseases. Therefore, HSPs have inhibitory effects on neuronal degeneration, which may provide the basis of neurotherapeutic development (Adachi et al., 2009). However, the protein aggregation of motor neurons cultures from iPSC carrying SOD1, TDP-43, and C9orf72 is not sufficient to upregulate HSPs (Seminary et al., 2018).

1-6-1 Heat shock protein70 (Hsp70)

The HSP70 promoter is used as a readout of neuronal stress, as it is activated by misfolded intracellular proteins in response to stresses such as oxidative stress, excitotoxicity, altered pH, temperature changes, and other abnormal conditions (Schlesinger, 2011). Elevation of hsp70 is seen in astroglial and motor neurons in ALS patients, as well as at low levels in the mutant SOD1 mice, suggesting that this is a disease-relevant physiological response to cellular stress (for review see (Kieran et al., 2004)).

Over-expression of HSP70 has conferred a potential neuroprotective therapy. The recombinant human HSP70 intraperitoneally injected three times weekly, at postnatal day 50 to G93A mice, it showed extended life span, promoted motor neurons survival, and increased of innervated neuromuscular junctions (Gifondorwa et al., 2007). The other follow up study of administration

recombinant human HSP70 from postnatal day 30 showed reducing pathophysiology in SOD1G93A mice (Gifondorwa et al., 2012).

HSP70 neuroprotective pathway is not well known. HSP70 was seen in the muscle cell in the peripheral tissue. There the HSP70 may maintain NMJ'S integrity and innervation of skeletal muscle due to increased HSP70 expression (Robinson et al., 2005). Using arimoclomol, a drug that up-regulates HSP70 led to an extend survival and improve motor performance at 75 days in symptomatic mice, but it failed to show any effects at 90 days (Kalmar and Greensmith, 2009; Kalmar et al., 2008). However, other studies have reported that an increase of chaperon proteins or elevation of HSP70 has no effect on ALS onset or survival in SOD1 mutant mouse models (Liu et al., 2005; Rohde et al., 2008).

Despite the variable effects of HSP70 in disease efficacy, the expression of HSP70 in stressed neurons is a good reporter for a stressed cell. In our model *sod1*G93Ros10 zebrafish, the bacterial artificial chromosome (BAC) was used. This DNA contains the *sod1* zebrafish gene promoter that drives the expression of zebrafish *sod1* gene that is mutated at position 93 (glycine to arginine, G93R). This transgene is in tandem with the zebrafish heat shock protein 70 (hsp70) promoter that drives the expression of the DsRed fluorescent protein; (Fig 1-2). Therefore, HSP70 expressions in stressed motor neurons would serve as a biomarker of stressed neurons in a drug screen. Tagging HSP70 promoter to a fluorescent DsRed molecule would allow us to perform further analysis of motor neuron's stress of treated fish in the future.

1-7 Work leading up to the project

1-7-1 *sod1*G93Ros10 ALS zebrafish model

The *sod1*G93Ros10 zebrafish transgenic line expresses mutant *sod1* at moderate levels. This model has been shown to have 4x fold higher *sod1* expression than the endogenous sod1 levels in wild type (WT) fish, with altered neuromuscular junctions showing a reduced overlap of pre- and post-synaptic markers in comparison to WT adult animals. This mutant line also showed loss of interneurons at 72 hpf, loss of motor neurons at adult stages, reduced survival, muscle weakness, and premature death (McGown et al., 2013; Ramesh et al., 2010).

The bacterial artificial chromosome (BAC) used contains the *sod1* zebrafish gene promoter, zebrafish *sod1* mutated at position 93 (glycine to arginine, G93R), as well as the zebrafish heat shock protein 70 (*hsp70*) promoter which drives expression of the DsRed fluorescent protein; (Fig 1-2). The *hsp70* promoter is used as a readout of neuronal stress, as it is activated by misfolded intracellular proteins in response to stresses such as oxidative stress, excitotoxicity, altered pH, temperature changes, and other abnormal conditions (Schlesinger, 2011). Heat shock response (HSR) proteins include hsp70, hsp90, hsp40 and hsp20, named according to their molecular weight. Elevation of hsp70 is seen in astroglia and motor neurons in ALS patients, as well as at low levels in the mutant SOD1 mice, suggesting that this is a disease-relevant physiological response to cellular stress (for review see (Kieran et al., 2004)). Further characterisation of the model published in 2013 demonstrated that mutant *sod1* zebrafish show neuronal stress in interneurons of the spinal cord at an early stage (72 hpf) before it is observed in motor neurons (McGown et al., 2013).

These features of mutant *sod1* zebrafish led to the development of drug screens utilising it. Selamectin was identified as neuroprotective in the *sod1*G93Ros10 model. This compound showed a reduction of stress in glycinergic inhibitory interneurons (McGown, 2014). Selamectin is a macrocyclic lactone. It modulates GABAergic and glycinergic inhibitory neurotransmission. (Lynagh et al., 2011; Sun et al., 2013). This finding when

taken with the studies outlined in section 1-5, further highlights the potential of ion channel modulation as a therapeutic target for ALS. We, therefore, set out to screen a library of ion channel modulators in this project.

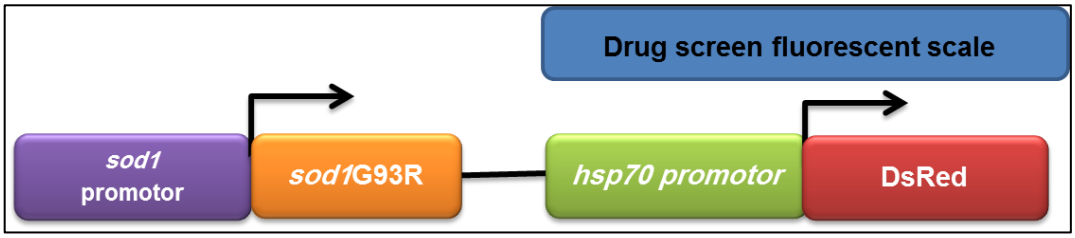

Figure 1-2: The construction of the *sod1*G93Ros10/ALS zebrafish**.** The *sod1* G93R open reading frame is driven by zebrafish *sod1* promoter. This mutant sod1 gene is in tandem to a drug screening gene that is composed of heat shock protein 70 (*hsp70*) gene, that drives the expression of fluorescent reported DsRed. The misfolding of *sod1*G93R is predicted to activate *hsp70* promoter, thus allowing identification of compounds that reduce protein misfolding.

1-7-2 *C9orf72* zebrafish ALS models

Given the multifactorial nature of ALS and multiple known genetic causes, we felt it would be important to validate findings in the *sod1*G93Ros10 ALS model in a second model based on a different genetic mutation. *C9orf72* zebrafish were therefore chosen to validate the modulation of neuronal stress by hits obtained from the *sod1* zebrafish screen.

The C9 ALS zebrafish model used in this project was generated in 2017 with independent lines carrying expressing the sense and anti-sense strands. The sense strand zebrafish has a forty-five hexanucleotide repeat expansion (HRE) of G4C2, and the anti-sense strand zebrafish has a thirty-nine HRE of C4G2.

Both of these models show DPR expression and reduction of swimming endurance. The $(G4C2)_{45}$ line has confirmed expression of poly-GR, -GA, and -GP, while the $(C4G2)_{39}$ line shows poly-PR, -PA, and -PG. The transgene constructs include a *Ubi* promoter that drives transcription of G4C2 or C4G2

repeats that are tagged with a V5 epitope to track DPR expression level and the *hsp70*-DsRed fluorescent stress readout as in the *sod1* zebrafish (see Fig. 1-3).

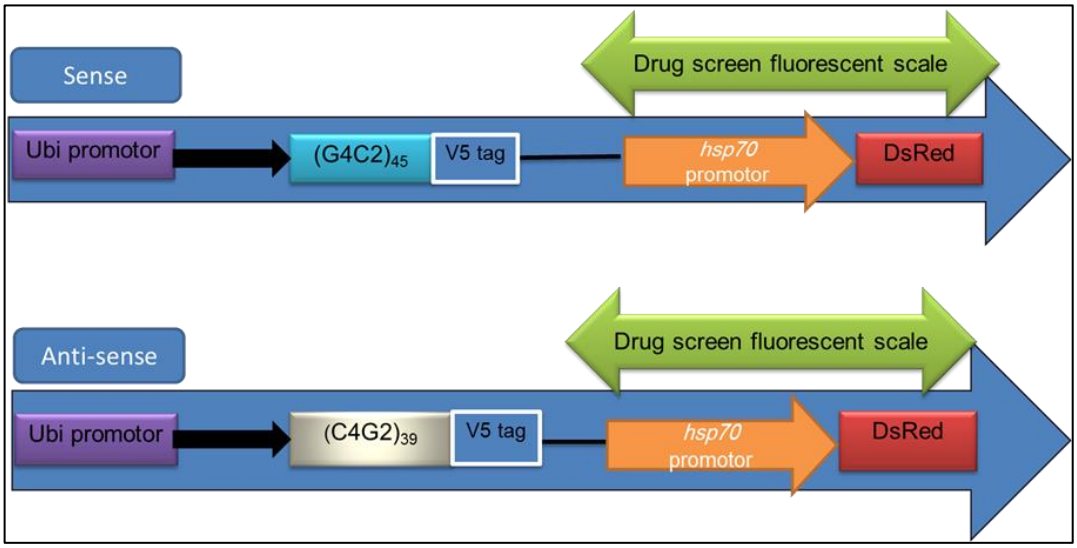

Figure (1-3): The construction of *C9ORF72 (sense and anti-sense)* ALS zebrafish. The ubiquitin (ubi) gene promoter drives the expression of sense $(G4C2)_{45}$ (top) or antisense $(C4G2)_{39}$ (Bottom) V5 epitope tag RNA. The sequence prior to the start of G4C2 and C4G2 repeats is devoid of any ATG, thus precluding ATG driven expression of DPRs. Thus, any V5 tagged DPR expression is exclusively RAN mediated translation. The *hsp70* promoter-DsRed gene is placed in tandem. It is predicted that DPRs would activate the stress response pathway and would serve as a tool to identify drugs that reduce DPR levels.

1-7 Hypothesis and aims

It is hypothesised that ion channel modulators may be of therapeutic benefit in ALS. The mutant *sod1*G93Ros10 zebrafish provides a robust *in vivo* ALS model that can be utilised for medium- to high-throughput drug screening, due to the incorporation of the *hsp70*-DsRed neuronal stress fluorescent reporter in the transgene construct. *C9orf72* HRE transgenic zebrafish provide an independent *in vivo* model for validation of ion channel modulators identified. We therefore set out to identify candidate novel neurotherapeutics relevant to multiple forms of cellular toxicity in ALS.

The specific aims of the project were as follow:

1. To screen the LifeArc (MRCT) library to identify ion channel modulators which modify the neuronal stress readout in *sod1*G93Ros10 zebrafish.
2. To validate the hits obtained from primary screening by establishing dose-response curves for neuronal stress readout.
3. To undertake behavioural analysis to determine whether the identified drugs show toxicity and/or sedative effects.
4. To investigate chemical structure relationships of the hit compounds.
5. To validate the most promising ion channel modulators identified in the *C9orf72* HRE zebrafish models.

By achieving these aims, we set out to identify compounds that can be taken forward into ALS mouse models for further pre-clinical validation.

CHAPTER 2

2-Materials and Methods

2-1 Animals:

2-1-1 The transgenic ALS zebrafish model: *sod*1G93Ros10 mutant zebrafish

Tg (*sod1*G93R;hsp70:DsRed) is referred to as G93Ros10-Sh1. The transgenic line utilised in this study was initially developed at Ohio State University, Columbus, OH. It was imported to the University of Sheffield, Sheffield, UK, in 2010. This line was generated according to the protocol previously set out in (Ramesh et al., 2010), (Fig. 2-1). The transgene contains a sod1 promoter that drives the expression of the zebrafish sod1 gene with a mutation in the conserved amino acid, from glycine (G) to arginine (R), at position 93. The transgene also contains a *hsp70* promoter, driving a DsRed reporter gene.

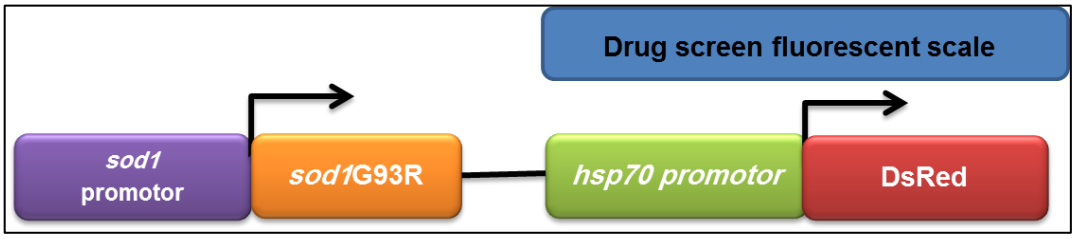

Figure 2-1: The construction of the *sod1*G93Ros10 zebrafish

2-1-2 Generation of *sod1*G93Ros10 embryos for screening

In all the zebrafish experiments in this thesis, the transgenic G93Ros10-Sh1 line was out crossed with the wild-type AB zebrafish strain. A male and female were set up in a breeding tank with a divider between them in the evening after feeding. The following day the dividers were removed from the tanks to allow the fish to mate and lay eggs. The fertilised eggs were filtered out of the water through a fine sieve. The embryos were transferred into and kept in sterile embryo medium (E3- NaCl 5.03 mM, KCL 0.17mM, $CaCl^2.2H2O$ 0.33Mm, MgSO4.7H2O 0.33 Mm) at 28ºC throughout the experimental procedure. All zebrafish used in this study were culled according to the

schedule 1 protocols, which were undertaken with a Home Office approved project license.

2-2 Dechorinating Method

The chorion was removed from the embryo by holding the chorion with two pairs of fine forceps and pulling the chorion apart, to allow the embryo to drop into the embryo medium. Care must be taken and a microscope used to avoid damaging the embryo within the chorion. Dechorination can be performed after 24 hpf at any time. An E3 media change was performed after dechorination to remove chorion debris, reduce the risk of fungal contamination, and to allow an optimal environment for embryo development.

2-3 LifeArc (formally MRCT) chemical compounds library and storage conditions

The medical research council technology (MRCT) library is a chemical library consisting of 4494 compounds. It is provided by the Medical Research Council Technology (now LifeArc). This library is stored in deep storage well plates within the SPOD system (Roylan) which prevents library damage. The library was delivered at 1mM dissolved in DMSO. The original libraries were shipped frozen and were stored at -80°C until the screening.

The SPOD system is a specialized drug storage system designed to extend the lifespan of compounds by controlling environmental conditions (atmospheric pressure of 0.5 PSI. oxygen level <10%, relative humidity <5%). The system maintains a high nitrogen environment to generate an inert environment with low O_2 and humidity levels, to reduce oxidation and hydrolysis of the compounds. The SPOD system also maintains a dark environment to prevent UV damage of the compounds (photolysis). 12 µl of each drug was dispensed from the library source plate to the Echo 384 LDV (Low dead volume) plate (Echo TM Qualified 384 well polypropylene microplate, clear, flat bottom, Ca t# P-05525). The transfer was performed using the Thermo Scientific Platemate Plus (Matrix Technologies Corp Thermo Scientific), the tips were cleaned after each cycle with an excess of distilled water and changed between drugs to avoid any cross-contamination.

Once imprinted onto the source plate (Echo 384 LDV plate), all screening plates were stored within the SPOD system for the duration of the screening.

2-4 InCell microscopy system at 2 dpf for genotyping the embryos

To identify zebrafish expressing the transgene at 48hpf, the high content imaging system, the InCell analyser 2200 (GE Healthcare) was used. The InCell can image multiwell plates in multiple wavelengths, allowing the rapid genotyping of ~1000 embryos per hour. Embryos at 2 dpf were loaded into 96 well plates (96 well black, µClear, Greiner Bio-One, Cat No:655096) in 150 µl of E3 media for imaging on the InCell analyser.
Images were taken in two channels: the DsRed wavelength (543 excitation and 604 emission) and brightfield. The wavelengths selected were both from Polychroic QUAD2 for brightfield (0.03s exposure) and DsRed (0.500s exposure) wavelengths to identify fish with transgene expression. The brightfield was used to identify any damage, changes in the morphology or abnormal developmental that may have occurred during dechorination or drug treatment. The full InCell imaging settings used were 2X Nikon objective, Plan Apo, CFI/60 lens, binning 4x4, and 2-D deconvolution. The large chip CCD camera was used to obtain high-resolution images with a CoolSNAP K4 2048x2048 pixel array (7.40 µm square pixel). A 1% power laser autofocus was used to obtain the best image focus for each well. The laser-based HWAF (Hardware autofocus) uses a 785 nm laser with the z-axis to determine the target and its location.

2-5 Drug plate preparation by using Echo 550 liquid handling system

The Echo550 liquid handling system was used to dispense the drug libraries into the zebrafish dosing plates. The Echo 550 liquid handling system uses acoustic energy to rapidly deliver multiple 2.5 nl droplets from the library plate (Echo™ 384 LDV plates/ source plates) to destination plates (96 well, uClear, Grenier). By using acoustic energy to dispense, the system has the capability of dispensing very low volumes 2.5 nl rapidly and accurately. This accelerates the transfer process, uses minimal drug library, and has no risk of cross-contamination as the transfer is done without tips. For the primary screen, 2 µl (2000 nl) of 1 mM stock concentration of each drug in the library was added to

a well. When the dispensing process has been completed, 150 µl of E3 was added to the wells by using the WellMate system (WellMate, Thermo Scientific, Matrix). Finally, 50 µl of (fish with E3) were loaded to make a final volume of 200 µl at 10 µM.

2-6 InCell microscopy system at 6dpf

Daily the individual embryos were checked under the light microscope to determine any toxicity and death. On day 6, Tricaine (MS-222 at 4.2 ml/100 ml E3 media) was added to each well to euthanise the fish. Then, the plates were scanned on the InCell plate reader (GE healthcare) to confirm all fish used in the screen were transgenic and identify fish with morphological defects due to drug toxicity. The incell settings used were the same as at 2dpf, but the exposure for DsRed was decreased to 0.100s due to increased fluorescence with age.

2-7 Drug screen fluorescent readout of cellular stress

At 6 dpf, the anesthetised fish were transfered into 96 well V-bottom plates (V-bottom, Clear, Greiner Bio-One, Cat No: 651101) in 50 µl of media. Each well was sonicated at 25% for 5 seconds using the Vibra cell sonication system (Sonics and Materials, Inc). The sonicated plates were centrifuged at 3000 G for 10 minutes (CWS ALC PK120 Centrifuge, T536 Bucket). 20 µl of the supernatant was then loaded onto 384 well plates (microplate, 384 well µClear®, black, Greiner Bio-One, Cat No: 781091)**.** DsRed fluorescence was measured using the Pheraster reader system at the excitation wavelengths 560 and 544 and emission wavelengths 645 and 590 respectively.

2-8 Statistical analysis

2-8-1 Statistical analysis utilised in the primary screen

The statistical parameter used to quantify this screen was the strictly standardized median difference (SSMD). SSMD represents the ratio of the median to the standard deviation. It measures the effect size of each compound by comparing it to the mean across the whole plate (Zhang, 2011). The logic is that the most test compounds in a test plate are most likely not to

affect, and any compound affecting will stand out. Therefore, the assay looks for outliers which may be activators or inhibitors of the DsRed signal. SSMD works to score every individual compound on the screen for its effect size above or below the mean. An SSMD value is denoted as β value and is average fold change penalized by the variability of the fold change among the compounds in the plate. This means that each compound has an effect size, which is representing the magnitude of the difference between the compound and the plate average. This allows for the scoring/grading of hits that is comparable between different plates in the screen.

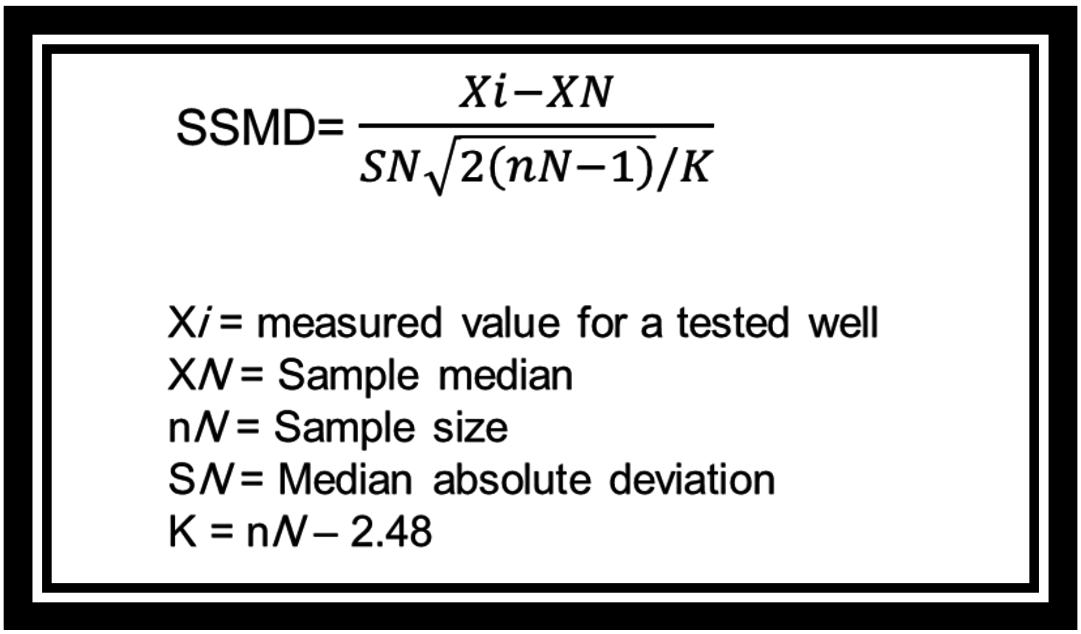

Figure 2-2: An equation of the calculation SSMD used in the primary high-throughput screen analysis.

In a high throughput drug screen, the majority of compounds will have little to no effect, and therefore the majority of the test compounds would have an SSMD score of around 0 in the plate as they do not have an effect. Therefore, a compound that causes an increased effect, such as an increase of DsRed fluorescence, would have a β value above zero SSMD scores. Conversely, compounds with an SSMD score below zero are reducing the DsRed fluorescence. SSMD uses a scoring system, as shown in Table 2.1, to grade the hits based upon effect size. The threshold for a compound being classified as a hit in this screen was set at β < -0.5 (weak) and < -1.0 (fairly moderate) for quality control of the screening experiments.

Table 2-1: SSMD thresholds score of the negatives and positives hits based on the β value. β values green colour represent SSMD threshold for selecting the inhibitor compounds, while β value red colour represent SSMD threshold for selecting the activator compounds Adapted from (PhD thesis (McGown, 2014)).

Effect subtype	Thresholds for negative SSMD	Thresholds for positive SSMD
No effect	β= 0	β= 0
Extremely Weak	− 0.25 < β <0	0.25 > β > 0
Very weak	− 0.5 < β < − 0.25	0.5 > β > 0.25
Weak	− 0.75 < β < − 0.5	0.75 > β > 0.5
Fairly weak	− 1 < β < − 0.75	1 > β > 0.75
Fairly moderate	− 1.28 < β < − 1	1.28 > β > 1
Moderate	− 1.645 < β < − 1.28	1.645 > β > 1.28
Fairly strong	− 2 < β < − 1.645	2 > β > 1.645
Strong	− 3 < β < − 2	3 > β > 2
Very strong	− 5 < β < − 3	5 > β > 3
Extremely strong	β < -5	β > 5

2-8-1-1 Quality control (QC)

The quality control of an assay is probably the most critical step in designing and validating an assay as it confirms the integrity of the identified hits. No biological screen is perfect due to experimental noise from the equipment used, the user, the compounds and the model systems used, but by fine-tuning a screen and obtaining the best QC measures, false hits can be minimised and the quality of data generated be improved.

It is important for each assay plate to contain a suitable number of the positives and negatives controls that can be used to ensure high-quality controls for each experiment. For a good high-throughput drug screening assay, it is critical to maintain a large drug effect window between the positive and negative controls. The industry-standard quality control (QC) for screening is to measure the sensitivity and specificity. The sensitivity of an assay is considered as to how many true hits are identified, while the specificity of an assay reflects how many false hits are identified.

The QC of each screened plate was quantified using the positive and negative controls in each plate and the sensitivity and the specificity was calculated in the following equation

Sensitivity= (True positives/(true positives+false negatives))*100

Specificity= (True negatives/(true negatives+false positives))*100

2-8-2 Statistical analysis of the secondary screen (dose-response)

The statistical analysis used was: one-way ANOVA analysis, Two-way ANOVA analysis, and Dunnet's comparison tests, Area under the curve, and T-test. Graph-pad prism 2017 was used to perform the statistical analysis and generate the graphs. The figures represent the dose-response analysis of the hit compounds to show the potency of the compounds compared to DMSO by using one-way ANOVA in the first screen and two-way ANOVA in a duplicate. This would allow us to make sure that a duplicate test from a new batch in different time shows the efficacy of hit compounds.

2-9 Secondary screen: The layout of the 96 well plates in the dose-response screen study

The 96 well plates layout of the secondary screen were divided depending on the type of screen being undertaken. The secondary screen performed were the dose-response study at a range of doses; therefore, the layout of the 96 well plates was different between the secondary screens screens.

2-9-1 The layout of the 96 well plate of the repeated hits screen

To confirm the true hits, each hit was repeated six times at 10µM. The layout of this screen was 6 wells of the positives control (riluzole), 6 wells of the negatives control (DMSO), and 10 columns of the repeated hits at 10 µM (Fig. 2-3).

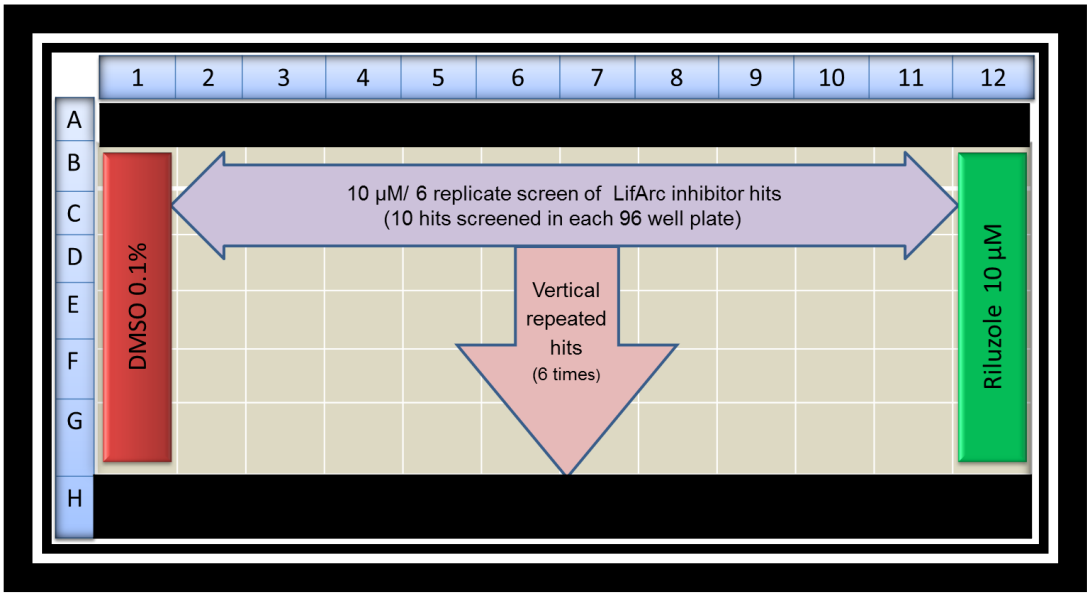

Figure 2-3: The layout of the repeated hits screen plate

2-9-2 The layout of the dose-response hits in the 96 well plate

The top hits were screened 5 times at a range of doses in a dose-response manner to look for compounds showing a good dose response profile. The layout of each 96 well plates was 6 wells of the positives control (riluzole), 6 wells of the negatives control, and 5 replicates for each of the doses (0.1 µM, 0.3 µM, 1.0 µM, 3.0 µM, 10 µM, and 20 or 30 µM) of two hits setting in 96 well plate, (Fig. 2-4).

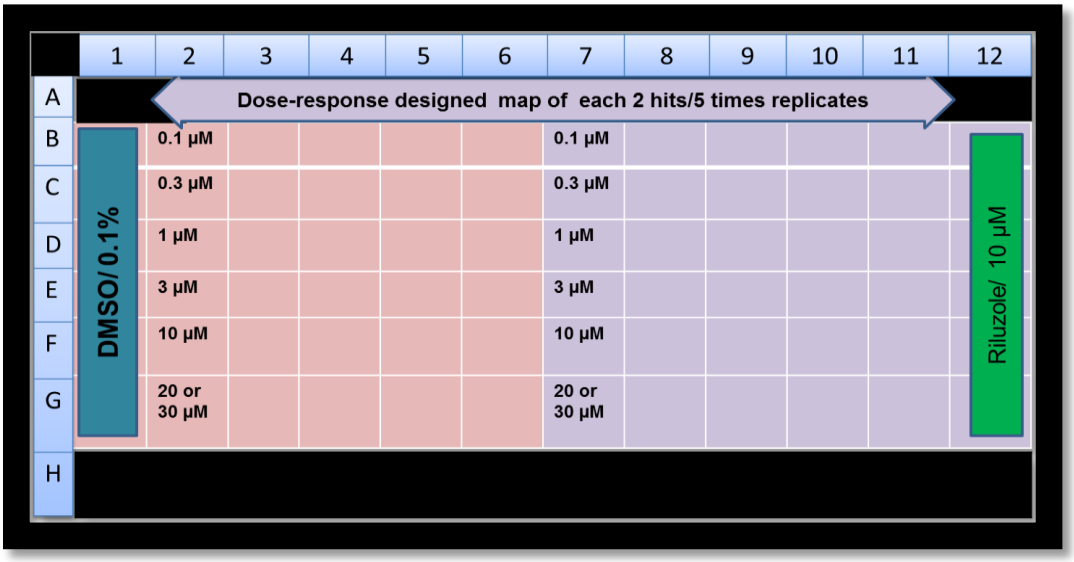

Figure 2-4: Shows the layout of the dose-response screen in the 96 well plate.

Also, the lower doses of the hits and related structure compounds layout were at 0.1 µM, 0.3 µM, 0.5 µM, 1.0 µM, 3.0 µM, 5 µM, and 10 µM/ 6 times each dose of one-hit setting in the 96 well plate, (Fig. 2-5).

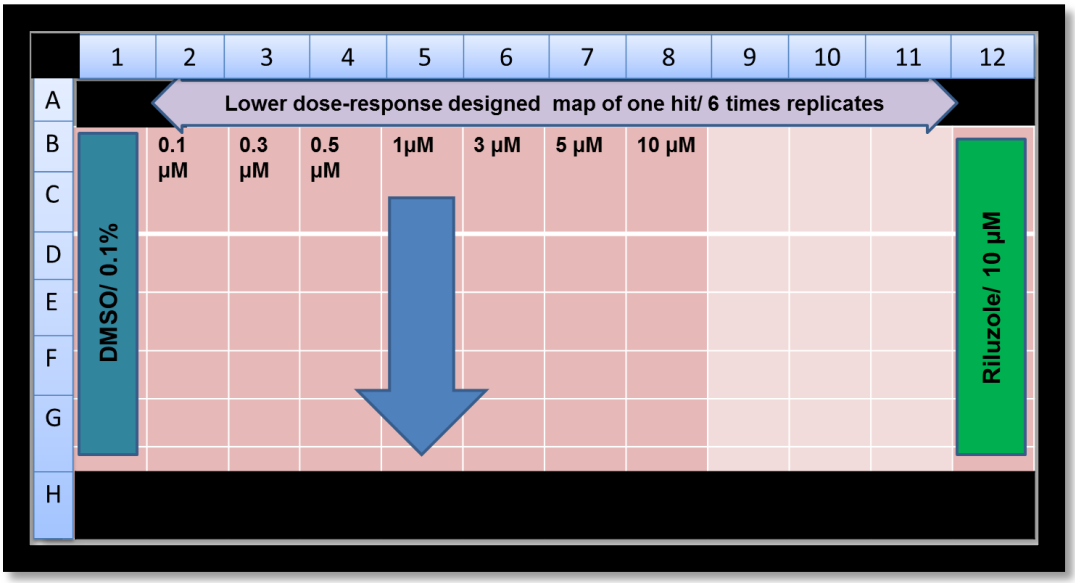

Figure 2-5: The layout of the lower dose-response screen of the hit and the related closet structure compounds.

2-10 Zebrafish behaviour analysis

This assay was used to detect gross changes in locomotor activity. Gross behavioral changes such as hyperactivity or hypoactivity are efficiently detected by our behavioural assays. Behavioural analysis was performed using the viewpoint software (Viewpoint Lab Sciences, Inc). This software allows the tracking of zebrafish behaviour in two different conditions (dark and light) with live location tracking of the embryos in a 96 well plate (96 well µClear, Greiner Bio-One) (one embryo in each well/ 200 µl). The programme detects movement in the 96 wells and tracks the movement of each embryo, splitting the movement speeds with different threshold parameters: >15 mm/s (fast movement) and <3 mm/s (slow movement) for 20 mins (10 mins/ dark and 10 mins/ bright).

For the dose-response screen study of the hits and analogues, the set up of tracking for the zebrafish behaviour was >15 mm as a fast movement and <5 mm as a slow movement for 5 mins each/4 cycles. This duration was sufficient for gross locomotor analysis and detecting light-dark response changes.

2-10-1 Power calculations and group size

The statistical power of a test of hypothesis is calculated as the probability of detecting an effect. This provides the confidence in the test of hypothesis of the study. More importantly power calculation is important prior to starting a study to estimate the number of observation (animals) required to detect a predetermined effect size in an experiment.

There are several factors effect that affect the study power. These are the α level (significance level), the difference between group means, the variability among the subjects in the study and the sample size. Sample size is a key factor in designing studies. Therefore, more samples would increase the precision of the study, although this is challenging as it would be ideal to have as few samples as possible when performing animal studies. The other factor that affects the group size is the magnitude of the significant difference between the groups being studied. Thus, very precise estimates of the true

population variability are required to more precisely calculate the power of the study (Jones et al., 2003).

The group size calculation should be designed before the research carried on. Therefore, when an experiment is designed, we want to be sure the study is worthwhile to get the answer. Altman developed a graph called Nomogram that relates the effect size, power and sample size (Figure 2-6).

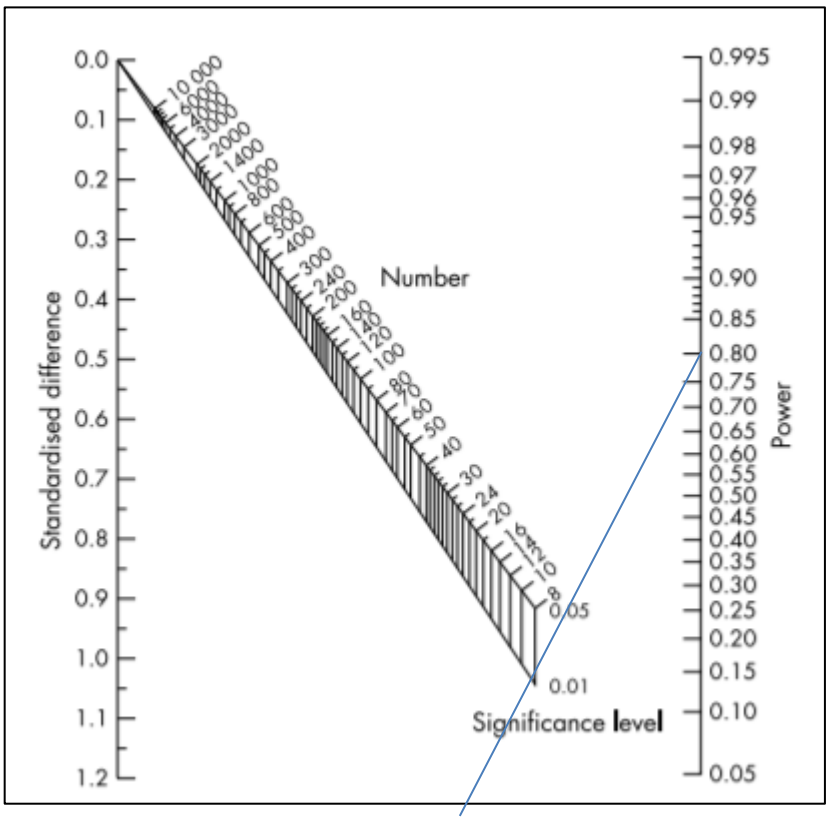

Figure (2-6): Nomogram developed by Altman to plot a relationship between effect size, power and sample size to determine optimal sample size (Whitley and Ball, 2002).

G*power is an online tool that can make similar calculations for number of samples required in a similar fashion (Faul et al., 2007). We utilised this software to analyze the N required for the screen. For example in our primary screen, when we analyze the b-value of negative control, it is an average of 0.247, while that of positive control riluzole is -4.05. The standard deviation of the combined group is 2.328. When performing a screen, in each plate we have at least 10 usable positive and negative controls and one test

compound. Thus, we can calculate the total number of samples for DMSO control and the test compound by performing the power calculation as shown below.

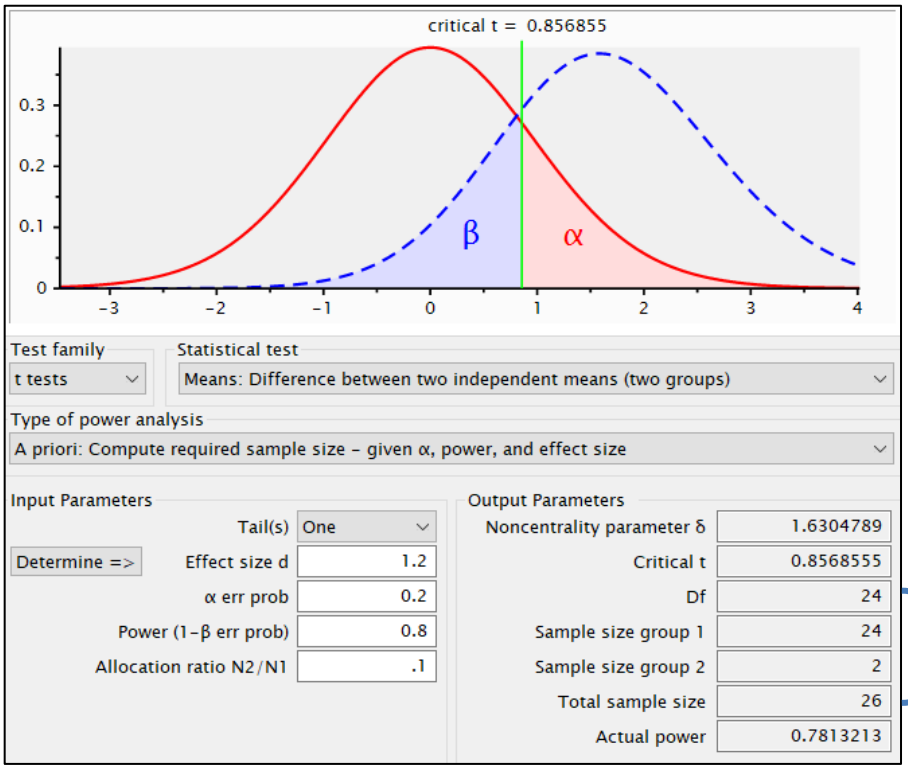

Figure (2-7): Sample size analysis. Analysis is based on riluzole and DMSO controls to arrive at N for DMSO control and test compound in the primary screen using G*Power software.

The effect size for detecting a compound like riluzole is 1.8 (d). We set hits to an effect size smaller than riluzole (d=1.2) and the power to 0.8 with 1 test compound/10 usable negative DMSO controls/ plate, the allocation ratio for two repeats of the screen is 0.1. Based on this, the sample size for DMSO control required is 24 (12+12 from each of the single screen) and N=2 for each of the test compound. Thus, based on this power calculation, it is reasonable to perform a duplicate screen, as it reduces the number of embryos required and makes the primary screen faster. Thus, any hits could be retested with larger N to confirm the hits in the primary screen.

The behaviour assay were performed on embryos at 6 dpf to detect the locomotion activity differences between treated embryos and the control (riluzole) during two environment conditions (light/dark). This would reveal the significant locomotion difference between hit-compounds treated embryos and riluzole treated (strong sedative effects) which would have a very large d value when we compare riluzole with DMSO control. Thus, it would be relatively easy to differentiate a strong sedative from non-sedative hit compounds.

Smaller behavioral effects of hypo and hyperactivity are much more difficult. When performing more subtle behavioral analysis, however, the effect size is very narrow and the standard deviation is large and thus, sample size of over 97/group is required to see a modest effect.

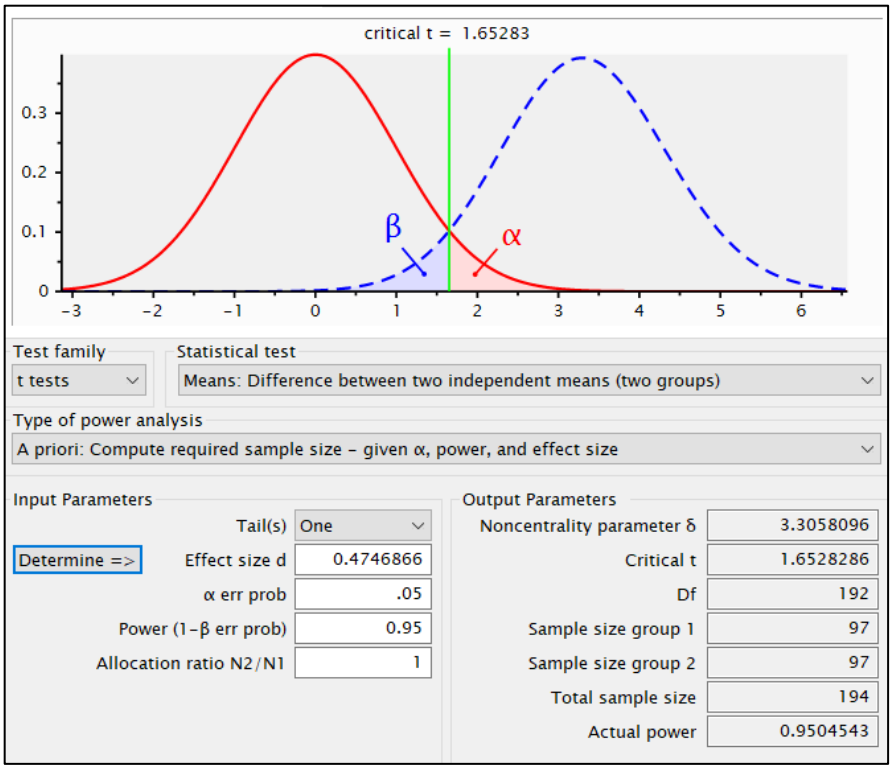

Figure (2-8): Sample size requirement for detecting a modest change in total locomotor activity in zebrafish larvae. Due to the small effect size in behavior of test compounds, sample size of 97/group is required to detect hypo or hyper activity. However, large effect size of 1.8 (such as complete sedation Vs non sedation) can be detected with small sample size as described in earlier figure.

This highlights that sample size is essential to detect precise differences and it also depends on the designed experiment. The lack of availability of the test compounds at sufficient amount precluded a more detailed behavioral analysis and only permitted separation of severe sedation or lack of sedation effects in test compounds.

2-11 Western blotting (WB)

Western blot was used to validate the inhibition of the neuronal stress of LifeArc's hits and quantify the inhibitory effects of compounds on dipeptide repeat protein (DPRs) expression in $(G4C2)_{45}$/C9 transgenic zebrafish.

2-11-1 Transgenic fish model C9 $(G4C2)_{45}$

The sense strand pure $(G4C2)_{45}$/C9 transgenic fish were generated in 2017 (unpublished). These fish carry 45 repeats of the GGGGCC (sense) repeats of containing no ATG start sites. The expression of the expansion was driven by zebrafish ubiquitin (*ubi*) promoter for ubiquitous expression. The expanded hexanucleotide repeats (G4C2) are in frame with a V5 peptide tag in all three frames so that any of the sense DPR's can be detected by the V5 tag. The transgene also carries a *hsp70*::DsRed in tandem to allow for the detection of the activation of heat shock stress response, potentially by DPR toxicity. Therefore, *hsp70*::DsRed is a fluorescent stress readout that could potentially be used as fluorescence based drug screen, as was done in the sod1 model (Fig. 1-3).

RAN translation of the *C9orf72* expansion in these fish produces DPR's, which are poly(glycine-alanine) (GA), poly(glycine-proline) (GP), and poly(glycine-arginine) (GR). These DPRs are predicted to cause toxicity in the C9$(G4C2)_{45}$ fish similar to those observed in ALS/*C9orf72* patients (Mori et al., 2013a). The C9$(G4C2)_{45}$ fish was mated with ABs wild-type zebrafish, and eggs were collected the following day. At 48 hpf, the genotyping was carried to identify transgenic fish (red fluorescence) and to check the development status of the fish.

2-11-2 Drugs treatment and protein assay quantifications

Drugs were loaded into 6 well plates, with 2 µl of 10 mM drug stock in 2 ml of E3 to have a final concentration of 10 µM. At 6 dpf, the fish were genotyped again to ensure the DsRed expression and detect any abnormal development of the fish during the treatment period (fish were monitored for developmental defects throughout the treatment). Fish were terminally anesthatised and RIPA buffer was added depending on the numbers of the fish. The calculation of RIPA buffer volume was

RIPA® = Number of the fish x 3 µl of RIPA buffer

(10 ml RIPA buffer + one tablet of proteinase inhibitor cocktail)

The samples in RIPA were sonicated in a 1.5 ml Eppendorf tube for 15 secs/ 25% amplitude. The samples were centrifuged for 4 mins / 17,000 rpm at 4ºC. The supernatant was used to quantify the protein using the protein standard (Biorad) on the spectrophotometer (Diode Array Spectrophotometer/ England). For the Bradford protein assay, 2 µl of each sample added into 1 ml of protein-dye reagent assay (1x). This was used to measure the protein concentration for each sample. The samples were normalised to 4 mg/ml with RIPA and then mixed 50:50 with Laemmli buffer (2x) to have a final sample concentration of 2 mg/ml.

The samples were heated to 93-96ºC for 5-10 mins to denature the proteins, and the samples were stored at -20ºC. All of the protein extraction processes were performed on ice to reduce any degradation.

2-11-3 Sodium Dodecyl Sulfate-Polyacrylamide denaturing Gel Electrophoresis (SDS-PAGE) Gel and transfer

The Mini-Protean Tetra Cell apparatus (Bio-Rad) was used for making SDS-PAGE gels. The resolving gel was a 15% gel for resolving smaller proteins, such as the DPR's. Glass plate's size of 1.0 mm was used for casting the gels. 15 ml falcons were used to prepare each (resolving + stacking) gels, Table 2-2. A small volume of isopropanol was added on top of the resolving gel solution to prevent any bubbles. After the gel was fully set, the isopropanol

was removed. The stacking gel was then added and a comb inserted, before allowing the gel to completely set. Care was taken throughout the gel pouring to prevent bubbles. The gels were put into the gel tank and filled up with a running buffer, Table 2-4, before removal of the combs to generate wells in the stacking gel. The loading of the samples was 4 µl of the ladder and 10 µl of each sample (10 µl of 2 mg/ml = 20 µg of protein per lane). The required voltage 50 mV/ 20 mins was applied to allow the ladder and the protein to reach the stacking/resolving gel interface. Then 150 mV was applied for 90 mins or until the ladder has sufficiently run on the gel.

After electrophoresis was completed, the stacking gel was separated and the resolving gel taken forwards for transfer. A Polyvinylidene difluoride (PVDF) membrane (0.2 mm) was activated in 100% methanol for 5 mins and then soaked in the transfer buffer. The transfer cassette was constructed in the transfer tray with buffer in the following order: sponge, 2x Waltman filter paper, gel, PVDF membrane, 2x Waltman filter papers, sponge, and then placed in the transferring tank. The transfer process started when connecting with the right power polarity (red to red and black to black) at 80 mV for 1 h. The tank includes an ice pack to avoid adverse effects from heating through the transfer process. The membrane was placed in a 50 ml falcon with 3 ml of blocking solution (5% of Non-Fat Dry Milk (in TBST)). The incubation of the membrane in the milk was at room temperature (RT) for 1 hour to block any nonspecific binding on the membrane. The primary antibodies were performed overnight at 4ºC on a roller, with an antibody specific concentration. The primary antibody was removed by TBST washes for 3 times/10 mins each before probing with the antibody specific horseradish peroxidase (HRP)-conjugated secondary antibody, Table 2-3, in 5% milk blocking for 1h at RT.

Table 2 2: The components of resolving and stacking gels used in western blot

Resolving gel (15%)

Components	Volume
Miller H2O	2.5 ml
30% ac/bis	5 ml
Resolving buffer (15%)	2.5 ml
APS (10%)	50 µl
Temed	10 µl

Resolving buffer (15%)/ PH 8.8/ 500 ml

Components	Volume
Tris/Trizma	90.85 g
SDS	2 mg

Stacking gel (5%)

Components	Volume
Miller H2O	5.8 ml
30% ac/bis	1.7 ml
Stacking buffer (5%)	2.5 ml
APS (10%)	50 µl
Temed	20 µl

Stacking buffer (5%)/ PH 6.8/ 500 ml

Components	Volume
Tris/Trizma	30.3 g
SDS	2 mg

2-11-4 G-box imaging

After the membrane was probed with the secondary antibodies, table (2-3), the membrane was washed 3 times/ 10 mins in TBST and imaged on the G-box (SynGene). Chemiluminescent ECL reagents A and B (1:1) were mixed in a 15 ml tube, incubated over the membrane for 1 min at RT, and visualised using the intellichemi program on the G-box. After imaging the membrane, it was stored in TBST at 4°C or re-probed with other antibodies, after removing the hrp signal with sodium azide treatment. (20 µl of (0.1% Sodium azide (in PBS))/ 10 ml of 5% milk blocking solution). Sodium azide is used to breakdown the HRP signal by inactivating the HRP bound to the membrane to allow different species of antibody to be probed on the same membrane.

2-11-5 Analysis of western blot

The ratio of the V5 signal of each band to the L10A signal (Ribosomal protein used as a control housekeeping protein) was calculated to standardise DPR expression levels. The ratio of each treatment was compared to the mean of DMSO for all experiments. The DsRed was quantified by the signal of DsRed/ the signal of β-tubulin (cytoskeletal protein used as a housekeeping protein) for each treatment and then compared to the DMSO treated samples.

2-12 Dot blot protein detection

A dot blot technique works by directly applying a protein onto the membrane without an electrophoresis step. It is used for detecting changes in protein levels within a small protein sample and for rapid analysis of protein levels. This technique was used to detect and quantify dipeptide repeat protein (DPR) in the *C9orf72* transgenic zebrafish.

2-12-1 *C9orf72* transgenic zebrafish ALS models

The *C9orf72* transgenic zebrafish were generated in 2017. Two transgenic lines were used. The sense $(G4C2)_{45}$ and antisense $(C4G2)_{39}$ transgenic zebrafish lines. The transgenic zebrafish express forty-five repeats of the hexanucleotide repeat expansion GGGGCC $(G4C2)_{45}$ (sense) and thirty-nine repeats of the hexanucleotide repeat expansion of CCCCGG $(C4G2)_{39}$ (antisense) as described in the section 1-6-2, (Fig 1-3).

2-12-2 Dot blot procedure

C9 fish were crossed with AB wild-type zebrafish and the eggs were collected on the following day. The fish were treated from 2 dpf to 5 dpf. At 5 dpf, embryos were culled under the schedule 1.

The sonication and the centrifugation of the samples were varied to optimise the protocol of the dot blot, table (6-2). The PVDF was activated in 100% methanol for 2-3 secs and the Waltman (filter paper) soaked in TBST for 5 mins and then placed (the filter paper + PVDF) into the dot blot cassette. Afterward, the blot cassette was tightly closed and the supernatants of

transgenic and non-transgenic of $(G4C2)_{45}$ and $(C4G2)_{39}$ fish were loaded with either the RIPA buffer or immunoparticipate (IP) cell lysis buffer in the 96 well dot plate, (Table 6-2). The 96 well dot blot cassette was applied to a vacuum pump turned to pull the samples from each well through the cassette and onto the membrane. The vacuum of the dot blot plate was performed for 15-20 mins. The membrane with bound protein was kept for 1h at room temperature (RT) for fixing the proteins onto the membrane by air drying. The dry membrane was then washed in TBST 2 times/ 15 mins and blocked in 5% milk low-fat blocking solution for 1h at RT. The membrane was incubated with V5 primary antibody (1:2000, Mouse Ab) overnight. The following day, the membrane was washed in TBST (6 times/ 5 mins), and then the membrane incubated with the appropriate secondary Ab (1:500, Goat anti-mouse HRP) for 1h at RT. After the secondary antibody, the membrane was washed in TBST (6 times/ 5mins). To image the membrane, the ECL substrates (1:1) were applied to the membrane for 1 min in a dark condition, and the image was taken by G-box. The membrane can be incubated in sodium azide as described in western blot for 1h prior to probing the membrane with other antibodies. The tubulin antibody (Rabbit anti-β-tubulin) was applied to the membrane in a dilution (1:500) overnight, along with the secondary AB (Goat anti-rabbit HRP). The membrane washed, and G-box used for the images. All the membranes were kept in TBST in the fridge after every test.

Table 2-3: List of antibodies

The type of antibodies	Targets	Company	Dilutions	Application	Species host	Products number
Primary	Tubulin	Sigma	1:10000	Overnight at 4℃	Mouse	T6119
Primary	V5	Thermofisher	1:2000	Overnight at 4℃	Mouse	R960-25
Primary	DsRed	Clontech	1:2000	Overnight at 4℃	Rabbit	632496
Primary	L10A	Santa Gruz	1:500	Overnight at 4℃	Mouse	JK-16
Secondary	HRP conjugate anti-mouse	BioRad	1:500	1h/ RT	Goat	172-1011
Secondary	HRP conjugate anti-rabbit	BioRad	1:500	1h/ RT	Goat	170-6515

Table 2-4: Components of the buffers

Components	Running buffer 5 L/ 1X	Transferring buffer (10 L/ 5X)	TBST-1X PH 7.6
NaCl			80.06 g
Glycine	190 mM	270 g	
TRIS	25 mM	150 g	21.6 g
Tween 20	41.4		0.1% (v/v)
SDS	3.5 mM		

Table 2-5: List of materials and reagents

Materials	Catalogue	Company	Source
MICROPLATE, 96 WELL, µCLEAR®, Black	655098	Greiner Bio-One	Germany
MICROPLATE, 384 WELL, µCLEAR®, BLACK	781091	Greiner Bio-One	Germany
6 **wells cytoOne plate, Clear**	7506	Greiner Bio-One	Germany
DMSO (anhydrous)	276855	Sigma-Aldrich	USA
Protease Inhibitor Cocktail (PIC)	P8340	Sigma-Aldrich	USA
Coomassie protein reagent	1856209	Thermoscientific	USA
TEMED	T3100	Melford	UK
Ammonium persulphate	A3678	Sigma-Aldrich	Japan
Isopropanol P	7500/17	Fisher Scientific	UK
Methanol	I M/4000/17	Fisher Scientific	UK
Sodium dodecyl sulfate	10090490	Fisher Scientific	UK
Triton™ X-100	T9284	Sigma-Aldrich	USA
Immobilon®-P Polyvinylidene difluoride membranes (PVDF)	IPVH00010	Millipore	UK
Chromatography papers (filter papers)	3030-917 GE	Healthcare	China
Chemiluminescent reagents	(EZ-ECL) 20-500-120	Biological Industries	Israel
Sodium azide	S8032	Sigma-Aldrich	Germany
TRIS	B2005	Melford	UK
Glycine	G0709	Melford	UK
Sodium chloride	11904061	Fisher Scientific	UK
TWEEN	20 233360010	Acros Organics	USA
Laemmli buffer (2X)	4% Sodium dodecyl sulphate (SDS), 20% glycerol, 10% 2-mercaptoethanol, 0.004% bromophenol blue, and 0.125 M Tris HCL; PH 6.8	Thermo Fisher & Fisher Scientific	USA & UK
RIPA buffer	EDTA,146.12g; 50 Tris HCL, 3.03g; 150 mM NaCl, 4.38 g; 0.5% NP40, 2.5 ml/50 ml	Thermo Fisher & Fisher Scientific	USA & UK
IP cell lysis buffer	EDTA 1ml; NaCl 15 ml; 50 mM HEPES 5.95 g; 10% glycerol; 0.5%(v/v) Triton x-100, 2.5ml; 8 mM Urea 240.24 g/ 50 ml	Thermo Fisher & Fisher Scientific	USA & UK

CHAPTER 3

3- Primary screening of the LifeArc (MRCT) library.

Hypothesis: The ion channel library designed to act on ion channels would identify hits that reduce neuronal stress in the *sod1* G93R zebrafish model of ALS.

3-1 Selection and storage of the LifeArc (MRCT) chemical compound library

The LifeArc library is composed of a collection of chemical small molecules dissolved in dimethyl sulfoxide (DMSO) as a solvent for the drugs. This library consists of a wide range of molecules specifically designed and predicted to be ion channel modulators. This library was chosen based on previous work where selamectin was identified as a hit compound in a neuroprotective screen in the *sod1*G93Ros10 mutant zebrafish line. Selamectin is known to modulate glycinergic activity (Lynagh et al., 2011), and it reduced neuronal stress in *sod1*G93Ros10 zebrafish (McGown, 2014).

Additionally, riluzole also modulates glutamate channels, and it was found to reduce neuronal stress and rectify interneuron dysfunction in the *sod1*G93Ros10 zebrafish model. Therefore, we hypothesised that by screening the LifeArc library in the *sod1*G93R zebrafish, we could identify novel ion channel modulators of potential therapeutic benefit for ALS. Ion channel dysfunction is involved in ALS pathology. For example, activation of persistent sodium channels and reduction of KCNA1, KCNA2, and KCNQ2 potassium channels has been identified in ALS, while ligand-gated ion channels such as NMDA and AMPA receptors are also modulated in ALS (Do-Ha et al., 2018). Small molecules that could potentially target these receptors may, therefore also ameliorate the disease course (Behan et al., 2013; Do-Ha et al., 2018).

The LifeArc library consists of 4494 compounds. For long term storage, it is kept at -80^{o}C in the dark in a sealed environment to avoid contamination, photolysis, hydrolysis, and oxidation. The screen was undertaken by transferring compounds into 384 well LDV plates (Labcyte), which are compatible with the Thermofisher PlateMate liquid handling system, as described in methods section 2.5. The LifeArc compound screening plates

were temporarily stored using the SPOD system (Roylan Development Technologies) in a low oxygen and moisture environment, to minimise oxidation and hydrolysis of the drugs over time. Monitoring of drug quality and degradation was performed weekly using the survey feature of the Echo550 system which can monitor DMSO content and volume changes to ensure that water contamination has not occurred.

3-2 Destination plate (96-well) design for screening

The destination plates used were 96-well Greiner µClear plates. In each 96-well plate, we included 12 negative control wells (DMSO) in columns 1 and 11, 12 positive control wells (riluzole) in columns 2 and 12, and 48 wells of LifeArc test compounds in columns 3-10. The wells for DMSO and riluzole were reversed on either side of the library compounds to minimise edge effects (Fig. 3-1). This plate loading allowed excellent quality control with large numbers of control wells. We utilised this large number of controls to ensure that the positive and negative control averages gave an accurate estimate of the effect size. The LifeArc library was provided at 1 mM and 10 mM concentrations. To achieve 10 µM (initial dose screen) in 200 µl (final volume in each well), 2000 nl or 200 nl of the compound was dispensed by the Echo550 in to each well.

We were keen to maintain the stock concentrations of DMSO and riluzole consistent with LifeArc stock concentrations throughout the study. Therefore, DMSO was used at 1% or 0.1% in 200 µl of E3, while riluzole was used at 10 µM, solubilised in 1% or 0.1% DMSO. Previous data showed a 54.4% reduction in DsRed fluorescence with 10 µM riluzole treatment in the *sod1*G93Ros10 zebrafish line (McGown et al., 2016). This study also showed that riluzole had a toxic effect when used at > 10 µM in *sod1*G93Ros10 zebrafish.

This screen is a unique high-throughput drug screen in the zebrafish *in vivo* ALS model (*sod1*G93Ros10) as it is the largest drug screen undertaken in a zebrafish model of ALS utilising the fluorescent stress readout provided by *hsp70*::DsRed.

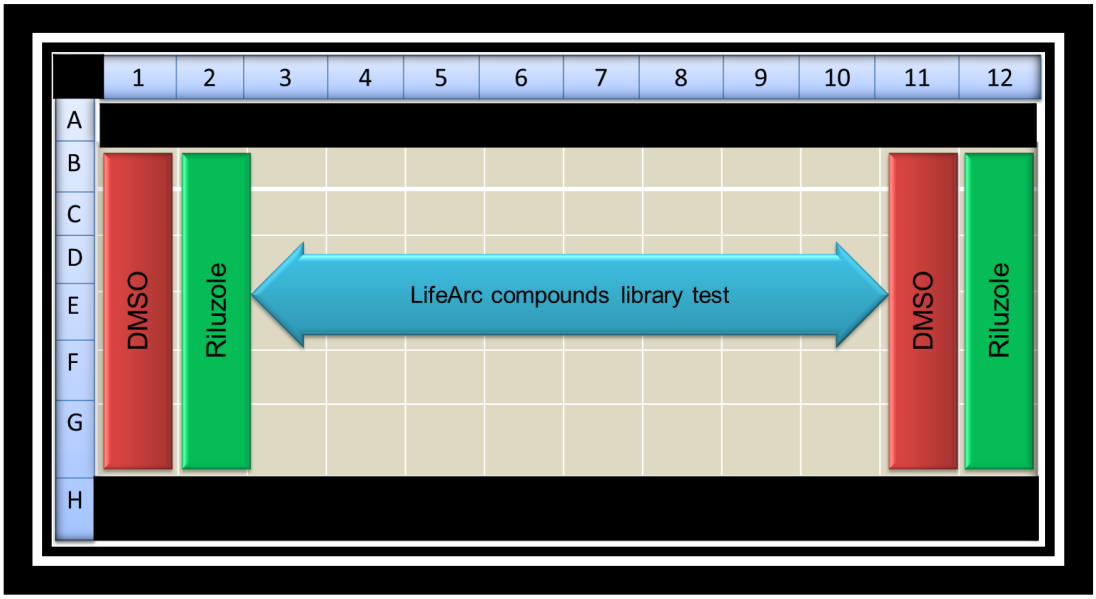

Figure 3-1: Destination plate design for the LifeArc compound library screen: Rows A & H are firewalls (to avoid possible dehydration issues), DMSO (-ve control) is in columns 1 & 11. Riluzole (+ve control) is in columns 2 & 12 of rows B-G. Columns 3-10 contain compounds of the LifeArc library.

3-3 Screening protocol

Eggs were collected following pair-mating of *sod1*G93Ros10 with wild-type AB zebrafish. Embryos were dechorionated manually at 24 hpf and kept in sterile embryo medium (E3) at 28ºC. Embryos were loaded manually into 96-well plates (one embryo in each well; approximately 150 µl E3/well) at 48 hpf, then the InCell imaging system (GE-Healthcare) used to genotype the fish on the basis of DsRed expression prior to screening. Transgenic embryos were pooled in a petri dish. Brightfield imaging was then used to ensure that the embryos were healthy and not damaged during dechorination. The Echo550 liquid handling system was used to dispense the compounds from a source plate (drug plate) to a fish plate (destination plate), with 2000 nl of each drug being added from a 1 mM source stock plate. The volume in each well at this stage was 150 µl of E3, then a transgenic embryo added to each well to give a final volume of 200 µl and 10 µM final drug concentration. The zebrafish were then kept at 28ºC in an incubator until 6 dpf (assay end-stage) with daily monitoring for toxicity. At 6 dpf any genotyping errors and drug toxicity effects were identified by imaging on the InCell system. The fish were terminally

anesthetised and then loaded into V-bottom plates (V-bottom, Clear, Greiner Bio-One, Cat No: 651101) in 50 µl of dissociation buffer, sonicated for 5 seconds at 25% amplitude using the Vibracell sonication system (Sonics and Materials, Inc), before being centrifuged at 3000 x *g* for 10 min. Twenty µl of each supernatant was loaded into a 384-well plate (384-well, µClear, Greiner Bio-One, Cat No: 781096) and DsRed fluorescence measured using the Pherastar system (BMG Labtech) using the protocol described in section 2-7. This protocol for high-throughput screening in *sod1*G93Ros10 zebrafish has been published elsewhere (McGown et al., 2016) and is illustrated in Fig. 3-2.

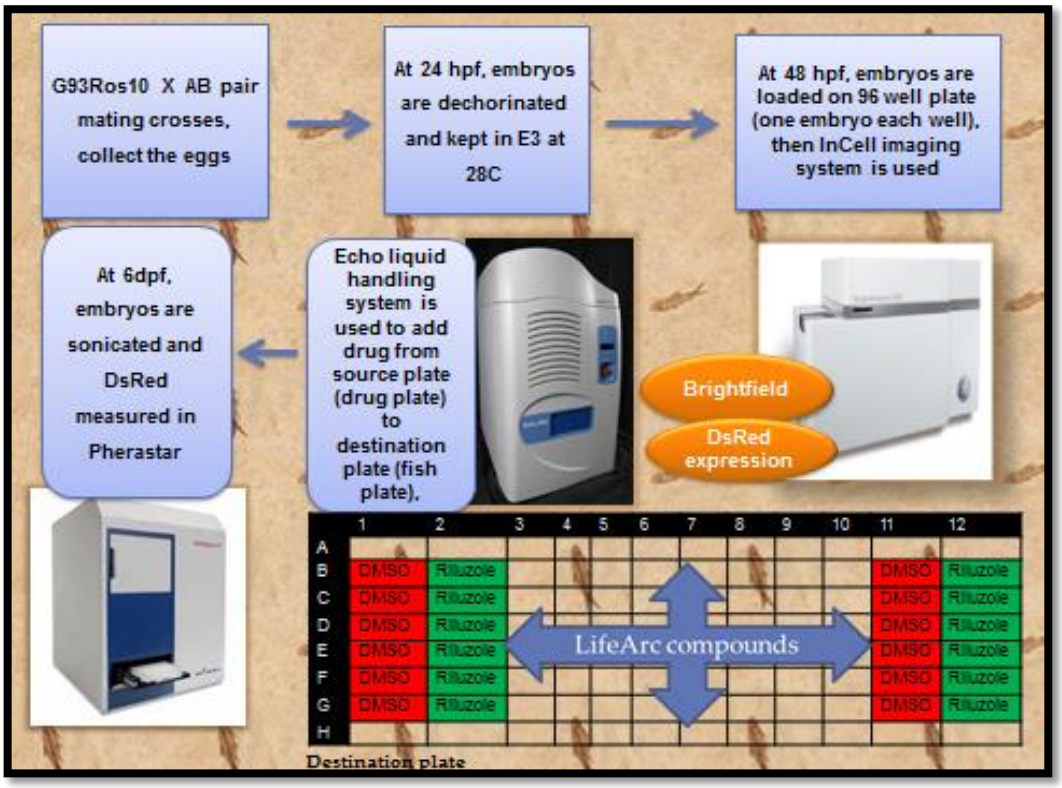

Figure 3-2: Flow-chart of the high-throughput screening protocol used in the *sod1*G93Ros10 zebrafish line.

3-4 Confirmation of the validity of riluzole as a positive control for DsRed-based screening

Riluzole was used as a positive control in the screening assay as it is the only FDA approved drug for ALS treatment. Importantly, riluzole was previously shown to reduce DsRed fluorescence in the *sod1*G93Ros10 model where it showed an average reduction of 54.4% in the DsRed signal at 10 µM. Riluzole was prepared as a 100 mM stock in DMSO and then diluted to 10 mM or 1 mM based on the stock concentration of the LifeArc compounds. Using the Echo550 liquid handling system, 200 nl or 2000 nl of riluzole was dispensed to a final concentration of 10 µM in 200 µl of E3. DMSO was used as a negative control in this screen at 0.1% or 1% concentration. DMSO is relatively safe, and zebrafish tolerate 0.1% and 1% well at 1-3 days post-hatching (Xiong et al., 2017). Throughout the screening performed for this thesis, riluzole showed a consistent inhibitory effect on the fluorescent readout of stress activation, with an average inhibition of 68% throughout the one year course of the screen, and with a low death rate (Fig. 3-3).

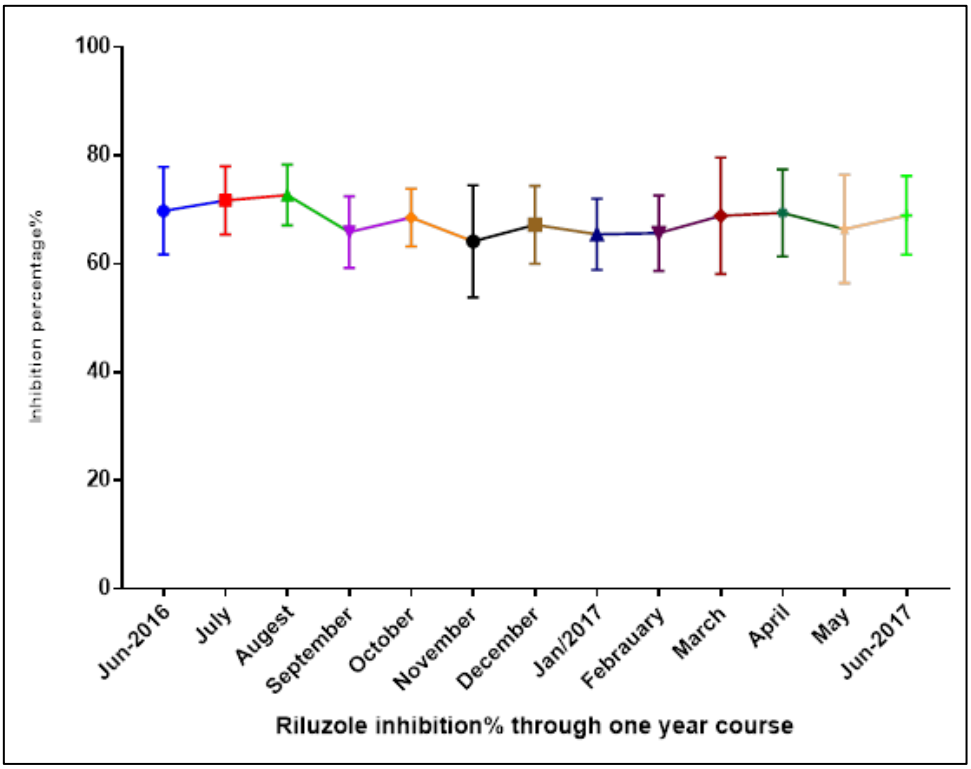

Figure 3-3. Riluzole showed an average inhibition in neuronal stress of 68% in the *sod1*G93Ros10 zebrafish line over the course of one year. N=36 for each

data point, n=12 technical replicates (individual fish) per experiment with 3 biological repeats per month.

3-5 Qualitative analysis of DsRed fluorescence in riluzole-treated embryos

The InCell 2000 (GE Healthcare) is an automated high-content imaging system which can capture images using multiple wavelengths as described in section 2-4. Imaging with the Incell showed that *sod1*G93Ros10 fish treated with riluzole had a reduction of DsRed fluorescence in the hindbrain, spinal cord and neuromasts at 6 dpf (Fig. 3-4). We could not perform quantitative analysis of screening plates using the InCell system due to the variable orientation of the fish in the wells meaning that many fish were not in focus when a plate was imaged. Hence many images were blurred (Fig. 3-5), although the fluorescence was visible.

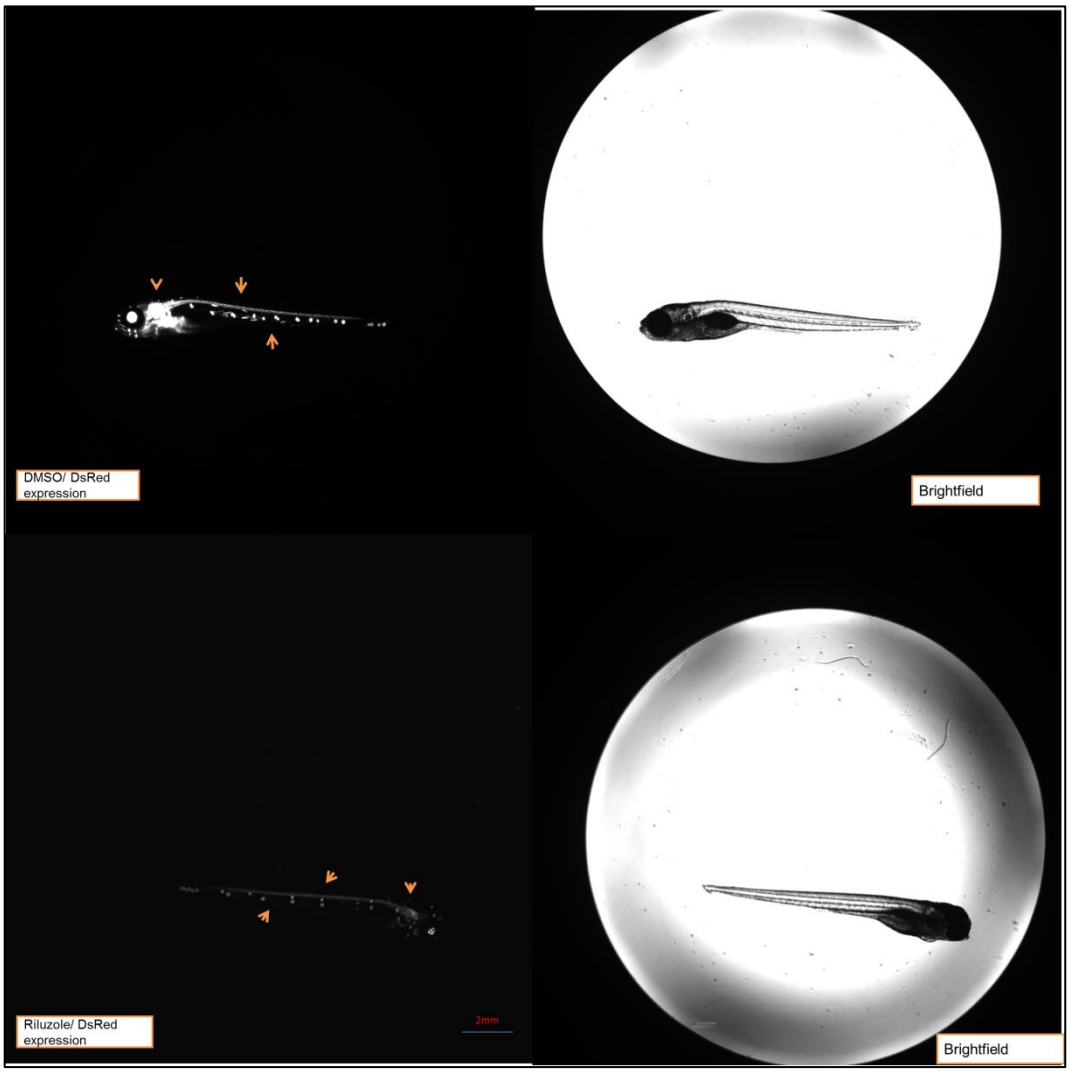

Figure 3-4: InCell images showing *sod1*G93Ros10 zebrafish at 6 dpf after exposure to 0.1% DMSO only (upper panel) or 10 µM riluzole in 0.1% DMSO (lower panel). The riluzole-treated fish has reduced DsRed fluorescence in the hindbrain, spinal cord, and neuromasts compared to the fish treated with DMSO alone.

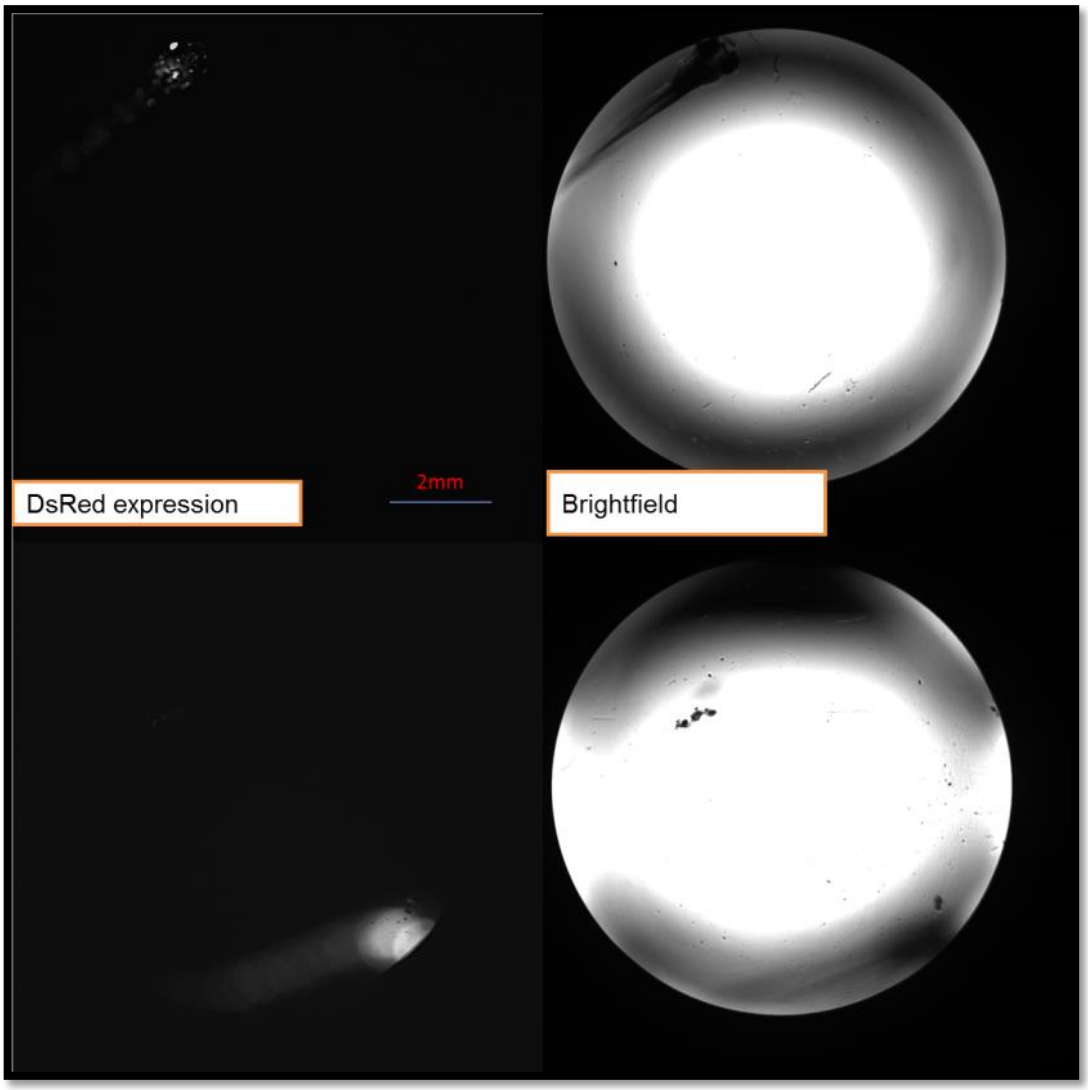

Figure 3-5: Unfavourably orientated fish at well edges showing fuzzy DsRed fluorescence due to poor focus, thereby preventing accurate quantitative analysis of fluorescence with the InCell system.

3-6 Assay statistics and quality control

Strictly standardized mean difference (SSMD) was used for statistical analysis in this screen (section 2.8). It has high applicability for screening approaches as only hits that stand out from the other test candidates will show a significant signal using SSMD. This reduces the need for multiple embryos on a primary screen such as the one we performed using single embryos. Therefore, SSMD provides a more accurate score of drug activity than another score, such as the Z score. SSMD measures the effect size of each compound by comparing any two random groups, while the Z score provides yes or no effect of the drug. SSMD is also represented as a graded score of the drug's effect based upon on β values, as shown in Table 2-1. After performing the initial screen, the screen was repeated, and all duplicate activators and inhibitors used to perform secondary screening (hits should show similar efficacy in both trials).

For optimal drug screening, it is essential to perform quality control analysis to ensure that the specificity and sensitivity are maintained at more than 90% throughout the screen. The specificity shows how many true negatives are observed in the screen. It should be in a higher percentage in each screen to reflect the accuracy of detecting true hits and avoiding false positive hits. In the same time, the sensitivity measures the detectable hits in the screen and should remain strong to ensure hits are not missed in the screen. Data analysis was performed at multiple SSMD thresholds to ensure that hits were not missed while maintaining the best balance between specificity and sensitivity. SSMD hit threshold scores were set up at $\beta < -0.5$ and < -1.0. The plates were analysed based upon these scales. False-positive numbers (negative controls showing as hits) and false-negative numbers (positive controls showing as negative numbers) were recorded for each plate and analysed to allow calculation of the sensitivity and specificity of each plate for quality control. False positives were calculated as the number of negative controls that showed up as a hit based upon the SSMD threshold. False negatives were calculated as the number of positive controls that did not reach the hit SSMD threshold. The sensitivity is a measure of how many hits are detected and the specificity is a measure of how accurate the assay is.

The percentage of true positives compared to false negatives is measured as sensitivity, while the measured percentage of true negatives compared to false positives is measured as the specificity.

3-6-1 Quality control with SSMD cut off based upon β < -0.5 in duplicate screens

An SSMD based upon β < -0.5 score allows only a small percentage of hit compounds showing up as false negatives and gave a sensitivity score of 95.76%. This is an excellent score in an *in vivo* primary screen. This confirmed that the assay revealed true hits at the cut off < -0.5. The specificity score of the screen at β < -0.5 was 82.29%. This means the screen will pick up some false positives. This lower specificity most likely reflects the variability inherent to any *in vivo* model or drug-screening assay.

3-6-2 Quality control with SSMD cut off <-1.0 in duplicate screens

The measured sensitivity and the specificity of the screen when shifted to SSMD based upon at β < -1.0 was more robust. The sensitivity was maintained at > 90%, but with a slight reduction than with β < -0.5, but the specificity was increased. At < -1.0, a very low number of false negatives and positives were detected, which lead to the sensitivity and specificity scores being 92.39% and 92.63%, respectively, as shown in Table 3-1. This is an excellent score in an *in vivo* primary screen. At this threshold, there was a slight decrease in the sensitivity of the assay, which might lead to some weaker hits being missed, but in comparison, there was stronger specificity leading to fewer false hits being detected.

Table 3-1: Quality control data in the duplicate screen for all plates based upon β < -0.5 and -1.0. It shows the true positive and negative rates with the incidence rates of false negatives and false positives to provide the percentage sensitivity and specificity.

β values	True+/ N=12	False-/ N=12	True-/N=12	False+/N=12	Sensitivity%	Specificity %
β < -0.5 Mean	10.12	0.45	9.46	2.04	95.76	82.29
SD	1.79	0.97	1.70	1.52	9.35	12.99
β < -1.0 Mean	9.76	0.80	10.67	0.85	92.39	92.63
SD	1.97	1.33	1.31	0.94	12.40	8.13

3-7 Compounds reducing DsRed fluorescence in the primary LifeArc library screen

The LifeArc library of 4494 compounds was screened in the duplicate to identify compounds that showed a reduction in DsRed fluorescence in *sod1*G93R mutant zebrafish. With the SSMD threshold set at β >-1.0 to <-0.5, 159 (3.53%) showed reduced DsRed fluorescence, while with the SSMD threshold set at β <-1.0, 55 (1.22% of the library) compounds were considered hits Table 3-2 and Table 3-3). These data confirmed that the SSMD score based upon β < -0.5 or < -1.0 is an appropriate threshold to identify reasonable numbers of hits that can be taken forward for secondary screening and hit validation.

Table 3-2: The number of primary hits showing a reduction in the *hsp70*:: DsRed fluorescent stress readout in duplicate screens.

SSMD threshold B values	Number of the inhibitor hits	Number screened	Percentage hits
>-1.0 - < -0.5	159	4494	3.53%
<-1.0	55	4494	1.22%
Total	214	4494	4.75%

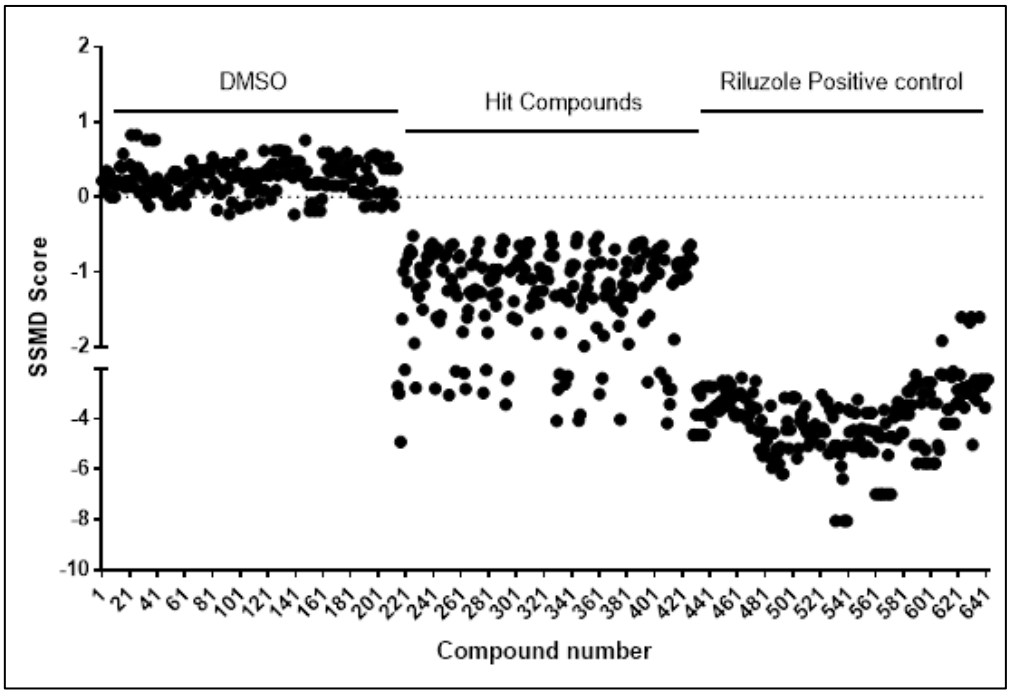

Figure 3-6: Summary of duplicate screen of primary inhibitor hit compounds of LifeArc ion channel library with negative (DMSO) and positive (riluzole) controls. Each dot represents average SSMD scores of a duplicate screen. Negative SSMD scores represent inhibitors. Hit compounds and Riluzole show negative SSMD scores. SSMD scores ≤ -0.5 in each of the duplicate screens were considered as hits.

3-8 Compounds increasing DsRed fluorescence in the primary LifeArc library screen

When a β threshold of > 1.0 was used, it detected 545 compounds that induced an increase of DsRed fluorescence in the duplicate screens of 4494 compounds. These compounds could be *hsp70* activators as some of these hits might be an auto-fluorescent. To determine how many of the compounds had a toxic effect at 10 µM concentration, daily inspection of embryos using a dissecting microscope was used to monitor for death or/and developmental abnormalities such as weak heartbeat and cardiac oedema. In total, 129 compounds were identified as toxic, causing death or severe abnormalities at 10 µM. This equates to 2.87% of the library.

Table 3-3: The number of compounds shows the activation of fluorescence and causes embryo death.

SSMD threshold	Number of the hits	Number screened	percentage
B > 1.0	545	4494	12.12%
Compounds caused death	129	4494	2.87%

3-9 Discussion

In the mutant *sod1*G93Ros10 zebrafish transgenic line, the fluorescent readout of the *hsp70*::DsRed reporter is utilised as a scale for the measurement of neuronal stress based upon of the activation of the *hsp70* promoter. This response can be utilised as a high-throughput screen and give a measure of the effect of each compound, either in reducing neuronal stress or activating the heat shock response. Previous work in the *sod1*G93Ros10 zebrafish identified selamectin as a modulator of glycinergic activity in *sod1*G93Ros10 (McGown, 2014). This work highlighted the potential key role of ion channels and their modulation in ALS cellular pathology. As a result, we set out to identify novel ion channel targeting drugs that could be utilised in ALS treatment. The LifeArc library was selected to screen in this model by measuring *hsp70*::DsRed fluorescence as an indicator of the anti-oxidant and/or protein misfolding stress (Ramesh et al., 2010). The library contains a large selection of novel compounds designed and predicted to act on ion channels. The efficacy screening window of the screen was high with an average of 68% reduction of the neuronal stress fluorescent readout for riluzole, the positive control, thus providing an ample window for screening. A high-throughput screen of LifeArc ion channel library is the most extensive focussed investigation of the ion channel modulating drugs in the *sod1* zebrafish model of ALS that has been published.

Riluzole is the only treatment currently given to ALS patients but its mechanism of action is not completely understood. It is a known anti-excitotoxic drug that acts by reducing glutamate-release and has also been shown to inhibit persistent sodium currents both *in vitro* and *in vivo* (Belluzzi and Urbani, 2000; Chang et al., 2010; Lazarevic et al., 2018). The efficacy of riluzole was consistent, with an average 68% reduction in the neuronal stress readout in *sod1*G93Ros10 zebrafish over the course of a year (Fig. 3-3). The activity of riluzole in this screen confirms that sod1-mediated toxicity measured in our assay is meaningful and increases the validity of hits identified in this assay. However, it should be noted that in a recent study using TDP-43, FUS, and SOD1G93A mouse models, riluzole did not improve

rotarod performance and/or extend survival in all of these ALS mouse models (Hogg et al., 2018).

This screen also demonstrated less toxicity than the previous spectrum library screen in the *sod1*G93Ros10 zebrafish (McGown et al., 2016). This could be due to the choice of the library. The spectrum library was more diverse including antibiotics, antifungal, and DNA intercalating drugs that may show high toxicity, while LifeArc was specifically targeted to ion channels, which may be potentially safer.

In high-throughput biological drug screening, the most commonly used method for scoring hits is the z score. A hit using the z score method is calculated as anything that has an effect size of more than three standard deviations away from the negative control. This gives a definitive yes or no answer for each drug being a hit in the screen. In the current screen, statistical analysis was based upon on the SSMD score. The SSMD score shows the power of the effect size of the drug by comparison to the negative control. This means that the SSMD score has some advantages compared to other high-throughput drug screening statistical methods, such as z score. This is because the z score needs three standard deviations of difference to be defined as a hit meaning weaker drugs may be missed, while SSMD allows a whole range of scores for the screen.

Additionally, z score analysis requires at least a triplicate sample size, while SSMD can utilise a single screen with a single replicate, thus reducing the cost and speed of screening. It grades a drug's effect from weak through to strong, thereby including weaker effects. This is particularly useful as drugs that have a weak effect in the screen may be more effective at different concentrations can still be detected and tested for dose-response to find the optimal drug concentration.

The primary screen of the 4494 LifeArc compounds screened in duplicate, at $\beta < -0.5$, there were 159 compounds identified that reduced DsRed fluorescence, while at the greater stringency of $\beta < -1.0$, 55 compounds showed reduced fluorescence. The assay, therefore, identified a reasonable number of hits to take forward for validation and dose-response screening to

identify lead candidates for further development. This confirmed the hypothesis of our initial screen.

At a β value ≥ 1, 545 compounds were found to increase DsRed fluorescence, equating to 12.1% of the total library. These compounds might include activators of the heat shock protein response (HSR). Hsp70 is up-regulated by the unfolded protein response (UPR) and other cell repair pathways, to try to improve cell survival. While transient activation of the HSR is thought to be beneficial, chronic activation of the HSR may have deleterious consequences. Misfolding of mutant SOD1 is thought to be an early step in toxicity. Therefore drugs that increase *hsp70* in the *sod1*G93Ros10 zebrafish might be beneficial as they may alleviate sod1 misfolding via further activation of the stress response. A therapeutic approach to upregulate the HSR using arimoclomol showed a beneficial effect when tested in G93A mutant SOD1 mice (Kieran et al., 2004). This compound improved motor performance and extended survival and is thought to act by the up-regulation of the heat shock proteins hsp70 and hsp90. This suggests that up-regulation of the heat shock pathway has potential neuroprotective effects in the context of neurodegenerative disease. Some of the compounds identified as activators were auto-fluorescent and carried through to the assay, providing false-positive results. Additionally, if a drug has a toxic effect, it could result in the activation of the heat shock response, again providing a false-positive result if activators were to be considered as potential hits.

Screening was performed at 10 μM, consistent with the optimal dose of riluzole and the most widely used dose in high throughput screens. 129 compounds caused death in the duplicate screens at this concentration. Death at 10 μM does not necessarily mean that a drug should be discounted. Such compounds may have efficacy at a lower concentration. Therefore, these compounds could be investigated at a lower concentration, such as 1 μM. Toxic compounds equated to 2.87% of the library, which was lower than was found with the Spectrum library screen, where 7.1% of 2000 compounds exhibited toxicity (McGown et al., 2016). As the Spectrum library contains a wide variety range of bioactive compounds and drugs, including known

cytotoxic ones, while the LifeArc library is designed against ion channels, a direct comparison of the two libraries is difficult.

CHAPTER 4

4-Secondary screening of the primary hit compounds

Hypothesis: Hits identified from primary screen would recapitulate and show repeatability.

4-1 Stratification of the primary screen hits

In total, 214 inhibitors with an SSMD score β < -0.5 were identified in the initial screen with 55 among these scoring <-1.0 SSMD score. These inhibitors were confirmed by the reproducible inhibition of the DsRed neuronal stress fluorescent readout in two independent primary screens. The next stage of the project was to carry out the key secondary screen studies in the *sod*1G93Ros10 mutant zebrafish to validate the hits, identify true hits and perform dose-response analysis of the hits obtained.

The precise design of the secondary screen is an essential step of any high-throughput screen. Secondary screens are critical for the identification of true positive hits and to remove any false positives. Secondary screens can be developed to provide more detailed information on each compound, such as effects on development and behavioural changes. Secondary screens can also provide in-depth information on any associated toxicity effects at different doses. The first stage of the secondary screen was to test whether the efficacy was reproducible and also identify any variability/toxicity associated with each hit compound. This was followed by the second stage where dose-response analysis of hits that show reproducible effects was performed.

4-1-1 Repeats of LifeArc's *hsp70*-DsRed fluorescent stress readout Inhibitor hits

The 214 inhibitors of neuronal stress from the primary screen were tested (6 replicates for each compound at 10 µM) to confirm and identify the compounds that show a reproducible inhibitory effect. Ninety-four of the initial

hits demonstrated reproducible effects based on a minimum cut off of ≥ 5% inhibition of the DsRed signal (Table 4-1).

The criteria for choosing reproducible inhibitory hits are explained below:

1. Inhibitors that showed efficacy in 6 of 6 repeats performed and demonstrated inhibition of ≥ 10%.
2. Inhibitors that showed effect in 83% of the repeats (5/6 repeats) and that averaged inhibition ≥ 5%.
3. As the hit numbers were small, we proceeded to select Inhibitors that showed effect in 67% of the repeats (4/6 repeats) and that averaged inhibition ≥ 5%, and also inhibitors that showed an effect in 50% of the repeats (3/6 repeats) and that averaged inhibition ≥ 5%. We also included one hit that demonstrated very strong activity (80%) in one of the replicates, assuming that it may show activity at a lower dose.

Therefore, based upon on these criteria, 94 compounds were identified for follow up in the dose-response study.

Table 4-1: The percent inhibition of DsRed signal at 10 µM in 6 replicates. The LifeArc Reference ID for each compound refers to the number of LifeArc plate, the column, and the row. Green colours represent an average inhibition as a % of each hit as compared to DMSO controls in at least 4 of 6 trials. The compounds in blue are averages of those that were more variable. Gray colours represent samples that showed no effect. Red colours are trials where the embryos died.

Plate number/ Row/ Column	LifeArc reference ID	Replicate 1	Replicate 2	Replicate 3	Replicate 4	Replicate 5	Replicate 6	Averages inhibition%	SD of inhibition%	Averages of DMSO	SD of DMSO
446K10	MRT00203281	71.38	55.54	66.70	45.42	15.75	47.07	50.31	19.84	0.27	9.25
465D07	MRT00215511	37.83	51.70	51.42	57.31	43.83	21.74	43.97	12.84	5.48	8.37
450E6	MRT00202252	34.50	34.70	30.34	31.19	29.69	17.38	29.63	6.36	-7.40	10.66
442I13	MRT00010424	33.70	20.78	14.07	28.61	4.82	7.23	18.20	11.59	-6.57	5.50
452D15	MRT00201271	30.61	29.75	39.66	29.93	19.76	23.16	28.81	6.88	0	5.84
450I20	MRT00202934	26.56	4.76	24.80	14.06	9.20	13.93	15.55	8.58	1.78	13.82
452I5	MRT00203248	24.00	27.21	26.64	25.16	10.02	26.31	23.22	6.56	0	5.84
444M3	MRT00200759	23.67	26.39	25.60	33.00	38.13	15.40	27.03	7.84	5.63	10.53
448K10	MRT00202938	23.28	25.21	27.01	27.36	11.41	14.10	21.40	6.90	-5.18	5.16
446D3	MRT00203393	23.21	13.52	20.65	10.16	24.31	15.00	17.79	5.74	2.49	14.48
446A6	MRT00203277	22.37	13.55	26.47	26.50	17.09	22.27	21.38	5.16	2.49	14.48
444K11	MRT00200762	21.60	24.00	12.65	32.37	28.66	22.92	23.70	6.73	0	9.56
444C6	MRT00200712	20.92	33.11	20.45	17.57	22.53	15.94	21.75	6.05	0.27	9.25

464B04	MRT00213771	20.74	32.14	30.15	21.13	9.28	32.67	24.35	9.09	5.48	8.37
448P014	MRT00203018	19.92	28.71	29.53	42.15	11.21	17.74	25.00	10.92	-5.18	5.16
442C19	MRT00203352	19.68	23.57	13.57	30.82	5.00	21.00	19.00	8.838	-6.57	5.50
446F004	MRT00201744	19.54	9.73	16.69	25.31	45.00	40.01	26.03	13.75	2.49	14.48
446O4	MRT00203275	19.35	44.22	28.79	6.00	40.37	28.00	27.77	14.00	0.27	9.25
450M13	MRT00202475	18.58	10.82	10.04	13.50	15.05	6.85	12.48	4.12	1.78	13.82
450F014	MRT00202041	17.46	22.61	7.85	16.89	19.51	28.85	18.86	6.94	1.78	13.82
452G5	MRT00203268	16.56	17.70	31.67	23.01	32.39	11.01	22.05	8.61	0	5.84
448E21	MRT00202679	14.50	22.69	22.00	25.07	40.54	7.18	22.00	11.21	0	7.74
446H16	MRT00040664	13.37	8.86	18.03	18.00	14.15	14.13	14.42	3.39	2.49	14.48
443K018	MRT00201502	14.60	14.56	8.04	16.66	15.85	23.91	15.60	3.41	2.49	14.48
452P6	MRT00201156	11.22	9.47	14.42	30.47	18.64	5.08	14.9	8.90	0	5.84
443P16	MRT00201623	11.05	44.56	17.41	39.45	22.13	4.84	23.24	15.74	0.27	9.25
445A13	MRT00201020	7.87	35.30	29.16	13.06	16.53	17.15	19.85	10.32	5.63	10.53
452I21	MRT00203254	6.20	13.46	29.18	24.29	4.56	17.73	15.90	9.78	0	5.84
443K010	MRT00201553	6.12	24.69	32.51	36.62	35.76	26.10	27.00	12.65	2.49	14.48

450G3	MRT00202662	12.00	8.35	26.09	29.05	12.91	16.52	17.48	8.28	1.78	13.82
464A1	MRT00215254	10.04	13.26	22.67	15.92	16.44	12.86	15.20	4.32	5.48	8.37
442I19	MRT00005242	30.11	25.08	27.40	41.27	33.40	16.49	29.00	8.31	-6.57	5.50
448G8	MRT00201898	24.87	23.14	32.17	35.76	19.07	17.79	25.47	7.16	0	7.74
442D20	MRT00004250	36.00	9.13	27.60	47.77	3.48	18.85	23.80	16.66	-6.57	5.50
444A15	MRT00200815	90.61	28.42	4.30	10.87	19.27	1.85	26.00	33.19	0	9.56
442/K9	MRT00003363	89.64	35.17	32.01	DEAD	36.55	25.36	43.75	26.01	-6.57	5.50
445B5	MRT00203524	36.68	26.00	-10.54	30.47	31.05	13.25	21.13	17.40	0.27	9.25
443D21	MRT00201582	42.65	37.69	30.39	53.85	46.84	-2.13	34.88	19.80	0.27	9.25
447K4	MRT00202006	22.16	21.77	46.85	0.30	8.00	37.78	22.80	17.49	0.27	9.25
447M15	MRT00201890	19.00	-3.15	19.87	18.53	60.17	17.35	21.94	20.67	0	7.74
452G14	MRT00201313	20.49	9.59	12.05	19.00	-2.00	16.71	12.63	8.21	0	5.84
442M19	MRT00203349	14.69	24.73	21.00	3.52	34.00	19.47	19.56	10.18	0	9.56
444O3	MRT00200770	14.04	21.00	23.07	22.00	9.46	-21.48	11.34	16.92	5.63	10.53
448P16	MRT00202655	11.73	18.52	9.30	16.70	14.67	-15.36	9.26	12.51	-5.18	5.16
449G9	MRT00202901	10.93	29.31	26.58	27.27	-10.25	10.84	15.78	15.21	0	7.74

450M12	MRT00202387	8.75	-4.07	26.49	9.85	26.38	8.83	12.70	11.81	1.78	13.82
450H7	MRT00202788	8.01	9.02	10.28	9.71	2.03	10.68	8.29	3.20	1.78	13.82
442/A13	MRT00028435	8.00	-2.13	30.29	52.65	23.23	46.16	26.36	21.25	-6.57	5.50
466B12	MRT00214364	7.76	1.66	13.42	10.00	6.78	10.17	8.28	4.00	-2.07	5.16
451H6	MRT00203197	5.63	14.30	14.23	-3.66	5.93	7.57	7.33	6.66	3.55	15.29
452M16	MRT00201197	5.43	4.62	6.85	-0.15	20.00	9.55	7.71	6.81	0	7.74
464F1	MRT00209832	7.22	22.28	4.36	16.72	14.29	4.57	11.57	7.32	5.48	8.37
452I9	MRT00203252	6.92	0.81	8.38	17.46	23.33	17.00	12.31	8.32	0	5.84
448N15	MRT00202375	5.11	42.11	24.32	7.14	10.30	-6.71	13.71	17.11	-5.18	5.16
444A5	MRT00200777	3.37	4.59	20.65	24.18	16.43	6.88	12.68	8.89	0	9.56
445L16	MRT00203486	0.78	17.40	21.11	18.03	20.36	7.35	14.17	8.21	5.63	10.53
446B6	MRT00202284	-4.69	26.66	6.25	4.65	26.06	13.44	12.06	12.49	2.49	14.48
464A4	MRT00213757	-5.00	14.59	15.51	12.37	21.80	8.68	11.33	9.08	5.48	8.37
450P018	MRT00202994	Dead	39.04	12.34	51.59	46.87	Dead	37.46	17.52	5.77	14.09
464A02	MRT00215326	27.46	3.38	18.00	21.81	-0.98	14.68	14.06	10.91	-5.48	5.66
449J12	MRT00202735	26.31	27.48	1.11	7.71	37.11	-8.64	15.18	17.76	2.13	6.30

464D3	MRT00209870	24.57	2.28	11.27	20.28	2.45	-5.72	9.19	11.65	5.48	8.37
452C11	MRT00203269	19.86	5.59	13.31	0.53	26.55	-4.29	10.25	11.79	0	5.84
444N18	MRT00200707	19.33	47.35	1.36	19.40	16.75	-3.17	16.84	17.79	0.27	9.25
450N010	MRT00202572	18.73	15.24	24.42	-6.15	1.70	40.39	15.72	16.54	1.78	13.82
443J22	MRT00201527	18.64	-3.47	21.22	5.00	11.28	-6.22	7.74	11.32	1.63	19.06
450H17	MRT00202281	18.16	17.58	15.40	2.52	-2.11	13.54	10.85	8.53	1.78	13.82
452G4	MRT00201233	17.74	22.23	3.20	4.14	21.32	11.39	13.34	8.40	0	5.84
444H20	MRT00200730	16.52	-4.40	8.12	11.65	4.49	9.90	7.71	7.14	0	9.56
447A21	MRT00202685	15.46	20.65	22.48	10.04	-6.00	-8.40	9.04	13.32	0.27	9.25
446/E12	MRT00203318	14.53	8.48	2.58	12.09	3.47	22.43	10.60	7.44	2.49	14.48
442B12	MRT00201470	12.05	4.30	5.00	-2.74	16.60	0.02	6.00	7.28	-6.57	5.50
442J6	MRT00201428	9.06	8.12	3.23	17.13	2.45	15.30	9.21	6.04	-6.57	5.50
443G20	MRT00201741	8.00	-2.83	20.00	6.68	-9.88	17.46	6.56	11.48	1.63	19.06
447L19	MRT00203098	7.05	11.18	12.67	20.81	4.35	4.31	10.06	6.29	-5.63	9.73
446P14	MRT00202461	6.61	12.35	1.27	-1.42	24.47	9.21	8.75	9.21	-7.40	10.66
443H21	MRT00201563	2.85	10.08	39.34	30.05	22.77	-7.88	16.20	17.70	1.63	19.06

443B8	MRT00055139	-1.47	9.00	7.20	47.36	12.44	-10.05	10.74	19.70	1.63	19.06
447L15	MRT00202665	-2.50	16.05	0.35	26.03	20.70	31.13	15.29	13.68	-5.63	9.73
450F10	MRT00202800	-3.04	27.61	14.23	0.72	6.39	9.42	9.22	10.90	0	7.74
445H18	MRT00203501	-3.71	-6.06	35.96	18.78	15.58	29.55	15.01	17.08	5.63	10.53
447B21	MRT00201895	-8.04	35.23	17.08	-8.62	13.44	25.30	12.39	17.72	0	19.40
448H18	MRT00202356	-8.21	-3.94	11.47	51.95	14.27	21.22	15.34	18.35	1.21	8.92
444I18	MRT00201081	-12.22	4.55	-9.58	5.71	46.96	15.63	8.51	21.49	0	9.56
446N12	MRT00202123	-5.27	2.00	14.80	13.26	14.89	9.70	8.23	8.20	-7.40	10.66
446A9	MRT00203592	12.18	-1.63	6.11	9.67	3.61	4.74	5.78	4.83	2.49	14.48
443E12	MRT00201701	6.98	13.33	dead	14.05	-6.18	-0.87	5.46	8.85	1.63	19.06
449A3	MRT00202245	5.21	-0.58	4.43	-5.65	6.05	21.29	5.12	9.07	-3.77	3.28
445M13	MRT00201059	4.20	35.20	7.95	3.26	12.46	-4.34	9.78	13.63	5.63	10.53
448I7	MRT00201967	3.90	10.39	25.93	12.62	-4.91	0.35	8.05	10.86	-5.18	5.16
464B1	MRT00209842	1.00	3.72	9.06	12.14	9.38	-1.90	5.56	5.48	5.48	8.37
443K9	MRT00057174	-3.99	3.66	8.72	10.81	4.06	9.32	5.43	5.71	2.49	14.48
464G4	MRT00213799	-12.91	2.39	-1.65	8.08	16.34	20.07	5.38	12.13	5.48	8.37

452P9	MRT00201383	3.15	86.14	-6.69	0.88	-15.85	-7.95	9.94	37.94	-8.88	20.04

The best inhibitors were the compounds that showed efficacy in all six samples when dosed at 10 µM. They showed a range of inhibition from 50.5% to 5%. We hypothesised that ones that showed weaker activity may show a larger effect at higher doses and chose to keep them for dose-response assays.

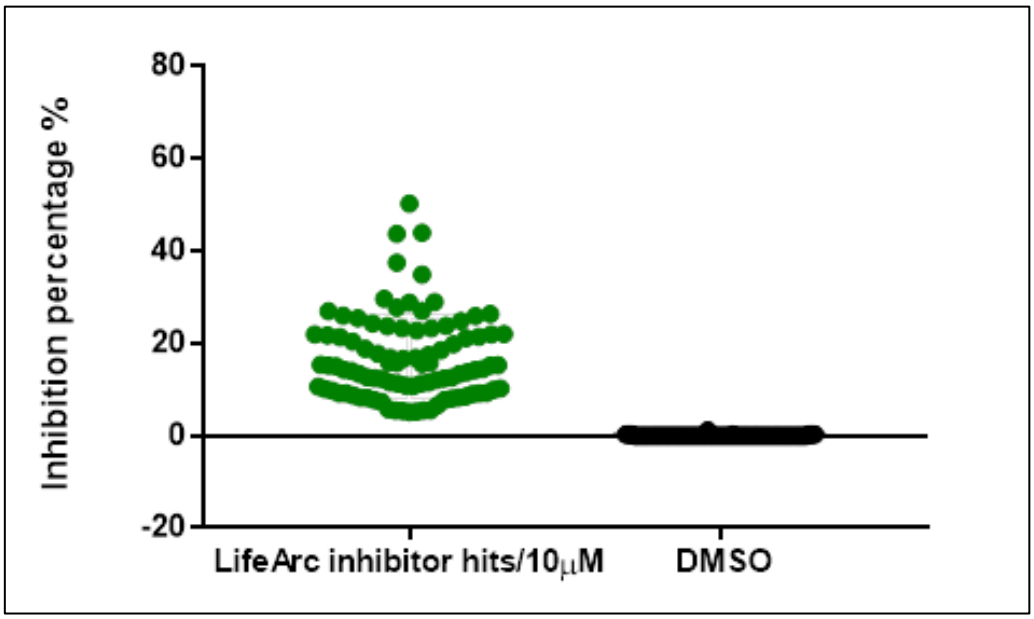

Figure 4-1: Shows an average of inhibition% of inhibitor hits compared to DMSO (negative controls). N=6 in each riluzole and DMSO treated.

Table 4-2: Stratification of the six replicates of inhibitory hits at 10 μM based upon a cut off ≥ 5% inhibition.

Cut off of DsRed inhibition %	Number of the hits
> 50%	1
> 40%	2
> 30%	2
> 20%	25
≥ 15%	17
> 10%	22
> 5%	25
Total	94

Table 4-2 and Fig. 4-1 show the number of hits identified by screening hits at 10 μM. The number of inhibitors with an average reduction of N > 30% was 5, while the number of reproducible inhibitors was larger at a lower criterion of 10% < N < 30%, with 64 confirmed hits. Also, some weak inhibitors were included between 5% < N < 10% and there were 25 hits in this category.

4-2 Dose-response analysis

Hypothesis: Ideal drug like candidates obtained from the screen will demonstrate dose response effect and good drug like properties.

Dose-response analysis is a highly informative secondary screen as it identifies the optimal dose for each compound and identifies the therapeutic window for each compound before toxicity is induced. A good hit should have a dose-response proportionate with the dosing and have minimal toxicity at higher doses. As the number of hits was small and manageable, dose-response analysis was performed on a total of 94 inhibitor hits that had been validated.

4-2-1 Dose-response study of LifeArc library inhibitors of the DsRed fluorescent stress readout in *sod1*G93Ros10 zebrafish

The doses were chosen on a log scale, starting from lower doses to higher doses as follows: 0.1 µM, 0.3 µM, 1.0 µM, 3.0 µM, 10 µM, and 20 µM or 30 µM (depend on the volum of the drug).

The number of identified inhibitor hits after the dose-response analysis with a good inhibition signature profile in the *sod1*G93Ros10 zebrafish was 13. These hits showed different responses ranging from a strong to moderate activity with some exhibiting toxicity at higher doses.

The following graphs show the dose-response of the 13 best inhibitor hits in terms of their dose-response profile. All of the dose-response studies were performed utilising five treated *sod1*G93Ros10 mutant zebrafish for each dose and this analysis was undertaken in a 96-well plate format. DMSO and riluzole were the negative and positive controls respectively, with six treated fish used for each control (see methods section for more details of the plate layout).

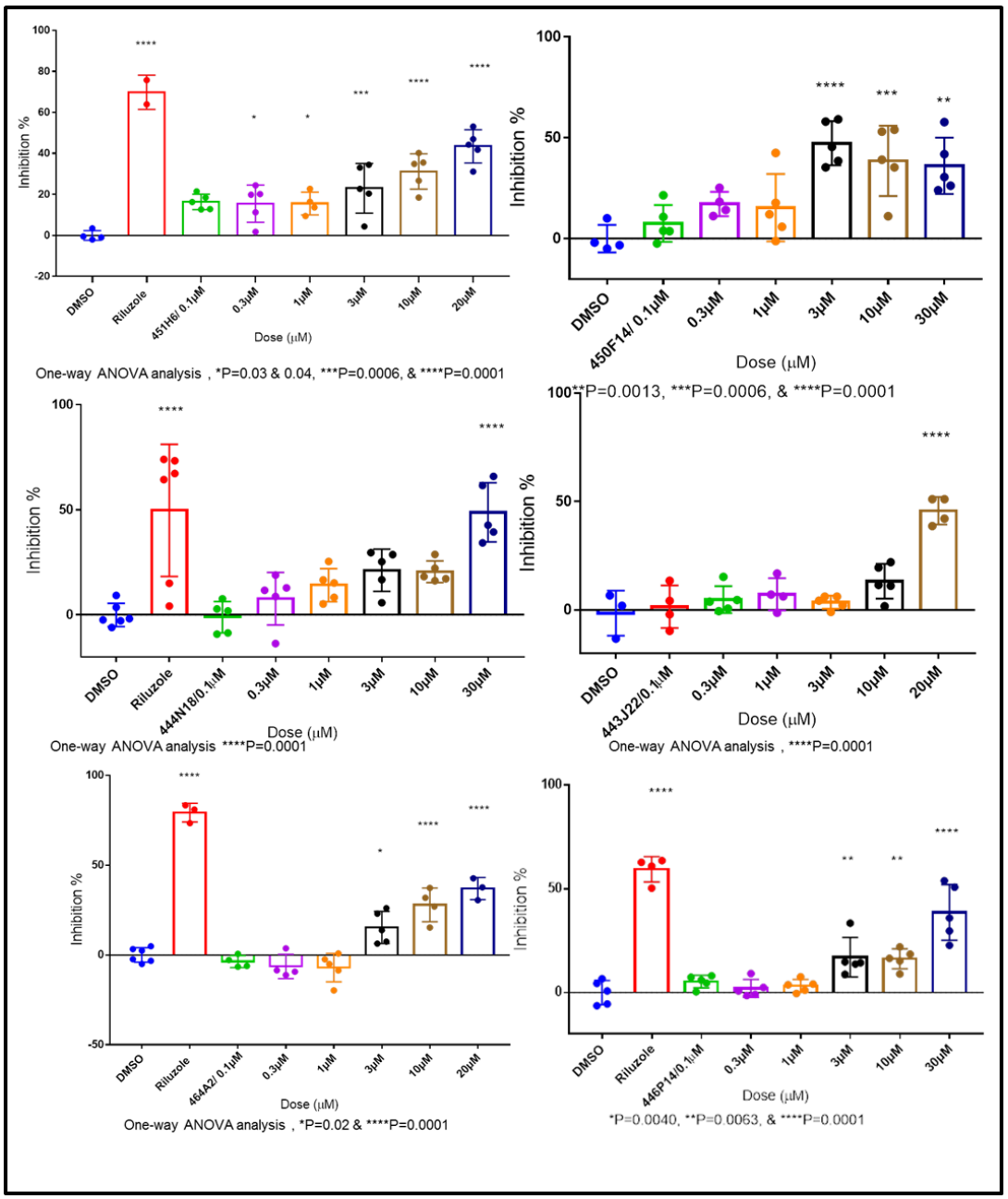

Figure 4-2: Dose-response of the most potent inhibitors from 0.1-20 or 30 µM. N=6 in DMSO (-ve) and riluzole (+ve) treated fish, and n=5 in LifeArc hit compound treated fish. Fish that displayed oedema were excluded from the analysis. One-way ANOVA statistical analysis was performed. Means and SD are shown on graphs. The compounds are 451H6(MRT002033197), 450F14(MRT00202041), 444N18(MRT00200707), 443J22(MRT00201527), 464A2(MRT00215326), & 446P14(MRT00202461).

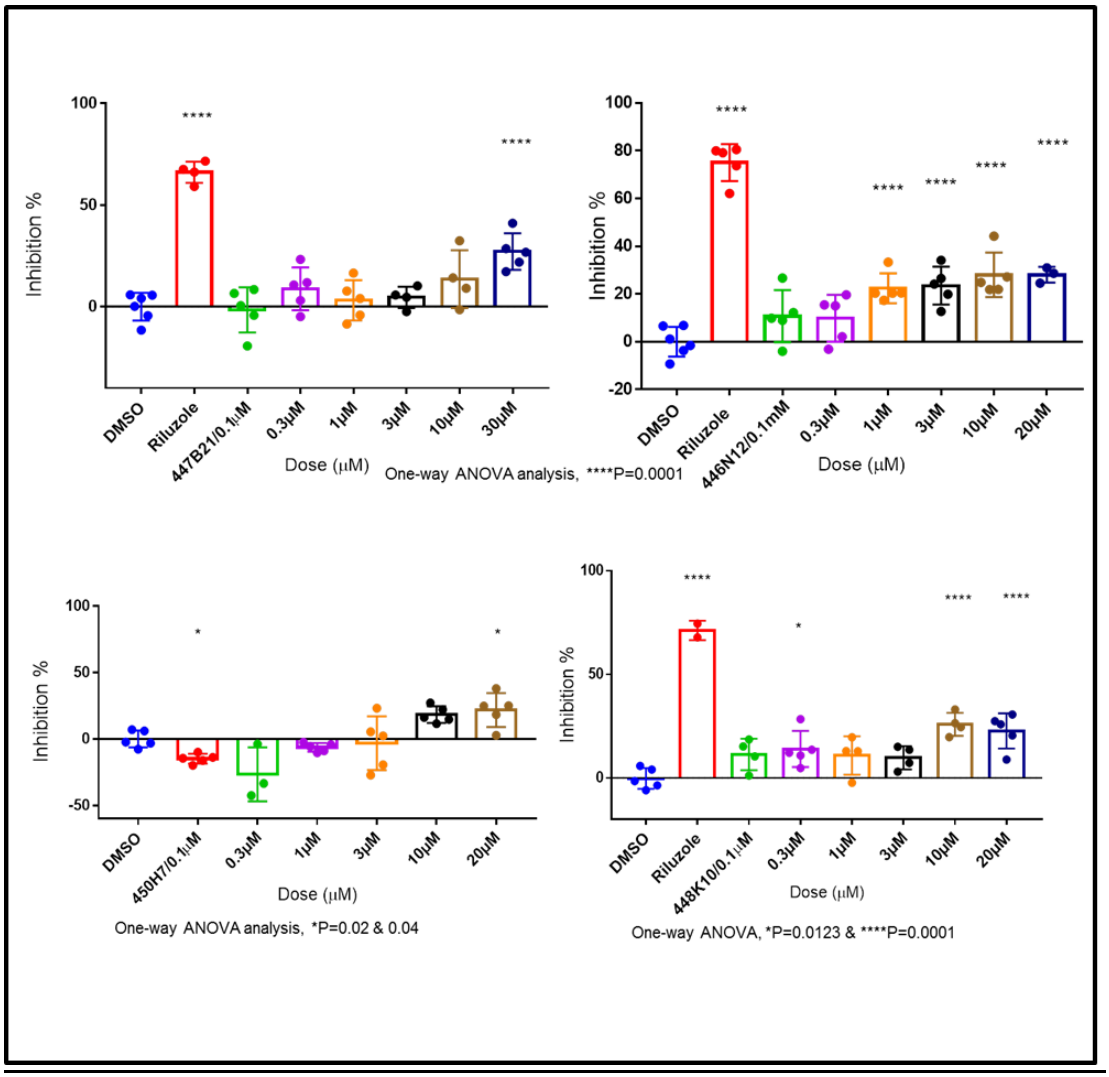

Figure 4-3: Dose-response of the moderately potent inhibitors from 0.1- 20 or 30 µM. N= 6 in DMSO (-ve) and riluzole (+ve), and n=5 in the *sod1*G93Ros10 zebrafish treated with LifeArc library hit compounds. Fish that displayed oedema were excluded from the analysis. One-way ANOVA statistical analysis was performed. Means and SD are shown. The compounds are 447B21(MRT00201895), 446N12(MRT00202123), 450H7(MRT00202788), & 448K10(MRT00202938).

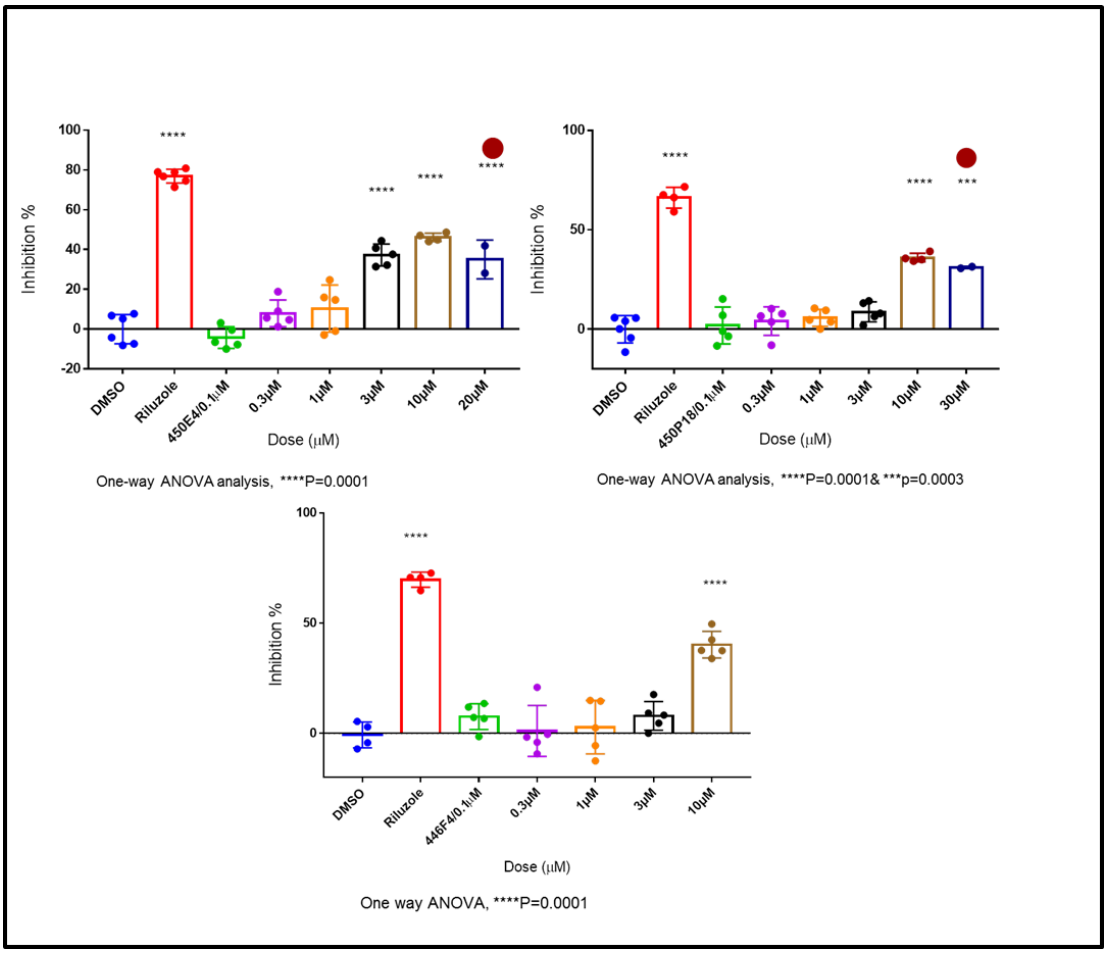

Figure 4-4 : Dose response of hits showing toxicity at higher doses of 20 µM and above. With these compounds, at the 20 µM dose, the number of the dead fish = 3 or it caused the death of all treated fish, such as when treated with 446F4/ MRT00201744. N= 6 in DMSO (-ve) and riluzole (+ve), and n=5 in the *sod1*G93Ros10 zebrafish treated with LifeArc compunds. Fish that displayed oedema were excluded from the analysis. One-way ANOVA statistical analysis was performed. Means and SD are shown. The compounds are 450E4(MRT00202253), 450P18(MRT00202994), & 446F4(MRT00201744).

All the tested compound groups were compared with the DMSO treated groups to identify inhibitor hits using a One-way ANOVA analysis.

Some hit compounds showed a significant reduction in the stress readout at a higher dose (10 µM, 20 µM, or 30 µM), but failed to show a consistent dose-response at lower doses (0.1-10 µM). This dose-response profile would not be ideal for further pre-clinical development and it might have multiple cellular targets so it is not useful for drug development.

As a result, 13 inhibitors were identified for further characterisation based on the dose-response screen. These hits showed different inhibition efficacy ranging from strong, through moderate, to weak activity with some causing death at higher doses (Figs. 4-2, 4-3, & 4-4). This secondary screen therefore allowed the classification of compounds based on their dose-response profile in the *sod1*G93Ros10 zebrafish.

4-2-2 Behavioral analysis of the hit compounds

Riluzole exhibits a sedative property and we hypothesised that compounds that showed reduced sedative activity, unlike riluzole, may be ideal for pre-clinical development as CNS side effects will be reduced. Behavioural analysis was undertaken on all of the hit compounds remaining after the dose-response study to explore whether any of the hit compounds showed sedative activity.

The ViewPoint ZebraBox behaviour system tracks the movement of fish to investigate their locomotor function and light-dark responses of animals. It also allows categorisation of the locomotor activity of the fish by generating a visual readout of movement. Red lines represent fast movement and green lines slower movement on the ViewPoint traces and show a trace of the total distance moved and allow visualisation of the activity of each fish. As the number of animals tested was low, a reliable quantitative assessment of locomotor behaviour was not possible due to the large variability observed between animals. This variability is typical with larval zebrafish. A good quantitative analysis would typically need 25-50 embryos per treatment dose. As we were limited by drug quantity, we were only able to perform a qualitative gross behavioural analysis to determine whether the compounds had a similar

sedative property as riluzole, or whether they gave a gross hypermotility phenotype. The study was set up to track the zebrafish larvae in two environmental conditions (dark + light) for 10 min. each. This was done in 96-well plates (HE-Health Greiner) with a threshold of 3 s/mm for slow movement and 15 s/mm for fast movement. In the analysis of the control groups, the DMSO-treated fish showed a normal locomotor activity in response to light/dark, while the riluzole-treated fish (10 µM) showed were sedated and showed no response to the light/dark cycle. It is known that riluzole causes a sedative effect in ALS patients. Interestingly, the hit compound-treated fish showed significantly higher locomotor activity as compared to riluzole, suggesting that the hits do not have strong sedative effects, and they responded to the light/dark cycles as expected in all doses up to 30 µM. Thus, these hits do not appear to have the limitations of riluzole. These results are presented in the following sections.

4-2-3 validation of dose-response study by secondary dose-response study

The primary dose-response study supplied a number of promising hits. Therefore, these hits were tested again in a duplicate screen to ensure that the results were reproducible. These hits exhibited a consistent reduction in DsRed fluorescence at 3, 10, & 20 or 30 µM, thus appearing to be bonafide pre-clinical leads for further exploration. The dose-response analysis led to the identification of three strong hits, three moderate hits, and some compounds that showed strong efficacy but also exhibited toxicity at higher doses.

The area under curve is utilised in drug screening to provide an individual activity value of compounds and compare them. When we performed an area under the curve analysis, the dose-response was comparable to that seen with the bar graphs. Two-way ANOVA analysis and Dunnett's multiple comparison test was performed to allow multiple comparisons between all the doses and with DMSO, and the significance levels are indicated for each dose in the subsequent figures. The variability between samples at some lower doses precluded significance due to higher noise.

4-2-3-1 Dose-response analysis of the strongest hits

The dose-response of all the inhibitor hit compounds showed strong inhibition of the DsRed fluorescence stress readout from 0.1-20 µM with ≥ 40% efficacy in the *sod1*G93Ros10 transgenic zebrafish. The compounds also showed a good dose-response profile with minimal/no toxicity, highlighting these compounds as strongs hit for further investigation.

4-2-3-1-1 MRT00202041(450F14) - referred as 2041

The compound 2041 showed one of the strongest inhibitions of the DsRed fluorescence, > 40% at 20 µM. It showed consistent inhibition of the DsRed neuronal stress readout with a significant reduction at the higher doses of 3,10, 20 or 30 µM, (Fig. 4-5). The first dose screen was from 0.1-30 µM, but then the highest dose was reduced to 20 µM because of drug volume limitations. The 2041-treated fish had normal development at each of the tested doses. The dose-response study of 2041 showed consistent inhibition with low variability (Fig. 4-5). The behavioural analysis of treated fish showed movement in all doses from 0.1- 20 µM in both environmental conditions (dark and light) (Fig. 4-6). This suggests that the compound is non-toxic at these doses.

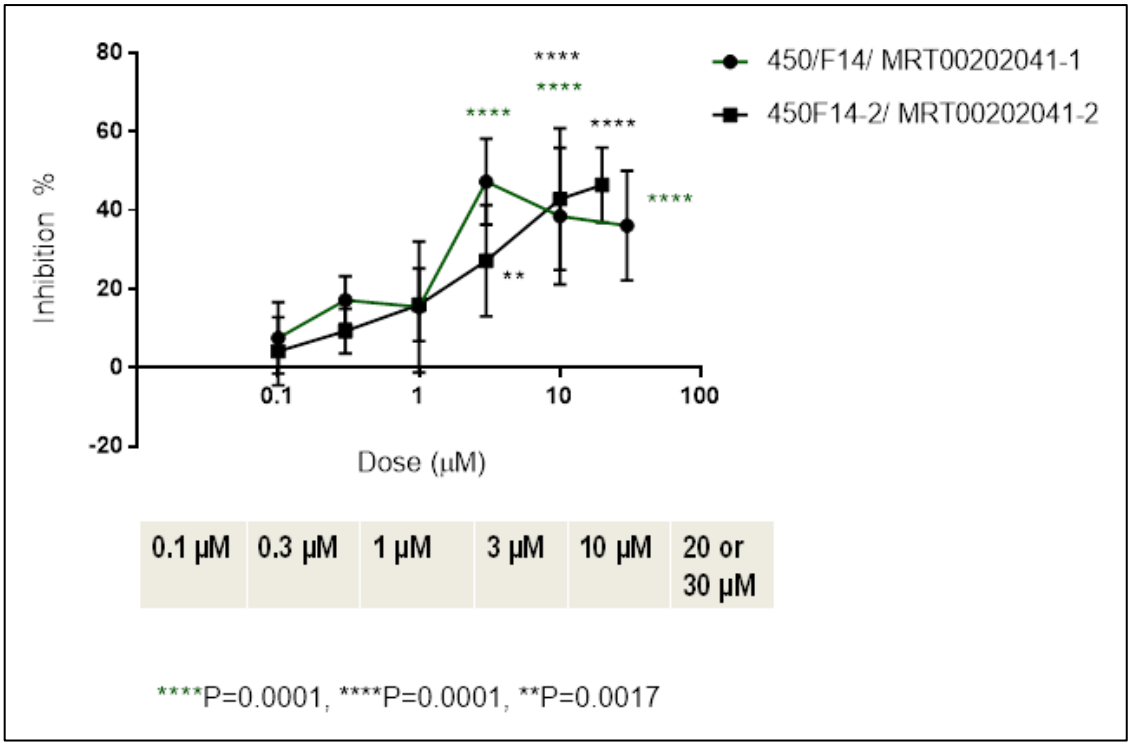

Figure 4-5: Compound 2041 is the most potent compound with strong inhibition of the DsRed neuronal stress fluorescence readout in a duplicate dose-response analysis in *sod1*G93Ros10 mutant zebrafish. N=5, Mean + SD of each dose is shown. Two-way ANOVA analysis and Dunnett's multiple comparison test were performed.

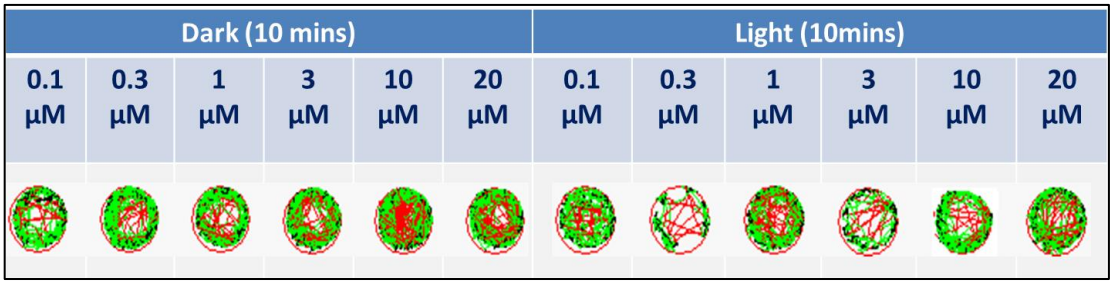

Figure 4-6: Locomotor activity of fish exposed compound 2041. No sedative effect was observed in the dark or light conditions over 10 min. Red lines represent fast movement, and the green lines represent slow movement at thresholds of 3 and 15 mm/s. One *sod1*G93Ros10 embryo was analysed in each well at 6 dpf after 4 days of drug exposure.

4-2-3-1-2 MRT00203197 (451H6) - referred as (3197)

Compound 3197 showed a strong and consistent inhibition of > 40% at 20 µM in the duplicate dose analysis. The efficacy of inhibition increased in a dose-dependent manner through 3,10, & 20 µM concentrations (Fig. 4-7). Treated fish showed normal development and normal locomotor activity (Fig. 4-8). It also did not cause death at higher doses.

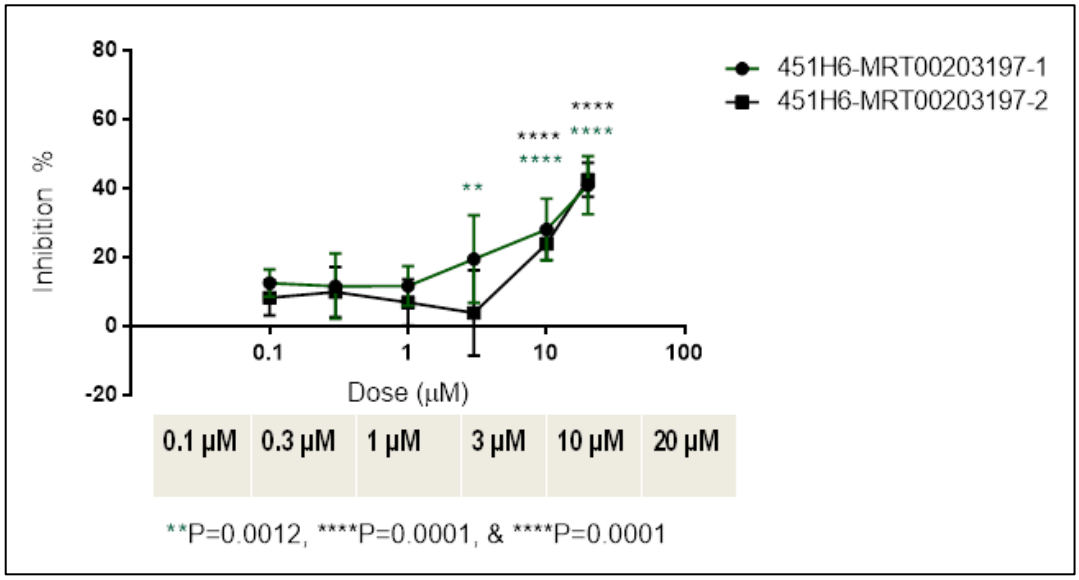

Figure 4-7: Dose-response profile of compound 3197. It showed inhibition at 3, 10 & 20 µM in the duplicate dose-response. N=5. Points and error bars represent the mean & SD at each dose. At dose 0.1 µM in the second test, the number of treated fish = 2 due to the inclusion of non-transgenic fish. Two-way ANOVA and Dunnett's multiple comparison tests were performed.

4-2-3-1-2-1 Behavioural analysis of dose-response to MRT00203197 (451H6) referred to as 3197

The behavioural analysis showed normal locomotor activity in both the dark and light conditions with all doses from 0.1-20 µM in the *sod1*G93Ros10 mutant zebrafish (Fig. 4-8). This is an interesting hit for follow up work, as it showed a good consistent reduction of neuronal stress from lower to higher doses, no effect on locomotor activity at all tested doses, and no death or abnormal development. This compound therefore gives a strong reduction in the stress readout without any sedative effects.

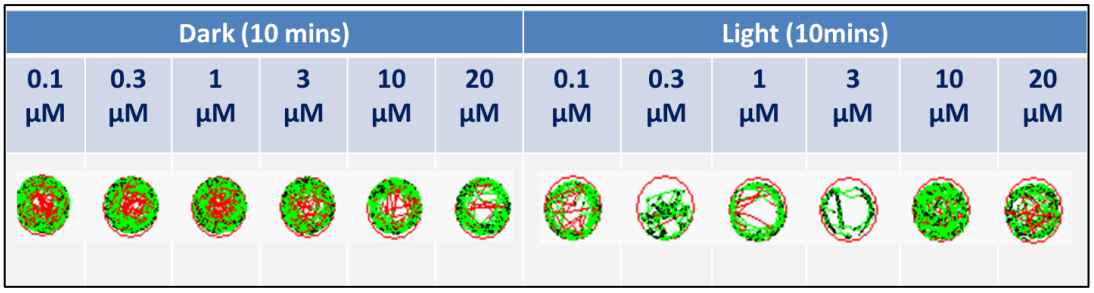

Figure 4-8: Locomotor activity of fish treated with compound 3197 at 0.1-20 µM doses in dark and light conditions. Red lines represent fast movement, and the green lines represent slow movement at thresholds of 3 and 15 mm/s. One *sod1*G93Ros10 embryo was analysed in each well at 6 dpf after 4 days of drug exposure.

4-2-3-1-3 MRT00215326 (464A2) - referred as (5326)

Dose-response analysis of the MRT00215326 compound showed a good dose-response profile from 0.1-20 µM, with > 36% inhibition of the stress readout at 20 µM in duplicate assays. Inhibition of neuronal stress started at 3 µM in both duplicates, and it showed a significant reduction of the DsRed fluorescence readout at 10 µM & 20 µM, as shown in (Fig. 4-9). This is an interesting hit for further investigation because the inhibition was dose-dependent and consistent.

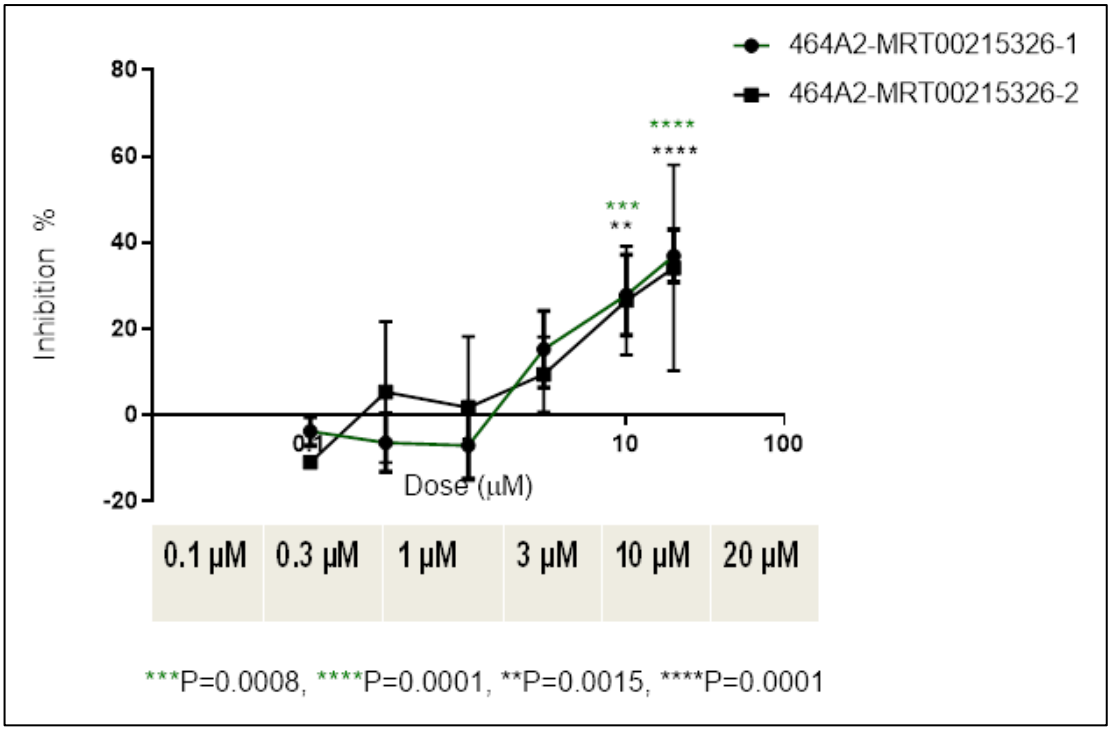

Figure 4-9: Compound 5326 was the third strongest hit with consistent dose-dependent inhibition at 3 µM, 10 µM, & 20 µM in the duplicate dose-response assays. N=5 except with the 0. 1 µM dose, where n=1 in the second screen due to drug-unrelated death of embryos.

4-2-3-1-3-1 Behavioural analysis of MRT00215326 (464A2) - referred to as 5326

The behavioural analysis of 5326 treated fish showed locomotor activity in dark and light conditions at all doses from 0.1-20 µM in the *sod1*G93Ros10 mutant zebrafish (Fig. 4-10). There was no apparent sedative activity at any of the doses.

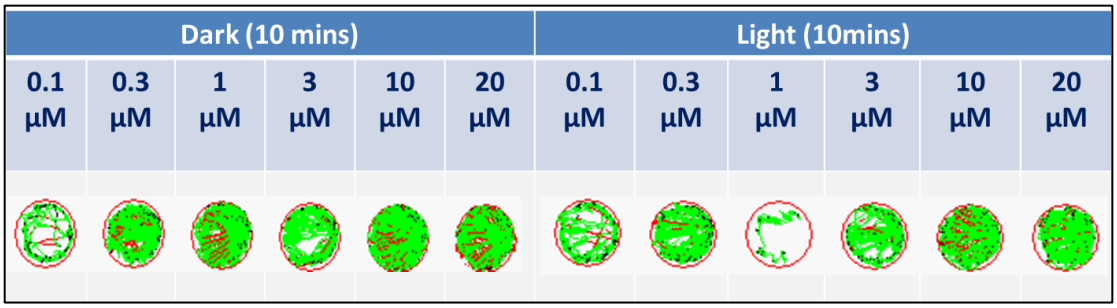

Figure 4-10: Compound 5326-treated *sod1*G93Ros10 zebrafish had normal locomotor activity in 0.1- 20 µM doses in light and dark conditions. Red lines represent fast movement, and the green lines represent slow movement at

thresholds of 3 and 15 mm/s. One *sod1*G93Ros10 embryo was analysed in each well at 6 dpf after 4 days of drug exposure.

4-2-3-2 Dose-response analysis of the moderate hits

Three moderate dose-response hits were identified with more than or equal to a 20% inhibition of DsRed fluorescence in the duplicate dose-response analyses. Thesehits showed consistent inhibition of *hsp70*::DsRed fluorescent stress readout with 0.1- 20 µM concentrations of the drug in *sod1*G93Ros10 zebrafish.

4-2-3-2-1 MRT00201895 (447B21) - referred as (1895)

The hit 1895 showed a moderate significant reduction effect of > 20% at the higher doses 30 µM and 20 µM in the duplicate analysis (Fig. 4-11). It showed a possible (insignificant) inhibition of the neuronal stress readout with 3 µM and a significant reduction at 10 µM and 20 µM. The first higher dose screen was at 30 µM and the second higher dose was reduced to 20 µM because of the limited volume of the drug available.

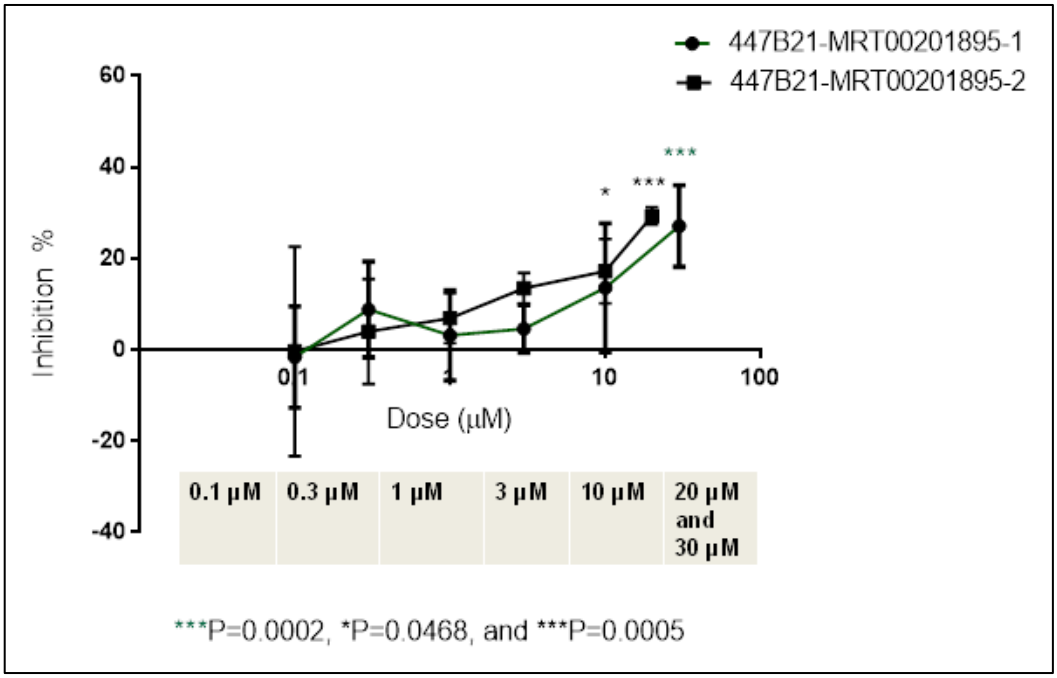

Figure 4-11: Compound 1895 showed a moderate reduction of the neuronal stress readout with consistent inhibition from 3 µM-20 µM in the duplicate dose-response analysis.

4-2-3-2-1-1 Behavioural analysis of MRT00201895 (447B21) - referred to as 1895.

The behavioural analysis of 1895 showed normal locomotor activity in both light and dark conditions at all doses from 0.1-20 µM in the *sod1*G93Ros10 mutant zebrafish (Fig. 4-12).

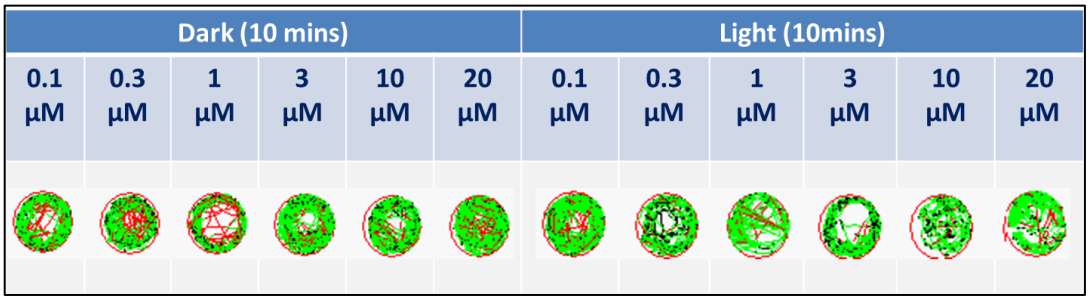

Figure 4-12: Compound 1895 treated *sod1*G93Ros10 zebrafish showed no sedative effect in the dark and light conditions. Red lines represent fast movement, and the green lines represent slow movement at thresholds of 3 and 15 mm/s. One sod1G93Ros10 embryo was analysed in each well at 6 dpf after 4 days of drug exposure.

4-2-3-2-2 MRT00202938 (448K10) - referred as (2938)

The compound 2938 showed a moderate, but significant reduction of the neuronal stress readout of > 20% at 10 µM and 20 µM in the duplicate dose-response analysis (Fig. 4-13). A significant effect was observed at 10 & 20 µM with no death or abnormal development in the duplicate dose-response analysis. For this compound, it would be interesting to investigate if higher doses showed greater activity.

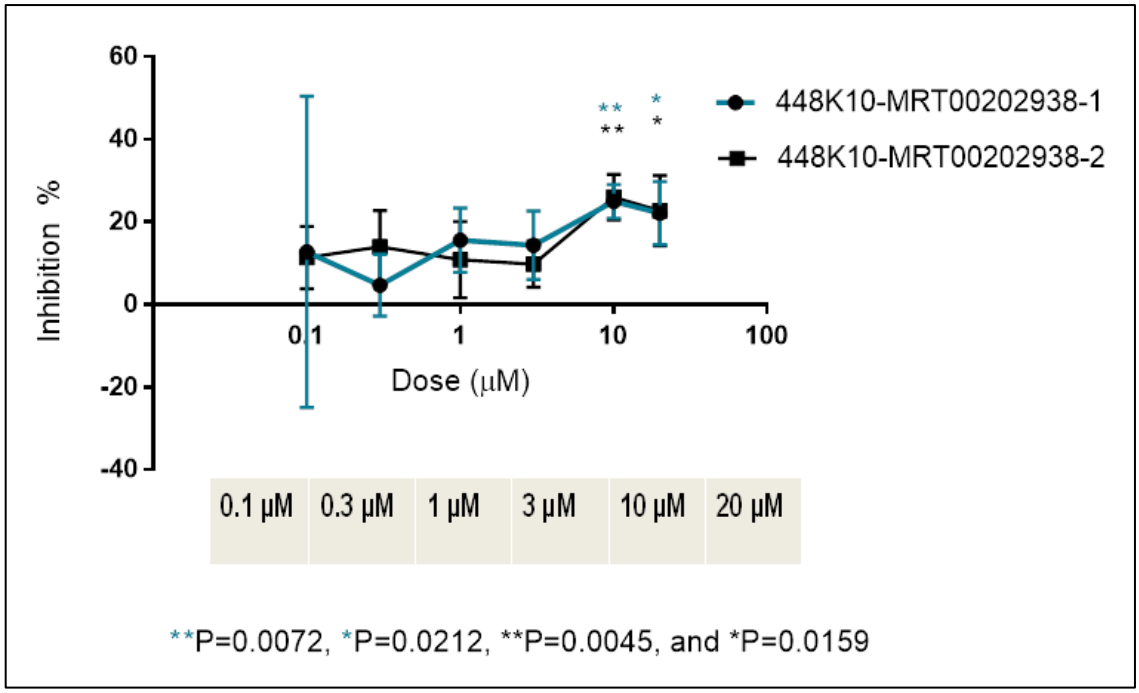

Figure 4-13: Compound 2938 showed an average inhibition of 20% at 20 µM in the neuronal stress readout in the duplicate dose-response analysis. At 0.1 µM in the first screen, two false values lead to a large SD.

4-2-3-2-2-1 Behavioural analysis of MRT00202938 (448K10) - referred to as 2938.

The behavioural analysis of compound 2938 showed normal movement activity at all doses from 0.1-20 µM in the *sod1*G93Ros10 mutant zebrafish in both light and dark conditions (Fig. 4-14).

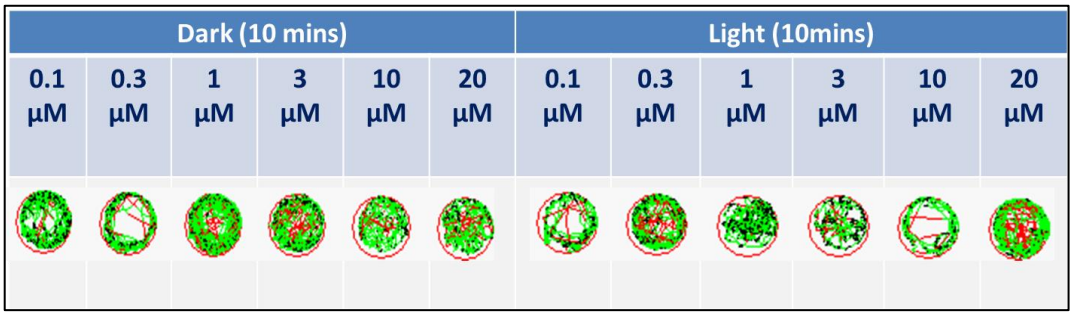

Figure 4-14: Compound 2938 had no sedative effect on the *sod1*G93Ros10 zebrafish in both light and dark conditions. Red lines represent fast movement, and the green lines represent slow movement at thresholds of 3 and 15 mm/s. One *sod1*G93Ros10 embryo was analysed in each well at 6 dpf after 4 days of drug exposure.

4-2-3-2-3 MRT00202788 (450H7) - referred as (2788)

The *sod1*G93Ros10 zebrafish treated with compound 2788 showed a moderate reduction of > 20% at 20 µM in the neuronal stress readout in the duplicate analysis. It showed a significant reduction in the DsRed stress readout of on average 24.1% at 20 µM (Fig. 4-15). The behavioural analysis showed normal locomotor activity in both environmental conditions (dark and light) with all doses from 0.1-20 µM (Fig. 4-16).

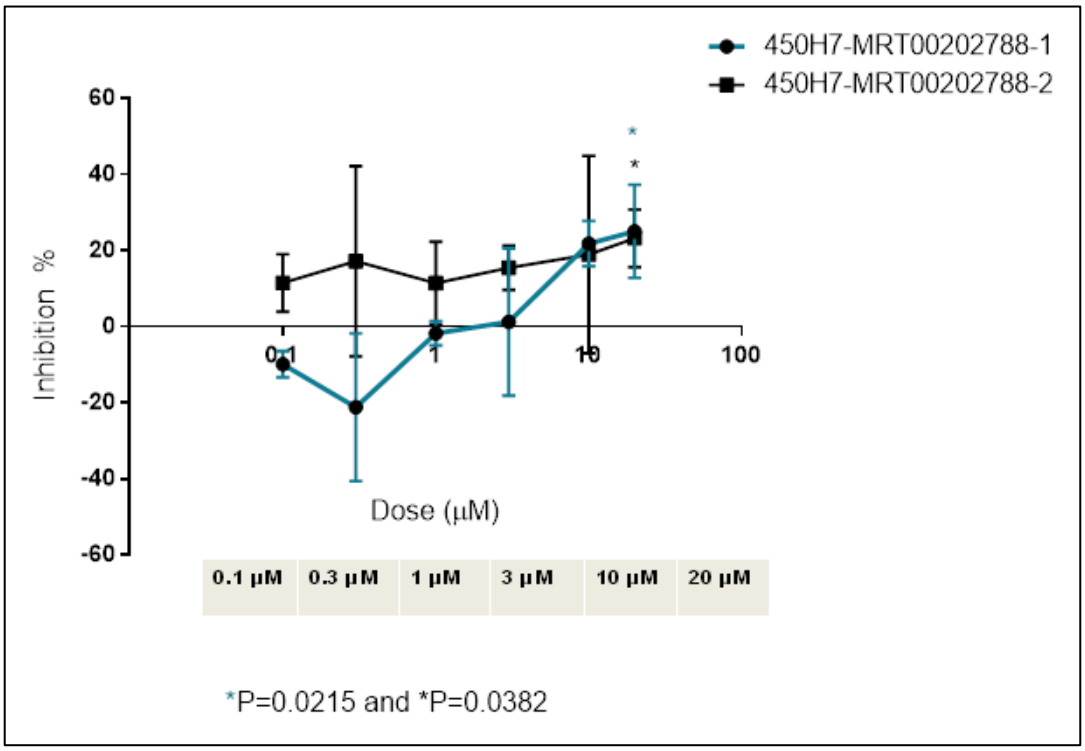

Figure 4-15: Compound 2788 has a moderate effect with inhibition of > 20% at 20 µM in duplicate dose-response. The different dose-response seen between the first and second analyses might be related to the use of a fresh drug batch in the second experiment.

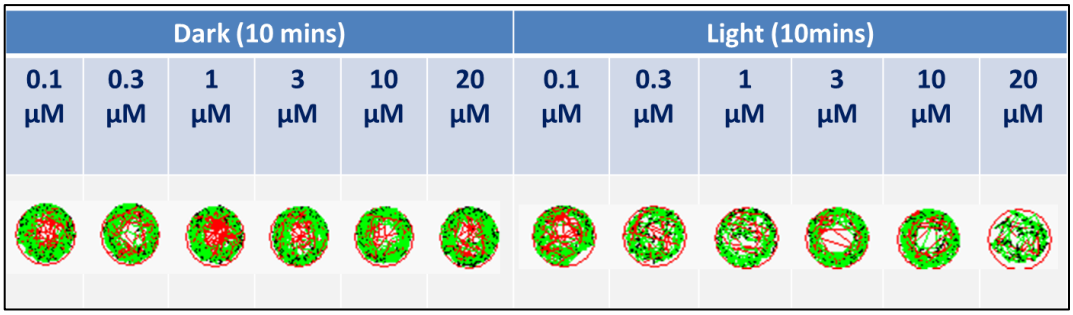

Figure 4-16: Compound 2788 had no sedative effect on the *sod1*G93Ros10 zebrafish in both light and dark conditions at all concentrations tested. Red lines represent fast movement, and the green lines represent slow movement at thresholds of 3 and 15 mm/s. One *sod1*G93Ros10 embryo was analysed in each well at 6 dpf after 4 days of drug exposure.

4-2-3-3 Dose-response of some hits that lack reproducibility in the second screen

The dose-response of some promising compounds showed a good dose-response in the first test from 0.1- 20 µM. However, the dose-response analysis failed to show the same level of reduction in the second repeat or showed a toxic effect. These compounds are listed in the section below.

4-2-3-3-1 Dose-response of MRT00202461 (446P14) and MRT00201527 (443J22) - referred to as 2461 and 1527

The dose-response analysis of 2461 and 1527 showed reproducibility issues between the first and second tests. The dose-response analysis of 2461 and 1527 showed a reduction of the *hsp70*::DsRed neuronal fluorescent stress readout of on average 39% and 42% at 30 µM and 20 µM respectively in the first test. The second dose-response analysis showed these compounds had a reduced activity of < 20% at 20 µM (Fig. 4-17). It is likely that this was caused by drug degradation between the first and the second tests. The Echo550 survey of these compounds showed a decrease of over 10% in the DMSO concentration between the first test and the second. To determine if this was the issue, we obtained a new batch of the drug from LifeArc to complete the dose-response studies of the hits and the related structural compounds discussed in the next chapter.

4-2-3-3-2 Dose-response of MRT00200707 (444N18), MRT00202123 (446N12), and MRT00201744 (446F4) - referred as 0707, 2123, and 1744 respectively

The first dose-response analysis of compounds 0707, 2123, and 1744 showed that all of these hits had strong activity on the stress readout from 0.1 to 30 µM in the *sod1*G93Ros10 zebrafish (Fig. 4-17). Issues with these compounds were noticed in the second analysis where the efficacy was limited and in some cases toxicity was observed at the highest dose. This raised the possibility of drug stability being an issue as the second test was performed using a drug from the stored library. However, due to fresh drug not being available for repeat testing, we are unable to make a definitive conclusion.

4-2-3-3-2-1 Dose-response of 0707

The first dose screen of compound 0707 showed reduction of the neuronal stress readout from 0.1-30 µM with an average reduction of 49% at 30 µM. The first test showed a dose-dependent effect with significant activity at 30 µM (Fig. 4-2), whilst the second test showed similar effects at lower doses, but however caused death at the highest dose of 20 µM (Fig. 4-17). Again, this issue was possibly thought to be related to the stability of this compound. The survey of DMSO showed shifts in DMSO concentration from 95% in the first test to 80% in the second, due to increased water content

4-2-3-3-2-2 Dose-response of 2123 and 1744: Lower reduction with the same death criteria at the higher doses between two screens

Compounds 2123 and 1744 had very similar reproducibility issues. Compound 1744 showed modest effects with a significant inhibition of the fluorescent stress readout, with an average of 38% inhibition at 10 µM, but it caused death at 30 µM (Fig. 4-4). In the second dosage analysis it showed a lesser effect at 0.1-20 µM, with an average of 11.8% reduction at 10 µM, and with death at 20 µM (Fig. 4-17).

The first dose-response analysis of compound 2123 showed moderate inhibition of > 20% at 20 µM. It showed moderate effects from 1-20 µM with average reductions of 22.37%, 23.47%, 27.99, and 28.05% respectively in the stress readout (Fig. 4-3). In the second test it showed a lower reduction than in the first and caused death at 10 and 20 µM (Fig. 4-17).

LifeArc ID hits	First screen 0.1µM | 0.3 µM | 1 µM | 3 µM | 10 µM | 20 or 30 µM	Second screen 0.1µM | 0.3 µM | 1 µM | 3 µM | 10 µM | 20 µM
MRT00202461	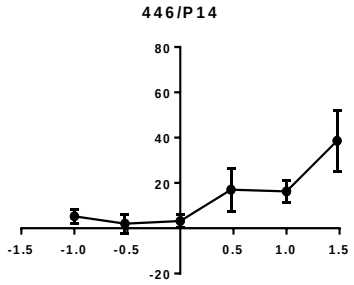	Lower reduction stress effects 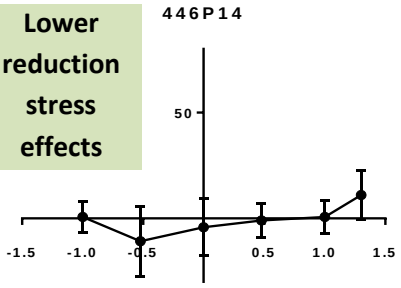
MRT00201527	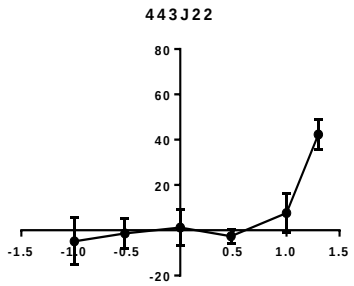	Lower reduction stress effects 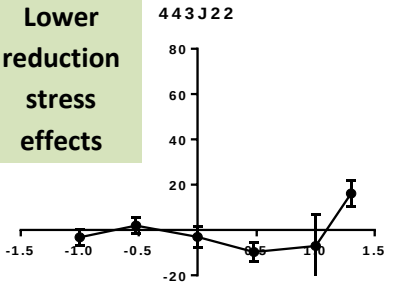
MRT00200707	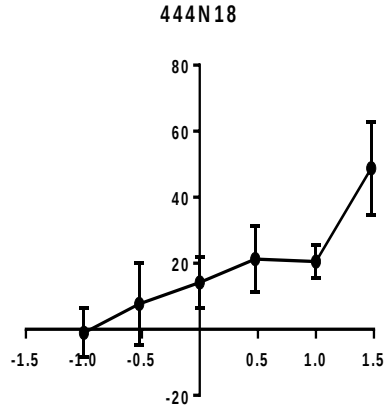	Dead fish at 20 µM 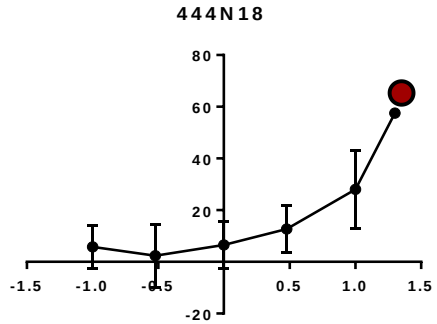

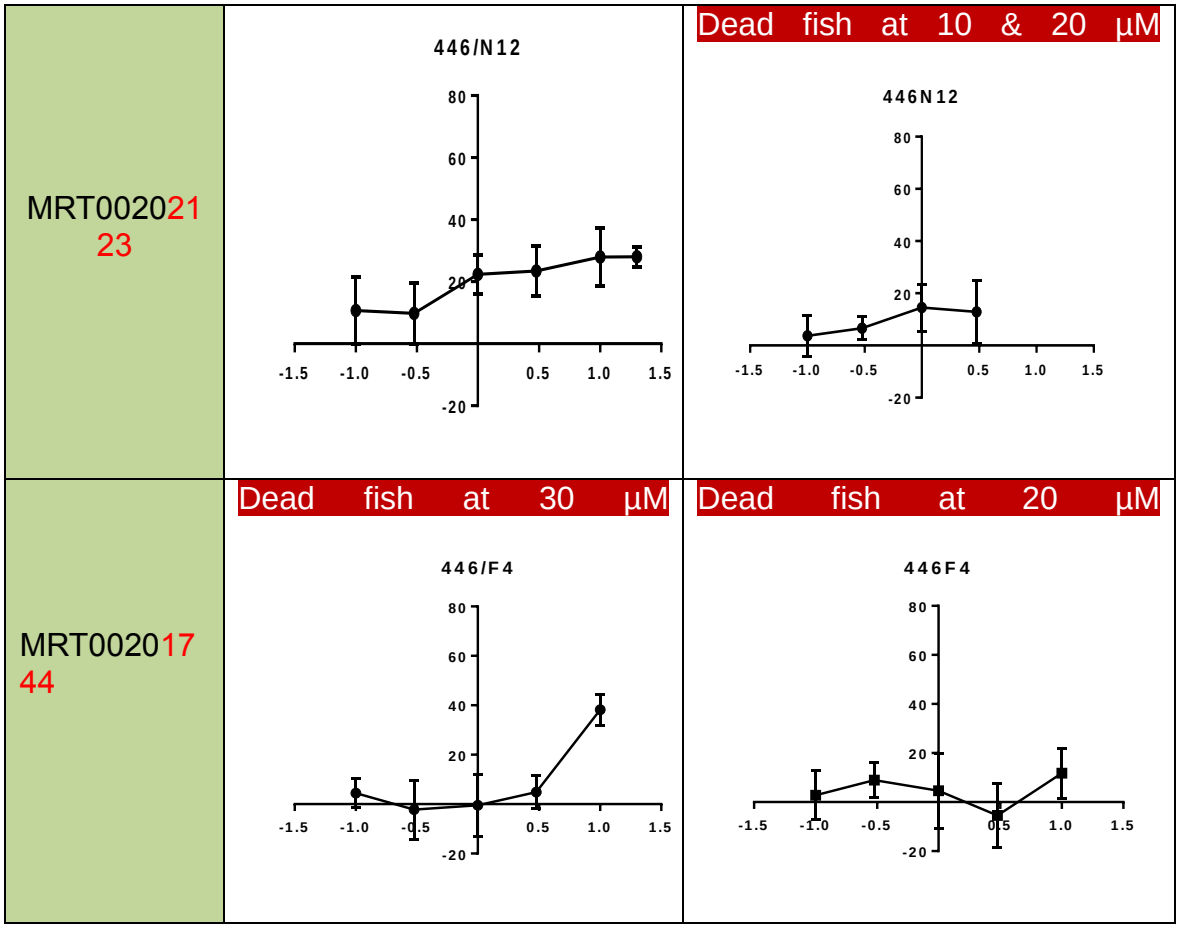

Figure 4-17: Log dose-response curves of hit compounds showed a good dose-response in the *sod1*G93Ros10 zebrafish in the first dose-response test, but showed lower activity or toxicity with the highest dose of 20 µM in the second replicate. The x-axis is a dose of the drug and Y-axis is the stress response.

4-2-3-4 Toxic response of MRT00202253 (450E4) - referred to as (2253), and MRT00202994 (450P18) - referred to as (2994) at higher doses

The dose-response analysis of compounds 2253 and 2994 showed a dose-dependent reduction in the neuronal stress readout over the 0.1-10 µM concentration range, with normal locomotor activity observed in both dark and light conditions. However, these compounds showed a toxic effect in the first and second dose-response tests at 20 or 30 µM, with three out of five treated fish dying. Therefore, these hit compounds appear to be toxic at higher doses and may not be suitable candidates to take forward for secondary screening.

The strongest effect was seen with 2253, showing a 46.19% decrease in the stress readout at 10 µM, although it appeared to be toxic at higher concentrations as it caused the death of three of five treated fish at 30 µM in the first dose-response test (Fig. 4-4). The second dose-response test showed dose-dependent inhibition from 0.1-20 µM with efficacy in inhibition at 10 and 20 µM, without any death or abnormal development upon visual inspection of the treated fish under a dissection microscope. The reduction percentages were very similar at 10 and 20 µM (48.9% and 48% respectively) (Fig. 4-18). This suggests that this hit has a strong inhibitory effect at 10 or 20 µM, but appears to potentially be toxic at higher concentrations of > 20 µM.

Another hit compound that showed a toxic profile was 2994. This compound showed a significant reduction in the DsRed readout of 36% at 10 µM, but it caused death at 20 µM (three fish of five dead) in the first dose-response test (Fig. 4-4). The second test showed similar effects from 0.1-20 µM with a 35.2% reduction at 10 µM, but caused death at 20 µM (Fig. 4-18). This led us to conclude that this compound may have a toxic effect at doses higher than 10 µM. The fish showed toxicity as indicated by oedema, abnormal development (seen at 5-6 dpf), and some deaths occurred after one or two days of 20 µM drug treatment.

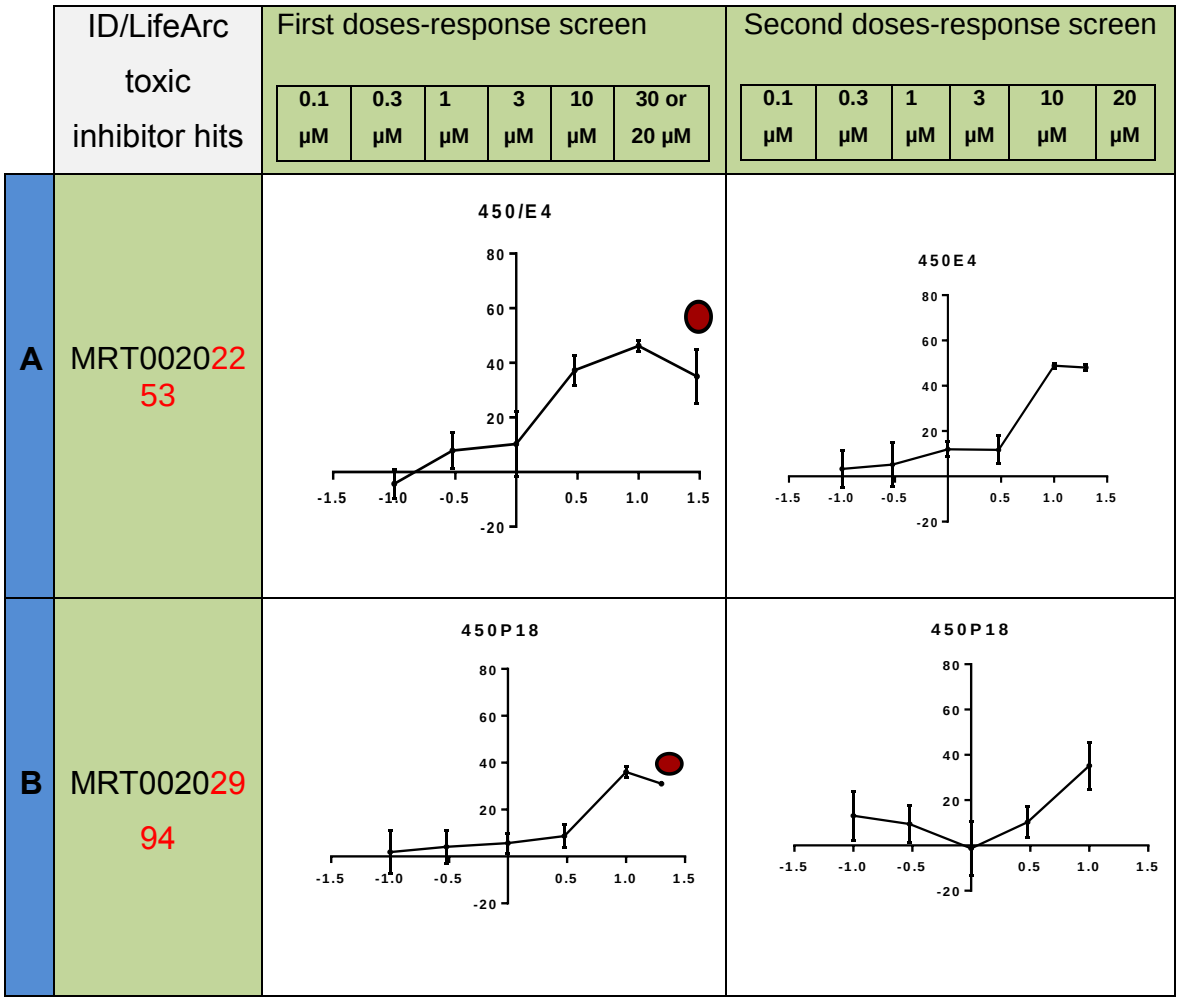

Figure 4-18: Showing hit inhibition of *hsp70*::DsRed fluorescent readout from 0.1-10 µM with a toxic effect response at higher doses (30 µM or 20 µM).

A-The compound 2253 showed a toxic effect at 30 µM in the first dose screen, while it had a good inhibition% at 10 & 20 µM of > 48% in the second dose screen.

A- At 20 µM dose, the compound 2994 showed toxic effects in duplicate doses screens in the *sod1*G93Ros10 zebrafish. 10 µM dose of this compound showed a good inhibition with an average of > 35% in duplicate screens. The x-axis is a dose of the drug and Y-axis is the stress response.

4-3 Whole body analysis of DsRed fluorescence at 6 dpf of fish treated with inhibitory compounds using the InCell imaging system

InCell imaging was performed at 6 dpf (4 days of treatment exposure), and images captured for fish treated with all 94 hit compounds from the primary screening. The images obtained showed that *sod1*G93Ros10 zebrafish treated with the most potent inhibitors had visibly reduced DsRed fluorescence in the hindbrain, and to a lesser extent in the spinal cord, than DMSO-treated fish (Fig. 4-19). The images of the moderately potent inhibitors of the neuronal fluorescent stress readout did not show obvious differences when compared to the DMSO controls. It is difficult to perform an image-based quantitation with the InCell system, as the orientation and positioning of fish in the wells could not be readily controlled. Nevertheless, these images suggest that the most potent compounds identified showed clear effects, attesting to the better sensitivity of the quantitative measurements obtained with the PHERAstar system.

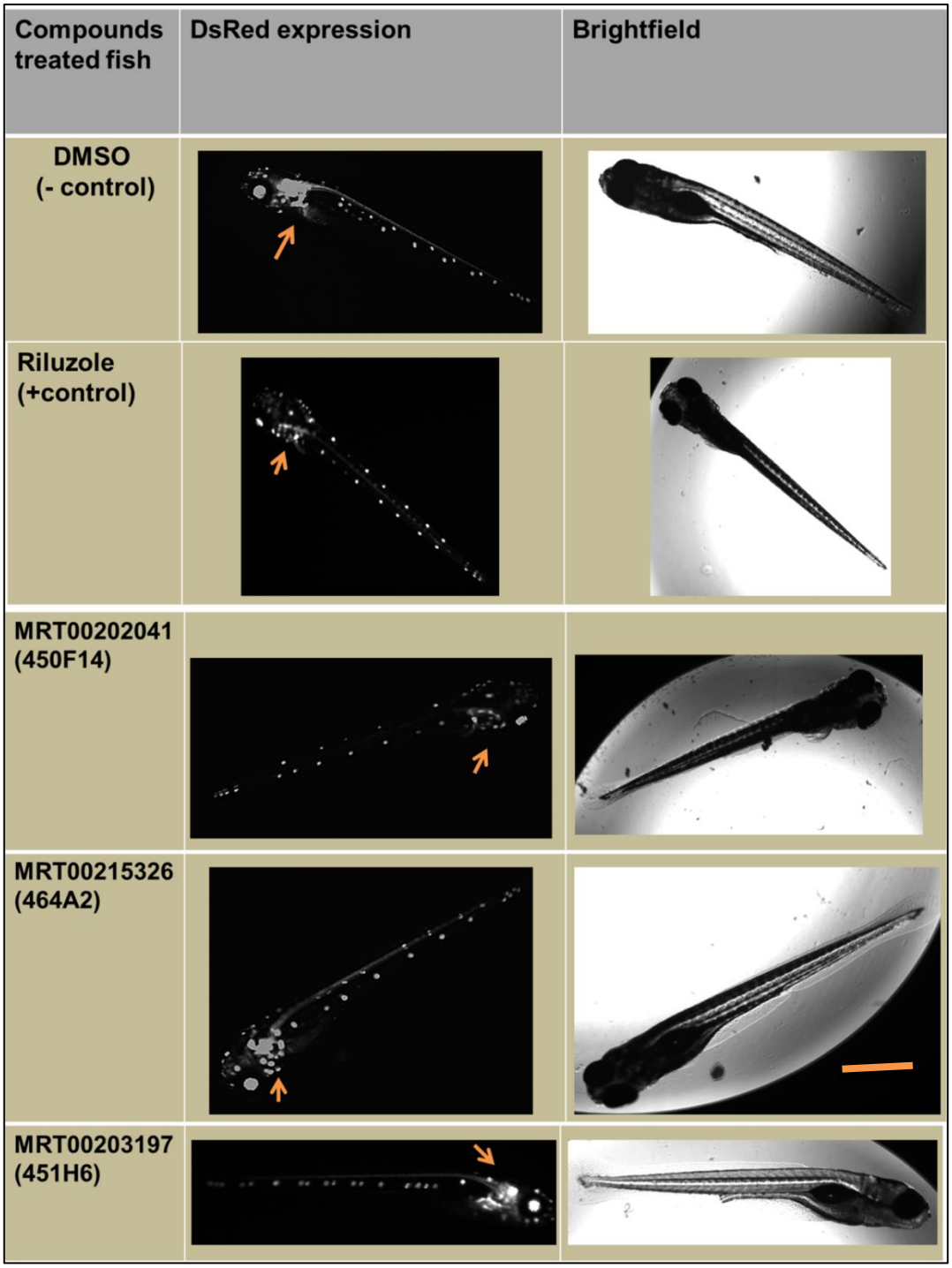

Figure 4-19: Whole-body imaging. DsRed fluorescence in the hindbrain was lower in 10 µM riluzole-treated and in *sod1*G93Ros10 zebrafish treated with the most potent LifeArc screen inhibitors at 6 dpf. The scale bars of all the images are 2 mm. Arrowheads represent DsRed signal.

4-4 Investigation of the chemical parameters of the top 13 inhibitors

The dose-response analysis of the hit compounds has identified three potent inhibitors of the neuronal stress readout, three moderate inhibitors, five inhibitors with potential stability issues, and two inhibitors, which showed toxicity at higher doses of 20 or 30 µM. The data generated from the screen was shared with LifeArc, who agreed to share with us the chemical and drug-like properties for the compounds. The chemical properties of each hit compound included information on the molecular weight (MW), stability, drug-like features, photosensitivity and blood-brain barrier permeability, as shown in Table 4-3 and these parameters are explained in the following section.

4-4-1 Chemical parameters

4-4-1-1 Intrinsic Property Forecast Index (iPFI)

Intrinsic Property Forecast Index (iPFI) is a chemical evaluation parameter that provides estimates of phototoxicity of compounds (Fournier et al., 2018). Phototoxic chemicals could be classified based on their ability to induce photosensitivity to UV light exposure. Nonphototoxic compounds are those having PIF < 2, low phototoxic potential at 2 < PIF < 5, while phototoxic compounds have PIF > 5 (Fournier et al., 2018). Each hit compound has a different PIF, as shown in a Table 4-3.

4-4-1-2 Quantitative Estimate of Drug-likeness (QED)

Quantitative Estimate of Drug-likeness (QED) is an estimate of a compound's drug-like properties that is based on molecular weight, whether it is hydrophopic or hydrophilic, and the tissue permeability of the compound. The scales of QED can be ranged from zero (undesirable properties) to one (most desirable properties) (Richard Bickerton ; et al, 2012). The QED score of each hit compound showed some having lower QED, while others had an excellent QED (Table 4-3).

4-4-1-3 CNS-MPO score

The central nervous system multi-parameter optimisation CNS-MPO score is a score to assess the blood-brain barrier permeability of compounds. This score is applied by weighting six physio-chemical parameters (clogP: partition coefficient calculation, clogD: distribution coefficient at ph=7.4, MW: molecular weight, TPSA: topological polar surface area, HBD: number of hydrogen bond donors, and pKa: most basic centre). The range of the CNS-MPO score is from 0-6. Typically a score of ≥ 4.0 is used for the selection of CNS penetrating compounds (Wager et al., 2010).

4-4-1-4 LogP chemical parameter

The partition constant log*P* is a prediction logarithm of solubility of a compound into two immiscible phases. It measures the propensity of a neutral (uncharged) compound to dissolve in an immiscible biphasic system of lipid (fats, oils, organic solvents) and water. It is used to predict oral bioavailability, blood-brain barrier permeability, and other biological parameters such as metabolism and excretion (see percepta batch modules online source www.acdlabs.com/products/percepta/batch).

Table 4-3: The chemical parameters and drug-like properties of each identified LifeArc hit compound. This data was provided by LifeArc.

LifeArc ID hits	iPFI	QED	CNS-MPO	MW	ACD-LogP	ACD-LogD	ACD-LogS	TPSA-NO
MRT00202041	5.55	0.6	5.5	318.3	1.55	1.55	-2.14	88
MRT00203197	4.87	0.85	5.34	371.4	2.87	2.82	-3.83	54
MRT00215326	3.79	0.82	5.01	419.3	2.79	2.79	-4.64	65
MRT00202253	4.46	0.77	5.83	349.4	1.46	1.46	-3.15	66
MRT00202994	5.22	0.8	5.72	305.3	2.22	2.22	-3.75	68
MRT00202788	5.77	0.7	5.42	363.4	2.77	2.77	-4.15	73
MRT00200707	5.75	0.78	5.83	282.3	2.75	0.79	-1.07	72
MRT00201895	6	0.78	5.31	363.4	3	3	-3.43	62
MRT00202938	5.64	0.76	5.72	375.4	2.64	1.94	-2.57	61
MRT00202461	4.87	0.85	5.56	318.8	2.87	2.87	-5.05	45
MRT00201744	6.86	0.68	4.36	375.5	3.86	3.86	-4.37	64
MRT00201527	6.34	0.84	3.84	404.9	4.34	4.34	-5.36	66
MRT00202123	6.98	0.79	4.35	331.4	3.98	3.98	-4.88	47

Quality	Colours
The higher quality of the chemical parameters	
The parameters are within the score, but the quality are graded from higher to lower scores	
Lower graded properties	
Toxic	

4-4-2 Hit compounds appear to have some related compounds with known biological activity in PubChem

Subsequent to analysis of the hit compounds, LifeArc provided potential targets that the hits could act on based on their structural similarity to compounds known to act on identified targets and/or their activity in biological assays obtained from PubChem, as shown in Table 4-4. This data suggests that some of the hit compounds could target the active binding site of these targets and may target similar biological pathways. This information helps to identify other compounds that impact these targets and identifies their potential mechanisms of action.

Table 4-4: Shows related compounds to the LifeArc inhibitor hits.

Compounds ID	Targets
CHEMBL1327271	Nothing showing as significant. Low confidence
CHEMBL186171	˷3 μM TrpV1 (group of ion channels receptors sensitive to damaged tissue) antagonist.
CHEMBL2313195	23 nM expoxide hydratase inhibitor.
CHEMBL210849	22 nM Ki against 5HT2A (excitatory serotonin G protein-coupled subtype receptors.
CHEMBL1610905	10 nM neuropeptide S receptor antagonist.
CHEMBL1500967	316 nM against ATM kinase (serine/threonine kinase)
CHEMBL485213	46nM IC50 ROCK kinase
CHEMBL1530615	~3uM against TDP43
CHEMBL485213	Most potent (158nM) as an activator of lysosomal alpha-glucosidase
CHEMBL1311980	Most significantly ~16uM against TDP43

4-5 Discussion

The work in this chapter aimed to validate true positive hit compounds from the primary screen of 4494 compounds. The primary high-throughput screen was a rapid initial screen that tested a large number of compounds and identified approximately 200 hits for further validation and investigation. To distinguish real hits from false positives, we developed secondary screens and further validation studies to test these positive hit compounds.

Secondary screening is an important key step in any high throughput screen, whether with an *in vitro* or in an *in vivo* model, as it is a crucial process for selection of pre-clinical lead compounds (McGown et al., 2016; Scull et al., 2019; Tsuburaya et al., 2018). Secondary screening is carried out on the positive primary screen hits and is designed to be more informative by providing more information on the reproducibility and dose-response of the hit compounds. This way, the most potent compounds that show good reproducibility and dose-response could move forward for further validation and pre-clinical studies in other model systems. Secondary screens are usually far lower throughput and generate more accurate and dosage information for each compound. In this chapter, we demonstrated that reduction of the neuronal stress readout by many of the hit compounds was reproducible and some of the compounds displayed a good dose-response curve, thus validating hits from the primary screen as bonafide candidates for further evaluation.

The first secondary screen performed was to repeat each drug (6 times at 10 µM) for all 214 primary screen hits. This was to confirm the reproducibility of the inhibitory effects of these hit compounds on the *hsp70*::DsRed fluorescent stress readout in the *sod1*G93Ros10 zebrafish.

The repeat screen at 10 µM of 214 primary inhibitor hits showed different categories of inhibitory effects, with some showing high and some showing weaker reproducibility. We retained the weaker hits for a more thorough dose-response analysis as the total hit numbers were manageable. Compounds 1527 and 2461 showed lower reproducibility at 10 µM, although they showed a significant inhibitory effect at 20 µM. However, compound 1527 displayed poor drug-like properties, although compound 2461 displayed better drug-like

properties, as shown in Table 4-3. Despite this, both of these compounds appear to demonstrate some stability issues, as they displayed lower or no effects in the repeat analysis.

Overall, the validation of hits from the primary screen conducted with multiple repeats at 10µM demonstrated that many of the hits identified were reproducible and were well tolerated and thus supported our hypothesis. Thus, these hits were appropriate for the next validation step, where dose-response was evaluated.

The dose-response screen was performed with 0.1, 0.3, 1, 3, 10 and 20 or 30 µM concentrations of the 94 inhibitors identified. This is a large window for drug effect and provides a dose profile signature for each hit. The dose-response screen identified 13 inhibitors that were classified into different inhibition categories based on their potency of inhibition. Additionally, ViewPoint behavioural analysis was performed to measure locomotor activity in dark and light conditions to detect any sedative effects of the compounds.

One of the strongest inhibitors was 2041. It showed inhibition of the stress readout with SSMD scores of -5.9 and -2.2 in the primary screens. The dose-response study of this hit showed a dose-dependent inhibitory effect on the neuronal stress readout when tested from 0.1-20 µM in duplicate studies. The efficacy of reduction was significant from 3-20 µM, showing the strongest inhibition of > 40% at 10 and 20 µM, with no obvious toxicity. This means that it could potentially be tested at a higher dose for an even stronger inhibitory effect. The viewpoint study for locomotor behaviour showed that 2041-treated fish had normal locomotor activity at all doses without any sedative effects, as opposed to riluzole, which strongly sedated fish. This is the most potent inhibitor identified with an inhibition percentage similar to riluzole at 10 µM, but with treated fish showing normal locomotor activity. Also, this hit showed the biophysical properties of a good drug-like molecule. It has a high CNS-MPO (blood-brain barrier and molecular distribution scale) score of 5.5, and a dose-response which is in a useful range in drug discovery, as shown in Table 4-3. Thus, this compound would be a strong candidate for further investigation for efficacy in other pre-clinical models, such as SOD1 G93A mice.

The dose-response study provided another strong lead candidate, which was 3197. This compound showed -2.3 and -0.6 SSMD scores in the first and second primary screens. The dose-response analysis of 3197 showed a good inhibition profile from 0.1-20 μM with inhibition in the range of 3 to 20 μM (> 40% at 20 μM) in the replicate study. The treated fish also showed good movement in dark and light conditions compared to riluzole. It also has good biophysical drug-like properties, except for its poor lipophilicity, stability, and photosensitivity. Thus, this drug may have difficulty in penetrating the CNS and its photosensitivity may require modification to improve its biological utility. Despite this, the compound would be worthy of further validation studies in zebrafish for measuring therapeutic benefit as it showed clear activity in reducing cellular stress. Further modification to enhance its drug-like properties may be required for pre-clinical studies in other animal models.

The third promising hit that came out of the dose-response study was 5326. Compound 5326 showed a good inhibition profile from 0.1-20 μM with reasonably potent inhibition of > 36% at 20 μM. The treated fish showed good locomotor activity at each of the tested doses. This compound displayed a good CNS permeability index, but other biophysical properties were not optimal, although they were not poor and hence this compound may be appropriate for further pre-clinical validation studies. To summarise, the dose-response study of 2041, 3197, and 5326 showed strong inhibition at 20 μM with an excellent locomotor profile and with biophysical measures that demonstrated desirable drug-like properties.

It is important to note that riluzole showed an average reduction of more than 65% of the neuronal stress readout in *sod1*G93Ros10 mutant zebrafish at 10 μM throughout this project, making it more potent that the hit compounds identified. However, it caused strong sedative effects in treated fish. The mechanism of riluzole action is predicted to be as an anti-excitotoxic agent by reducing glutamate release, but it has also been suggested to modulate GABA receptors and decrease persistent sodium ion channel currents. The LifeArc library is comprised of predicted ion channel receptor modulator compounds. However, the strongest hits showed inhibition effects of around > 40% with little effect on locomotor activity, indicating that these compounds do not have

sedative properties. This suggests that they might work on ion channels different from the targets of riluzole. Thus, these compounds may be useful for elucidating novel pathological mechanisms in ALS.

The three moderate inhibitors of the neuronal stress readout identified showed a good inhibition profile from 0.1-20 µM. These hits were 1895, 2938, and 2788. All of these hits showed significant inhibition of ≥ 20% at 20 µM in duplicate dose-response assays. Treated fish also displayed normal locomotor activity in all tested doses from 0.1-20 µM. Interestingly, these moderate inhibitors displayed poorer biophysical profiles as compared to the most potent hit compounds, suggesting that improvement in their drug-like properties may enhance their biological activity. This needs to be investigated in the future.

The dose-response studies also identified five inhibitors that, despite showing the desired biological activity, did not display good biophysical properties. These were compounds 2461, 1527, 0707, 2123, and 1744. Compounds 2461, 1527, 0707, and 1744 showed the highest reduction of > 40% at high doses of 20 or 30 µM. The other inhibitor 2123 showed a moderate inhibition effect of > 20% at 20 µM. These inhibitors appeared to have stability issues because they showed high variability in their inhibitory effects in the duplicate dose-response study. The biophysical parameters of compounds 1527, 2123 and 1744 demonstrated relatively poor scores for biodistribution, lipophilicity, photosensitivity, and CNS-MPO. Compounds 0707 and 2461, however, display average biophysical values with poorer scores for photosensitivity and biodistribution respectively.

It is interesting to note that the identified inhibitors predominantly displayed good CNS-MPO scores, thus reflecting that a zebrafish CNS-targeted screen can provide lead compounds with good BBB quality. Hence it is a suitable organism to identify and pre-screen compounds with excellent to moderate drug-like properties.

Compounds 2253 and 2994 were two hits from the same family that displayed functional inhibition of DsRed expression at 10 µM with an average 47% and 35.5% respectively in the duplicate dose-response studies. However, these inhibitors caused the death of the treated larvae at higher doses of 20 and 30

µM. Hits that display toxicity at higher doses need to be evaluated carefully, as the observed inhibition at 10 µM may potentially represent mild toxicity as the DsRed fluorescence was not normalised to any reference protein expression, meaning that lower DsRed levels may reflect toxicity.

Toxicity associated with drugs can be caused by a variety of factors related to the drug itself, but may also be specific to the biological system (zebrafish in this case) or potential drug intermediates that show toxicity after *in vivo* metabolism of the drug in the liver and kidneys. General toxicity could be confirmed by testing the compounds in a different *in vivo* model and mammalian cell lines, as well as by looking at the chemical structure of the compounds to identify possible toxic intermediates.

The dose-response assays of some hits showed a reduction of the neuronal stress fluorescent readout of ≥ 40% in the first screen, then failed to show the same level of reduction in the second repeat or showed a toxic effect. There is a high probability that this issue might be related to the compound's stability, with degradation occurring over time due to prolonged storage in DMSO. Also, a second batch of some drugs were ordered due to lack of sufficient quantity for a full dose-response study. The Echo550 system can survey the DMSO percentage for each drug aliquot. This provides an idea of how much water has been absorbed into the DMSO and is an indicator of drug hydrolysis and potential breakdown. In the first dose-response analysis, the DMSO% in each well was between 90-95%, whereas this dropped to 70-77% in the second. This is one potential reason why some drugs did not show the same effect on both analyses as some drugs in the library may be susceptible to hydrolysis and breakdown. The toxicity of some in the repeat study may also be related to the batch quality.

It is necessary to mention that the dose-response studies with the LifeArc inhibitors revealed some hit compounds with structural similarity to some compounds with known targets in PubChem. These compounds work via different targets that might be potential neurotherapeutic targets for ALS therapy in the future. One of these compounds targets TRPV4 (Transient receptor potential vanilloid 4). This is a Ca^{2+} permeable receptor which shows increased

expression in various brain regions, including cerebral cortex, hippocampus, thalamus, cerebellum, and spinal cord in the SOD1G93A mouse (Lee et al., 2012). This suggests it has a role in ALS and inhibitors of it may provide a neuroprotective role in ALS. Another potential target is the neurotransmitter serotonin (5-hydroxytryptamine; 5-HT) and the 5HT2A class of receptor in particular. Serotonin is highly expressed in the raphe nuclei of the brainstem. The 5HT2A class belongs to the G-protein coupled receptor superfamily. The denervation of serotonergic inputs may lead to glutamate toxicity and loss of motor neurons in ALS, and also the disruption of serotonergic control over mesencephalic dopaminergic connections between basal ganglia nuclei and cortico-thalamic networks has been suggested to be involved in Parkinson's disease (Vermeiren et al., 2018). This highlights that serotonin receptors may be a potential target for investigating the neuroprotective agents identified in this project.

ATM kinase is the primary DNA repair kinase, and defective ATM-mediated double-strand DNA break repair has been reported as a pathological consequence of C9orf72 expansion toxicity in ALS (Walker et al., 2017). ATM kinase might therefore be a potential target for addressing genomic instability in MNDs. Another potential target that is listed is ROCK kinase which mediates microglial phenotypes. The activation of ROCK signalling is associated with the activated M1 microglia state with the increased pro-inflammatory cytokine release and decreased anti-inflammatory cytokine production (Roser et al., 2017). Lysosomal alpha-glucosidase is an enzyme that has been linked with ALS progression (Pagliardini et al., 2015). This enzyme was identified as a potential clinical biomarker of diagnosis and prognosis in ALS patients.

Interestingly two compounds that target TDP-43 were identified in PubChem, as shown in Table 4-4; these showed similar features to the hit compounds. TDP-34 is a hallmark aggregation protein in neurodegenerative diseases including ALS (Neumann et al., 2006). It would be interesting to screen more analogues of these compounds to determine whether the compounds bind or interact with TDP-43. The modulation of these targets by the hits identified will be useful to determine whether any of the hits identified work through these mechanisms in the future.

To conclude, the dose-response assays of the LifeArc library hit compounds revealed dose-dependent inhibition of neuronal stress in the *sod1*G93Ros10 zebrafish model. It also identified potential targets that may be impacted by the hits, although none of the compounds identified in the screen were structurally identical to the compounds that act on these targets, except for some overall similarity. Thus, testing of compounds known to act on the specific targets identified would help clarify whether these pathways modulate the stress readout in our zebrafish-based assay. This study also identified hits that demonstrated good drug-like properties, which can be taken forward for further pre-clinical validation studies. This demonstrates the advantages of performing screens in zebrafish as a major aspect of drug development, as it has the potential to identify drug-like molecules through rapid *in vivo* screening.

CHAPTER 5

5- Further analysis of hit and related closest structure compounds in the *sod1*G93Ros10 zebrafish model

Hypothesis: Structurally related compounds to hit compounds may show similar efficacy in reducing neuronal stress in the *sod1* G93R zebrafish model of ALS.

The primary high-throughput screen identified 214 inhibitors of the neuronal stress fluorescent readout in the *sod1*G93Ros10 zebrafish. Of these, 94 inhibitors showed a reproducible effect in the secondary screens and 13 compounds showed a good dose-response profile. We took these 13 lead hits and aimed to increase our understanding of these compounds, by focusing on their activity and screening a small library of closely structurally-related compounds.

In collaboration with LifeArc, a systematic review of the structures of the 13 hit compounds was performed; we aimed to look for common chemical motifs to identify structures to facilitate structure-activity relationship analysis.

The review from the chemists at LifeArc identified no clustering of hits to a specific common structure. This is most likely due to the relatively low number of hits (13) but also that some of the compounds were relatively poorly annotated with little known about their cellular targets. LifeArc then provided us with a small bespoke library of closely related compounds based on similarity to each of the hits. LifeArc's chemical analysis identified and provided us with 46 compounds that displayed structural similarity at grade > 0.4 and at < 0.9 (grades of structural similarity of the hit compounds to the closest structure compounds). Therefore, we screened these 46 compounds for effect on the fluorescent stress readout in sod1 zebrafish and performed dose-response experiments. We aimed to generate extra data to identify novel core structures that may help identify novel active binding sites, targets and therapies for ALS/MND.

5-1 Screening of the inhibitory hit componds and their analogues in the *sod1*G93Ros10 ALS zebrafish

LifeArc supplied 46 compounds that were the previously identified hits and their related structural analogues of > 0.5 to investigate the structural activity of the hits and analogues compounds on the fluorescent stress readout in the *sod1*G93Ros10 model. These 46 compounds were screened in triplicate at 10 µM in the *sod1*G93Ros10 model to determine their inhibitory effects on the stress readout (Table 5-1).

The screen of 46 compounds at 10 µM showed confirmation of previously identified hits, some analogues that showed no effect, and some that showed significant inhibitory activity. This suggests that some of the analogues may share a common chemical space or binding target with the original hit compound.

5-2 Dose-response study of the hit and related compounds

The concentrations used for the dose-response analysis of each chemical family was based on the effect size of the inhibition of each compound at 10 µM in the *sod1*G93Ros10 zebrafish. Hits that showed relatively strong inhibition with analogues that showed activity at 10 µM in triplicate experiments were taken forward to a dose-response analysis at higher range of doses (0.1, 0.3, 1, 3, 10 and 30 µM). The compounds that showed toxicity at 10 µM were tested for dose-response at lower doses of 0.1, 0.3, 0.5, 1, 3, 5, and 10 µM.

The dose-response study of the hits and their related closest structure compounds was to generate a signature dose profile for each family of compounds. With a dose-response profile for each family of compounds, we then aimed to identify the structure-activity relationships (SAR) of the hits and analogues, leading to further understanding of the SAR for further lead development.

Table 5-1: Percentage inhibition of the hits and the closest related structure compounds on the fluorescent stress readout in the *sod1*G93Ros10 zebrafish. Three replicate experiments were performed at 10 µM dose. Green represents the original hits; orange is the related structure compounds.

LifeArc ID compounds	Closest Hit_similarity	Inhibition% of 1st screen/10 µM	Inhibition% of 2nd screen/10 µM	Inhibition% of 3rd screen/10 µM	Average of inhibition% of 3 times screen/10 µM
MRT00202041	1	dead	45.72	dead	45.72
MRT00228648	0.75	22.00	-21.15	-24.00	-7.71
MRT00230055	0.61	-7.50	dead	dead	-7.50
MRT00203197	1	26.47	36.80	8.32	23.86
MRT00029113	0.5	-0.57	5.29	5.60	3.44
MRT00028775	0.47	dead	-0.54	19.25	9.35
MRT00022114	0.47	20.37	-4.26	-4.67	3.81
MRT00215326	1	45.84	44.13	17.45	35.80
MRT00215308	0.74	10.03	52.60	6.23	23.00
MRT00215317	0.67	-1.66	-1.82	-9.94	-4.47
MRT00200707	1	23.39	21.77	38.67	27.94
MRT00020039	0.52	11.66	32.81	18.03	20.83
MRT00201895	1	2.61	13.05	-6.81	2.94
MRT00224992	0.58	dead	dead	dead	dead
MRT00228558	0.52	dead	-14.34	dead	-14.34
MRT00186102	0.44	9.37	37.39	5.310	17.36
MRT00202788	1	29.13	dead	dead	29.13
MRT00201890	0.66	dead	dead	dead	dead
MRT00225551	0.61	16.14	-18.00	-6.86	-2.90
MRT00203050	0.55	6.20	-25.59	11.14	-2.75
MRT00231859	0.55	-4.12	-6.00	3.34	-2.22
MRT00202938	1	33.00	25.16	11.74	23.30
MRT00202994	1	46.58	15.54	dead	31.06
MRT00202426	0.63	13.82	-22.75	-2.00	-3.60
MRT00202461	1	9.74	dead	dead	9.74
MRT00202253	1	dead	39.53	dead	39.53
MRT00198109	0.7	dead	26.33	dead	26.33
MRT00222455	0.61	-10.65	19.28	-14.66	-2.01
MRT00194502	0.59	-12.67	dead	-13.07	-13.00
MRT00238721	0.56	4.58	14.52	-17.15	0.65
MRT00202123	1	33.31	44.53	10.07	29.30
MRT00261052	0.79	59.23	54.65	55.08	56.32
MRT00261262	0.71	43.46	dead	dead	43.46
MRT00259092	0.7	44.48	23.64	22.49	30.20
MRT00167967	0.68	-14.09	3.11	-12.37	-7.78
MRT00018034	0.65	12.43	19.82	6.18	12.81
MRT00010793	0.65	17.41	34.42	10.57	20.80
MRT00261211	0.62	13.90	-5.90	5.49	4.50
MRT00201744	1	67.44	dead	dead	dead
MRT00151164	0.63	13.56	12.74	-17.17	3.04
MRT00036455	0.51	-4.00	5.68	-17.14	-5.13
MRT00201527	1	20.13	35.43	-0.76	18.26
MRT00201554	0.88	dead	2.47	-7.52	-2.52
MRT00201537	0.79	9.38	-3.13	dead	3.12
MRT00201513	0.7	5.38	12.77	-27.70	-3.17
MRT00201541	0.7	-10.83	13.63	-2.32	0.15
MRT00201707	0.69	-3.55	4.00	-7.73	-2.44

For simplicity, all the hit and related closest structure compounds are referred to by the four last numbers of their LifeArc ID. Table 5-1 shows that hit compounds 3197 and 1527 confirmed their previous inhibitory effects, but none of the analogue compounds showed any effect on the fluorescent stress readout in *sod1*G93Ros10 zebrafish. Compounds 5326 and 0707 again showed reproducible inhibition, with the closest analogues (5308 and 0039, respectively) also showing a significant reduction in the DsRed signal. Therefore, the dose-response for these groups was carried out at the higher dose range (0.1-30 µM). The following compounds: 2041 and the analogue 0055, 2253 and the analogue 8109, 2788 and the analogue 1890, and 1744 and the analogue1164, were all screened at lower doses (0.1-10 µM) due to death of the treated fish at 10 µM. Compound 2123 and the analogues 1052, 1262, 9092, 8034, and 0793, showed different inhibition effects at 10 µM. The analogues 1052, 9092, 8034, and 0793 showed a higher inhibitory effect at 10 µM, while the analogue 1262 caused death of the treated fish at 10 µM. Compounds 2938, 2994, and 2461 did not have any structurally related similar compounds. Therefore, the dose-response was not performed on these hit compounds as it had previously been done. The 1895 family of compounds did not show a reduction of the fluorescent stress readout at 10 µM. Therefore, the dose-response was not performed.

5-2-1 Hit 2041 family

The dose-response study of 2041 and its analogue 0055 was performed at the lower range of doses (0.1, 0.3, 0.5, 1, 3, 5, and 10 µM) due to the death of the treated fish at 10 µM.

5-2-1-1 Dose-response study of 2041

The dose-response analysis of 2041 showed a reproducible reduction of the neuronal stress readout with an average inhibition effect of 28% at 3, 5, and 10 µM (Fig. 5-1). These results confirmed the previous reduction seen in dose-response analysis of the original hits with an average 36% and 46% at 30 µM and 20 µM respectively, in the *sod1*G93Ros10 zebrafish. It is also showed locomotor activity in light and dark environmental conditions over 4 x 5 min

cycles (Fig. 5-2). However, this fresh batch of 2041 led to a lower percentage inhibition at 3, 5 and 10 µM than before with abnormal development of the treated fish (oedema) observed at 5 and 6 dpf. It would therefore be necessary to undertake toxicity screening to ensure the drug has no toxic side effects before further pre-clinical testing.

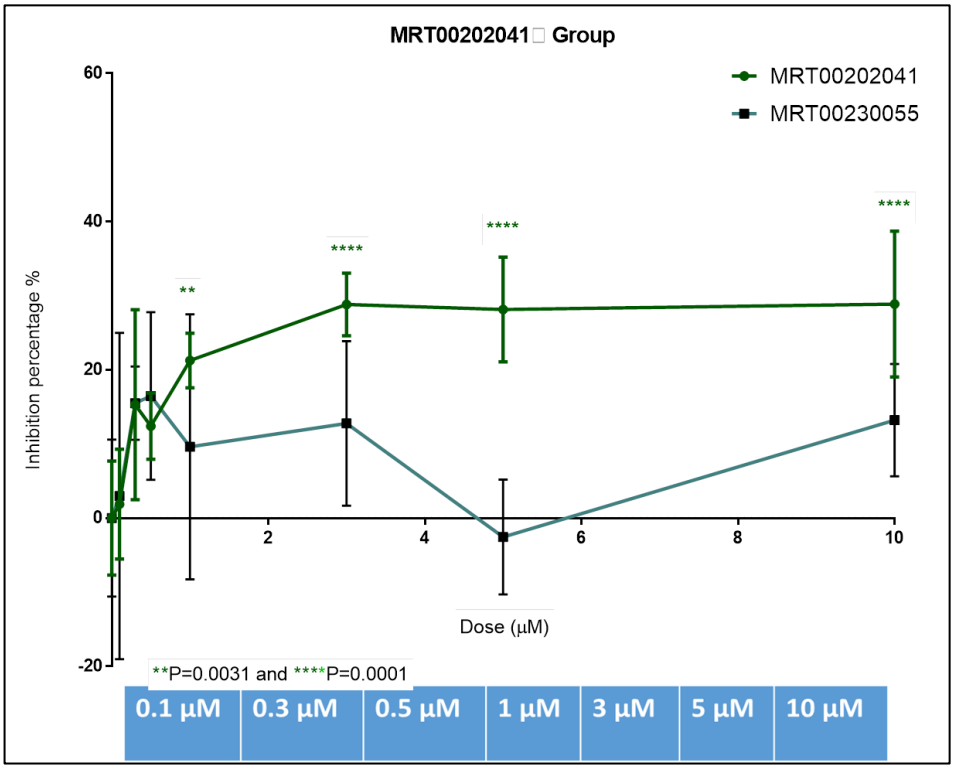

Figure 5-1: Dose-response structure-activity analysis of compound 2041 with a significant reduction of the fluorescent signal at 1, 3, 5, & 10 µM. The analogue 0055 showed a small effect on the inhibition of the DsRed signal in the *sod1*G93Ros10 zebrafish. Two-way ANOVA analysis and Dunnett's multiple comparison test was performed. N=6. The points and bars are the mean and SD.

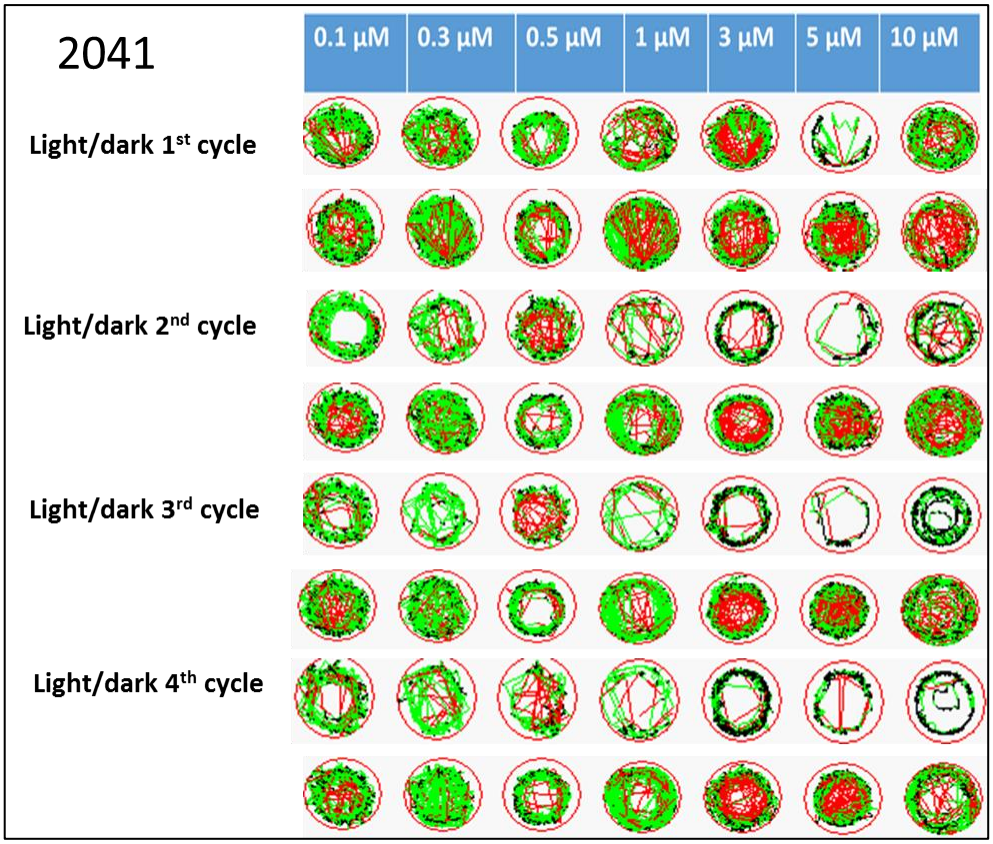

Figure 5-2: Locomotor activity of *sod1*G93Ros10 zebrafish treated with compound 2041 at doses from 0.1-10 µM in light/dark conditions. N=1 in each well.

5-2-1-2 Dose-response study of 0055, a related compound to 2041

Hit compound 2041 has two analogues that show related structure similarity scores of 0.75 and 0.61. These analogues are 8648 and 0055. The analogue 8648 did not show any reduction of neuronal stress, but it seemed to have an activation effect on the *hsp70*::DsRed stress readout at 10 µM. However, this should be confirmed before any further study. The analogue 0055 caused the death of the treated fish at 10 µM in duplicate experiments. Therefore, the dose-response study was carried out of the analogue 0055 at the lower dose range.

The dose-response analysis of compound 0055 showed a very weak reduction in fluoresence at 0.1-20 µM (Fig. 5-1). The inhibitory effect of the analogue was on average 13% at 10 µM, far lower than the original hit compound. Therefore, the dose-response analysis showed this analogue did not show efficacy similar to the hit compound.

5-2-2 Hit compound 3197 family

Compound 3197 was identified previously as the strongest inhibitory hit in the primary screen, with an average inhibition of more than 40% at 20 µM. This hit compound has three closely related analogues that have a similarity of > 0.5. The analysis of 3197 at 10 µM (3 replicates) confirmed the reduction of the neuronal stress readout in the *sod1*G93Ros10 zebrafish. However, the screening of the analogues at 10 µM (3 replicates) did not show any reduction of the DsRed signal. Hence, this family of analogues did not show similar effects to the original hit compound in the neuronal stress assay in the *sod1*G93Ros10 zebrafish at 10 µM dose. Therefore, no dose-response studies of the analogues were carried out.

5-2-3 Compound 5326 family - the most potent hit from the primary screen

Compound 5326 and related analogues were tested in triplicate at 10 µM. The hit compound 5326 showed a reduction of the DsRed signal with an average of 35.0%, which confirmed the previous studies where an average 30.3% and 38.3% was seen at 10 µM and 20 µM. Compound 5326 has two related structure compounds, with similarity scores of 0.74 and 0.67, respectively (compounds 5308 and 5317).

At 10 µM in triplicates, the analogue 5308 showed a modest inhibition of the neuronal stress readout with an average reduction of 23.0%, while the other analogue 5317 showed no reduction of the stress readout in the *sod1*G93Ros10 zebrafish (Table 5-1). Therefore, the dose-response analysis was performed with 5326 and the analogue 5308 alone.

5-2-3-1 Dose-response of the original hit compound 5326

The dose-response analysis of compound 5326 was performed at the higher doses (0.1, 0.3, 1, 3, 10 and 30 µM) because its inhibition was 35.8% at 10 µM and normal development of the treated larvae was seen.

The dose-response study of 5326 showed dose-dependent inhibition of the stress readout from 0.1-30 µM and displayed no overt sedative effect on

locomotor behaviour (Figs. 5-3 and 5-4). It showed a significant reduction in DsRed fluorescence with an average of 36.3% at 30 µM (Fig. 5-3). Normal development of the treated fish was also seen at all doses. This suggests that this drug has the potential to be a good candidate lead to progress.

5-2-3-2 Dose-response of the analogue 5308, a related structure to the hit compound 5326

The dose-response study of the analogue 5308 showed a reproducible dose-dependent reduction of the stress readout from the lower doses to the higher doses (0.1-30 µM) in duplicate screens (Fig. 5-3). Average inhibition of 22.7% and 18.2% was seen at 10 µM respectively in the two trials. At 30 µM, it showed significant inhibition with average reductions of 36.8% and 46.0% in the first and second tests (Fig. 5-3). The treated larvae displayed normal development and locomotor activity (Fig. 5-4).

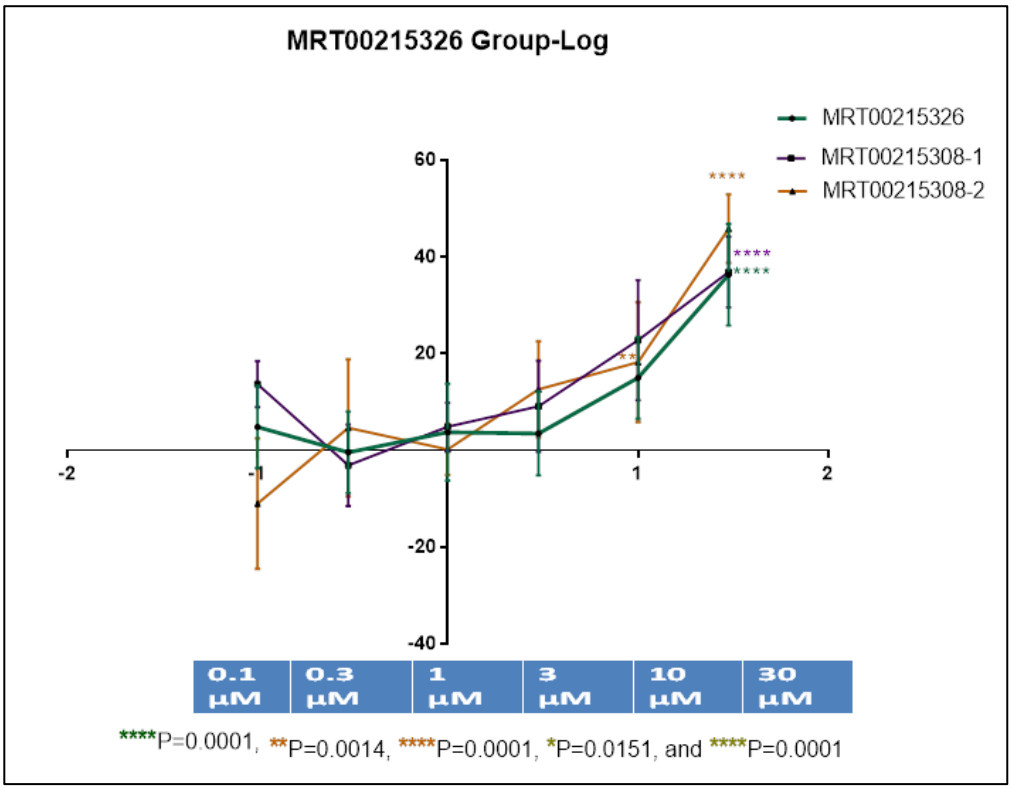

Figure 5-3: Effect on stress readout of the 5326 family compounds. Both members of this family showed a significant reduction at 30 µM. Two-way ANOVA analysis and Dunnett's multiple comparisons was performed. N=5. The points and bars are the mean and SD.

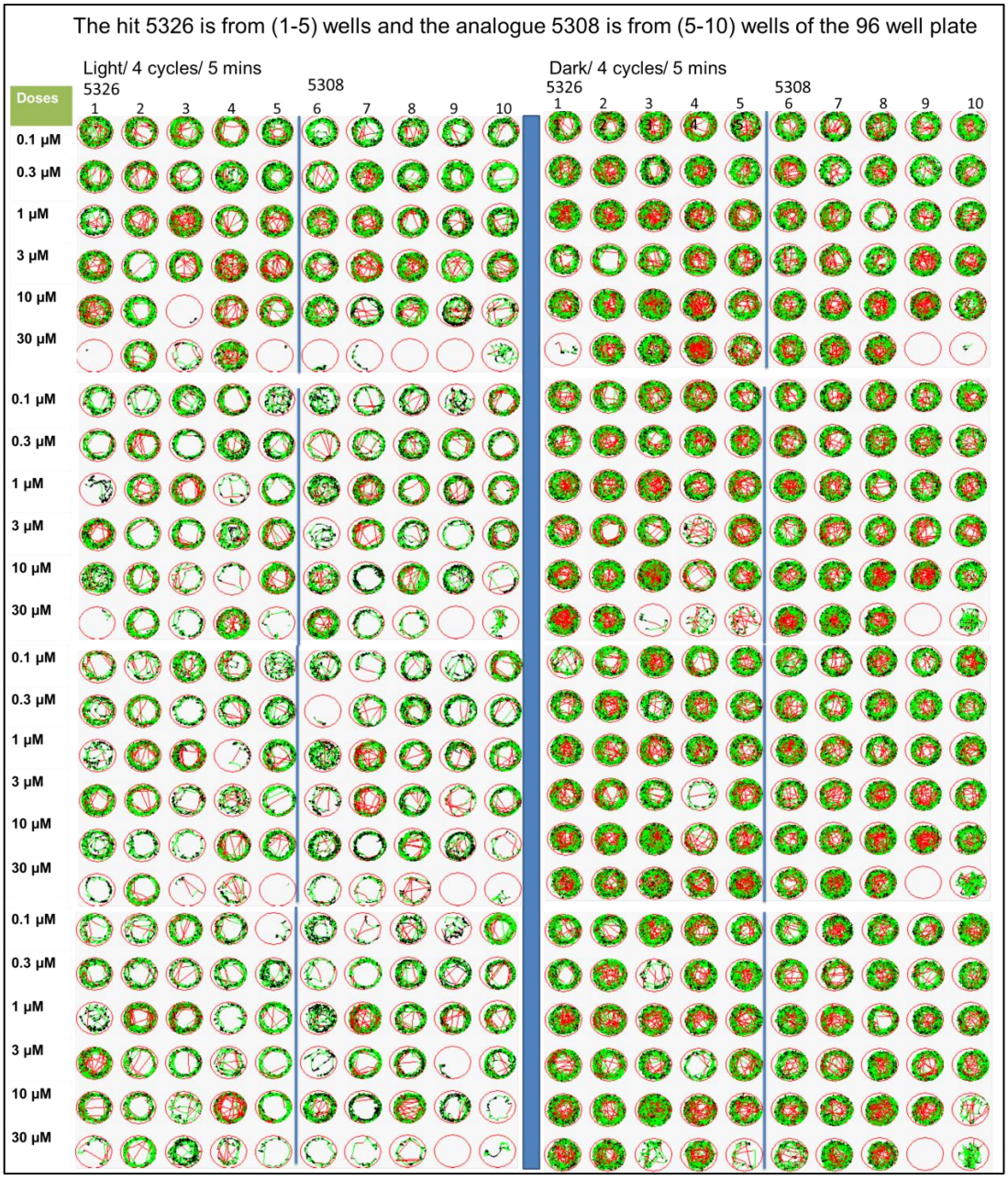

Figure 5-4: Locomotor activities of fish treated with the hit compound 5326 and its analogue 5308 at doses from 0.1-30 µM in 96 well plate format. There was no fish in the 9th well of the 30 uM row. N=1 in each well.

5-2-4 Hit compound 0707 family

The previous dose-response profile of 0707 showed reproducible reduction of the stress readout, but with some stability issues. The dose-response study with a fresh aliquot of 0707 with (3 replicates at 10 µM) showed a reproducible reduction of the neuronal stress fluorescent readout, with an average reduction of 27.9%. Normal development of embryos was seen with no obvious sedative effects (Table 5-1). This hit compound had one analogue with a similar structure score of 0.52, compound 0039. The triplicate analysis of 0039 at 10 µM showed reproducible inhibition of the stress response, with an average reduction of 20.8%, normal growth and no sedative effects.

5-2-4-1 Dose-response screen of the hit 0707

The dose-response analysis of 0707 showed a good consistent inhibition of the neuronal stress readout and had a strong dose-response profile in the *sod1*G93Ros10 zebrafish at the doses 0.1-10 µM (Fig. 5-5). It had a significant reduction in stress activity of < 20% at 10 µM and the larvae displayed normal locomotor activity (Fig. 5-6), but it caused death of the treated fish at 30 µM. This confirmed what was seen in the previous dose-response analysis, as shown in chapter 4 (Fig. 4-17).

The first dose-response analysis of the analogue 0039 showed significant inhibition from 0.1-10 µM with an average of 29.7% at 10 µM (Fig. 5-5). However, the analogue 0039 caused death of the treated fish at 30 µM, which is a similar effect to the original hit compound. Therefore, to test for dose-dependent inhibition by the analogue 0039, the repeat study was performed at lower doses of 0.1-10 µM.

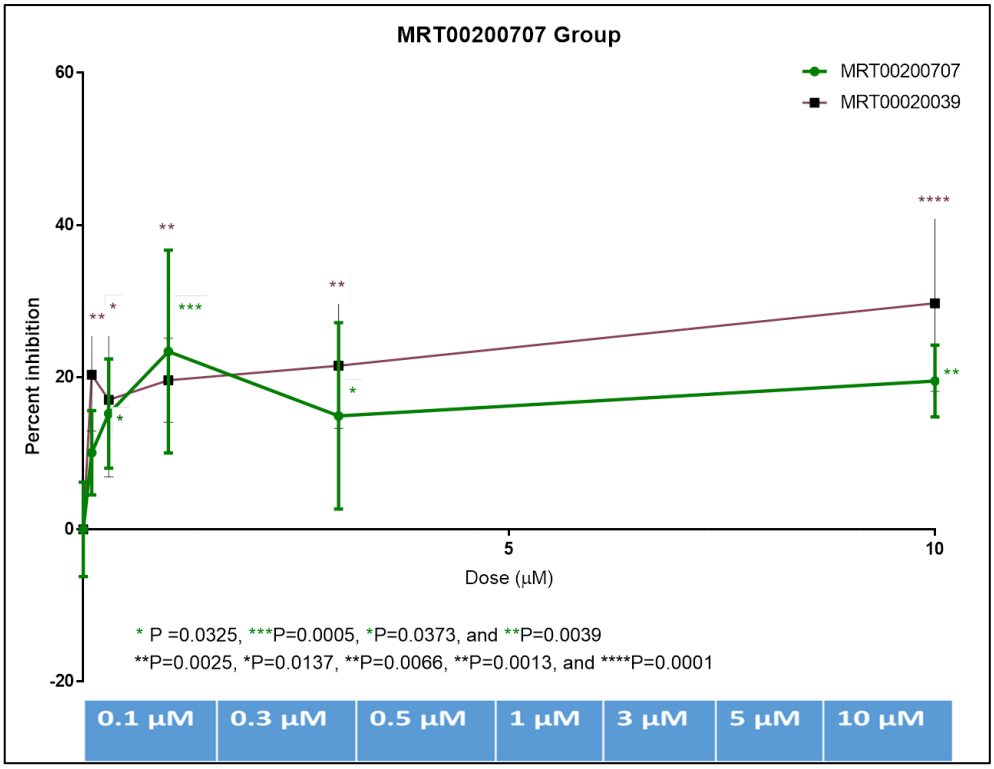

Figure 5-5: Dose-response signature profiles of the hit compound 0707 and its analogue 0039. This family showed a significant reduction of the stress fluorescent readout, but it caused death at 30 µM. The two compounds show similar reduction of the stress readout in the *sod1*G93Ros10 model. Two-way ANOVA analysis and Dunnett's multiple comparison test was performed. N=6. The points and bars are the mean and SD.

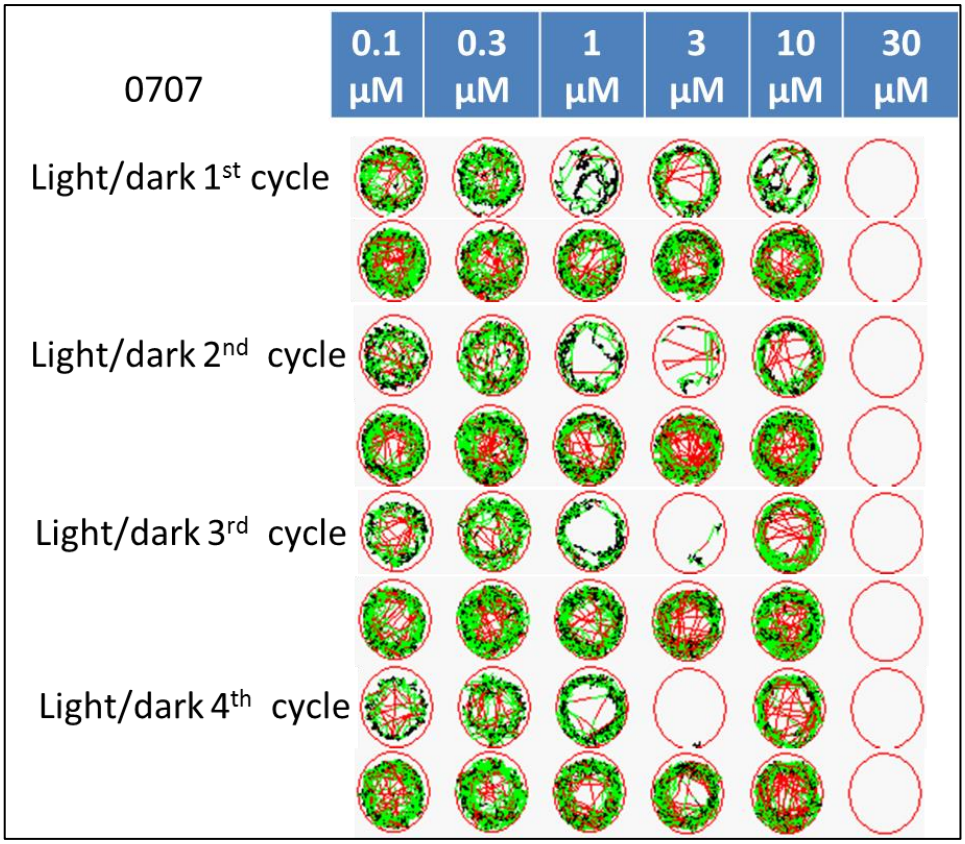

Figure 5-6: ViewPoint behaviour analysis of fish treated with 0707 at 0.1-30 µM at 6 dpf. The highest concentration of the drug was toxic. N=1 in each well.

5-2-4-2 Dose-response study of compound 0039, a closely related structure to 0707

The dose-response analysis of the analogue 0039 showed this compound gave reproducible inhibition of the stress response from the lower doses to the higher doses (0.1-10 µM). It showed significant inhibition of 19% at 5 µM, while it showed 17.4% and 42.4% inhibition at 10 µM in two separate trials respectively (Fig. 5-7). The analogue treated larvae also displayed normal locomotor activity indicating the lack of any sedative effects for this compound (Fig. 5-8).

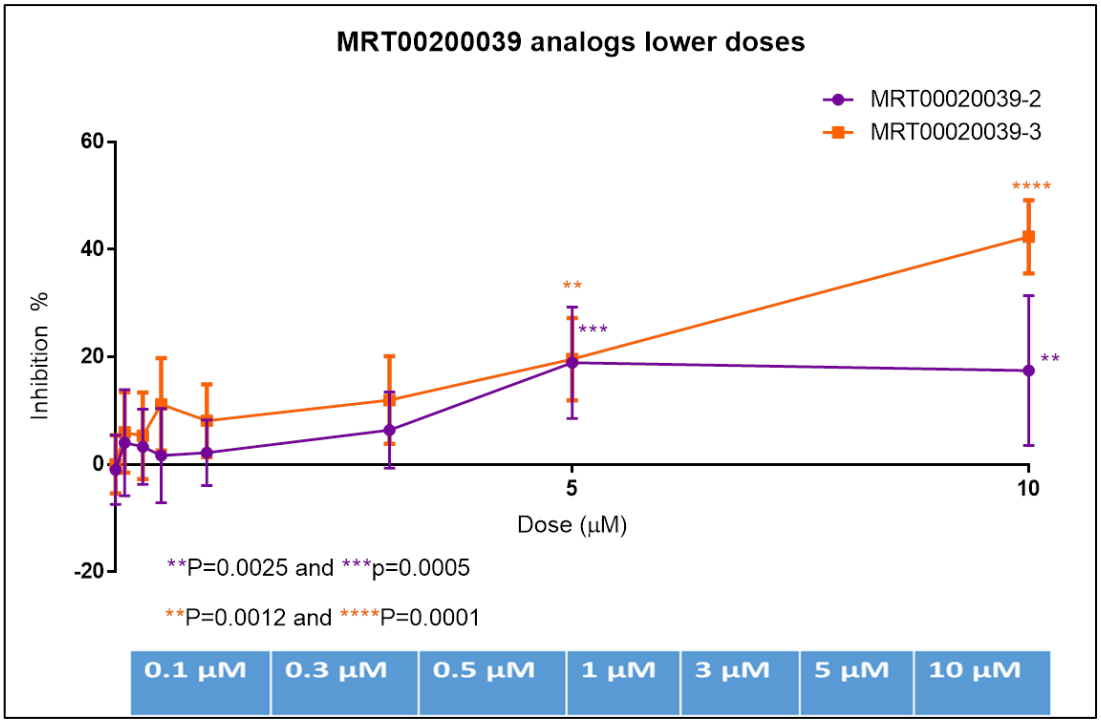

Figure 5-7: Dose-response screen of the 0707 analogue 0039 with a significant reduction in the stress readout seen at 5 and 10 µM in the *sod1*G93Ros10 model. Two-way ANOVA analysis and Dunnett's multiple comparison tests were performed. N=6. The points and bars are the mean and SD.

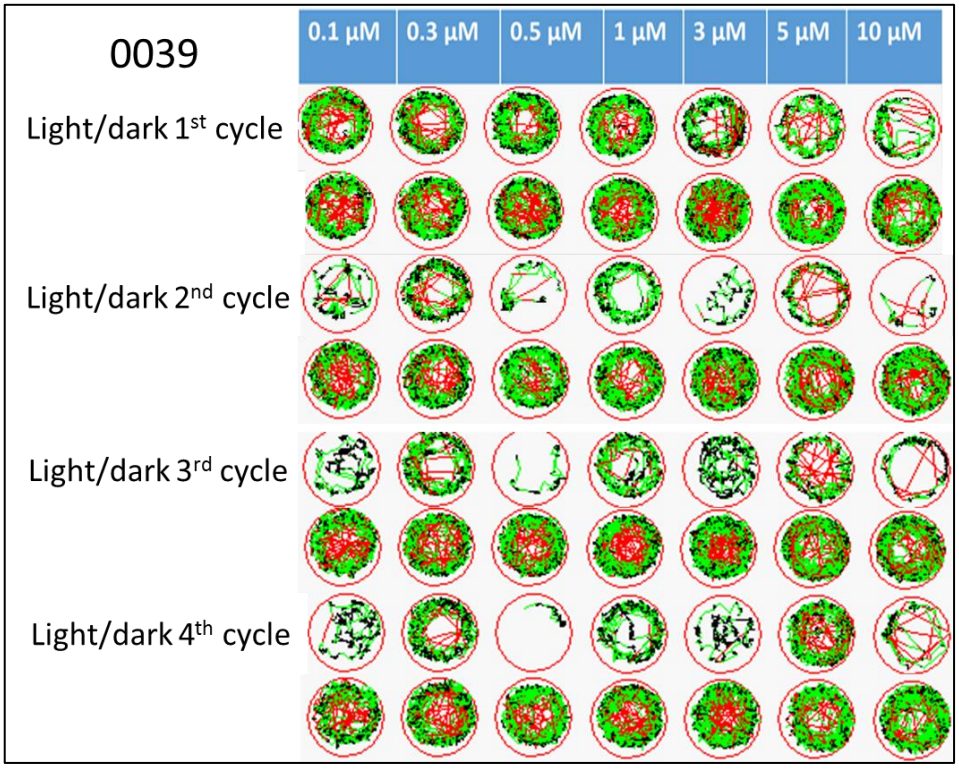

Figure 5-8: Locomotor activity of fish treated with the 0707 analogue 0039 at doses from 0.1-10 µM at 6 dpf in light/dark conditions. N=1 in each well.

5-2-5 Hit compound 2123 family

The repeat test of the hit compound 2123 with a fresh batch of drug at 10 µM showed a moderate inhibition of the neural stress readout, with an average reduction of 29.3% in the *sod1*G93Ros10 zebrafish (Table 5-1). This confirmed the reduction in DsRed signal previously shown. This hit compound had seven related structures with a similarity score of > 0.6. These compounds are 1052, 1262, 9092, 7967, 8034, 0793, and 1211. All of these compounds showed a reproducible inhibition of the stress readout except 7967 and 1211. Therefore, the dose-response study was carried out on the five analogues to investigate their dose-response characteristics.

The dose-response analysis of this family was performed at the higher doses of 0.1, 0.3, 1, 3, 10, and 30 µM the first time. In the second and third repeats, it was performed at the lower doses of 0.1, 0.3, 0.5, 1, 3, 5, and 10 µM due to the limited volume of the drugs supplied.

5-2-5-1 Dose-response study of the original hit compound 2123

The previous dose-response analysis of 2123 showed a modest inhibition effect, with the potential issue of drug stability. Dose-response assays with a fresh aliquot of drug were carried out, and confirmed a consistent inhibitory effect (Fig. 5-9). It showed reproducible effects at 0.1-30 µM with normal growth of the treated fish and a significant inhibition of the stress response at 3, 10, and 30 µM, with reductions of 23.4%, 24.6%, and 32.4% respectively. The fish treated with 2123 at 0.1-30 µM displayed normal locomotor activity (Fig. 5-10).

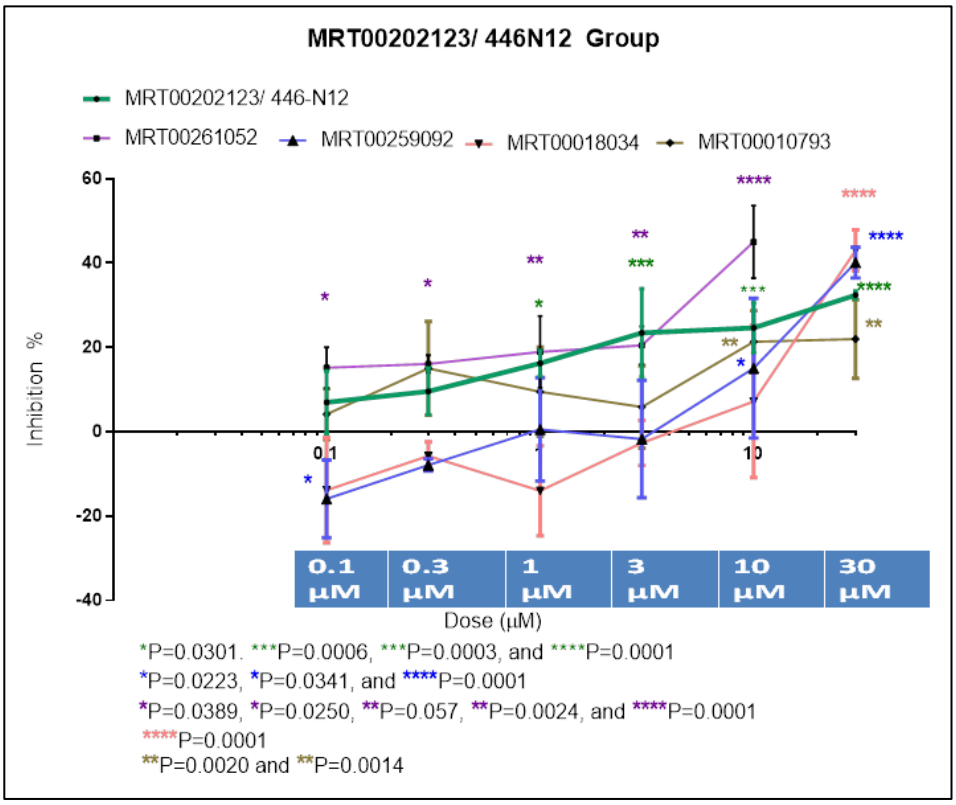

Figure 5-9: Dose-response analysis of the original hit 2123 and its closely related structure compounds. The dose-response study of this family demonstrated a similar inhibition profile across this family in the *sod1*G93Ros10 zebrafish. All the compounds in this group showed significant inhibitory effects at 30 µM. Two-way ANOVA analysis and Dunnett's multiple comparison tests were performed. N=5. The points and bars are the mean and SD.

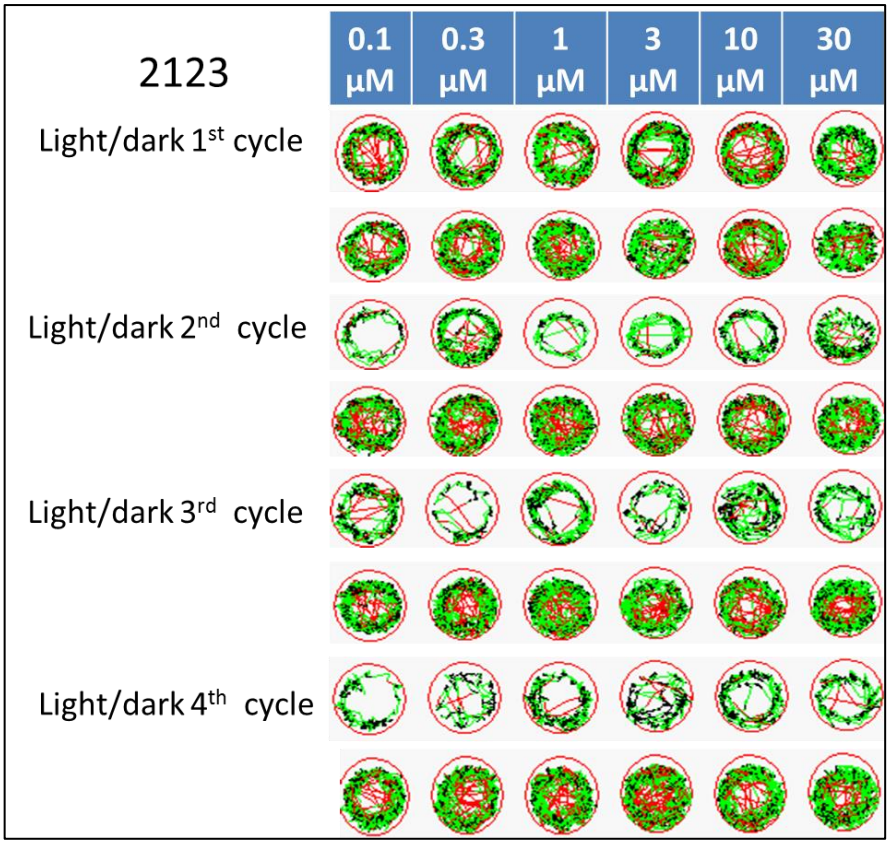

Figure 5-10: Locomotor activity of the fish treated with the original hit compound 2123 at 6 dpf in light/dark conditions (4 x 5 min. cycles).N=1 in each well.

5-2-5-2 Dose-response study for compound 1052, an analogue of hit compound 2123

The analogue 1052 has a structural similarity score of 0.79 with 2123. This analogue showed a reproducible reduction of the stress readout with an average of 56.3% at 10 µM (triplicates). Therefore, dose-response analysis for this analogue was performed at the higher concentration range (0.1-30 µM). It showed a significant lower reduction of the stress readout of 15.2%, 16.1%, 19.0%, and 20.5% at 0.1, 0.3, 1 and 3 µM doses respectively. At higher doses, the inhibition jumped to 45% at 10 µM, but with death of the treated fish observed at 30 µM (Fig. 5-9).

5-2-5-3 Dose-response study of 2123 analogue 1262

The analogue 1262 has a related closest structure similarity score of 0.71 to 2123. This compound caused death of the treated *sod1*G93Ros10 zebrafish at 10 µM (Table 5-1). Therefore, the dose-response study was carried out using the lower range of doses rather than higher doses.

The duplicate dose-response tests of 1262 showed a consistent stress reduction in the stress readout with a significant effect at 10 µM of 22.9% and 34.0%, respectively (Fig. 5-11). A third repeat showed a reduction in the stress readout of 24.7%, 37.8%, and 49.3% at 3, 5, and 10 µM respectively. However, abnormal development of some fish was seen at these doses (Fig. 5-12). Therefore, although compound 1262 displayed a dose-dependent effect on the neuronal stress readout, it may have toxicity as shown by the abnormal shape of some of the treated fish.

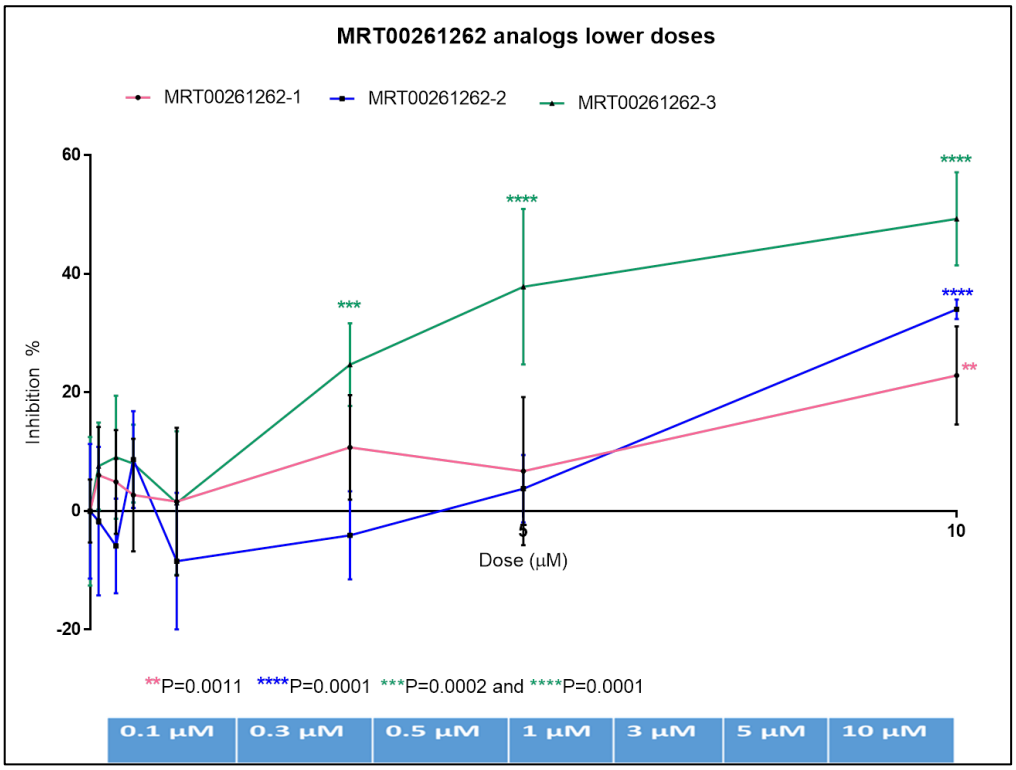

Figure 5-11: Three dose-response tests of the analogue 1262. On all occasions a significant reduction of the fluorescent stress readout was seen at 10 µM. These doses were from different batches kept them separate. N=6. The points and bars are the mean and SD.

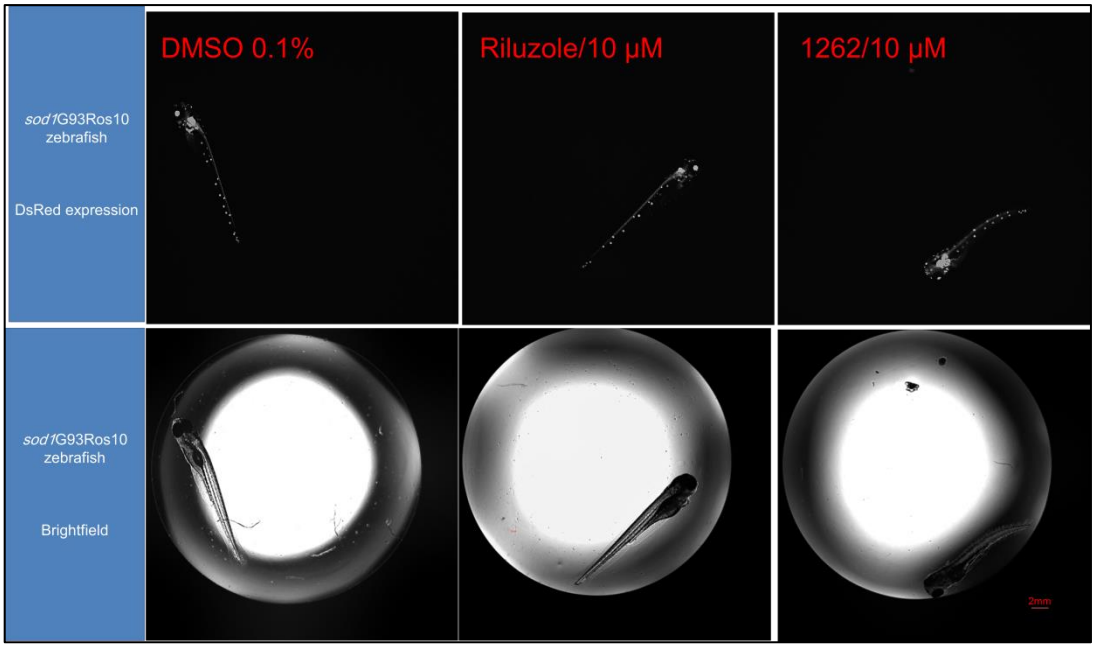

Figure 5-12: InCell imaged of an abnormal shape (a small size) of the *sod1*G93Ros10 zebrafish treated with the analogue 1262 at 10 µM compared to DMSO and riluzole treated.

5-2-5-3-1 Behavioural analysis of *sod1*G93Ros10 zebrafish treated with the 2123 analogue 1262

Daily monitoring and visual inspection of the treated fish suggested that the *sod1*G93Ros10 zebrafish treated with compound 1262 showed hyperactivity at 3 dpf and 4 dpf in response to the higher doses (3, 5, and 10 µM). When we performed the quantitative analysis of locomotor activity via the ViewPoint behavioural analysis system of the fish treated with this compound at 6 dpf, it showed that at higher doses hyperactivity was observed (Figure 5-13). When light dark analysis was conducted, this hyperactivity was more pronounced in the light conditions (Figure 5-14, 5-15) in duration and distance plots respectively. As the N are small these results and are not conclusive. Further study of this analogue is required to confirm this observation.

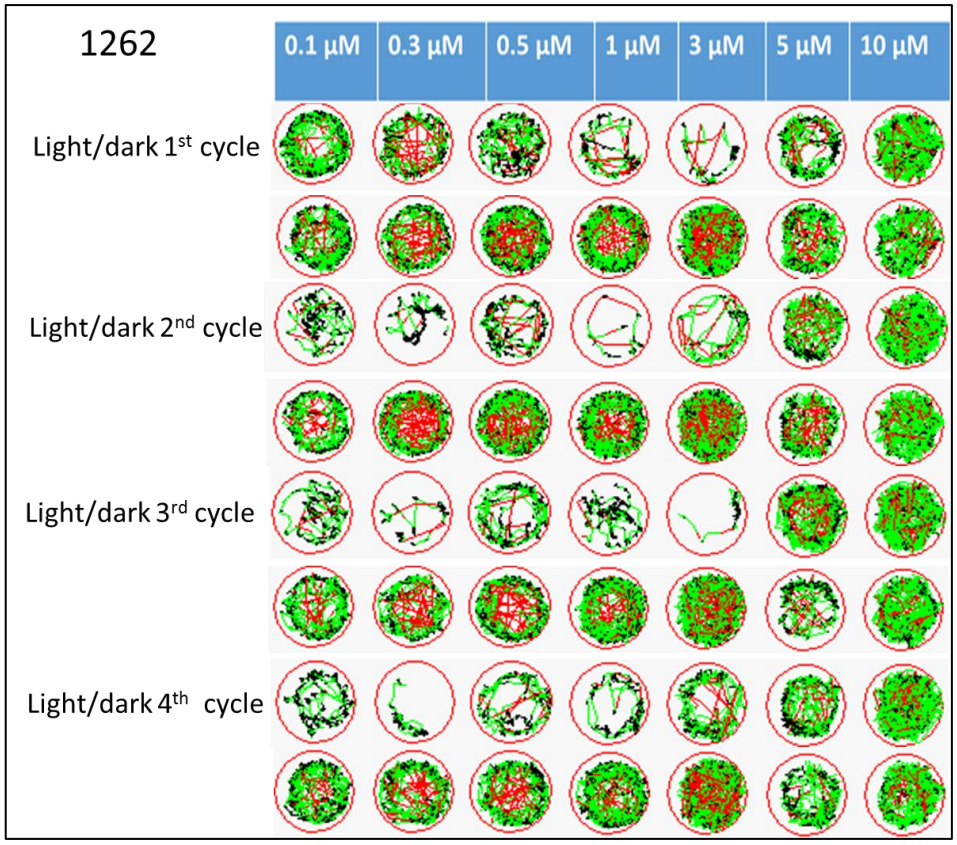

Figure 5-13: Locomotor activity of fish treated with the 1262 analogue at doses from 0.1-10 µM at 6 dpf in light/dark conditions(4 x 5 min. cycles). N=1 in each well.

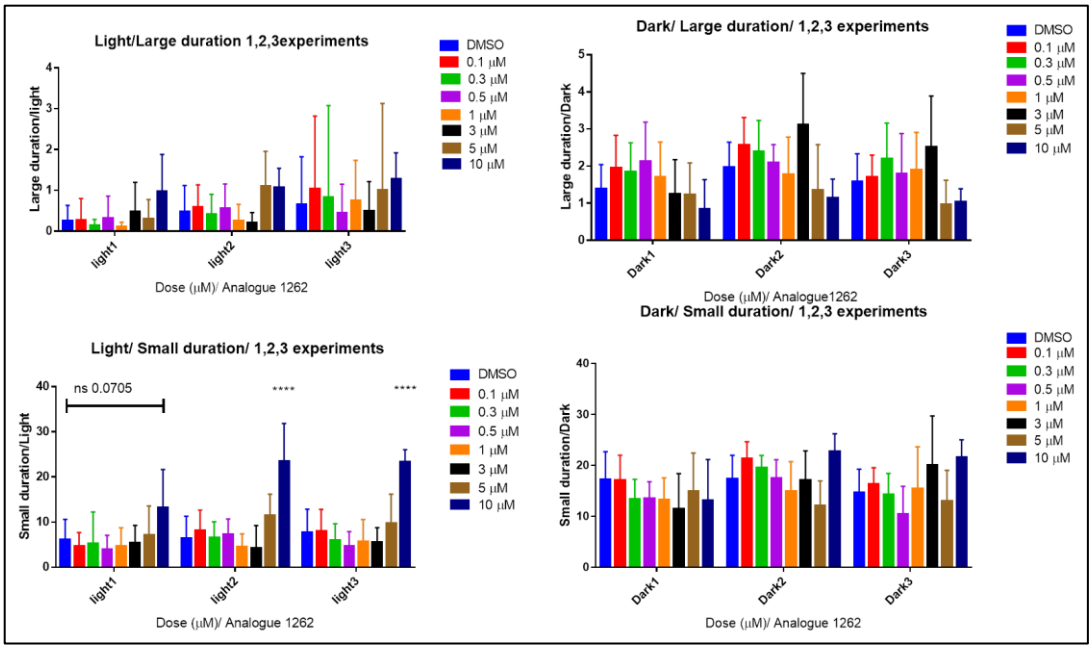

Figure 5-14: Quantitative analysis of small and large duration of *sod1*G93Ros10 zebrafish treated with 1262 treated at 10 µM. It showed in small light duration

potentially had different behavior than DMSO. Three independed experiment and further analysis is required with increased the samples. Two-way ANOVA analysis and Dunnett's multiple comparison tests. N=6. The points and bars are the mean and SD.

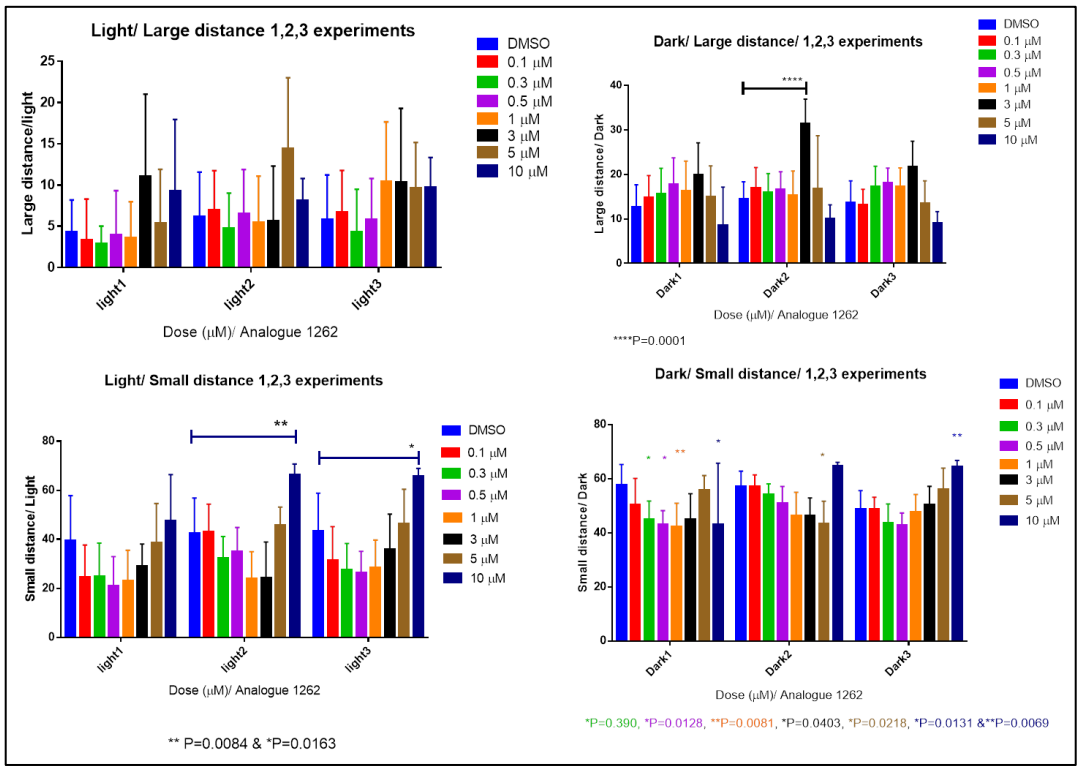

Figure 5-15: Quantitative analysis of the small and large distance of the *sod*1G93Ros10 zebrafish treated with the 1262 analogue in the light/dark cycle. We could not confirm the hyperactivity of the treated fish at 6 dpf. Two-way ANOVA analysis and Dunnett's multiple comparison tests. N=6. The points and bars are the mean and SD.

5-2-5-4 Dose-response study of the analogue 9092 a related closest structure of the original hit compound 2123

The analogue 9092 has a structural similarity score of 0.70 to the hit 2123. The screen of this analogue at 10 µM showed a reproducible reduction of the neuronal stress readout with an average of 30.20% in the *sod1*G93Ros10 zebrafish, (table 5-1). Therefore, the dose-response study of this analogue was carried out at a higher dose (0.1, 0.3, 1, 3, 10 and 30) µM.

The initial dose-response study showed that this analogue gave a dose-dependent reduction of the stress readout with significant reductions of 15.1%

and 40.1% at 10 µM and 30 µM respectively (Fig. 5-9). To confirm the effect of this analogue, the dose-response analysis was repeated again, although without the 30 µM dose to save the compound for further studies.

The lower range dose-response screen of 9092 again showed dose-dependent effects from the lower doses to the higher doses (Fig. 5-16). It showed a significant reduction at 3, 5, and 10 µM of on average 16.3%, 21.7%, and 35.6% respectively across two trials. Larvae exposed to this compound showed normal locomotor activity (Fig. 5-17).

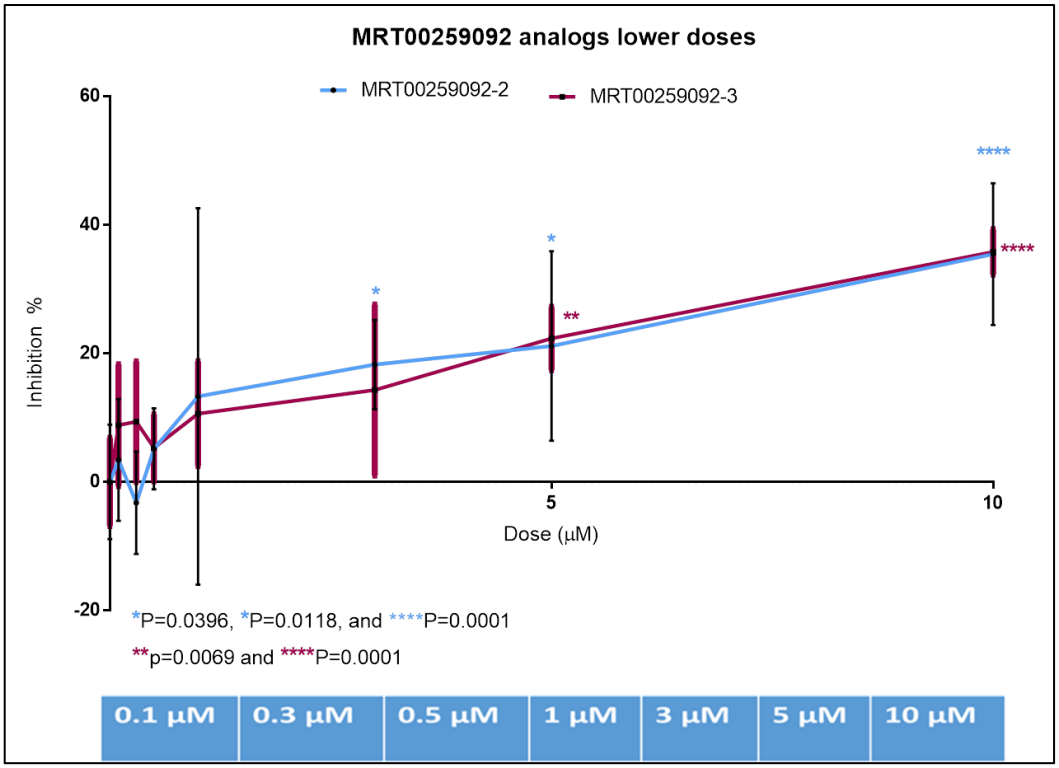

Figure 5-16: Dose-response analysis of compound 9092 on the neuronal stress assay in *sod1*G93Ros10 zebrafish. Two-way ANOVA analysis and Dunnett's multiple comparison tests were performed. N=6. The points and bars are the mean and SD.

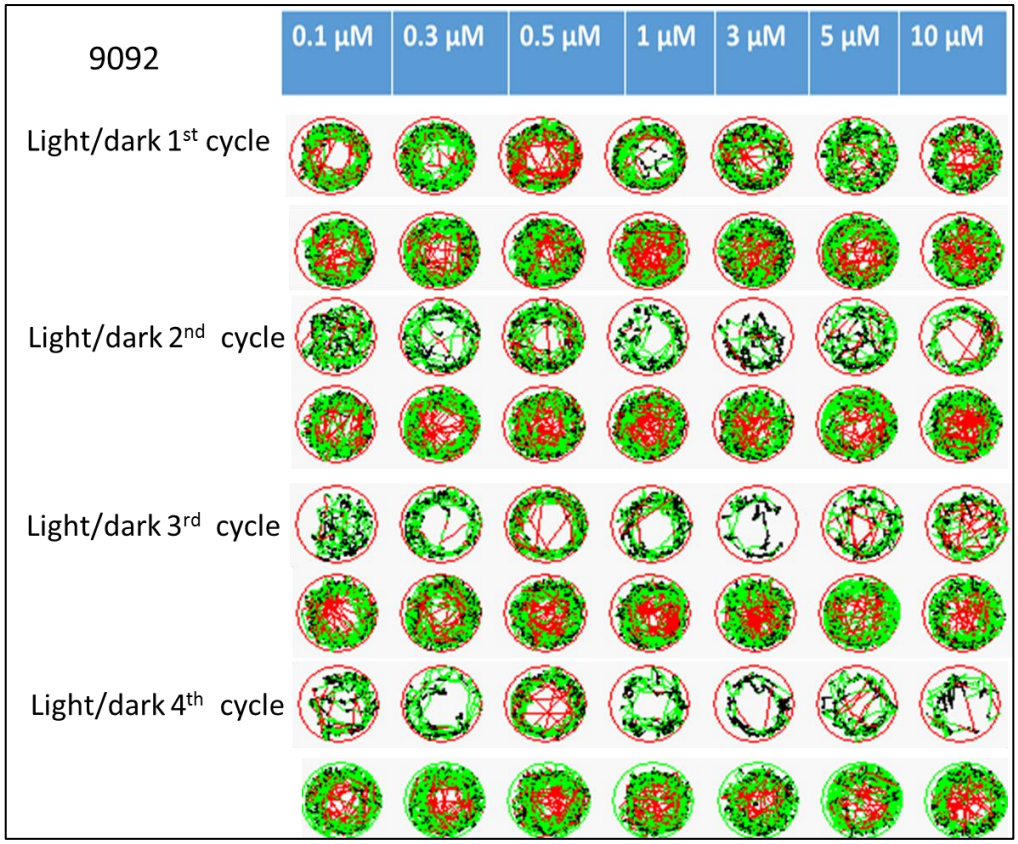

Figure 5-17: Locomotor activity of fish treated with the 2123 analogue 9092. N=1 in each well.

5-2-5-5 Dose-response study of compound 0793, a related closest structure of the original hit compound 2123

The analogue 0793 showed a structure similarity score of 0.65 to the hit compound 2123. Compound 0793 showed a reduction in the DsRed signal at 10 µM (triplicates) with an average of 20.8% in the *sod1*G93Ros10 zebrafish (Table 5-1). Dose-response analysis of this analogue was performed at 0.1-30 µM. It showed a reduction in the DsRed signal at the lower doses with > 20% reduction at 10 µM and 30 µM (Fig. 5-9).

The second and third dose-response analyses were performed at the lower range of doses (0.1, 0.3, 0.5, 1, 3, 5, and 10 µM) due to shortage of the compound. These repeat experiments showed that 0793 had little to no effect on reducing the stress response at lower doses (0.1-5 µM). It showed a potentially modest reduction at 10 µM of < 20% (Fig. 5-18), but this was not

significant. The dose-response profile of this analogue suggests this compound has at best a modest effect of reducing neuronal stress in the fluorescent readout assay at 10 µM.

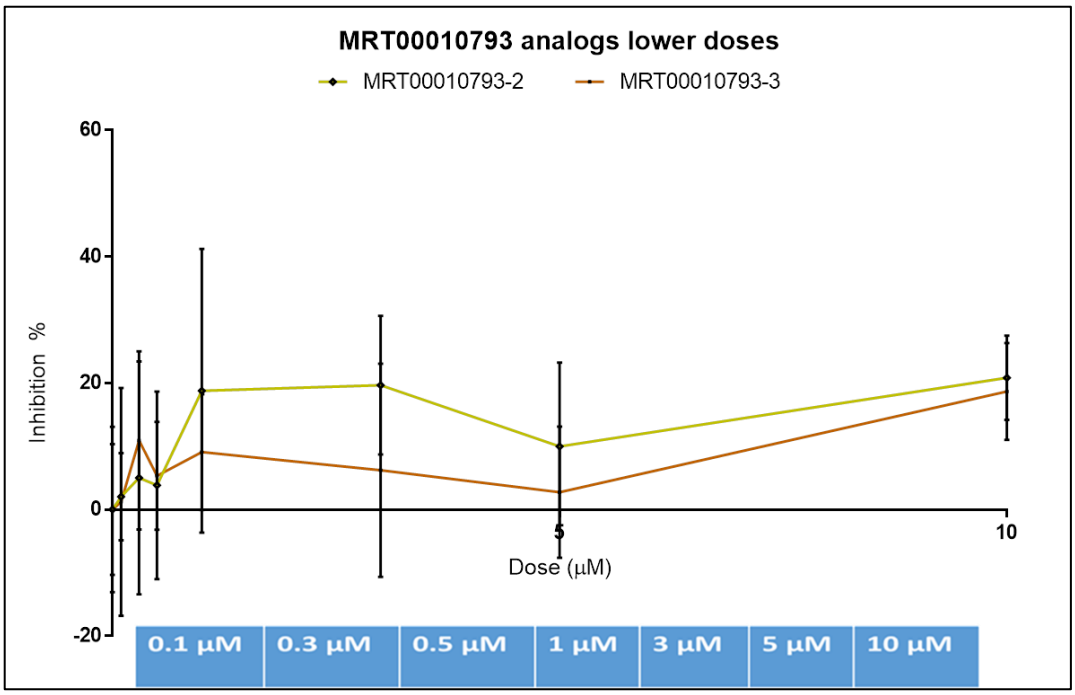

Figure 5-18: Dose-response profiles for compound 0793 in the neuronal stress assay in the *sod1*G93Ros10 zebrafish. No significant effects were observed. N=6.

5-2-5-6 Dose-response study for compound 8034, a related closest structure of compound 2123

Compound 8034 showed a structural similarity score of 0.68 to the original hit compound 2123. The earlier triplicate test of this analogue at 10 µM showed a modest inhibition with an average reduction of 12.8% in the fluorescent stress readout in the *sod1*G93Ros10 zebrafish. A dose-response study of this analogue was carried out and showed no significant inhibition of activity at 0.1-10 µM (Fig. 5-9). This analogue showed a non-significant reduction of the stress response at 10 µM of 7.17% while displaying a significant 43% inhibition at 30 µM. Thus, the analogue 8034 was excluded from further study because of its poor dose-response profile.

5-2-6 Dose-response study of the original hit compound 1744 family

The repeat analysis with a fresh batch of compound 1744 caused death of the treated fish at 10 µM and so it confirmed the toxicity of this compound at higher doses, as previously seen (Fig. 4-17).

This compound had two related closest compounds, 1164 and 6455 with structural similarity scores of 0.63 and 0.51 respectively. Compound 6455 did not show reduction of fluorescence in the DsRed neuronal stress assay at 10 µM, while the analogue 1164 showed a reduction with an average of 13.2% in duplicate tests (Table 5-1). Therefore, the dose-response study of this family of drugs was performed at the lower dose range (0.1, 0.3, 0.5, 1, 3, 5, and 10 µM).

Repeat dose-response analysis of the original hit compound 1744 showed little to no activity at 0.1-5 µM. At 10 µM, the reduction in DsRed fluorescence on this occasion was 56.8% (Fig. 5-19), although two fish of six died, suggesting some toxicity. The dose-response screen of the analogue 1164 showed no reduction in DsRed fluorescence at any dose (Fig. 5-19). Therefore, the dose-response profile of this family did not show a reproducible reduction of the fluorescent stress readout in the *sod1*G93Ros10 zebrafish. The previous dose-response screen showed it caused the death of fish treated at 20 µM (Fig. 4-17). This suggests that compound 1744 might also have a toxic effect at 10 µM giving the reduction in fluorescence.

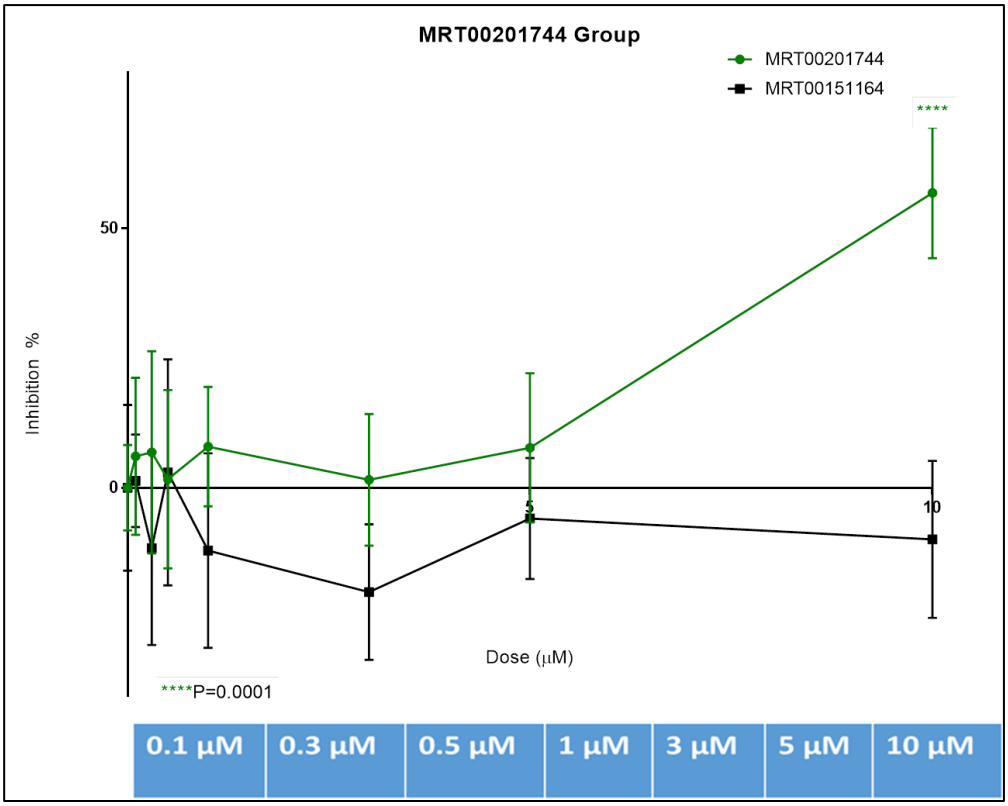

Figure 5-19: Dose-response profiles of the original hit compound 1744 and the related closest structure compound 1164 in the *sod1*G93Ros10 zebrafish. N=6. Two fish died when treated with 1744 at 10 µM. The points and bars are the mean and SD.

5-2-7 Hit compound 2253 family

The fresh aliquot of the original hit compound 2253 tested at 10 µM caused the death of the treated fish. Also, testing at 10 µM of four related closest structure compounds: 8109, 2455, 4502, and 8721 with similarity scores of 0.7, 0.61, 0.59, and 0.56 respectively; showed that the analogue 8109 caused death of the fish and the others displayed no activity. Therefore, the dose-response study was performed on the original hit compound 2253 and the related closest structure compound 8109 at lower doses (0.1-10 µM) to identify a sub-toxic dose and see if any effect on the neuronal stress readout could be detected.

5-2-7-1 Dose-response study of the hit 2253

The dose-response analysis of the original hit compound 2253 showed a reproducible dose-response profile, with low and variable reduction of the fluorescent stress readout at 0.1-1 µM and a significant reduction in the DsRed signal at 3-10 µM, with average reductions of 28.4%, 48.9%, and 46.7% respectively. However, two of six of the treated fish at 5 and 10 µM showed abnormal development (oedema). Also, the compound caused death in the previous dose-response analysis at 20 and 30 µM (Fig. 4-18, A), suggesting this compound has toxic effects at doses above 5 µM.

5-2-7-2 Dose-response study of 8109 a related closest structure compound to the hit 2253

The analogue 8109 has a structural similarity score of 0.70 to the original hit compound 2253. Testing at 10 µM of the analogue 8109 caused death of the treated fish. Therefore, the dose-response screen was performed at the lower dose range (0.1-10 µM).

The dose-response analysis of the analogue 8109 showed a variable non-significant reduction in the DsRed stress response at 0.1-0.5 µM. It showed a significant reduction at 1-10 µM with an average > 30% at 3 and 5 µM and 40.5% at 10 µM in duplicate analyses (Fig. 5-20). However, it also caused abnormal development (oedema) at 3-10 µM.

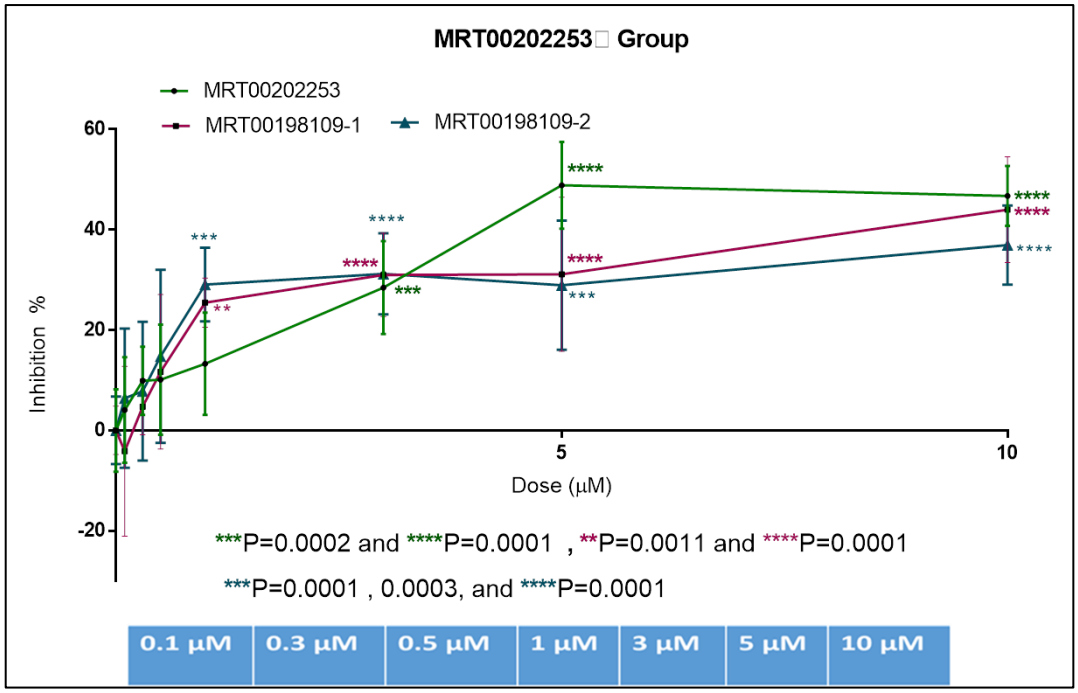

Figure 5-20: Dose-response profiles of the original hit compound 2253 and related closest structure compound 8109. The graphs show the consistent reduction in the stress readout due to this family in the *sod1*G93Ros10 zebrafish. Two-way ANOVA analysis and Dunnett's multiple comparison test was performed. N=6. The points and bars are the mean and SD.

5-2-8 Dose-response study of the original hit compound 2788 family

When the hit 2788 was screened at 10 µM in triplicate, it caused the death of the treated fish, as shown in Table 5-1. This hit compound has four related closest structure compounds: 1890, 5551, 3050, and 1859. Three of these compounds showed no reduction in the DsRed stress activity at 10 µM, the exception being compound 1890 (Table 5-1). This analogue showed the same effect as the hit compound, causing death of the treated fish at 10 µM. Therefore, the dose-response study was carried out at the lower dose range (0.1-10 µM).

The dose-response study of the original hit compound 2788 and the analogue 1890 showed that this family of compounds did not have a reproducible effect in reducing the DsRed stress activity in the *sod1*G93Ros10 zebrafish. Compound 2788 showed no reduction of the fluorescent stress readout, while the analogue had a significant reduction of the stress response at 3 µM, but it caused the death of the treated fish at 5 and 10 µM (Fig. 5-21). The dose-response profile of this family therefore does not show reproducible dose-dependent effects on the neuronal stress fluorescent readout in the *sod1*G93Ros10 zebrafish.

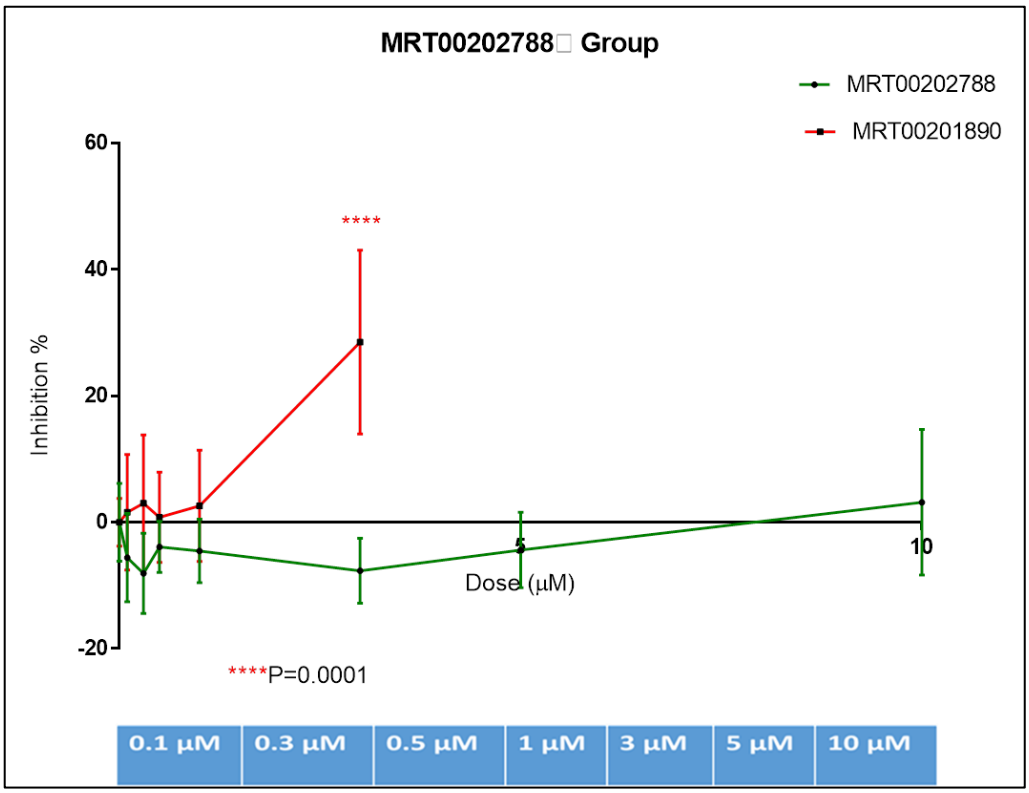

Figure 5-21: Dose-response profiles of the original hit compound 2788 and its analogue 1890 in the *sod1*G93Ros10 zebrafish. Two-way ANOVA analysis and Dunnett's multiple comparison test was performed. N=6. The points and bars are the mean and SD.

5-3 Discussion

The identification and validation of lead hits from high-throughput screening is the aim of drug discovery. To improve the quality of the identified hits and gather structure-activity relationships, we obtained structurally related compounds from LifeArc and identified compounds that modulated the stress readout in this chapter. Good structure-activity relationships obtained from analogues can be used to predict the nature of the binding of compounds to protein-ligand pockets on biological targets (Eskildsen et al., 2014; Klug et al., 2019).
The structure-activity relationship approach, in combination with proteomics, allows deconvolution of receptor-drug complexes, thereby identifying novel targets and molecules impacting on them. Therefore, in the future, by tagging the lead compounds and isolating proteins that interact with the test molecules, we will be able to understand better the targets these molecules act on.

Therefore, we tested the original hits and their analogues (46 compounds) at 10 µM in triplicate trials. This confirmed the inhibitory effect of compounds 2041 and 3197 and revealed four hit compounds (5326, 0707, 2123 and 2253) which are with their related compounds displayed a structure-activity relationship, as shown in Table 5-2.. It will be worthwhile to carry on further investigations and validation studies.

One of the most promising aspects of this part of the project was that the compounds identified by this *in vivo* screening approach displayed features that drug-like molecules exhibit. This is rare with in-silico and *in vitro* screens. The *in vivo* screen requires that the drug is bioavailable, non-degradable by enzymes that detoxify compounds, relatively safe, and CNS penetrant for CNS indications. When we examined the drug-like properties of the hit compounds, we noted that most of them have a good CNS-MPO score, which is widely used in CNS drug therapy development for assessing biodistribution properties (most show green or yellow for the biodistribution scores) (Table 5-3).

Table 5-2: Chemical structure of the hit compound families and the structure relationship neuronal stress readout of the *hsp70*-DsRed activity in the *sod1*G93Ros10 zebrafish

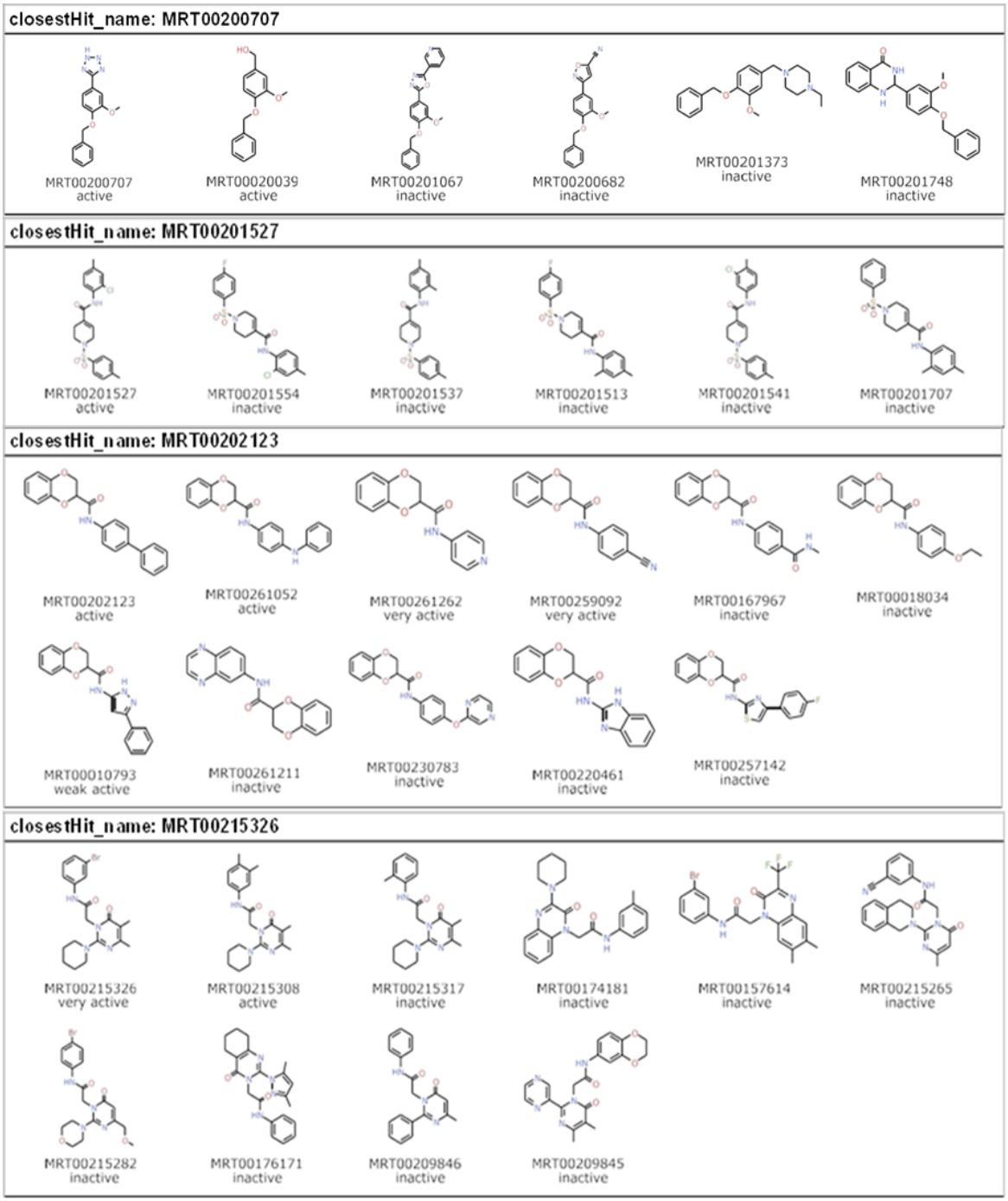

Table 5-3: The physiochemical properties of identified hit compound families.

LifeArc ID hits	iPFI	QED	CNS-MPO	MW	ACD-LogP	ACD-LogD	ACD-LogS	TPSA-NO
MRT00202041	5.55	0.6	5.5	318.3	1.55	1.55	-2.14	88
MRT00203197	4.87	0.85	5.34	371.4	2.87	2.82	-3.83	54
MRT00215326	3.79	0.82	5.01	419.3	2.79	2.79	-4.64	65
MRT00202253	4.46	0.77	5.83	349.4	1.46	1.46	-3.15	66
MRT00200707	5.75	0.78	5.83	282.3	2.75	0.79	-1.07	72
MRT00202123	6.98	0.79	4.35	331.4	3.98	3.98	-4.88	47

Although all of the hit compounds did not display cluster activity, an interesting point arising from this study is that the hit and related structure compounds showed structural-functional similarity associated with different size effects as described in the following section:

- Hit compounds 2041 and 3097 showed strong effect size on inhibition of the *hsp70*-DsRed neuronal stress readout, but the analogues of these failed to show any activity. Therefore, these compounds need investigating further with a much larger set of analogues.
- Compound 2123 and its analogue 9092 showed consistent dose-response profiles with significant modest inhibition of the stress readout at 10-30 µM. At 30 µM, the inhibition effect was on average > 30% and 40.1%, respectively. It appears that these compounds have some structure-activity relationship to warrant further dissection of the optimal structure for the largest activity.
- The most potent hit family that modulated the *hsp70*-DsRed neuronal stress is the hit compound 5326 and its analogue 5308. Both showed a significant modest inhibition effect of > 35%. These compounds also demonstrated some structure-activity relationship and further refinement of optimal structural features needs performing.
- Hit compound 2253 and its analogue 8109 also demonstrated a structure-activity relationship. These compounds showed consistent dose-response profiles in the *sod1*G93Ros10 zebrafish. They showed a significant inhibitory effect from 3-10 µM. At 10 µM, the hit compound

displayed > 45%, and the analogue displayed > 40% modulation of the neuronal stress readout. However, despite the evidence of some structure-activity relationship of these compounds, they caused abnormalities of the treated fish at 10 μM and thus the toxicity profile of other analogs needs investigating to determine whether the efficacy and toxicity seen in this family can be separated. Therefore, it is worth investigating other analogues in the future.

Therefore, it is clear that this study identified a number of hit compounds whose analogues showed activity in the zebrafish assay thus validating our hypothesis. This suggests that there is potential among these to further explore the chemical space and develop more optimal compounds. The identification of distinct structure-activity relationships greatly enhances the potential of this assay to identify and characterise molecular targets that these compounds act on. Electrophysiological studies could be utilised to determine which types of channels are modulated by the compounds and this could provide novel cellular targets leading to more understanding of ALS pathology.

In general, the chemical properties of the compounds identified in the zebrafish screen displayed a good CNS-MPO. However, compounds 3197 and 5326 displayed lower ADME properties. ADME is a recorded score of the absorption, disruption, metabolic, and excretion properties, including LogP, LogS, and LogD (shaded yellow in Table 5-3). Therefore, these potentially interesting compounds require improvement of their bioactivity profile to increase their potency and make more bio-available compounds in the future.

In summary, this chapter described the application of dose-response and structure-activity relationships to identify potential therapeutics that reduce neuronal stress and provided some preliminary data for conducting more in-depth structure-activity studies in the future. We have identified four different classes of compounds that display stress-reducing activity that show no sedative properties, potentially representing a significant improvement over riluzole. These should form the basis for developing pre-clinical leads that are superior to riluzole in the future.

CHAPTER 6

6-Testing hit compound efficacy in the *C9orf72*/$(G4C2)_{45}$ transgenic zebrafish model of ALS

Hypothesis: Compounds that show efficacy in reducing neuronal stress in the *sod1* G93R zebrafish model may show similar efficacy in a *C9orf72* zebrafish model of ALS/FTD by reducing neuronal stress and/or reducing synthesis of toxic dipeptide repeat proteins.

C9orf72 is the most common causative gene for ALS/FTD. The mutation is a hexanucleotide repeat expansion (HRE) of GGGGCC (G4C2) within an intronic region of the *C9orf72* gene. It accounts for 40% of familial ALS cases and 4-6% of sporadic ALS (DeJesus-Hernandez et al., 2011; Freibaum et al., 2015; Renton et al., 2011). As mentioned previously in the introduction, there are three proposed mechanistic hypotheses for cytotoxicity of the C9 repeat expansion. The first hypothesis is that a reduced C9 protein production leads to haploinsufficiency. The second hypothesis is that the expanded RNA has toxic properties, supported by the identification of RNA foci and the sequestration of the RNA-binding proteins into them. The third hypothesis is the production of five dipeptide repeat proteins (DPRs) from sense strand (G4C2) and antisense strand (C4G2). These DPRs are produced without a traditional AUG translation start codon but rather by repeat-associated non-AUG (RAN) translation, and these DPRs are predicted to have toxic properties via aggregation and sequestration of nuclear and cytosolic proteins (Donnelly et al., 2013; Haeusler et al., 2014; Zhang et al., 2015; Zu et al., 2013).

It also has been reported that phosphorylated TDP-43 inclusions and p62 NCI (neuronal cytoplasmic inclusions) are associated with C9 repeat expansion DPRs. However, p62 is much more abundant in neuronal cytoplasmic inclusions in the cerebellum and hippocampus than p-TDP-43 in these areas (Al-Sarraj et al., 2011; Schipper et al., 2016). Recently, glutamate and AMPA excitotoxicity have been linked with the *C9orf72* HRE expansion and may contribute to the death of motor neurons (Selvaraj et al., 2018; Westergard et al., 2019). Moreover, SOD1 inclusion in C9 patients have been reported and may suggest a crossover in mechanisms between different ALS mutations (Forsberg et al., 2019). Therefore, we hypothesised that the LifeArc library hit compounds we

identified might modulate excitotoxicity and may show activity in the *C9orf72* zebrafish model. We tested the hit compounds and related structures in the novel *C9orf72* transgenic zebrafish for effects in reducing *C9orf72*-mediated neuronal stress.

6-1 Analysis of *Hsp70*-DsRed fluorescent stress readout in the *C9orf72*/$(G4C2)_{45}$ zebrafish model

The C9 transgenic zebrafish line used is described in the methods section. The sense $(G4C2)_{45}$ transgenic line has forty-five hexanucleotide expansion repeats, which are predicted to be long enough to cause pathogenic DPR expression. These zebrafish show expression of the major DPRs, including poly-(GR), poly-(GA), and poly-(GP), and show a progressive decline in swimming performance (unpublished data).

The construct expressed in the C9 transgenic zebrafish (G4C2) is driven by a Ubiquitin (Ubi) promoter, with 45 repeats of G4C2 and a V5 epitope tag in all three reading frames to allow the detection of all sense strand-derived DPRs (Fig. 6-1). Also, the construct contains the *hsp70*-DsRed fluorescent stress readout, similar to that used in the *sod1*G93Ros10 zebrafish *in vivo* ALS model for drug screening.

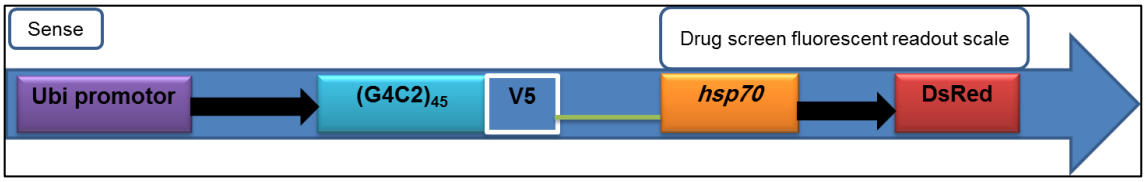

Figure 6-1: Transgene structure of the *C9orf72*/$(G4C2)_{45}$ sense strand zebrafish.

6-1-1 Effect of riluzole on the *hsp*70-DsRed fluorescent stress readout in the *C9orf72*/$(G4C2)_{45}$ zebrafish

Riluzole showed a reduction of the *hsp70*-DsRed fluorescent stress readout at 10 µM in the *C9orf72*/$(G4C2)_{45}$ zebrafish, with an average reduction of 39.2% (Fig. 6-2). The *C9orf72*/$(G4C2)_{45}$ zebrafish treated with 10 µM riluzole showed normal growth through the treatment at 2-6 dpf. Riluzole-treated fish showed

reduced locomotor activity, as was seen in the *sod1* zebrafish, due to its known sedative effects (Fig. 6-3). This suggests that excitotoxicity may play a role in the pathogenesis of *C9orf72*/$(G4C2)_{45}$ zebrafish as riluzole has been shown to have anti-excitotoxic properties (Bensimon, 1994).

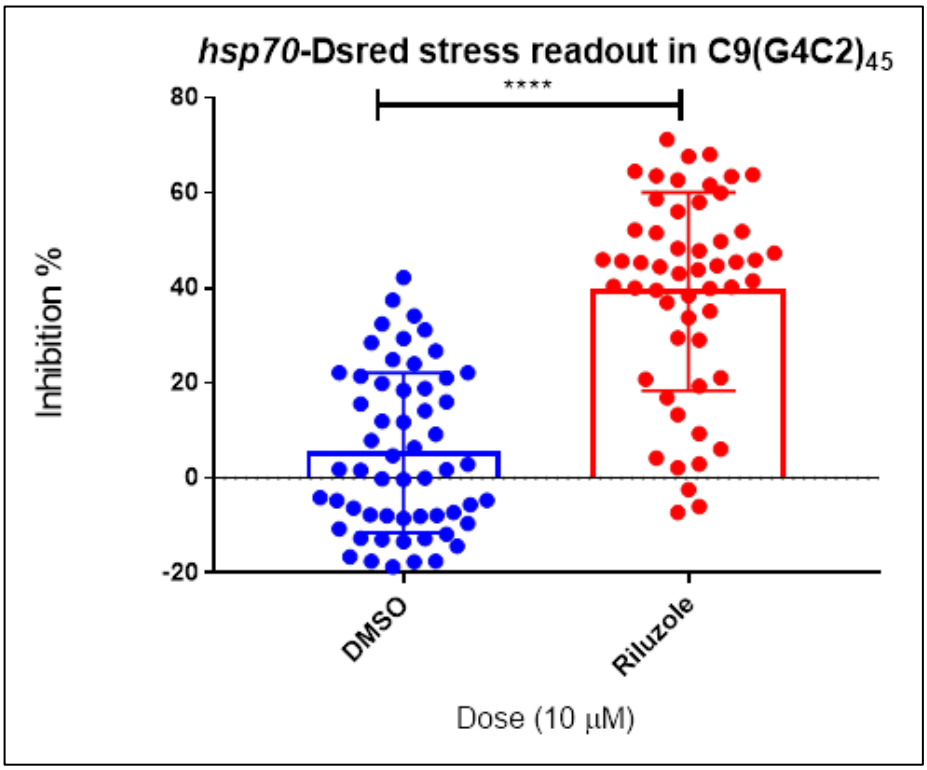

Figure 6-2: Riluzole caused a significant reduction in the *hsp70*-DsRed fluorescent stress readout at 10 µM in the *C9orf72*/$(G4C2)_{45}$ zebrafish. T-test analysis. ****P=0.0001. N=60 each. Data pooled from two independent experiments, different clutches were pooled on each occasion. Error bars represent mean ± SD.

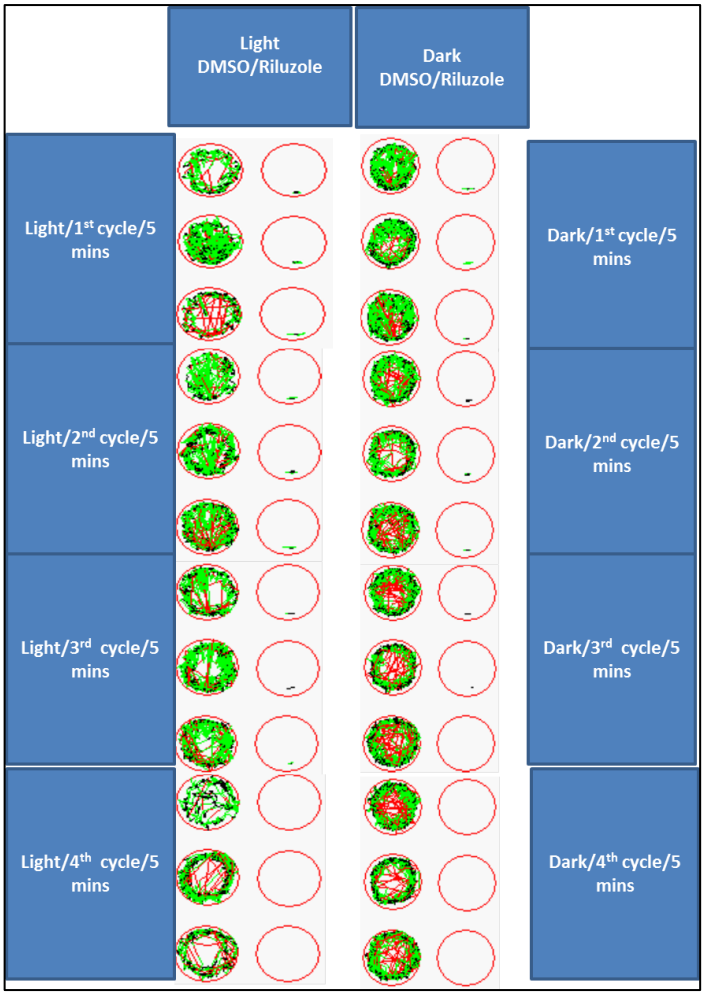

Figure 6-3: Behavioural tracking of 10 µM riluzole and DMSO-treated *C9orf72*/$(G4C2)_{45}$ zebrafish. Riluzole-treated fish show sedated behaviour compared with DMSO controls at 6 dpf. Four cycles of 5 min. light & dark exposure was used. N=1 in each well.

6-1-1-1 Images of DMSO control and riluzole-treated *C9orf72*/$(G4C2)_{45}$ zebrafish at 6 dpf

The InCell imaging system was used for imaging the *C9orf72*/$(G4C2)_{45}$ zebrafish at 6 dpf. The images of the treated fish were taken at the end of the drug exposure after the fish had been anaesthetised with MS-222. Upon visual inspection, DsRed expression in the riluzole-treated fish was lower in the hindbrain, spinal cord and muscle than in DMSO control fish (Fig. 6-4).

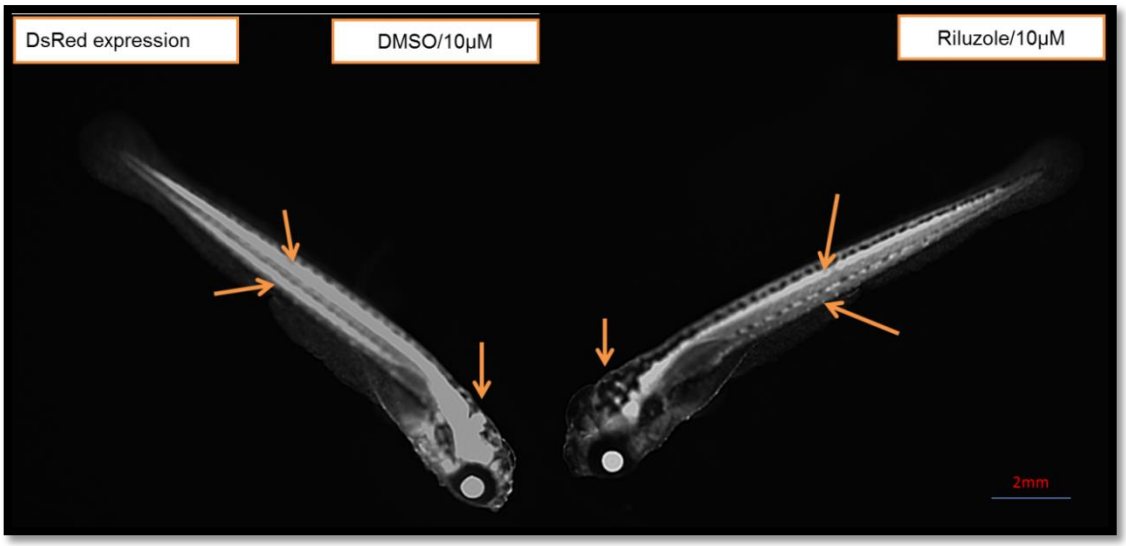

Figure 6-4: DsRed expression in 10 μM riluzole-treated *C9orf72*/$(G4C2)_{45}$ zebrafish appeared lower than in DMSO control fish at 6 dpf. Images were taken using the InCell system. Arrows indicate fluorescence in the hindbrain, spinal cord and the muscle.

6-1-2 *Hsp70*-DsRed screen of LifeArc hit compounds and structurally related compounds in the *C9orf72*/$(G4C2)_{45}$ zebrafish

The activity screen of the 46 previously identified compounds (hits and analogues) was performed at 10 μM in the *C9orf72*/$(G4C2)_{45}$ transgenic zebrafish. Embryos were exposed to the compounds at 2 dpf and culled at 6 dpf under schedule 1 procedure. This screen identified four hits that reduced neuronal stress in the *C9orf72*/$(G4C2)_{45}$ zebrafish. These compounds were 1744, 1052, 1262 and 2994, all of which showed a significant reduction in the fluorescent stress readout, with an average of 48.1%, 29.2%, 41.6%, and 31.6% respectively, compared to DMSO controls (Fig. 6-5). The fish were screened in triplicate and showed normal growth with no visible drug toxicity. However, compound 2994 showed much variability in its effect with a large standard deviation (SD), leading to its exclusion from further validation studies. Also, we noticed upon visual inspection and InCell imaging that analogue 1262-treated fish were shorter than DMSO only treated fish. This will be discussed in more detail later.

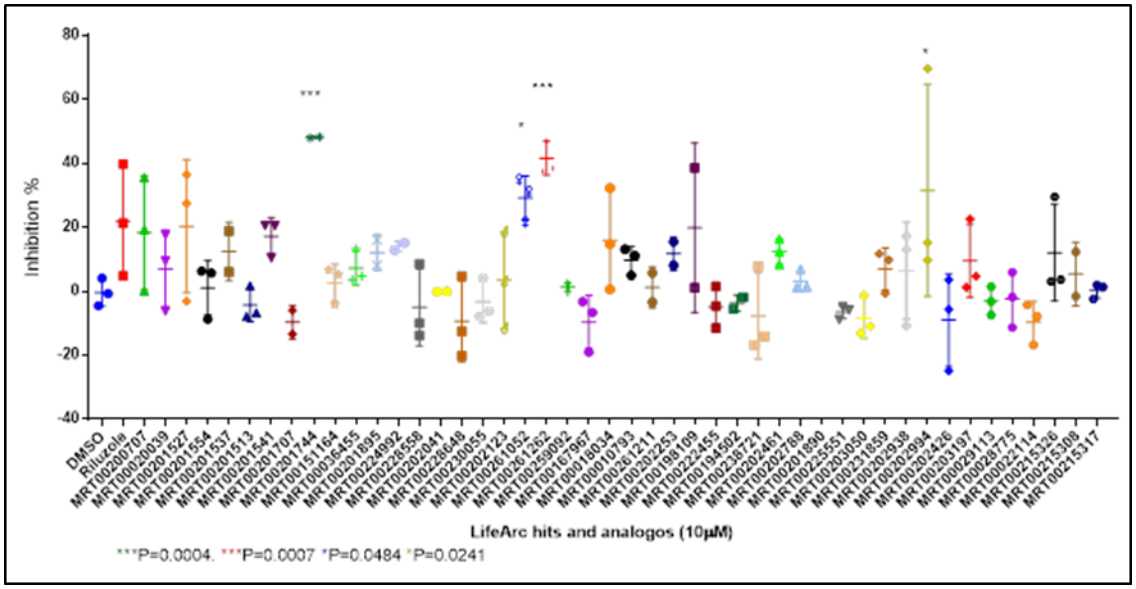

Figure 6-5: Effect of the LifeArc hit compounds and analogues on the fluorescent stress readout assay in *C9orf72*/(G4C2)$_{45}$ zebrafish. One-way ANOVA analysis was performed. N=3.

The other interesting result from assaying DsRed fluorescence in the *C9orf72*/(G4C2)$_{45}$ zebrafish was that some compounds with similar structures (i.e. hits and analogues) showed an inhibition of the stress readout. These were the hit compound 1527 and its analogue 1541, and the hit compound 0707 and its analogue 0039. 1527 and 1541 showed reductions in the stress readout of on average 20.3% and 17.2%, respectively. The hit compound 0707 and its analogue 0039 showed reduction of on average 27.4% and 7.0%, respectively. The other interesting aspect of this pair of compounds is that they showed reduction of the DsRed fluorescent readout in the *sod1*G93Ros10 zebrafish as well. This suggests 0707 and 0039 may have a shared pathological target in both *C9orf72*/(G4C2)$_{45}$ and *sod1*G93Ros10 zebrafish. To summarise, analysis of the *hsp70*-DsRed fluorescent stress readout in the *C9orf72*/(G4C2)$_{45}$ zebrafish identified a number of compounds that reduced neuronal stress in this model, including some with structure-function relationships. These compounds were selected for further investigation as they showed a robust reduction in DsRed fluorescence.

We hypothesised that one potential mechanism by which these drugs may be acting is by reducing DPR levels. Reducing DPR load may reduce toxicity, which, in turn, would lead to a reduction of the *hsp70*-DsRed readout. To answer this question, we performed western blotting for V5-tagged DPRs in treated and control zebrafish to see if we could detect an effect.

6-2 Western blot (WB) of *C9orf72*/$(G4C2)_{45}$ zebrafish treated with LifeArc hit compounds.

6-2-1 Investigation of riluzole (+ve control) and LifeArc hit compounds on DPR expression

The identified hits from the *hsp70*-DsRed fluorescent stress assay were investigated for their effects on DPR expression in the *C9orf72*/$(G4C2)_{45}$ zebrafish. This experiment was performed similar to the DsRed assay; fish were exposed to compounds from 2-6 dpf at 10 µM. Twenty-five fish were treated with each drug in 6-well plates containing 2 ml of media per well. At 6 dpf, the fish were anesthetised with MS-222 and then transgenic zebrafish (expressing *hsp70*-DsRed) were identified using the InCell high-throughput imaging microscope. The transgenic fish were then disrupted by sonication, and the proteins quantified and prepared for SDS-PAGE as described in the methods section.
In C9 zebrafish, the V5 tag is used to visualise the DPRs expression. Ribosomal protein RLP10A (L10A) was used as a reference protein. L10A levels should not be affected by drug treatment. The ratio of the V5 band signal intensity was normalised to that of L10A to quantify changes in DPR expression.

6-2-1-1 WB testing effect of riluzole treatment in *C9orf72*/$(G4C2)_{45}$ zebrafish

WB anlaysis showed that riluzole did not reduce V5-DPR levels (135% vs. 100% for DMSO control; Figs. 6-6 and 6-7). This suggests that riluzole might target other downstream cellular mechanisms in the *C9orf72*/$(G4C2)_{45}$ zebrafish as it showed 39.2% reduction in the DsRed fluorescent stress readout previously. To determine whether the fluorescence readout correlates with DsRed expression levels, western blotting of riluzole-treated embryos for DsRed expression was

performed. WB for DsRed suggested that riluzole reduced the DsRed protein expression (44.9% vs. 100% relative to DMSO control; Figs. 6-8 and 6-9).

6-2-1-2 WB to investigate effect of LifeArc hit compounds and analogues

The LifeArc hit compounds from showed distinct effects on DPR levels in the *C9orf72*/$(G4C2)_{45}$ zebrafish. Hit compound 1527 showed a significant reduction of 26.3% in V5-DPR levels when analysed across three experiments. While its analogue 1541 also appears to show a reduction in DPR levels in Fig. 6-6, the variance across three experiments led to a larger SD and precluded any statistical significance. All other compounds tested showed no apparent reduction by WB (Fig. 6-6), and no significant effects were observed for the other compounds after quantification (Fig. 6-7).

WB of *C9orf72*/$(G4C2)_{45}$ zebrafish for DsRed expression, however, showed a significant reduction in fish treated with 0707, 1052, 1527, 1541 and 1262 of 37.12%, 36.4%, 33.4%, 26.0%, and 23.8% respectively, despite the variability observed between samples (Figs. 6-8 and 6-9). The other compounds, 0039 and 1744, did not show a significant reduction in DsRed levels by WB, but the DMSO control samples showed a large variance which decreased the statistical power of the analysis. With an increase in the number of samples analysed, the statistical analysis could be more reflective of actual differences. The fluorescent readout of DsRed expression obtained using the PheraStar gives a far more accurate quantitative measure than ECL western blotting.

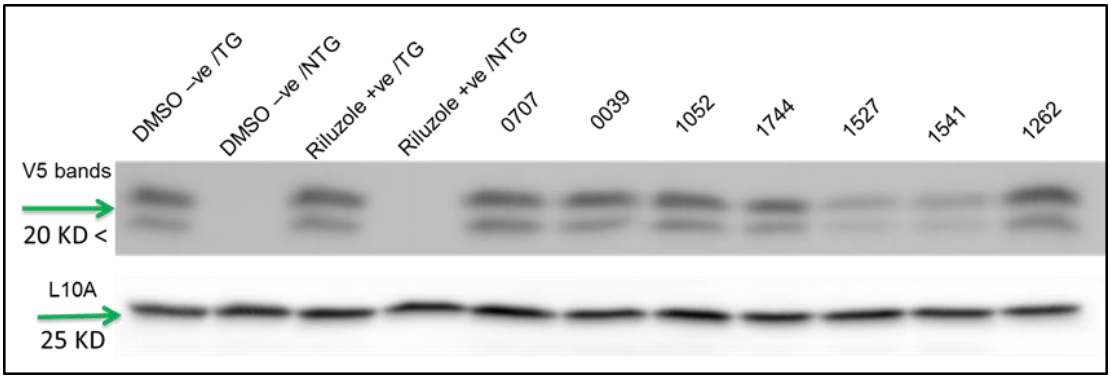

Figure 6-6: Representative WB of the V5-tagged DPRs and L10A in the *C9orf72*/(G4C2)$_{45}$ zebrafish. No V5 signal is seen in the NTG zebrafish extracts. Hit compound 1527 and its analogue 1541 show reduced levels of V5-DPR expression. Drug exposure was from 2-6 dpf. Each blot = 23±2 pooled embryos.

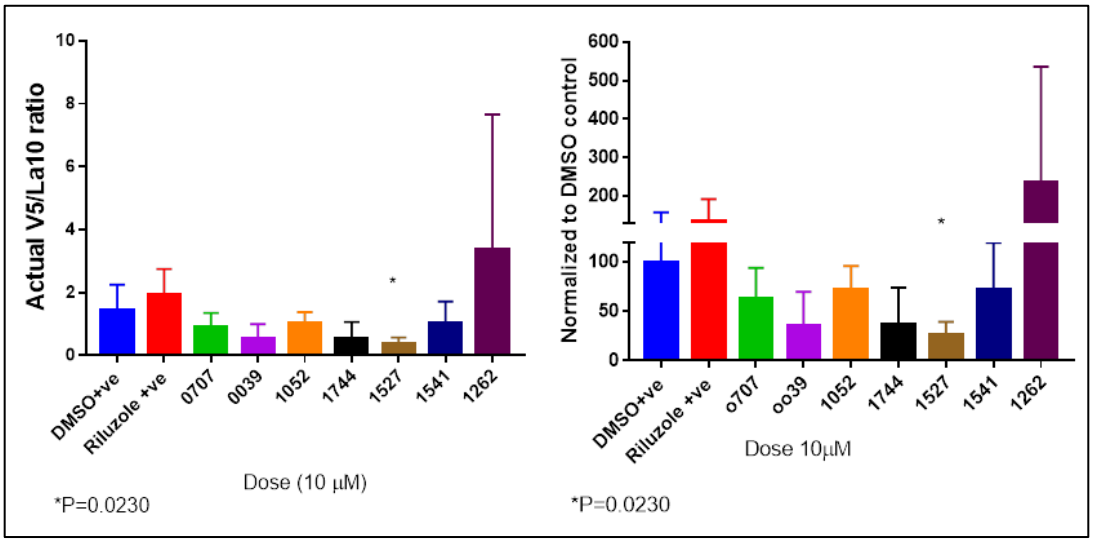

Figure 6-7: WB quantification. Raw V5/L10A ratio and data normalised to DMSO control shown. Significant reduction of V5-DPRs is seen in *C9orf72*/(G4C2)$_{45}$ zebrafish treated with hit compound 1527. T-test analysis of 3 independent repeats; 23±2 pooled embryos per condition. *p<0.05

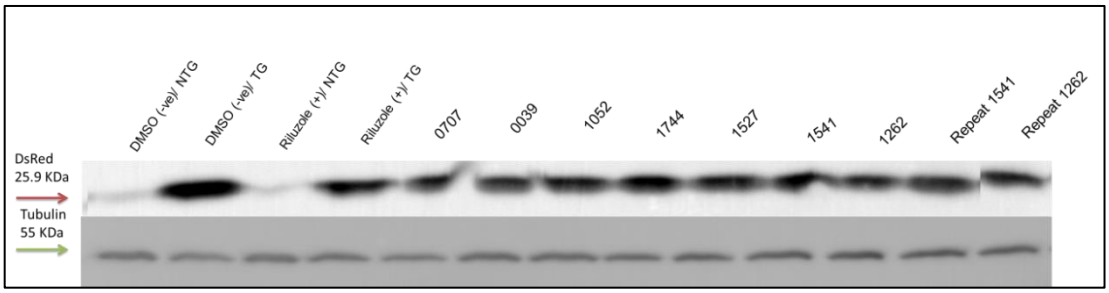

Figure 6-8: WB for DsRed and tubulin expression in the *C9orf72*/$(G4C2)_{45}$ zebrafish. No DsRed expression is seen in NTG zebrafish. Drug exposure was from 2-6 dpf. 23±2 embryos pooled per treatment.

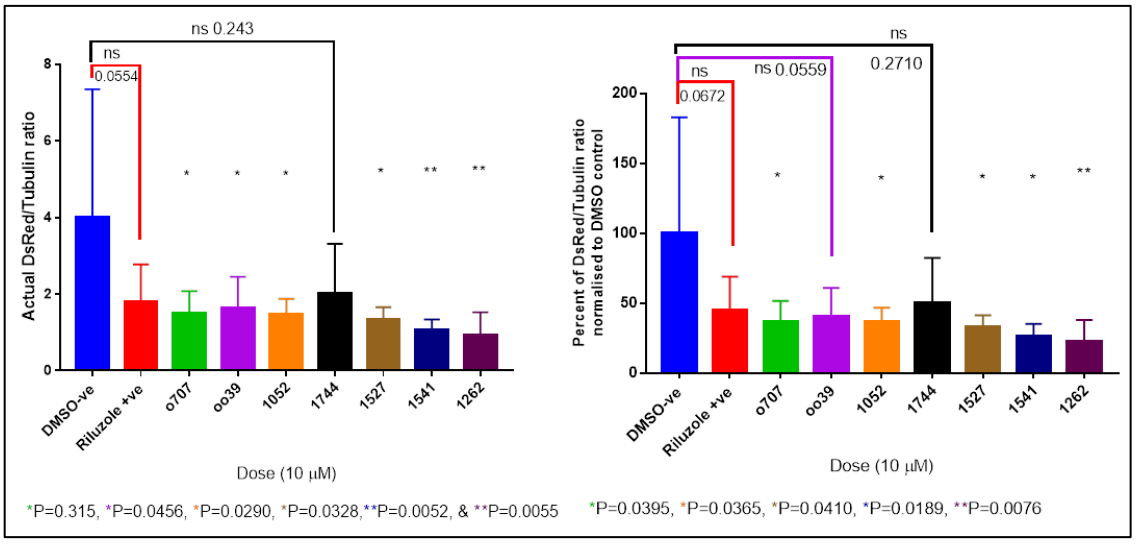

Figure 6-9: Shows the actual DsRed/Tubulin ratio and normalised to DMSO in the C9$(G4C2)_{45}$ zebrafish at 6 dpf. Three trials. DMSO showed that a big SD leads to an effect on normalised DsRed/Tubulin in each sample. One-way ANOVA analysis and Dunnett's multiple comparisons test. *p<0.05, **p<0.01

6-2-1-3 Potential DPR upregulating activity of LifeArc compound 1262 in *C9orf72*/(G4C2)$_{45}$ zebrafish

Western blotting of *C9orf72*/(G4C2)$_{45}$ extracts from fish treated with compound 1262 suggested a possible increase in V5-DPR expression compared to DMSO (235% compared to DMSO; Figs. 6-6 and 6-7), although this difference was not statistically significant and needs confirmation by further analysis. Interestingly phenoytpic monitoring of *C9orf72*/(G4C2)$_{45}$ zebrafish treated with 10 µM compound 1262 throughout the treatment window suggested visible hyperactivity in treated larvae at 2 and 3 dpf. Similar observations were made when *sod1* zebrafish were treated with high doses (3, 5, and 10 µM) of this compound. Unfortunately, we could not confirm hyperactivity quantitatively via the ViewPoint behavioural analysis system because we did not have sufficient volume of the drug to perform this study with large samples (25) of *C9orf72*/(G4C2)$_{45}$ treated fish. However, upon visual monitoring, we noticed that the treated larvae had lower locomotor activity compared to DMSO treated fish at 6dpf. This was noticed as well in the *sod1*G93Ros10 zebrafish (see dose-response analysis of sod1 zebrafish treated with 1262 in Chapter 5). This suggests that a detailed behavioural analysis study should be considered with 1262 treated embryos from 2 dpf to 6 dpf to confirm the effects on locomotor activity in the future.

Although compound 1262 gave a reduction in DsRed fluorescence in *C9orf72*/(G4C2)$_{45}$ zebrafish, the larvae showed morphological abnormalities when compared to DMSO control and riluzole-treated fish (Fig. 6-10). This was seen in *sod1*G93Ros10 zebrafish as well. This might be an indicator of toxicity occurring and may explain the tentative observation of higher DPR levels in the treated *C9orf72*/(G4C2)$_{45}$ fish. Exploration of mutant sod1 aggregation in the *sod1*G93R zebrafish model would highlight whether this compound modulates protein misfolding or not.

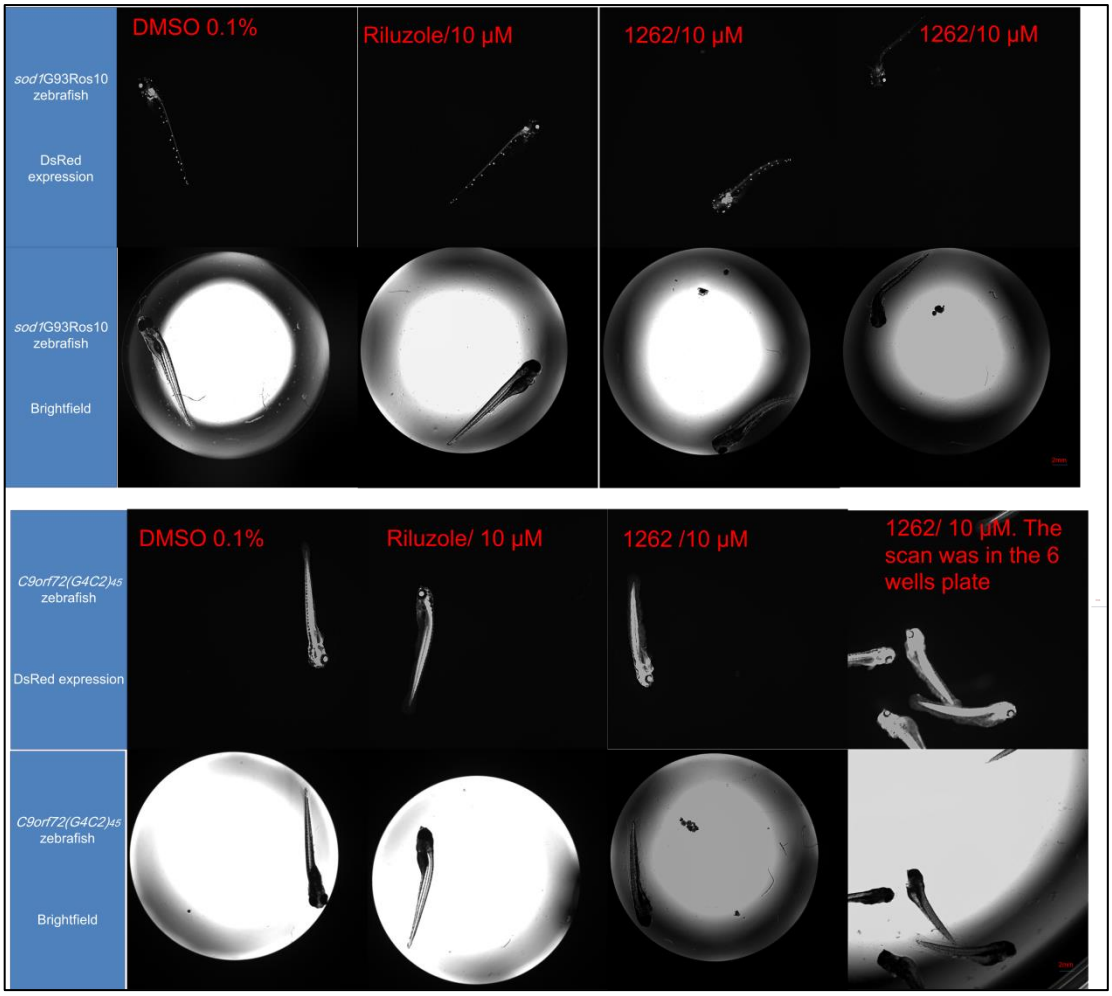

Figure 6-10: InCell imaging demonstrating abnormal growth of *sod1*G93Ros10 and *C9orf72*/$(G4C2)_{45}$ zebrafish treated with 1262 compared to DMSO control and riluzole-treated larvae at 6 dpf. The curvature of the body is seen in many of the treated fish. With 96-well plate, n=1 larva per well. With 6-well plates, n= 25 per well. The scanning of the 6-well plates was performed by dividing each well into 20 sectors.

To summarise, the significant attenuation of DPR levels by compound 1527 in treated zebrafish is potentially very interesting as it was accompanied by a significant reduction in DsRed levels. Compound 1527 and its analogue 1541 merit further investigation to determine whether this family of compounds has an effect on DPR levels. Further exploration of this chemical space would be necessary for the further development of this class of compounds. It may be worth investigating these compounds in the SOD1G93A and C9orf72 mouse models to validate their efficacy on disease processes.

6-3 Development of a *C9orf72*/$(G4C2)_{45}$ high-throughput screen:

6-3-1 Dot blot drug development screen

The dot blot provides a high-throughput, reproducible, rapid, and cheap method to detect proteins. It is limited when compared to western blotting as the molecular size of the proteins in samples is not differentiated. Therefore, high levels of non-specific background staining in samples limit the utility of dot blotting. The advantages and disadvantages of dot blotting and WB are listed in Table 6-1. If an antibody is highly specific it will serve as a useful high-throughput screening tool with faster screening time (Zhang et al., 2019) as samples are directly applied to membranes without electrophoresis and transfer steps in a multi-well plate format (Renart and Martinez, 1996).

With the validation of the V5 antibody to detect V5-DPRs from western blotting, we began developing a novel DPR-based drug screen in the *C9orf72*/ zebrafish using both sense and anti-sense transgenic lines ($(G4C2)_{45}$ and $(C4G2)_{39}$) starting from 2 to 5 dpf. We aimed to identify compounds that modulate DPR levels using the dot blot method.

Table (6-1): The advantages and disadvantages of dot blot & WB procedures

Features	Dot blot	Western blot (WB)	Advantages	Disadvantages
Applying protein	Direct adsorb onto the membrane by filtration method via a vacuum champer	Indirect by using (SDS-PAGE) electrophoresis gels and then transfer onto membrane	Dot blot	WB
Resolving protein	Not applicable.	Resolving of the proteins depending on the molecular size by employing the polyacrylamide concentration and gel running buffer (SDS & Tris-glycine)	WB	Dot blot
Ladder protein	Not applicable	Applicable	WB	Dot blot
Cost	Cheapest	Expensive	Dot blot	WB
Employ	Quantitative and qualitative study for analysis of large similar samples. High-throughput rapid screen. Designing for suitable of the parameter before proceeding to a advance analysis.	Quantitative study for small similar samples. For more advance process (a validation study).	Dot blot & WB	WB
Time	Shorter	Longer	Dot blot	WB
Sensitivity	Higher sensitivity	Lower sensitivity than dot blot	Dot blot	WB
Membrane	PVDF & Nitrocellulose	PVDF	Dot blot	WB
The number of the samples	Lower number of the samples (one fish or two fish)	Large number of the samples (>20 fish)	Dot blot	WB
Detective protein	Higher detective protein, but it uses a large volume of the samples.	Higher detective proteins with a small volume of the samples	WB	Dot blot
Variability	Higher as it is a direct applied on the membrane.	Lower variability, but the bands are sensitive for any wrong steps.	WB	Dot blot

6-3-2 Transgenic C9orf72 zebrafish

As described in the methods section, the *C9orf72* sense $(G4C2)_{45}$ and anti-sense $(C4G2)_{39}$ transgenic zebrafish used to develop the dot blot drug screen. The V5-tagged DPRs expressed in sense $(G4C2)_{45}$ zebrafish are poly-(GR), -(GA) and –(GP), while the anti-sense $(C4G2)_{39}$ zebrafish show V5-tagged poly-(PA), -(PR) and –(GP) expression. The transgene constructs for both transgenic lines are shown in Fig 6-11.

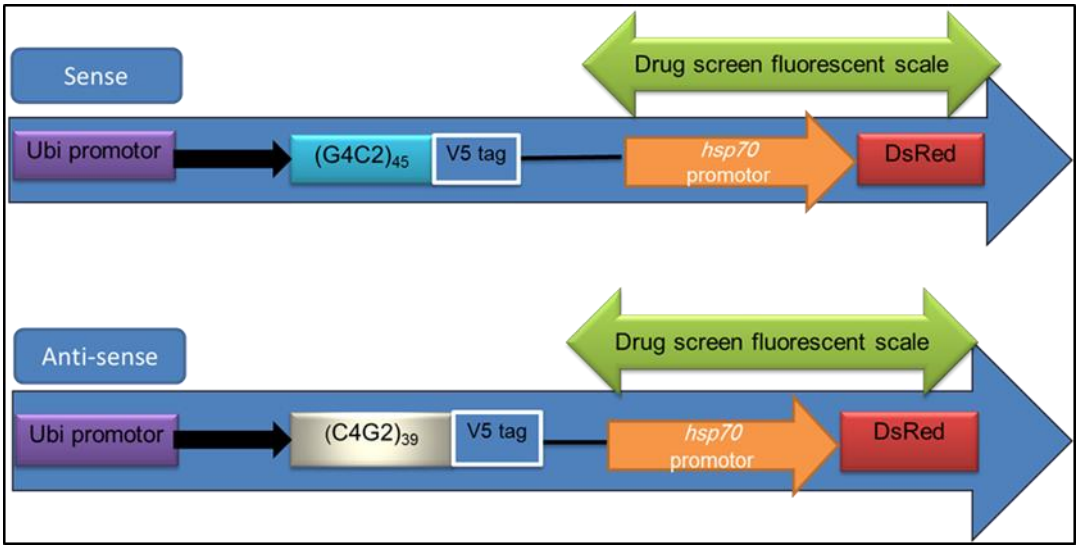

Figure 6-11: Transgene structure of C9$(G4C2)_{45}$ and C9$(C4G2)_{39}$ zebrafish lines.

The initial dot blot procedure was performed by sonicating the embryos into RIPA buffer. We then tested different set ups to detect V5 signals and reduce the variability of the samples, as shown in Table 6-2. We started by performing sonication in the wells of V-bottom plates at 25% for 20 s, then used 1.5 ml plastic micro-centrifuge tubes with sonication amplitude of 20% for 15 s to reduce sample loss by misting during sonication (Table 6-2). The sonication of individual embryos in the wells of a V-bottom plate was found to produce extreme variability in the protein extraction because some of the samples were lost during the sonication step due to a small well size and low volume (50 µl). We concluded that the best extraction procedure was using 1.5 ml plastic tubes to sonicate the samples at 20% power for 15 s in immunoprecipitation (IP) cell lysis buffer (100 µl), as shown in Table 6-2.

Table 6-2: This table shows a number of optimisation experiments performed with different conditions for development of a dot blot based drug screen in the C9orf72 zebrafish.

Experiments	Zebrafish Transgenic line	The amount to sonicate	Samples placed to sonicate	Amplitude of the sonication/ Time	How many fish used	Application of lysis buffer	Centrifuging	Extraction of the supernatant	Membranes	V5 signals	Conclusions of the results
1st	(C4G2)39 TG/NTG	50 µl of (RIPA lysis buffer +PIC)	V-bottom	25%/ 20 secs	One fish/two fish. 3 samples of each	RIPA + PIC (50 µl before sonication + 150 after sonication)	3000 r/ 10 mins	Serial dilution (25%,50%, 75%)	PVDF (0.45mm)	Good V5 signals in (75%) of one fish and two fish (75%)	✓Good V5 signals of 75% dilution of one fish. ✓Good V5 signals of 75% dilution of two fish ✓Variable V5 expressions between different clutches
2nd	(C4G2)39 TG/NTG Treated and untreated trazodone (50 µM)	50 µl	V-bottom	25%/ 20 secs	One fish/two fish. 6 samples of each	RIPA + PIC (The same application before)	3000 r/ 10 mins	75% of the supernatant	PVDF (0.45mm)	Variable V5 signals	
3rd	(C4G2)39 and (G4C2)45 TG/NTG treated and untreated trazodone (50 µM)	50 µl	V-bottom	30%/10 secs	One fish/two fish. 6 samples of each	RIPA + PIC (The same application before)	3000 r/ 10 mins	75% of the supernatant	PVDF (0.45mm)	C4G2: Good signal and strong signals in the two fish, but with a variable expression. G4C2: Strong V5 signal in one and two, but with variable expressions	✓Weaker V5 expression and variable in one fish of C4G2. ✓Strong V5 signals in one and two G4C2 fish, but it was variable.
4th	(C4G2)39 TG/NTG treated and untreated trazodone (50 µM)	50 µl	V-bottom	25%/ 5 secs	One fish/two fish. 6 samples of each	RIPA + PIC (50 µl before sonication + 160 after sonication) To get much proteins extraction	3000 r/ 10 mins	75% of the supernatant	PVDF (0.45mm)	Higher noise background led to loose the V5 signal	
5th	(C4G2)39 TG/NTG treated and untreated trazodone (50 µM)	50 µl	V-bottom	25%/ 5 secs	One fish/ two fish. 6 samples of each	RIPA + PIC (50 ml before sonication + 150 ml after sonication)	3000 r/ 10 mins	75% of the supernatant + sediment	PVDF (0.2mm)	Not good signals	✓ Sediment clogged the pore
6th	(C4G2)39 TG/NTG treated and untreated trazodone (50 µM)	50 µl	V-bottom	20%/15 secs	One fish/two fish. 6 samples of each TG/NTG	IP cell lysis (50 ml before sonication + 150 ml after sonication)	6000 rpm/4 mins/ 4ºC	75% of the supernatant	Nitrocellulose	Very weak V5 signal	
7th	(C4G2)39 and (G4C2)45 TG/NTG	100 µl	Eppendorf tube (1.5 ml)	20%/15 secs	One fish. 6 samples of each C9 fish TG/NTG	IP cell lysis (100ml before sonication + 100ml after sonication)	17000 rpm/4 mins/ 4ºC	75 µl and 100 µl of the supernatant	PVDF (0.45mm)	Strong V5 signals were in the G4C2 fish, but it was not detected In the C4G2 fish	✓Strong V5 signals in the G4C2
8th	(G4C2)45 TG/NTG	100 µl	Eppendorf tube (1.5 ml)	20%/15 secs	One fish. 4 samples of each TG/NTG	IP cell lysis (The same application before)	17000 rpm/4 mins/ 4ºC	25 µl, 50 µl ,75 µl and 100 µl of the supernatant	PVDF (0.45mm)	Strong V5 signals were in the 75 µl G4C2 fish and were a leak in 100 µl and very weak in the other concentrations	✓Strong V5 signals in 75 µl of the supernatant in the G4C2.
9th	(G4C2)45 TG/NTG	100 µl	Eppendorf tube (1.5 ml)	20%/15 secs	One fish of 3 samples of TG/NTG in each lysis buffer	RIPA buffer and IP cell (100 ml before and after)	17000 rpm/4 mins/ 4ºC	75 µl and 100 µl of the supernatant	PVDF (0.45mm)	Strong V5 signals were in the G4C2 fish with using IP cell lysis buffer , while no V5 signals were in the RIPA buffer.	✓Strong V5 signals in the 75 µl and 100 µl of the supernatant in the IP cell lysis than RIPA.

It is important to note that we performed a serial dilution of one fish (25%, 50%, and 75% dilution of raw extract) and 75% dilution of two fish extracts in the first experiment to create and develop a standard curve of varying amounts of protein. This would allow us to determine whether the dot blot signal is in the linear range and also to identify the most suitable volume of sample required for detecting a robust V5 signal from a single larva, or whether two larvae are required for optimal signal to noise detection. However, we had problems with this due to the variability of samples from clutch to clutch with the $(C4G2)_{39}$ line (Fig. 6-12). This could be related to the sonication process as some samples were lost as an aerosol during the sonication process in the V-bottom plates. Also, the study was performed at 2-5 dpf, a rapidly growing stage that could result in variability between embryos/larvae.

For the actual dot-blotting, a vacuum pump was used to pull 200 µl (total of extract made up with lysis buffer) samples through the membrane. After blocking the PVDF or Nitrocellulose membranes were probed with the mouse anti-V5 antibody (primary antibody) and then goat anti-mouse secondary antibody. The membranes were imaged after saturation with ECL substrates, as described in the methods section.

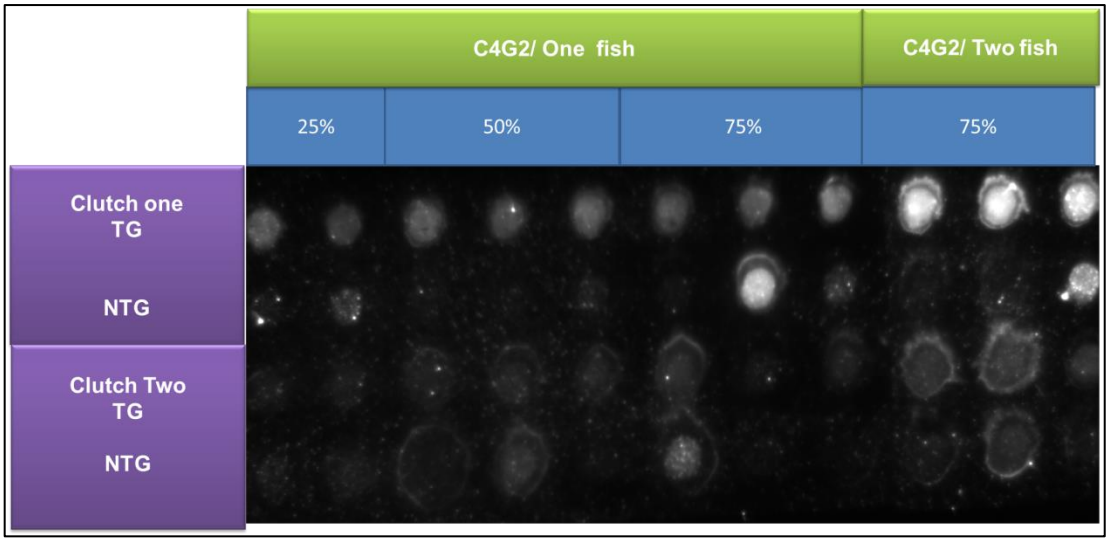

Figure 6-12: V5 signals obtained C9(C4G2)$_{39}$ with different concentrations of extract. The V5 signal was generally clearer in the TG fish than NTG fish but with some contamination of NTG wells, especially in row 2. Two clutches of C9(C4G2)$_{39}$ zebrafish were used in this experiment. A PVDF membrane (0.45 mm) was used. Sonication was performed in V-bottom plates.

6-3-2-1 Standardisation of the dot blot screen in the C9orf72 zebrafish

Dot blotting of C9(C4G2)$_{39}$ and C9(G4C2)$_{45}$ zebrafish extracts showed good V5 signals after sonication of the larvae in 100 µl of extraction buffer in 1.5 ml tubes at 20% amplitude for 15 seconds. This gave more reproducible results than using V-bottom plates for sonication. The volume was sufficient to extract the supernatant and separate it from insoluble material. PVDF (0.45 mm) membranes were used.

We used IP cell lysis buffer as the ingredients of the IP cell lysis buffer include DTT and urea (8 M), see Table 2-5. DTT and urea are used as denaturing agents with the capability to solubilise insoluble protein aggregates. It showed stronger V5 signals in the (G4C2)$_{45}$ from one fish than (C4G2)$_{39}$ (Fig. 6-13). The (G4C2)$_{45}$ fish showed specific V5 signals when we used 100 µl or 75 µl of the supernatant, while the (C4G2)$_{39}$ fish extracts did not show V5 signals when IP cell lysis buffer was used, as shown in Fig. 6-13.

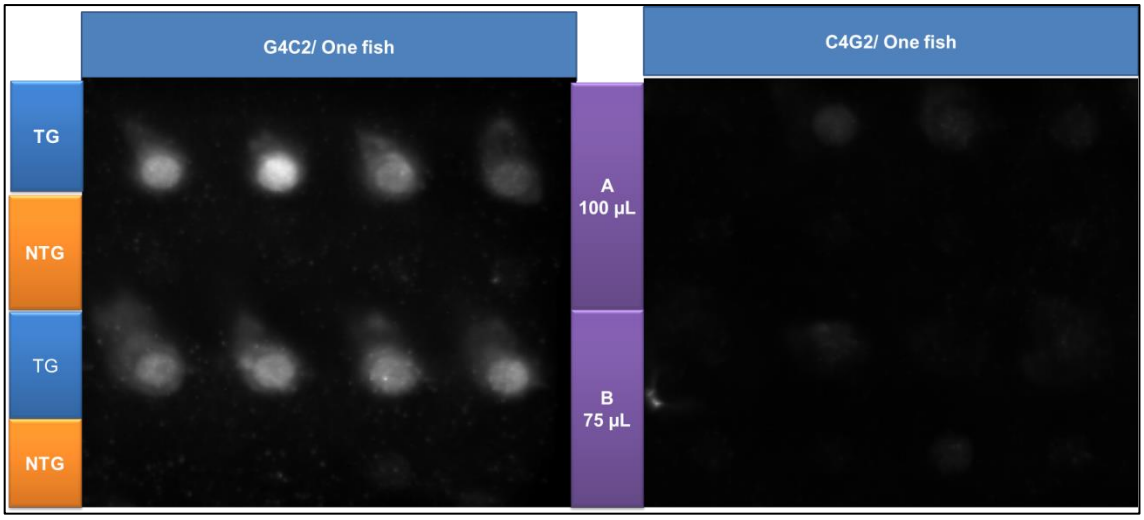

Figure 6-13: V5-DPR expression measured by dotblot. Specific signals were obtained with C9(G4C2)$_{45}$ extracts but not with C9(C4G2)$_{39}$ extracts. PVDF membrane (0.45 mm) was used. All G4C2 and C4G2 fish were from a single clutch. Samples in A were 100 µl of supernatant + 100 µl of IP lysis buffer. Samples in B were 75 µl of supernatant + 125 µl of IP lysis buffer.

The results showed that:

- ✓ The V5 signals were detected in the extracts from a single transgenic fish (TG) and were absent in the non-transgenic fish (NTG) samples, as shown in Fig. 6-13.
- ✓ The V5 expressions are stronger when two embryo extracts are used, rather than an extract from a single embryo Fig. 6-12.
- ✓ The signal of V5 expression is strong to detect in the C9(G4C2)$_{45}$ line.

6-4 Discussion

Hexanucleotide repeat expansion (HRE) in the *C9ORF72* gene is the most common causative mutation in familial and sporadic forms of ALS. It accounts for 40% of fALS and 3-4% of sALS. It is linked with other causative genes, such as *SOD1* and *TARDBP* through common mechanisms such as aggregation (Dedeene et al., 2019; Forsberg et al., 2019). *C9orf72* HRE was recently also shown to promote Tau phosphorylation and lead to toxicity in *Drosophila* (He et al., 2019). As *C9orf72* is the most commonly known ALS causing gene with some potential interaction with *SOD1* mediated ALS, we explored whether the hits from the *sod1*G93Ros10 zebrafish drug screen also modulated the stress phenotype of the *C9orf72* HRE transgenic zebrafish. We also developed tools to perform a high-throughput drug screen using this novel model.

The *C9orf72* zebrafish ALS *in vivo* models were generated in 2017. They express sense $(G4C2)_{45}$ and anti-sense $(C4G2)_{39}$ HREs respectively and produce DPRs, which are hypothesised to be one of the proposed cytotoxic pathologies of C9orf72 HREs. Moreover, recent evidence has been reported that increased glutamate activity induces stress in glutamatergic motor neurons in *Drosophila* and in the spinal cord and motor cortex derived from patients leading to increase DPR synthesis (Westergard et al., 2019; Xu and Xu, 2018). This support our hypothesis of investigating the LifeArc hit compounds in *C9orf72* zebrafish and testing whether they have any effect on the rate of DPR production. Therefore, the LifeArc hit compounds and their closest structure related compounds were tested in the *C9orf72* zebrafish. These compounds showed reduced neuronal stress using the *hsp70*-DsRed fluorescent stress readout in the *sod1*G93Ros10 zebrafish. We therefore investigated whether these compounds reduce neuronal stress in the C9$(G4C2)_{45}$ zebrafish line and modulate *C9orf72* toxicity.

The LifeArc hit compounds and analogues (46 compounds) were screened in the $(G4C2)_{45}$ zebrafish to tets their activity on the *hsp70*-DsRed fluorescent stress readout. This line was chosen due to the $(G4C2)_{45}$ line having higher DPR expression with lower variability, therefore any changes in expression are easier to detect. The screen identified three compounds, 1744, 1052, and 1262,

that reduced the neuronal stress *hsp70*-DsRed fluorescent readout with an average of 48.1%, 29.2% and 41.6% respectively.
Also, this screen showed a structure-activity relationship in two groups of compounds. These were the hit compound 0707 and its analogue 0039, and the hit compound 1527 and its analogue 1541. Therefore five compounds (0707, 0039, 1744, 1052, and 1262) modulated activity of the *hsp70*-DsRed neuronal stress readout in both ALS *in vivo* models. This may suggest a common mechanism shared by the two mutations leading to common drug targets that can modulate neuronal stress. These sets of data will allow further refinement of the structures of the hit compounds in the future.

One aspect of the *hsp70*-DsRed neuronal stress readout screen in the *C9orf72* fish was that it showed some variance in the effect of riluzole and some of the LifeArc compounds between different clutches of embryos and between different generations of fish used for testing in this new model. This needs to be further explored and standardised over clutches and further generations to ensure generational stability of the repeats and phenotypes. Therefore, it will be necessary to ensure controls are maintained for each clutch when performing a drug screen in the *C9orf72* zebrafish so that each clutch can be compared to its own control group. In the future, it will be important to perform studies to identify variability between different clutches, as was performed in the *sod1*G93Ros10 zebrafish. This will reduce the potential for false positives and negatives, enhancing the applicability of this model for use in a high-throughput screen.
The other investigation that was performed in the C9(G4C2)$_{45}$ zebrafish was the DPR assay. Production of DPRs is one of the hallmark features of *C9orf72* pathophysiology, and some of the active compounds obtained from testing the fluorescent modulation of stress in the C9 zebrafish were shown to reduce DPR levels in the C9(G4C2)$_{45}$ transgenic zebrafish using western blotting. Compound 1527 showed a significant reduction of V5-DPR expression when normalised against DMSO controls (26.3%) (Fig.6-7). The analogue 1541 may also demonstrate a reduction of V5-DPR expression, but its effects were variable, reducing statistical power, so further repeats of this experiments are needed. The potential for two compounds with a similar structure modulating DPR levels

is interesting as it provides a chemical scaffold that can be utilised for further structure-function analysis using synthetic chemistry.

Although these hit compounds reduced DPR levels, a key requirement for neurotoxicity, the mechanism of their action is still unclear. The synthesis of DPRs in the *C9orf72* zebrafish model requires aberrant export of the HRE RNA, followed by cytosolic RAN translation of DPRs. It has been shown that the nuclear transport of HRE RNA in a *Drosophila C9orf72* ALS model was mediated by the nuclear export adaptor SRSF1 (Hautbergue et al., 2017). The compounds identified here may modulate SRSF1 or other processes to reduce DPRs. The nuclear pore structure shows some similarity to ion channels and thus, it is possible that some of these hits may directly modulate the nuclear export of HRE mRNA (Beck and Hurt, 2017; Gatenby, 2019).

Interestingly, it was recently shown that neuronal excitation and stress modulates RAN translation in an *in vitro C9orf72* model resulting in neuronal vulnerability and increased DPR production (Westergard et al., 2019). Activating glutamate receptors or optogenetically stimulating neuronal activity led to increased HRE associated non-AUG (RNA) translation leading to increased DPR production in primary cortical neurones and patient-derived motor neurons. Furthermore, it was suggested that some downstream events may be implicated in DPR synthesis. One of these events is activation of the integrated stress response (ISR), which leads to an increase in RAN translation. This enhancement was reduced on modulating the phosphorylation of eif-2α, a key stress response factor in mediating RAN translation. However, it is still unclear how neuronal excitation and ISR enhanced RAN translation. In our own laboratory, it was shown that heat shock stress enhanced RAN translation of DPRs (unpublished data). Further exploration of these pathways and the effects of our hit compounds will be required to identify the exact molecular targets involved in this process.

The other potentially interesting observation from the WB for DPRs in the C9(G_4C_2)$_{45}$ zebrafish concerned compound 1262. This suggested a possible divergence between DPR levels and the DsRed stress readout. On some occasions, this compound appeared to show increased DPR levels, however,

this same compound consistently showed a reduction of the DsRed signal. Further repeats are needed to validate this observation, but potential mechanisms for increased DPR production while reducing *hsp70*-DsRed activity may be:

- Activation of the ubiquitin promotor leading to induction of expression of the $(G4C2)_{45}$ transgene leading to an increase of the DPR levels.
- Blocking of *hsp70* transgene activity in both the $C9(G4C2)_{45}$ and *sod1*G93Ros10 zebrafish.
- Hyperactivity in embryos between 2-4 dpf increased neuronal activity which is related to increased RAN translation as described (Westergard et al., 2019), so the hyperactivity induced by compound 1262 may enhance RAN translation.

As the LifeArc compound 1527 showed a significant modulation of the DPR expression levels, it is worth investigating this compound at higher doses as it was safe and tolerated in the fish treated at 10 µM. The effect on individual DPR species in the $C9(G4C2)_{45}$ zebrafish could also be examined with DPR-specific antibodies rather than the V5 antibody.

Due to the poor quantitative nature of western blotting, it would be good to use a more quantitative method to test the effect of the LifeArc compounds on DPR modulation. We did not perform such additional tests as our study was limited by the low drug volume provided. Also, it will be critical to test different clutches as clutch variability in the *C9orf72* zebrafish needs to be addressed. Genotyping fish prior to treatment would also reduce variability caused by contamination with non-transgenic fish. WB for DsRed showed that most of the hit compounds significantly reduced DsRed expression, but the statistical analysis was again limited by the variance seen with WB.

Overall, the most exciting result of testing the LifeArc hit compounds from the *sod1*G93Ros10 screen in the $C9(G4C2)_{45}$ zebrafish was that some compounds consistently reduced the fluorescence-based readout in both models. It is possible that these hits have reliable effects on the stress axis involved in ALS pathology by targeting other cellular mechanisms, rather than DPR toxicity.

The dot blot results with the *C9orf72* sense $(G4C2)_{45}$ and anti-sense $(C4G2)_{39}$ fish has supplied promising preliminary data for performing a high-throughput screen in the *C9orf72* zebrafish in the future. It confirmed the presence of detectable V5-DPR expression in single embryos screen of both sense and anti-sense transgenic lines (Figs. 6-12 and 6-13). It did, however, show that the V5-DPR signals obtained when using two $(C4G2)_{39}$ embryos are stronger than the signals from single embryos. However, it must be acknowledged that the dot blot assay is sensitive but variable in its current form, and it will be necessary to use multiple single clutches of *C9orf72* fish to compensate for clutch variability and create linear standards for the DPR protein concentrations. This currently limits the capacity for high throughput screening.

To summarise the findings with the *C9orf72* lines, the *hsp70*-DsRed fluorescent stress readout assay was successfully used to identify compounds to take forward for further validation studies. This study also identified at least one compound that reduces DPR levels in the $(G4C2)_{45}$ zebrafish. Thus, the *C9orf72* pure HRE transgenic zebrafish showed strength as an *in vivo* model for performing screening and validation of drugs that modulate DPR levels and show promise for use as in high-throughput screening in the future.

CHAPTER 7

7- Discussion

7-1 Was the *sod1*G93Ros10 zebrafish an appropriate *in vivo* model for the LifeArc high-throughput screen?

Various genes associated with divergent cellular mechanisms have been implicated in ALS pathology. This has led to a host of emerging new drugs and therapeutic targets aimed at reducing the disease progression, obtained from screens with *in vivo* and/or *in vitro* models. SOD1G93A mice are the most common pre-clinical *in vivo* model used in the drug discovery process for ALS (Turner and Talbot, 2008). However, one of the main challenges of drug discovery in ALS has been the failure to translate of many positive compounds (pre-clinical data) from the SOD1G93A mice into positive clinical trials. The hypotheses for the cause of these failures are that the model may be limited due to its dependence on different scale outcomes, such as the quantitative analysis of motor neuron survival, gait analysis, rotarod performance, littermate variability, etc. However, manypre-clinical studies may not have been designed correctly or with sufficient power (Van Damme et al., 2017; Scott et al., 2008). One of the issues with this mouse model is the 14-fold higher expression of mSOD1 due to a large number of gene copies, which leads to early-onset disease symptoms and early death at four months of age. This does not directly mimic what is seen in human patients, that have later disease onset and less aggressive disease course. Also, many mouse studies begin drug treatments pre-symptomatically, which is not possible in human patients. This means that a drug may work, but that the window for therapeutic effect is pre-symptomatic. This highlights the need for the ALS research field to focus on the identification of early-disease biomarkers and other disease-causing genes thus enabling the earlier identification and treatment of patients where the drugs may have a higher chance of efficacy. This concept can be applied in a small vertebrate *in vivo* model, such as the *sod1*G93Ros10 zebrafish (Ramesh et al., 2014), but it is challenging in mice.

Another issue is that SOD1 mutations account for a very small subset of ALS with quite a different disease pathology to other genetic models of ALS. This

may mean that a positive therapeutic effect in one model may not translate to other ALS subtypes and that a multiple genetic models approach is needed before proceeding to clinical trials. This raises the issue of addressing and improving study designs in terms of having fewer limitations, reducing the cost, and enabling a shorter time scale. Therefore, within a very complex disease such as ALS where there are models based on different genetic forms, it seems that a better-balanced screen of multiple models would increase the likelihood of a positive impact of therapy in clinical trials. The understanding of primary disease pathways, when applied to specific genetic models, should provide better performance in high-throughput drug screening and identification of new clinical therapeutics in an expeditious manner.

To try to enable better-informed drug screening efforts in the ALS field and support drug discovery, a high-throughput drug screen was conducted using *sod1*G93Ros10 zebrafish. The aim was to identify novel structural compounds that modulate ion channels. Riluzole, the drug approved for treating ALS is thought to act through modulating Ca++ ion through the channel. Thus, ion channels are among the bonafide targets demonstrated in ALS. The *sod1*G93Ros10 zebrafish show interneuronal defects during the larval stages (72 hpf) (McGown et al., 2013), before any loss of motor neurons. Interneuron loss in ALS has been seen in neuropathological studies (Maekawa et al., 2004; Nihei et al., 1993). Previous drug screens in the *sod1*G93Ros10 zebrafish identified riluzole and selamectin, two compounds that target ion channels and their receptors, as neuroprotective agents. These were shown to modulate neuronal stress in *sod1*G93Ros10 zebrafish model via reducing glycinergic transmission in transgenic zebrafish (PhD Thesis (McGown, 2014). Selamectin also demonstrated pro-neurogenic potential and promoted neurogenesis in the zebrafish brain (Sun et al., 2013). This was shown to be mediated via γ2-containing $GABA_A$ receptors in pluripotent stem cells (PSCs) (Sun et al., 2013). Additionally, emerging evidence has shown that ion channel pathways are potential therapeutic targets in *in vivo* and *in vitro* ALS models (Bonifacino et al., 2019; Milanese et al., 2014). Compounds such as ivermectin (Andries et al., 2007) that inhibited the excitotoxicity of ion channels, including AMPA receptors, extended lifespan in the SOD1G93A mouse. The vulnerability of motor neurons

is due to a reduction in inhibitory interneuron innervation which modulates their excitability. Thus interneuronopathy plays an important role in human ALS through modulating the excitability of motor neurons (Martin, 2012; Turner and Kiernan, 2012).

Oral administration of the AMPA receptor antagonist perampanel rescues the loss of motor neurons, ameliorates motor dysfunction, and ameliorates TDP-43 pathology in the ADAR2 mouse model of sporadic ALS (Akamatsu et al., 2016). This mouse exhibits a progressive ALS phenotype caused by a knockdown of the adenosine deaminase ADAR2 which catalyses RNA editing at the Q/R site of GluA2 (Akamatsu et al., 2016). This study further highlights how ion channel therapy might be a potential target for ALS in the future, and also the importance of AMPA receptors as one of the major glutamate receptors involved in the cellular toxicity of ALS.

The *sod1*G93Ros10 zebrafish ALS *in vivo* vertebrate model mimics numerous phenotypic and pathogenic features of ALS that make it more desirable than other *in vivo* invertebrate models, such as *c. elegans* or *Drosophila*, for performing a high-throughput screen as they are still small and amenable for large scale screens. Besides the zebrafish being easier to genetically manipulate, transparent during early development and drugs are easily to apply for screening in aqueous medium make them very useful in high throughput *in vivo* screening. A small number of pairs of zebrafish can lay over 2000 embryos which allowed us to screen around 550 compounds in a week. Moreover, it is a unique *in vivo* model that includes in its construction the *hsp70*-DsRed neuronal stress fluorescent readout. This is a neuronal reporter of cellular stress that is activated as a result of the toxic insult caused by misfolding of the msod1 protein. This allowed us to utilise the *hsp70*-DsRed fluorescent readout for drug screening. This fluorescent readout could also be used for other MND models involving proteinopathy and other neurodegenerative diseases such as Parkinson's disease and Alzheimer's disease which also involve protein misfolding and aggregation. HSPs are part of a protective cellular mechanism termed the unfolded protein response (UPR) which is controlled by stresses such as increased temperature (Dukay et al., 2019). In this transgenic fish

model, the mutation of *sod1* caused cellular stress toxicity, and the UPR is activated to induce *hsp70* expression to overcome protein aggregation and promote cell survival. These distinct features of the *sod1*G93Ros10 zebrafish make it a very appropriate vertebrate model for conducting a high-throughput LifeArc ion channel focussed drug screen.

In this project, drug treatment was for four days between 2-6 dpf, the early stage of development in the *sod1*G93Ros10 zebrafish spanning embryo and larval stages. The *sod1*G93Ros10 zebrafish showed interneuronal defects during the larval stages (72 hpf) (McGown et al., 2013) and interneuron loss has been seen in human pathological studies (Maekawa et al., 2004; Nihei et al., 1993). Thus the neuronal stress observed in our zebrafish G93R model may mimic the early non-phenotypic stages of disease and provide a useful tool for discovering drugs that modulate early pathological processes. This coupled with early diagnosis of ALS patients with biomarkers that allow diagnosing of early prodromal stage of disease will allow early disease intervention and potentially allow delay in disease onset and/or progression.

In terms of high-throughput drug screening in zebrafish, multiple studies have screened libraries of compounds and explored phenotypes relevant to different areas, such as cancer, psychology, and metabolism. These screens have used developmental, gene expression and behavioural analyses. Here we utilized a fluorescent readout, which provides a simple quantative readout for analysis. Additionally, most high throughput screens in vitro utilize the Z-score, which is not amenable for *in vivo* models. We utilised an SSMD score in our screen due to the potential benefits of this analysis. The SSMD score is more suitable with an *in vivo* readout than the Z-score in a high-throughput drug screen for a number of reasons. It calculates the median of the differences across the whole plate divided by the standard deviation of the variations of the plate (Zhang, 2011). This allows measurement of the fold change for each drug in each well of the plate, while the Z-score would be a readout of the variability of two values by calculating the average of the signals divided by the standard deviation. The SSMD score accounts for the positive controls, negative controls, and the tested compounds, while the Z-score does not account for the positive and negative controls. The Z-score does not record the strength of the difference of each

compound leading to missing of weaker effects which may just be due to sub-optimal dose.

This study was the first high-throughput drug screen in an *in vivo* MND zebrafish model that has been performed on small ion channel modulating compounds. Despite this accomplishment, the screen could have been improved by more automation. Use of an automated embryo dechorionation system, automatic plating of embryos and the ability to sonicate large numbers of embryos at a time, such as by using a sonicating water bath, would all have significantly improved the throughput to higher levels. This would have allowed more time for characterisation of hits from the screen, potentially in a mouse model.

7-2 Testing riluzole and the LifeArc library in *sod1*G93Ros10 and *C9orf72* zebrafish

Riluzole and Edaravone are the only two licensed drug treatments for ALS, with both showing a modest effect on slowing progression of the disease. Riluzole was the first drug licensed for ALS, extends survival by 3–4 months and is a known anti-excitotoxic drug, thought to act via inhibition of glutamate receptors and persistent Na^+ channels, as well as other ion channels, at the synapse (Azbill et al., 2000; Bensimon, 1994; Vucic et al., 2013). However, the precise mechanism of its effect is still unknown. With riluzole treatment in the zebrafish, we saw a reduction of more than 65% in the *hsp70*-DsRed neuronal stress readout in the mutant *sod1* model and of more than 40% in the $C9(G4C2)_{45}$/sense zebrafish. This allowed the production of a significant reduction window in neuronal stress compared to the negative control (DMSO) in the high-throughput drug screen and enhanced the sensitivity of detecting actual positive hits. However, it is essential to mention that riluzole has anesthetic properties (Mantz et al., 1992), which were evident in the *sod1*G93Ros10 and C9orf72 zebrafish. This highlights the need for a new therapy for ALS. Ion channels are one of the potential targets in ALS treatment. Therefore, we investigated the ion channel library (LifeArc) in the *sod1*G933Ros10 zebrafish to identify modulators of neuronal stress and enable a better understanding of the cellular mechanisms underlying ALS pathology.

Interestingly, riluzole showed no reduction of the DPR expression level in the treated C9(G4C2)$_{45}$ fish in spite of reduced DsRed expression. This indicates that riluzole may not act directly on DPR-mediated toxicity and has a more general cellular protective role, possibly via reducing excitotoxicity. It could be that riluzole inhibits persistent sodium channels ($I_{Na}P$) in interneurons during an earlier stage of disease than with the motor neurons (Benedetti et al., 2016; Tazerart et al., 2007). The sedative properties of riluzole seen in the zebrafish lead to a reduction in locomotor activity. This may result from inhibition of currents and action potentials via ion channel inhibition.

It is essential to note that ion channel modulators seem to have potential therapeutic value in ALS models, as shown by the modulation of the glycinergic inhibitory stress response in the *sod1*G93Ros10 zebrafish by selamectin (McGown, 2014), and by the significant reduction by more than 60% of the DsRed stress response in riluzole treated fish in this study. It remains to be determined whether amelioration of neuronal stress at later stages by these compounds improves survival of motor neurons, as was shown in recent studies related to modulation of cellular glutamate excitotoxicity (Akamatsu et al., 2016; Bonifacino et al., 2019; Shi et al., 2019) including activation of the glial glutamate transporter EAAT2 (Kong et al., 2014).

7-3 A successful *sod1*G93Ros10 zebrafish informative dose-response profile for LifeArc's hits

The successful high-throughput screening performed in the *sod1*G93Ros10 zebrafish identified a small panel of lead compounds that could now be taken forward to pre-clinical studies in mice. The secondary screen of the hits defined a dose-response profile for each of the inhibitors, their closest structural analogues, and provided some data on the potential side effects of each compound. This highlights the power of this high-throughput screen and the secondary screens conducted. It has generated a large amount of data for each compound that would not be possible to obtain in other vertebrate models without incurring huge cost and ignoring the time constraints that would be involved. Zebrafish have the advantage over *in vitro* assays that the whole organism is being screened, with a functional CNS, therefore providing more

information about the effect of the drugs on cell-cell interactions and identifying potential off-target toxic side effects. However, the zebrafish is still a small vertebrate organism with a relatively simple CNS (e.g. no motor cortex) compared to humans.

A large number of high-throughput drug screens with *in vitro* ALS models have been conducted. A major advantage of cell lines is that they represent a simple phenotype and single genotype without exogenous and endogenous interference. An excellent high-throughput performance can be obtained if the target and the cellular pathway are known and the cellular models provide this target, such as screening of a library of anti-oxidant drugs in NSC34 cells (Barber et al., 2009) or an *in vitro* abnormal apo-SOD1(G37R)$^{S\text{-}S}$ oligomerisation screen of 640 FDA-approved drugs for reduced oligomerisation (Anzai et al., 2016). However, this would be impossible for a blinded screen of drugs that are synthesised to work via ion channels, such as the LifeArc library. Also, the use of an *in vivo* model allows monitoring of the consequence of the drugs on motor-neuron degeneration, survival, and NMJ defects; this is not possible in simple cellular models. In addition, the *hsp70*-DsRed fluorescent readout in the *sod1*G93Ros10 zebrafish increases the power of utilising zebrafish for this screen. Therefore, the zebrafish *in vivo* model has clear advantages over cellular models for performing this research.

Recent studies have applied the invertebrate model *C. elegans* for conducting a high-throughput screen and then utilised zebrafish and mice for validation studies (Bose et al., 2019; Patten et al., 2017). These studies measured the effect of drugs on *C. elegans* locomotor activity as a measure of neuromuscular transmission. Subsequent validation studies in different genetic zebrafish ALS models and then mice allowed data of increasing potential therapeutic impact to be obtained. To improve understanding of the mechanisms through which the drugs from high-throughput drug screens act, we could express reporters of particular cellular pathways implicated in ALS such as autophagy or oxidative stress resporters, e.g. the Nrf2-ARE reporter, in the *sod1*G93Ros10 zebrafish. This reporter would offer a vital opportunity to investigate lead compounds obtained from various *in vitro* drug screens in an *in vivo* ALS model in an efficient manner.

While the screen performed in this thesis has identified compounds reducing the hsp70::DsRed stress readout, the data from this screen still has some limitations because the mechanism by which this cellular stress readout is reduced is still unknown. It will therefore now be necessary to further investigate and validate the effects of the identified compounds on msod1 gene expression, protein misfolding and/or aggregation. This could be achieved by determination of levels of misfolded msod1 protein using western blotting and of the level of RNA expression of the msod1 gene by qPCR.

Another important thing to investigate regarding the effects of the drugs identified before proceeding to a pre-clinical study in mice is to determine their effects at the adult stage. Histological analysis should be performed to determine any improvement in motor neuron survival, NMJ defects, glycinergic and glutamatergic dysfunctions. Also, a motor behaviour study should be conducted on the *sod1*G93Ros10 adult zebrafish to determine if the hits improve adult motor function in the treated fish. However, such a study would be costly as it requires a much greater amount of the drugs to be performed than is currently available.

7-4 Utility of C9orf72 zebrafish enhances drug development in ALS therapy

The C9 zebrafish have been shown to produce the predicted DPR species due to RAN translation of the hexanucleotide repreat expansion, which is one of the hypothesised forms of cellular toxicity in the HRE-C9 gene (Shaw, 2018). Analysis of hits from the initial screen using the sod1 G93R fish in the C9-HRE fish identified one compound, 1527, that significantly reduced the *hsp70*-DsRed neuronal stress response and the expression level of the DPR proteins Fig (6-5, 6-6, & 6-7). Also, compound 1541, which showed a structure relationship with compound 1527 also modulated DPR levels in the C9$(G4C2)_{45}$ zebrafish. Therefore, these compounds appear to have beneficial effects in two distinct genetic models of ALS, increase the potential impact for ALS drug development therapy by this study. Testing of the initial hits that decreased the stress readout in the *sod1*G93Ros10 zebrafish in the C9-HRE zebrafish also revealed some compounds that modulated the *hsp70*::DsRed fluorescent stress readout, without modulating DPR levels. These compounds were hit 0707 and its

analogue 0039, along with compound 1262. Further validation studies of these compounds will be important as they appear to work regardless of the genetic trigger for the disease. This may mean they work on one of the more general disease mechanisms and may therefore potentially be beneficial in sporadic ALS cases too.

Recently, eif2α and SR-rich splicing factor SRSF1, have been demonstrated to modulate DPR production in *C9orf72* disease models (Halliday et al., 2017; Hautbergue et al., 2017). Potentially, ion channels in the nuclear envelope may be involved in nuclear transport and gene transcription. Nuclear ion channels have the essential function of generating ion gradients across the nuclear membrane (Matzke et al., 2010). Therefore, the effects of compounds from the LifeArc screen on the C9-HRE zebrafish revealed that it may be useful to focus in the future on the role of nuclear channels in ALS pathobiology.

7-5 The limitation of the work and the models

This research was screened ion channel small chemical molecules in the *sod1*G93Ros10 and *C9ORF72* ALS zebrafish. It showed significantly a higher impact of performing a high-throughput drug screen *in vivo* ALS zebrafish and it candidates a novel ion channel hit-compound family of ALS drug development. It significantly revealed a novel ion channel hit family that reduced a novel biological target in *C9orf72* zebrafish. However, this work was included some limitation. One of these limitations was a biological target. The library was synthesised to work via ion channel receptors, but this was not a determination of a particular biological target. Therefore, the screen was blinded and it was a time consumption which prevented performing a quantitative study of loss of motor neurons or a histology study of CNS or integrity of NMJ's dysfunction analysis. Also, the volume of the drug was limited which did not allow us for further analysis.

The other important point of the limitations was on the fluorescent stress readout of *hsp70*-DsRed in the *sod1*G93Ros10 zebrafish because the mechanism by which this cellular stress readout is reduced is still unknown. It will therefore now be necessary to further investigate and validate the effects of the identified compounds on msod1 gene expression, protein misfolding and/or aggregation.

This suggests a cellular stress reporter would be an essential of performing a faster high-throughput drug screen in the *sod1*G93Ros10 zebrafish. The utilising of *C9ORF72*-ALS zebrafish was also showed some limited impact of testing the efficacy of a novel ion channel hit-compounds due to it is still a novel pure *C9ORF72* zebrafish and using different generation of this transgenic line appeared some variability from one clutch to another. This should be addressed in the future to facilitate a high-throughput drug screen in the *C9ORF72* zebrafish in the future.

7-6 Future work

Multiple cellular mechanisms are involved in ALS pathology, but key druggable pathways are yet to be identified. This project, with its limited-time scope, offers preliminary results that can be built on with future mechanistic and validation studies. As mentioned earlier, analysis of *sod1* and C9-HRE transgene expression in response to drug treatment would elucidate the activity of each compound on the transcription of the mutant genes. By investigating the lead hit compounds at an adult stage in both the *sod1*G93Ros10 zebrafish and C9-HRE zebrafish we will be able to monitor for amelioration of loss of MNs, NMJ defects, swimming strength and extension of survival which will be very important as these studies would provide an insight into effects on the underlying cellular pathology and determine whether these drugs alter the later stages of the disease process.

Further investigation is required on the C9-HRE zebrafish because these fish have not been fully characterised, and more work is needed to understand the observed effects of drugs in this fish. Dose-response studies of the identified hits in these transgenic C9-HRE fish would provide information on the optimal dosing required to modulate the levels of DPR proteins. Further, the activity of the hits on production of the various DPRs that show varying toxicity in the sense and anti-sense C9 zebrafish ALS models will be valuable.

SRSF1 is a key modulator of nuclear export of the HRE RNA and eif2a is important for RAN translation. Thus, the modulation of SRSF1 or eif2α in the C9-HRE zebrafish treated with compound 1527 could be investigated to identify whether modulation of these factors occurs in response to drug treatment.

These studies could also be performed using an *in vitro* model that expresses DPRs and shows toxicity to obtain more mechanistic insight. Further mechanistic information on the drug action could be obtained using *in vitro* systems to study the nuclear export of the mutant RNA in *C9orf72* models.

Compound 1527 and its analogues (1541, 1537, 1513, 1554, 1707) could be novel drugs targeting the modulation of DPRs in the C9-HRE zebrafish (sense and anti-sense) for further development. Another interesting future study would be further investigation of compound 0707 and its analogue 0039 along with compound 1262, due to them showing activity on the *hsp70*::DsRed readout in both ALS zebrafish models (sod1 and C9-HRE). Identification of the molecular target of these compounds might identify a novel target for modulating neuronal stress in ALS.

C9 zebrafish show DsRed expression in the muscle as well as the hindbrain and spinal cord. A histological study of the effect of the drugs could be conducted to identify which tissues show the greatest reduction in DsRed expression and how the drugs impact DPR levels in the different tissue compartments.

A critical future project would be to develop a DPR-based high-throughput screen to identify DPR modulating targets and compounds in the C9-HRE fish. This could be performed using dot-blotting or ELISA. ELISA is a more sensitive and quantifiable technique than the dot-blotting, but it would be more costly for a high-throughput drug screen than dot-blotting. Genetic modifier screens could be applied in an unbiased fashion to look for genetic factors that could reduce DPR load, but these screens are much simpler in invertebrate models such as *C. elegans* and *Drosophila*.

Conducting a targeted drug screen through synthesis of various analogues of the hits obtained in this project would provide a better understanding of the structure-activity relationship and identify a strong lead compound to reduce DPR levels. This would also allow for a further assessment of the active site binding of the hits and enable exploration of targets. It could also lead to enhancement of the selection of a novel candidate molecule for pre-clinical studies in rodents.

7-6 Conclusions

This project is a realistic example of a high-throughput *in vivo* drug screen in a zebrafish ALS model. It confirmed the power of the *sod1*G93Ros10 ALS zebrafish by screening 4494 compound LifeArc chemical library targeting ion channels. It provided extensive data for further ALS drug discovery with a high sensitivity and specificity of more than 90%. It detected inhibitors (4.21%) and activators (12.10%) of neuronal stress in the sod1G93Ros10 model. A unique dose-response profile of the lead hits was obtained among over 100 dose-response screens, and a behaviour analysis profile for each compound was obtained. It identified compounds that that reduced toxic DPR levels as well as reducing neuronal stress in pure C9orf72 HRE zebrafish. It therefore confirmed that ion channels are a viable target for future ALS therapy. This project opens up a vast area for chemical and genetic investigations to better understand the cellular pathophysiology of SOD1 and C9orf72 ALS, as well as other MNDs, and identify candidates for future ALS therapy.

8- References

Adachi, H., Katsuno, M., Waza, M., Minamiyama, M., Tanaka, F., and Sobue, G. (2009). Heat shock proteins in neurodegenerative diseases: Pathogenic roles and therapeutic implications. Int. J. Hyperth. *25*, 647–654.

Aggarwal, S., and Cudkowicz, M. (2008). ALS Drug Development: Reflections from the Past and a Way Forward. Neurotherapeutics *5*, 516–527.

Akamatsu, M., Yamashita, T., Hirose, N., Teramoto, S., and Kwak, S. (2016). The AMPA receptor antagonist perampanel robustly rescues amyotrophic lateral sclerosis (ALS) pathology in sporadic ALS model mice. Sci. Rep. *6*, 1–7.

Al-Chalabi, A., Jones, A., Troakes, C., King, A., Al-Sarraj, S., and Van Den Berg, L.H. (2012). The genetics and neuropathology of amyotrophic lateral sclerosis. Acta Neuropathol. *124*, 339–352.

Al-Sarraj, S., King, A., Troakes, C., Smith, B., Maekawa, S., Bodi, I., Rogelj, B., Al-Chalabi, A., Hortobágyi, T., and Shaw, C.E. (2011). P62 positive, TDP-43 negative, neuronal cytoplasmic and intranuclear inclusions in the cerebellum and hippocampus define the pathology of C9orf72-linked FTLD and MND/ALS. Acta Neuropathol. *122*, 691–702.

Al, Stephen F. Traynelis, et al (2010). Glutamate Receptor Ion Channels: Structure, Regulation, and Function. Pharmacol. Rev. *26*, 406–474.

Andries, M., Van Damme, P., Robberecht, W., and Van Den Bosch, L. (2007). Ivermectin inhibits AMPA receptor-mediated excitotoxicity in cultured motor neurons and extends the life span of a transgenic mouse model of amyotrophic lateral sclerosis. Neurobiol. Dis. *25*, 8–16.

Anzai, I., Toichi, K., Tokuda, E., Mukaiyama, A., Akiyama, S., and Furukawa, Y. (2016). Screening of Drugs Inhibiting In vitro Oligomerization of Cu/Zn-Superoxide Dismutase with a Mutation Causing Amyotrophic Lateral Sclerosis. Front. Mol. Biosci. *3*, 1–11.

Armstrong, G.A.B., and Drapeau, P. (2013). Loss and gain of FUS function impair neuromuscular synaptic transmission in a genetic model of ALS. Hum. Mol. Genet. *22*, 4282–4292.

Ash, P.E.A., Bieniek, K.F., Gendron, T.F., Caulfield, T., Lin, W.L., DeJesus-Hernandez, M., Van Blitterswijk, M.M., Jansen-West, K., Paul, J.W., Rademakers, R., et al. (2013). Unconventional Translation of C9ORF72 GGGGCC Expansion Generates Insoluble Polypeptides Specific to c9FTD/ALS. Neuron *77*, 639–646.

Atanasio, A., Decman, V., White, D., Ramos, M., Ikiz, B., Lee, H., Siao, C., Brydges, S., Larosa, E., Bai, Y., et al. (2016). C9orf72 ablation causes immune dysregulation characterized by leukocyte expansion , autoantibody production , and glomerulonephropathy in mice. Nat. Publ. Gr. *16*, 23204.

Azbill, R.D., Mu, X., and Springer, J.E. (2000). Riluzole increases high-affinity glutamate uptake in rat spinal cord synaptosomes. Brain Res. *871*, 175–180.

Baldwin, K.R., Godena, V.K., Hewitt, V.L., and Whitworth, A.J. (2016). Axonal transport defects are a common phenotype in Drosophila models of ALS. Hum. Mol. Genet. *25*, 2378–2392.

Bannwarth, S., Ait-El-Mkadem, S., Chaussenot, A., Genin, E.C., Lacas-Gervais, S., Fragaki, K., Berg-Alonso, L., Kageyama, Y., Serre, V., Moore, D.G., et al. (2014). A mitochondrial origin for frontotemporal dementia and amyotrophic lateral sclerosis through CHCHD10 involvement. Brain *137*, 2329–2345.

Barber, S.C., and Shaw, P.J. (2010). Oxidative stress in ALS: Key role in motor neuron injury and therapeutic target. Free Radic. Biol. Med. *48*, 629–641.

Barber, S.C., Higginbottom, A., Mead, R.J., Barber, S., and Shaw, P.J. (2009). An in vitro screening cascade to identify neuroprotective antioxidants in ALS. Free Radic. Biol. Med. *46*, 1127–1138.

Barua, S., Kim, J.Y., Yenari, M.A., and Lee, J.E. (2019). The role of NOX inhibitors in neurodegenerative diseases. IBRO Reports *7*, 59–69.

Battaglia, G., and Bruno, V. (2018). Metabotropic glutamate receptor involvement in the pathophysiology of amyotrophic lateral sclerosis: new potential drug targets for therapeutic applications. Curr. Opin. Pharmacol. *38*, 65–71.

Beck, M., and Hurt, E. (2017). The nuclear pore complex: Understanding its function through structural insight. Nat. Rev. Mol. Cell Biol. *18*, 73–89.

Behan, Á.T., Breen, B., Hogg, M., Woods, I., Coughlan, K., Mitchem, M., and Prehn, J.H.M. (2013). Acidotoxicity and acid-sensing ion channels contribute to motoneuron degeneration. Cell Death Differ. *20*, 589–598.

Belluzzi, O., and Urbani, A. (2000). Riluzole inhibits the persistent sodium current in rat cortical neurones. Pflügers Arch. J. Physiol. *440*, R23–R23.

Benatar, M. Lost in translation: Treatment trials in the SOD1 mouse and in human ALS. Neurobiol. Dis. 1–13.

Benedetti, L., Ghilardi, A., Rottoli, E., De Maglie, M., Prosperi, L., Perego, C., Baruscotti, M., Bucchi, A., Del Giacco, L., and Francolini, M. (2016). INaP selective inhibition reverts precocious inter- and motorneurons hyperexcitability in the Sod1-G93R zebrafish ALS model. Sci. Rep. *6*, 1–20.

Bensimon (1994). A controlled trial of Riluzole in Amyotrophic Lateral Sclerosis. N. Engl. J. Med. *330*, 587–591.

Bhat, A.H., Dar, K.B., Anees, S., Zargar, M.A., Masood, A., Sofi, M.A., and Ganie, S.A. (2015). Oxidative stress, mitochondrial dysfunction and neurodegenerative diseases; a mechanistic insight. Biomed. Pharmacother. *74*, 101–110.

Biferi, M.G., Cohen-Tannoudji, M., Cappelletto, A., Giroux, B., Roda, M., Astord, S., Marais, T., Bos, C., Voit, T., Ferry, A., et al. (2017). A New AAV10-U7-Mediated Gene Therapy Prolongs Survival and Restores Function in an ALS Mouse Model. Mol. Ther. *25*, 2038–2052.

Boccitto, M., Lamitina, T., and Kalb, R.G. (2012). Daf-2 signaling modifies mutant sod1 toxicity in c. elegans. PLoS One *7*, 1–8.

Boeynaems, S., Bogaert, E., Michiels, E., Gijselinck, I., Sieben, A., Jovičić, A., De Baets, G., Scheveneels, W., Steyaert, J., Cuijt, I., et al. (2016). Drosophila screen connects nuclear transport genes to DPR pathology in c9ALS/FTD. Sci. Rep. *6*, 7–14.

Bonifacino, T., Provenzano, F., Gallia, E., Ravera, S., Torazza, C., Bossi, S., Ferrando, S., Puliti, A., Van Den Bosch, L., Bonanno, G., et al. (2019). In-vivo genetic ablation of metabotropic glutamate receptor type 5 slows down disease progression in the SOD1G93A mouse model of amyotrophic lateral sclerosis. Neurobiol. Dis. *129*, 79–92.

Van Den Bosch, L., Van Damme, P., Bogaert, E., and Robberecht, W. (2006). The role of excitotoxicity in the pathogenesis of amyotrophic lateral sclerosis. Biochim. Biophys. Acta - Mol. Basis Dis. 1762, 1068–1082.

Bose, P., Tremblay, E., Maois, C., Narasimhan, V., Armstrong, G.A.B., Liao, M., Parker, J.A., Robitaille, R., Wen, X.Y., Barden, C., et al. (2019). The Novel Small Molecule TRVA242 Stabilizes Neuromuscular Junction Defects in Multiple Animal Models of Amyotrophic Lateral Sclerosis. Neurotherapeutics 3–18.

Bostock, H., Sharief, M.K., Reid, G. and, and Murray, N.M.F. (1995). Axonal ion channel dysfunction in amyotrophic lateral sclerosis. JAMA Neurol. *118*, 217–225.

Bowman, T. V., and Zon, L.I. (2010). Swimming into the future of drug discovery: In vivo chemical screens in zebrafish. ACS Chem. Biol. *5*, 159–161.

Boyd, J.D., Peter Lee-Armandt, J., Feiler, M.S., Zaarur, N., Liu, M., Kraemer, B., Concannon, J.B., Ebata, A., Wolozin, B., and Glicksman, M.A. (2014). A high-content screen identifies novel compounds that inhibit stress-induced TDP-43 cellular aggregation and associated cytotoxicity. J. Biomol. Screen. *19*, 44–56.

Bozzo, F., Mirra, A., and Carrì, M.T. (2017). Oxidative stress and mitochondrial damage in the pathogenesis of ALS: New perspectives. Neurosci. Lett. *636*, 3–8.

Bruijn, L.I., Becher, M.W., Lee, M.K., Anderson, K.L., Jenkins, N.A., Copeland, N.G., Sisodia, S.S., Rothstein, J.D., Borchelt, D.R., Price, D.L., et al. (1997). ALS-linked SOD1 mutant G85R mediates damage to astrocytes and promotes rapidly progressive disease with SOD1-containing inclusions. Neuron *18*, 327–338.

Bruni, G., Rennekamp, A.J., Velenich, A., McCarroll, M., Gendelev, L., Fertsch, E., Taylor, J., Lakhani, P., Lensen, D., Evron, T., et al. (2016). Zebrafish behavioral profiling identifies multitarget antipsychotic-like compounds. Nat. Chem. Biol. *12*, 559–566.

Bursch, F., Kalmbach, N., Naujock, M., Staege, S., Eggenschwiler, R., Abo-Rady, M., Japtok, J., Guo, W., Hensel, N., Reinhardt, P., et al. (2019). Altered calcium dynamics and glutamate receptor properties in iPSC derived motor

neurons from ALS patients with C9orf72, FUS, SOD1 or TDP43 mutations. Hum. Mol. Genet. *00*, 1–16.

Cacabelos, D., Ramírez-Núñez, O., Granado-Serrano, A.B., Torres, P., Ayala, V., Moiseeva, V., Povedano, M., Ferrer, I., Pamplona, R., Portero-Otin, M., et al. (2016). Early and gender-specific differences in spinal cord mitochondrial function and oxidative stress markers in a mouse model of ALS. Acta Neuropathol. Commun. *4*, 1–14.

Casafont, I., Bengoechea, R., Tapia, O., Berciano, M.T., and Lafarga, M. (2009). TDP-43 localizes in mRNA transcription and processing sites in mammalian neurons. J. Struct. Biol. *167*, 235–241.

Catterall, W. a (2000). From Ionic Currents to Molecular Mechanisms : The Structure and Function of Voltage-Gated Sodium Channels. Neuron *26*, 13–25.

Catterall, W.A. (2011). Voltage-Gated Calcium Channels. Cold Spring Harb Perspect Biol *3*, 1–373.

Chang, Q., and Martin, L.J. (2016). Voltage-gated calcium channels are abnormal in cultured spinal motoneurons in the G93A-SOD1 transgenic mouse model of ALS. Neurobiol. Dis. *93*, 78–95.

Chang, G., Guo, Y., Jia, Y., Duan, W., Li, B., Yu, J., and Li, C. (2010). Protective effect of combination of sulforaphane and riluzole on glutamate-mediated excitotoxicity. Biol Pharm Bull *33*, 1477–1483.

Chapman, A.L., Bennett, E.J., Ramesh, T.M., De Vos, K.J., and Grierson, A.J. (2013). Axonal Transport Defects in a Mitofusin 2 Loss of Function Model of Charcot-Marie-Tooth Disease in Zebrafish. PLoS One *8*, 267–276.

Chen-Plotkin, A.S., Lee, V.M.-Y., and Trojanowski, and J.Q. (2010). TAR DNA-binding protein 43 in neurodegenerative disease. NIH Public Access *6*, 211–220.

Chen, H.J., Mitchell, J.C., Novoselov, S., Miller, J., Nishimura, A.L., Scotter, E.L., Vance, C.A., Cheetham, M.E., and Shaw, C.E. (2016). The heat shock response plays an important role in TDP-43 clearance: Evidence for dysfunction in amyotrophic lateral sclerosis. Brain *139*, 1417–1432.

Chew, J., Gendron, T.F., Prudencio, M., Sasaguri, H., Castanedes-casey, M., Lee, C.W., Jansen-west, K., Kurti, A., Murray, M.E., Bieniek, K.F., et al. (2015). C9ORF72 repeat expansions in mice cause TDP-43 pathology, neuronal loss, and behavioral deficits. *348*, 1151–1154.

Chiu, A.S., Gehringer, M.M., Welch, J.H. and, and Neilan, B.A. (2011). Does α-amino-β-methylaminopropionic acid (BMAA) play a role in neurodegeneration.pdf. 3728–3746.

Ciura, S., Lattante, S., Le Ber, I., Latouche, M., Tostivint, H., Brice, A., and Kabashi, E. (2013). Loss of function of C9orf72 causes motor deficits in a zebrafish model of amyotrophic lateral sclerosis. Ann. Neurol. *74*, 180–187.

Cooper-Knock, J., Shaw, P.J., and Kirby, J. (2014). The widening spectrum of

C9ORF72-related disease; Genotype/phenotype correlations and potential modifiers of clinical phenotype. Acta Neuropathol. *127*, 333–345.

Corbin-Leftwich, A., Mossadeq, S.M., Ha, J., Ruchala, I., Le, A.H.N., and Villalba-Galea, C.A. (2016). Retigabine holds $K_V 7$ channels open and stabilizes the resting potential. J. Gen. Physiol. *147*, 229–241.

Corti, S., Donadoni, C., Ronchi, D., Bordoni, A., Fortunato, F., Santoro, D., Del Bo, R., Lucchini, V., Crugnola, V., Papadimitriou, D., et al. (2009). Amyotrophic lateral sclerosis linked to a novel SOD1 mutation with muscle mitochondrial dysfunction. J. Neurol. Sci. *276*, 170–174.

Da Costa, M.M.J., Allen, C.E., Higginbottom, A., Ramesh, T., Shaw, P.J., and McDermott, C.J. (2014). A new zebrafish model produced by TILLING of SOD1-related amyotrophic lateral sclerosis replicates key features of the disease and represents a tool for in vivo therapeutic screening. DMM Dis. Model. Mech. *7*, 73–81.

Cozzolino, M., Ferri, A., Valle, C., and Carr, M.T. (2013). Mitochondria and ALS: Implications from novel genes and pathways. Mol. Cell. Neurosci. *55*, 44–49.

Van Damme, P., Robberecht, W., and Van Den Bosch, L. (2017). Modelling amyotrophic lateral sclerosis: Progress and possibilities. DMM Dis. Model. Mech. *10*, 537–549.

Dedeene, L., Van Schoor, E., Race, V., Moisse, M., Vandenberghe, R., Poesen, K., Van Damme, P., and Thal, D.R. (2019). An ALS case with 38 (G4C2)-repeats in the C9orf72 gene shows TDP-43 and sparse dipeptide repeat protein pathology. Acta Neuropathol. *137*, 853–856.

DeJesus-Hernandez, M., Mackenzie, I.R., Boeve, B.F., Boxer, A.L., Baker, M., Rutherford, N.J., Nicholson, A.M., Finch, N.C.A., Flynn, H., Adamson, J., et al. (2011). Expanded GGGGCC Hexanucleotide Repeat in Noncoding Region of C9ORF72 Causes Chromosome 9p-Linked FTD and ALS. Neuron *72*, 245–256.

Deng, H.-X., Shi, Y., Furukawa, Y., Zhai, H., Fu, R., Liu, E., Gorrie, G.H., Khan, M.S., Hung, W.-Y., Bigio, E.H., et al. (2006). Conversion to the amyotrophic lateral sclerosis phenotype is associated with intermolecular linked insoluble aggregates of SOD1 in mitochondria. Proc. Natl. Acad. Sci. U. S. A. *103*, 7142–7147.

Deng, H., Chen, W., Hong, S., Boycott, K.M., George, H., Siddique, N., Yang, Y., Fecto, F., Shi, Y., Zhai, H., et al. (2012). Mutations in UBQLN2 cause dominant X-linked juvenile and adult onset ALS and ALS/dementia. *477*, 211–215.

Deng, H.X., Chen, W., Hong, S.T., Boycott, K.M., Gorrie, G.H., Siddique, N., Yang, Y., Fecto, F., Shi, Y., Zhai, H., et al. (2011). Mutations in UBQLN2 cause dominant X-linked juvenile and adult-onset ALS and ALS/dementia. Nature *477*, 211–215.

Do-Ha, D., Buskila, Y., and Ooi, L. (2018). Impairments in Motor Neurons, Interneurons and Astrocytes Contribute to Hyperexcitability in ALS: Underlying

Mechanisms and Paths to Therapy. Mol. Neurobiol. *55*, 1410–1418.

Dolphin, A.C. (2018). Voltage-gated calcium channels: Their discovery, function and importance as drug targets. Brain Neurosci. Adv. *2*, 1–20.

Donnelly, C.J., Zhang, P.W., Pham, J.T., Heusler, A.R., Mistry, N.A., Vidensky, S., Daley, E.L., Poth, E.M., Hoover, B., Fines, D.M., et al. (2013). RNA Toxicity from the ALS/FTD C9ORF72 Expansion Is Mitigated by Antisense Intervention. Neuron *80*, 415–428.

Dukay, B., Csoboz, B., and Tóth, M.E. (2019). Heat-Shock Proteins in Neuroinflammation. Front. Pharmacol. *10*, 1–22.

Dupuis, L., Gonzalez De Aguilar, J.L., Oudart, H., De Tapia, M., Barbeito, L., and Loeffler, J.P. (2004). Mitochondria in amyotrophic lateral sclerosis: A trigger and a target. Neurodegener. Dis. *1*, 245–254.

Elden, A.C., Kim, H.J., Hart, M.P., Chen-Plotkin, A.S., Johnson, B.S., Fang, X., Armakola, M., Geser, F., Greene, R., Lu, M.M., et al. (2010). Ataxin-2 intermediate-length polyglutamine expansions are associated with increased risk for ALS. Nature *466*, 1069–1075.

Eskildsen, J., Redrobe, J.P., Sams, A.G., Dekermendjian, K., Laursen, M., Boll, J.B., Papke, R.L., Bundgaard, C., Frederiksen, K., and Bastlund, J.F. (2014). Discovery and optimization of Lu AF58801, a novel, selective and brain penetrant positive allosteric modulator of alpha-7 nicotinic acetylcholine receptors: Attenuation of subchronic phencyclidine (PCP)-induced cognitive deficits in rats following oral ad. Bioorganic Med. Chem. Lett. *24*, 288–293.

Fang, M.Y., Markmiller, S., Vu, A.Q., Javaherian, A., Dowdle, W.E., Jolivet, P., Bushway, P.J., Castello, N.A., Baral, A., Chan, M.Y., et al. (2019). Small-Molecule Modulation of TDP-43 Recruitment to Stress Granules Prevents Persistent TDP-43 Accumulation in ALS/FTD. Neuron *103*, 1–18.

Faul, F., Buchner, A., Erdfelder, E., and Mayr, S. (2007). A short tutorial of GPower. Tutor. Quant. Methods Psychol. *3*, 51–59.

Feng, H.L., Leng, Y., Ma, C.H., Zhang, J., Ren, M., and Chuang, D.M. (2008). Combined lithium and valproate treatment delays disease onset, reduces neurological deficits and prolongs survival in an amyotrophic lateral sclerosis mouse model. Neuroscience *155*, 567–572.

Ferrante, R.J., Browne, S.E., Shinobu, L. a, Bowling, a C., Baik, M.J., MacGarvey, U., Kowall, N.W., Brown, R.H., and Beal, M.F. (1997). Evidence of increased oxidative damage in both sporadic and familial amyotrophic lateral sclerosis. J. Neurochem. *69*, 2064–2074.

Foran, E., and Trotti, D. (2009). Glutamate Transporters and the Excitotoxic Path to Motor Neuron Degeneration in Amyotrophic Lateral Sclerosis. Antioxid. Redox Signal. *11*, 1587–1602.

Forman, M.S., Trojanowski, J.Q., and Lee, V.M.Y. (2007). TDP-43: a novel neurodegenerative proteinopathy. Curr. Opin. Neurobiol. *17*, 548–555.

Forsberg, K., Graffmo, K., Pakkenberg, B., Weber, M., Nielsen, M., Marklund, S., Brännström, T., and Andersen, P.M. (2019). Misfolded SOD1 inclusions in patients with mutations in C9orf72 and other ALS/FTD-associated genes. J. Neurol. Neurosurg. Psychiatry *0*, 1–9.

Fournier, J.F., Bouix-Peter, C., Duvert, D., Luzy, A.P., and Ouvry, G. (2018). Intrinsic property forecast index (iPFI) as a Rule of thumb for medicinal chemists to remove a phototoxicity liability. J. Med. Chem. *61*, 3231–3236.

Francois-Moutal, L., Scott, D.D., Felemban, R., Miranda, V.G., Sayegh, M.R., Perez-Miller, S., Khanna, R., Gokhale, V., Zarnescu, D.C., and Khanna, M. (2019). A small molecule targeting TDP-43's RNA recognition motifs reduces locomotor defects in a Drosophila model of ALS. ACS Chem. Biol. 14, 1–27.

Freibaum, B.D., Lu, Y., Lopez-Gonzalez, R., Kim, N.C., Almeida, S., Lee, K.-H., Badders, N., Valentine, M., Miller, B.L., Wong, P.C., et al. (2015). GGGGCC repeat expansion in C0ORF72 compromises nucleocytoplasmic transport. Nature *525*, 129–133.

Freischmidt, A., Wieland, T., Richter, B., Ruf, W., Schaeffer, V., Müller, K., Marroquin, N., Nordin, F., Hübers, A., Weydt, P., et al. (2015). Haploinsufficiency of TBK1 causes familial ALS and fronto-temporal dementia. Nat. Neurosci. *18*, 631–636.

Gatenby, R.A. (2019). The Role of Cell Membrane Information Reception, Processing, and Communication in the Structure and Function of Multicellular Tissue. Int. J. Mol. Sci. *20*, 1–13.

Gendron, T.F., Bieniek, K.F., Zhang, Y.J., Jansen-West, K., Ash, P.E.A., Caulfield, T., Daughrity, L., Dunmore, J.H., Castanedes-Casey, M., Chew, J., et al. (2013). Antisense transcripts of the expanded C9ORF72 hexanucleotide repeat form nuclear RNA foci and undergo repeat-associated non-ATG translation in c9FTD/ALS. Acta Neuropathol. *126*, 829–844.

Gendron, T.F., van Blitterswijk, M., Bieniek, K.F., Daughrity, L.M., Jiang, J., Rush, B.K., Pedraza, O., Lucas, J.A., Murray, M.E., Desaro, P., et al. (2015). Cerebellar c9RAN proteins associate with clinical and neuropathological characteristics of C9ORF72 repeat expansion carriers. Acta Neuropathol. *130*, 559–573.

Gifondorwa, D.J., Robinson, M.B., Hayes, C.D., Taylor, A.R., Prevette, D.M., Oppenheim, R.W., Caress, J., and Milligan, C.E. (2007). Exogenous Delivery of Heat Shock Protein 70 Increases Lifespan in a Mouse Model of Amyotrophic Lateral Sclerosis. J. Neurosci. *27*, 13173–13180.

Gifondorwa, D.J., Jimenz-Moreno, R., Hayes, C.D., Rouhani, H., Robinson, M.B., Strupe, J.L., Caress, J., and Milligan, C. (2012). Administration of recombinant heat shock protein 70 delays peripheral muscle denervation in the SOD1 G93A mouse model of amyotrophic lateral sclerosis. Neurol. Res. Int. *2012*.

Giovanni Manfredi and Hibiki Kawamata (2016). Mitochondria and endoplasmic reticulum crosstalk in amyotrophic lateral sclerosis. Physiol. Behav. *176*, 139–

148.

Gomez-Deza, J., Lee, Y.-B., Troakes, C., Nolan, M., Al-Sarraj, S., Gallo, J.-M., and Shaw, C.E. (2015). Dipeptide repeat protein inclusions are rare in the spinal cord and almost absent from motor neurons in C9ORF72 mutant amyotrophic lateral sclerosis and are unlikely to cause their degeneration. Acta Neuropathol. Commun. *3*, 1–7.

Guerrero, E.N., Wang, H., Mitra, J., Hegde, P.M., Stowell, S.E., Liachko, N.F., Kraemer, B.C., Garruto, R.M., Rao, K.S., and Hegde, M.L. (2016). TDP-43/FUS in motor neuron disease: Complexity and challenges. Prog. Neurobiol. *145–146*, 78–97.

Gurney, M.E., Pu, H., Chiu, A.Y., Dal Canto, M.C., Polchow, C.Y., Alexander, D.D., Caliendo, J., Hentati, A., Kwon, Y.W., Deng, H.-X., et al. (1994). Motor neuron degeneration in mice that express a human Cu,Zn superoxide dismutase mutation. Science (80-.). *264*, 1772–1775.

Haeusler, A.R., Donnelly, C.J., Periz, G., Simko, E.A.J., Shaw, P.G., Kim, M.S., Maragakis, N.J., Troncoso, J.C., Pandey, A., Sattler, R., et al. (2014). C9orf72 nucleotide repeat structures initiate molecular cascades of disease. Nature *507*, 195–200.

Halliday, M., Radford, H., Zents, K.A.M., Molloy, C., Moreno, J.A., Verity, N.C., Smith, E., Ortori, C.A., Barrett, D.A., Bushell, M., et al. (2017). Repurposed drugs targeting eIF2α-P-mediated translational repression prevent neurodegeneration in mice. Brain *140*, 1768–1783.

Hardiman, O., , Ammar Al-Chalabi2 , Adriano Chio3 , Emma M. Corr , Giancarlo Logroscino, Wim Robberecht, Pamela J. Shaw, Z.S., and Berg, and L.H. van den (2017). Amyotrophic lateral sclerosis. Nat. Rev. Dis. Prim. *3*, 1–17.

Hautbergue, G.M., Castelli, L.M., Ferraiuolo, L., Sanchez-Martinez, A., Cooper-Knock, J., Higginbottom, A., Lin, Y.H., Bauer, C.S., Dodd, J.E., Myszczynska, M.A., et al. (2017). SRSF1-dependent nuclear export inhibition of C9ORF72 repeat transcripts prevents neurodegeneration and associated motor deficits. Nat. Commun. *8*, 1–18.

Hayward, C., Brock, D.J.H., Minns, R.A., and Swingler, R.J. (1998). Homozygosity for Asn86Ser mutation in the CuZn-superoxide dismutase gene produces a severe clinical phenotype in a juvenile onset case of fALS. Med. Genet. *35*, 174–176.

He, H., Huang, W., Wang, R., Lin, Y., Guo, Y., Deng, J., Deng, H., Zhu, Y., Allen, E.G., Jin, P., et al. (2019). Amyotrophic Lateral Sclerosis-associated GGGGCC repeat expansion promotes Tau phosphorylation and toxicity. Neurobiol. Dis. *130*, 1–10.

Hilton, J.B., Mercer, S.W., Lim, N.K.H., Faux, N.G., Buncic, G., Beckman, J.S., Roberts, B.R., Donnelly, P.S., White, A.R., and Crouch, P.J. (2017). Cu II (atsm) improves the neurological phenotype and survival of SOD1 G93A mice and selectively increases enzymatically active SOD1 in the spinal cord. Nat. Publ. Gr. 1–11.

Ho, W.Y., and Ling, S.-C. (2019). Elevated FUS levels by overriding its autoregulation produce gain-of-toxicity properties that disrupt protein and RNA homeostasis. Autophagy *0*, 1–3.

Hogg, M.C., Halang, L., Woods, I., Coughlan, K.S., and Prehn, J.H.M. (2018). Riluzole does not improve lifespan or motor function in three ALS mouse models. Amyotroph. Lateral Scler. Front. Degener. *19*, 438–445.

Howe, K., Clark, M.D., Torroja, C.F., Torrance, J., Berthelot, C., Muffato, M., Collins, J.E.J.E., Humphray, S., McLaren, K., Matthews, L., et al. (2013). The zebrafish reference genome sequence and its relationship to the human genome. Nature *496*, 498–503.

Islam, M.T. (2017). Oxidative stress and mitochondrial dysfunction-linked neurodegenerative disorders. Neurol. Res. *39*, 73–82.

Jean Mantz; et al (1992). Anesthetic properties of riluzole (54274 RP), a new inhibitor of glutamate neurotransmission. Anesthesiology *76*, 844–848.

Jiang, J., Zhu, Q., Gendron, T.F., Saberi, S., McAlonis-Downes, M., Seelman, A., Stauffer, J.E., Jafar-nejad, P., Drenner, K., Schulte, D., et al. (2016). Gain of Toxicity from ALS/FTD-Linked Repeat Expansions in C9ORF72 Is Alleviated by Antisense Oligonucleotides Targeting GGGGCC-Containing RNAs. Neuron *90*, 535–550.

Johnson, J.O., Mandrioli, J., Benatar, M., Abramzon, Y., Van Deerlin, V.M., Trojanowski, J.Q., Gibbs, J.R., Brunetti, M., Gronka, S., Wuu, J., et al. (2010). Exome Sequencing Reveals VCP Mutations as a Cause of Familial ALS. Neuron *68*, 857–864.

Johnson, J.O., Pioro, E.P., Boehringer, A., Chia, R., Feit, H., Renton, A.E., Pliner, H.A., Abramzon, Y., Marangi, G., Winborn, B.J., et al. (2014). Mutations in the Matrin 3 gene cause familial amyotrophic lateral sclerosis. Nat. Neurosci. *17*, 664–666.

Jones, S.R., Carley, S., and Harrison, M. (2003). An introduction to power and sample size estimation. Emerg. Med. J. *20*, 453–458.

Kabashi, E., Lin, L., Tradewell, M.L., Dion, P.A., Bercier, V., Bourgouin, P., Rochefort, D., Bel Hadj, S., Durham, H.D., Velde, C. Vande, et al. (2009). Gain and loss of function of ALS-related mutations of TARDBP (TDP-43) cause motor deficits in vivo. Hum. Mol. Genet. *19*, 671–683.

Kabashi, E., Brustein, E., Champagne, N., and Drapeau, P. (2011). Zebrafish models for the functional genomics of neurogenetic disorders. Biochim. Biophys. Acta - Mol. Basis Dis. *1812*, 335–345.

Kalmar, B., and Greensmith, L. (2009). Activation of the heat shock response in a primary cellular model of motoneuron neurodegeneration - Evidence for neuroprotective and neurotoxic effects. Cell. Mol. Biol. Lett. *14*, 319–335.

Kalmar, B., Novoselov, S., Gray, A., Cheetham, M.E., Margulis, B., and Greensmith, L. (2008). Late stage treatment with arimoclomol delays disease

progression and prevents protein aggregation in the SOD1G93A mouse model of ALS. J. Neurochem. *107*, 339–350.

Kaur, S.J., McKeown, S.R., and Rashid, S. (2016). Mutant SOD1 mediated pathogenesis of Amyotrophic Lateral Sclerosis. Gene *577*, 109–118.

Kieran, D., Kalmar, B., Dick, J.R.T., Riddoch-Contreras, J., Burnstock, G., and Greensmith, L. (2004). Treatment with arimoclomol, a coinducer of heat shock proteins, delays disease progression in ALS mice. Nat. Med. *10*, 402–405.

Kiernan, M.C., Vucic, S., Cheah, B.C., Turner, M.R., Eisen, A., Hardiman, O., Burrell, J.R., and Zoing, M.C. (2011). Amyotrophic lateral sclerosis. Lancet *377*, 942–955.

King, O.D., Gitler, A.D., and James, S. (2012). The tip of the iceberg: RNA-binding proteins with prion-like domains in neurodegenerative disease. Brain Res *1462*, 61–80.

Kliveny, et al (2006). Neuroprotective effects of (-)-epigallocatechin-3-gallate in a transgenic mouse model of amyotrophic lateral sclerosis. Neurochem. Res. *31*, 1263–1269.

Klug, D.M., Diaz-Gonzalez, R., Pérez-Moreno, G., Ceballos-Pérez, G., García-Hernández, R., Gomez-Pérez, V., Ruiz-Pérez, L.M., Rojas-Barros, D.I., Gamarro, F., González-Pacanowska, D., et al. (2019). Evaluation of a class of isatinoids identified from a high-throughput screen of human kinase inhibitors as anti-sleeping sickness agents. PLoS Negl. Trop. Dis. *13*, 1–12.

Kong, J., and Xu, Z. (1998). Massive mitochondrial degeneration in motor neurons triggers the. J Neurosci *18*, 3241–3250.

Kong, Q., Chang, L.C., Takahashi, K., Liu, Q., Schulte, D.A., Lai, L., Ibabao, B., Lin, Y., Stouffer, N., Mukhopadhyay, C. Das, et al. (2014). Small-molecule activator of glutamate transporter EAAT2 translation provides neuroprotection. J. Clin. Invest. *124*, 1255–1267.

Kuo, J.J., Siddique, T., Fu, R., and Heckman, C.J. (2005). Increased persistent Na(+) current and its effect on excitability in motoneurones cultured from mutant SOD1 mice. J. Physiol. *563*, 843–854.

Kwiatkowski, et al (2009). All use subject to JSTOR Terms and Conditions in the FUS / TLS Gene Mutations on Chromosome 16 Cause Familial Amyotrophic Lateral Sclerosis. Science (80-.). *323*, 1205–1208.

Landers, J.E., Melki, J., Meininger, V., Glass, J.D., Van Den Berg, L.H., Van Es, M.A., Sapp, P.C., Van Vught, P.W.J., McKenna-Yasek, D.M., Blauw, H.M., et al. (2009). Reduced expression of the Kinesin-Associated Protein 3 (KIFAP3) gene increases survival in sporadic amyotrophic lateral sclerosis. Proc. Natl. Acad. Sci. U. S. A. *106*, 9004–9009.

Lau, A., and Tymianski, M. (2010). Glutamate receptors, neurotoxicity and neurodegeneration. Pflugers Arch. Eur. J. Physiol. *460*, 525–542.

Lazarevic, V., Yang, Y., Ivanova, D., Fejtova, A., and Svenningsson, P. (2018).

Riluzole attenuates the efficacy of glutamatergic transmission by interfering with the size of the readily releasable neurotransmitter pool. Neuropharmacology *143*, 38–48.

Lee, J.C., Joo, K.M., Choe, S.Y., and Cha, C.I. (2012). Region-specific changes in the immunoreactivity of TRPV4 expression in the central nervous system of SOD1G93A transgenic mice as an in vivo model of amyotrophic lateral sclerosis. J. Mol. Histol. *43*, 625–631.

Li, J., and Le, W. (2013). Modeling neurodegenerative diseases in Caenorhabditis elegans. Exp. Neurol. *250*, 94–103.

Ling, S.-C., Polymenidou, M., and Cleveland, D.W. (2013). Converging mechanisms in ALS and FTD: Disrupted RNA and protein homeostasis. Physiol. Behav. *79*, 416–438.

Liu, J., Shinobu, L.A., Ward, C.M., Young, D., and Cleveland, D.W. (2005). Elevation of the Hsp70 chaperone does not effect toxicity in mouse models of familial amyotrophic lateral sclerosis. J. Neurochem. *93*, 875–882.

Liu, Q., Shu, S., Wang, R.R., Liu, F., Cui, B., Guo, X.N., Lu, C.X., Li, X.G., Liu, M.S., Peng, B., et al. (2016a). Whole-exome sequencing identifies a missense mutation in hnRNPA1 in a family with flail arm ALS. Neurology *87*, 1763–1769.

Liu, Y., Pattamatta, A., Zu, T., Reid, T., Bardhi, O., Borchelt, D.R., Yachnis, A.T., and Ranum, L.P.W. (2016b). C9orf72 BAC Mouse Model with Motor Deficits and Neurodegenerative Features of ALS/FTD. Neuron *90*, 521–534.

Logroscino, G., Traynor, B.J., Hardiman, O., Chió, A., Mitchell, D., Swingler, R.J., Millul, A., Benn, E., and Beghi, E. (2010). Incidence of amyotrophic lateral sclerosis in Europe. J. Neurol. Neurosurg. Psychiatry *81*, 385–390.

Lynagh, T., Webb, T.I., Dixon, C.L., Cromers, B.A., and Lynch, J.W. (2011). Molecular determinants of ivermectin sensitivity at the glycine receptor chloride channel. J. Biol. Chem. *286*, 43913–43924.

Mackenzie, I.R.A., Bigio, E.H., Ince, P.G., Geser, F., Neumann, M., Cairns, N.J., Kwong, L.K., Forman, M.S., Ravits, J., Stewart, H., et al. (2007). Pathological TDP-43 distinguishes sporadic amyotrophic lateral sclerosis from amyotrophic lateral sclerosis with SOD1 mutations. Ann. Neurol. *61*, 427–434.

MacRae, C.A., and Peterson, R.T. (2015). Zebrafish as tools for drug discovery. Nat. Rev. Drug Discov. *14*, 721–731.

Maekawa, S., Al-Sarraj, S., Kibble, M., Landau, S., Parnavelas, J., Cotter, D., Everall, I., and Leigh, P.N. (2004). Cortical selective vulnerability in motor neuron disease: A morphometric study. Brain *127*, 1237–1251.

Mahmoud, S., Gharagozloo, M., Simard, C., and Gris, D. (2019). Astrocytes Maintain Glutamate Homeostasis in the CNS by Controlling the Balance between Glutamate Uptake and Release. Cells *8*, 3–27.

Martin, L.J. and C.Q. (2012). Inhibitory Synaptic Regulation of Motoneurons: A New Target of Disease Mechanisms in Amyotrophic Lateral Sclerosis. Mol

Neurobiol. *45*, 30–42.

Maruyama, H., Morino, H., Ito, H., Izumi, Y., Kato, H., Watanabe, Y., Kinoshita, Y., Kamada, M., Nodera, H., Suzuki, H., et al. (2010). Mutations of optineurin in amyotrophic lateral sclerosis. Nature *465*, 223–226.

Mathis, S., Goizet, C., Soulages, A., Vallat, J.M., and Masson, G. Le (2019). Genetics of amyotrophic lateral sclerosis: A review. J. Neurol. Sci. *399*, 217–226.

Matsumoto, G., Stojanovic, A., Holmberg, C.I., Kim, S., and Morimoto, R.I. (2005). Structural properties and neuronal toxicity of amyotrophic lateral sclerosis-associated Cu/Zn superoxide dismutase 1 aggregates. J. Cell Biol. *171*, 75–85.

Mattiazzi, M., D'Aurelio, M., Gajewski, C.D., Martushova, K., Kiaei, M., Flint Beal, M., and Manfredi, G. (2002). Mutated human SOD1 causes dysfunction of oxidative phosphorylation in mitochondria of transgenic mice. J. Biol. Chem. *277*, 29626–29633.

Matzke, A.J.M., Weiger, T.M., and Matzke, M. (2010). Ion channels at the nucleus: Electrophysiology meets the genome. Mol. Plant *3*, 642–652.

McAllum, E.J., Roberts, B.R., Hickey, J.L., Dang, T.N., Grubman, A., Donnelly, P.S., Liddell, J.R., White, A.R., and Crouch, P.J. (2015). ZnII(atsm) is protective in amyotrophic lateral sclerosis model mice via a copper delivery mechanism. Neurobiol. Dis. *81*, 20–24.

McGown, A. (2014). Developing and validating a high-throughput drug screen in a zebrafish model of amyotrophic lateral sclerosis. Thesis. Univ. Sheff. 1–210.

McGown, A., McDearmid, J.R., Panagiotaki, N., Tong, H., Al Mashhadi, S., Redhead, N., Lyon, A.N., Beattie, C.E., Shaw, P.J., and Ramesh, T.M. (2013). Early interneuron dysfunction in ALS: Insights from a mutant sod1 zebrafish model. Ann. Neurol. *73*, 246–258.

McGown, A., Pamela, D., Shaw, J., and Ramesh, T. (2016). ZNStress: a high-throughput drug screening protocol for identification of compounds modulating neuronal stress in the transgenic mutant sod1G93R zebrafish model of amyotrophic lateral sclerosis. Mol. Neurodegener. *56*, 3–11.

McGurk, L., Berson, A., and Bonini, N.M. (2015). Drosophila as an in vivo model for human neurodegenerative disease. Genetics *201*, 377–402.

McMillan, C.T., Russ, J., Wood, E.M., Irwin, D.J., Grossman, M., McCluskey, L., Elman, L., Van Deerlin, V., and Lee, E.B. (2015). C9orf72 promoter hypermethylation is neuroprotective. Neurology *84*, 1622–1630.

Mead, R.J., Higginbottom, A., Allen, S.P., Kirby, J., Bennett, E., Barber, S.C., Heath, P.R., Coluccia, A., Patel, N., Gardner, I., et al. (2013). S[+] Apomorphine is a CNS penetrating activator of the Nrf2-ARE pathway with activity in mouse and patient fibroblast models of amyotrophic lateral sclerosis. Free Radic. Biol. Med. *61*, 438–452.

Merrilees, J., Klapper, J., Murphy, J., Lomen-Hoerth, C., and Miller, B.L. (2010). Cognitive and behavioral challenges in caring for patients with frontotemporal dementia and amyotrophic lateral sclerosis. Amyotroph. Lateral Scler. *11*, 298–302.

Milanese, M., Giribaldi, F., Melone, M., Bonifacino, T., Musante, I., Carminati, E., Rossi, P.I.A., Vergani, L., Voci, A., Conti, F., et al. (2014). Knocking down metabotropic glutamate receptor 1 improves survival and disease progression in the SOD1G93A mouse model of amyotrophic lateral sclerosis. Neurobiol. Dis. *64*, 48–59.

Miller, T., Pestronk, A., David, W., Rothstein, J., Simpson, E., Appel, S.H., Andres, P.L., Mahoney, K., Allred, P., Alexander, K., et al. (2013). A Phase I, Randomised, First-in-Human Study of an Antisense Oligonucleotide Directed Against SOD1 Delivered Intrathecally in SOD1-Familial ALS Patients. Lancet Neurol *12*, 435–442.

Min, H.J., Cho, I.R., Srisuttee, R., Park, E.H., Cho, D.H., Ahn, J.H., Lee, I.S., Johnston, R.N., Oh, S., and Chung, Y.H. (2009). Hexachlorophene suppresses β-catenin expression by up-regulation of Siah-1 in EBV-infected B lymphoma cells. Cancer Lett. *276*, 136–142.

Moens, T.G., Niccoli, T., Wilson, K.M., Atilano, M.L., and Birsa, N. (2019). C9orf72 arginine - rich dipeptide proteins interact with ribosomal proteins in vivo to induce a toxic translational arrest that is rescued by eIF1A. Acta Neuropathol. *137*, 487–500.

Mordes, D.A., Prudencio, M., Goodman, L.D., Klim, J.R., Moccia, R., Limone, F., Pietilainen, O., Chowdhary, K., Dickson, D.W., Rademakers, R., et al. (2018). Dipeptide repeat proteins activate a heat shock response found in C9ORF72 - ALS / FTLD patients. 1–13.

Mori, K., Weng, S.-M.M., Arzberger, T., May, S., Rentzsch, K., Kremmer, E., Schmid, B., Kretzschmar, H.A., Cruts, M., Van Broeckhoven, C., et al. (2013b). The C9orf72 GGGGCC repeat is translated into aggregating dipeptide-repeat proteins in FTLD/ALS. TL - 339. Science *339*, 1335–1338.

Myszczynska, M., and Ferraiuolo, L. (2016). New in vitro models to study amyotrophic lateral sclerosis. Brain Pathol. *26*, 258–265.

Nagai, M., Aoki, M., Miyoshi, I., Kato, M., Pasinelli, P., Kasai, N., Brown, R.H., and Itoyama, Y. (2001). Rats expressing human cytosolic copper-zinc superoxide dismutase transgenes with amyotrophic lateral sclerosis: associated mutations develop motor neuron disease. J. Neurosci. *21*, 9246–9254.

Narayan, M., Peralta, D.A., Gibson, C., Zitnyar, A., and Jinwal, U.K. (2015). An optimized InCell Western screening technique identifies hexachlorophene as a novel potent TDP43 targeting drug. J. Biotechnol. *207*, 34–38.

Neumann, M. (2009). Molecular neuropathology of TDP-43 proteinopathies. Int. J. Mol. Sci. *10*, 232–246.

Neumann, M., Sampathu, D.M., Kwong, L.K., Truax, A.C., Micsenyi, M.C.,

Chou, T.T., Bruce, J., Schuck, T., Grossman, M., Clark, C.M., et al. (2006). Ubiquitinated TDP-43 in Frontotemporal Lobar Degeneration and Amyotrophic Lateral Sclerosis. Science (80-.). *314*, 130–133.

Newman, M., Ebrahimie, E., and Lardelli, M. (2014). Using the zebrafish model for Alzheimer's disease research. Front. Genet. *5*, 1–10.

Nihei, K., McKee, A.C., and Kowall, N.W. (1993). Patterns of neuronal degeneration in the motor cortex of amyotrophic lateral sclerosis patients. Acta Neuropathol. *86*, 55–64.

Nishimura, A.L., Mitne-Neto, M., Silva, H.C.A., Richieri-Costa, A., Middleton, S., Cascio, D., Kok, F., Oliveira, J.R.M., Gillingwater, T., Webb, J., et al. (2004). A mutation in the vesicle-trafficking protein VAPB causes late-onset spinal muscular atrophy and amyotrophic lateral sclerosis. Am. J. Hum. Genet. *75*, 822–831.

Niswender, C.M., and Conn, P.J. (2010). Metabotropic Glutamate Receptors: Physiology, Pharmacology, and Disease. Annu. Rev. Pharmacol. Toxicol. *50*, 295–322.

O'Rourke, J.G., Bogdanik, L., Muhammad, A.K.M.G., Gendron, T.F., Kim, K.J., Austin, A., Cady, J., Liu, E.Y., Zarrow, J., Grant, S., et al. (2015). C9orf72 BAC Transgenic Mice Display Typical Pathologic Features of ALS/FTD. Neuron *88*, 892–901.

Oakes, J.A., Davies, M.C., and Collins, M.O. (2017). TBK1: a new player in ALS linking autophagy and neuroinflammation. Mol. Brain *10*, 1–10.

Oeda, T., Shimohama, S., Kitagawa, N., Kohno, R., Imura, T., Shibasaki, H., and Ishii, N. (2001). Oxidative stress causes abnormal accumulation of familial amyotrophic lateral sclerosis-related mutant SOD1 in transgenic Caenorhabditis elegans. Hum. Mol. Genet. *10*, 2013–2023.

Ohta, Y., Nomura, E., Shang, J., Feng, T., Huang, Y., Liu, X., Shi, X., Nakano, Y., Hishikawa, N., Sato, K., et al. (2019). Enhanced oxidative stress and the treatment by edaravone in mice model of amyotrophic lateral sclerosis. J. Neurosci. Res. *97*, 607–619.

Pagliardini, V., Pagliardini, S., Corrado, L., Lucenti, A., Panigati, L., Bersano, E., Servo, S., Cantello, R., D'Alfonso, S., and Mazzini, L. (2015). Chitotriosidase and lysosomal enzymes as potential biomarkers of disease progression in amyotrophic lateral sclerosis: A survey clinic-based study. J. Neurol. Sci. *348*, 245–250.

Pandey, U.B., and Nichols, C.D. (2011). Human Disease Models in Drosophila melanogaster and the Role of the Fly in Therapeutic Drug Discovery. Drug Deliv. *63*, 411–436.

Pansarasa, O., Bordoni, M., Diamanti, L., Sproviero, D., Gagliardi, S., and Cereda, C. (2018). Sod1 in amyotrophic lateral sclerosis: "ambivalent" behavior connected to the disease. Int. J. Mol. Sci. *19*, 1–13.

Papsdorf, K., and Richter, K. (2014). Protein folding, misfolding and quality control: The role of molecular chaperones. Essays Biochem. *56*, 53–68.

Parakh, S., and Atkin, J.D. (2016). Protein folding alterations in amyotrophic lateral sclerosis. Brain Res. *1648*, 633–649.

Parkinson, N., Ince, P.G., Smith, M.O., Highley, R., Skibinski, G., Andersen, P.M., Morrison, K.E., Pall, H.S., Hardiman, O., Collinge, J., et al. (2006). ALS phenotypes with mutations in CHMP2B (charged multivesicular body protein 2B). Neurology *67*, 1074–1077.

Patten, S.A., Aggad, D., Martinez, J., Tremblay, E., Petrillo, J., Armstrong, G.A.B., La Fontaine, A., Maios, C., Liao, M., Ciura, S., et al. (2017). Neuroleptics as therapeutic compounds stabilizing neuromuscular transmission in amyotrophic lateral sclerosis. JCI Insight *2*, 1–20.

Peters, O.M., Ghasemi, M., and Brown Jr., R.H. (2015). Emerging mechanisms of molecular pathology in ALS Find the latest version : Emerging mechanisms of molecular pathology in ALS. J. Clin. Invest. *125*, 1767–1779.

Pieri, M., Carunchio, I., Curcio, L., Mercuri, N.B., and Zona, C. (2009). Increased persistent sodium current determines cortical hyperexcitability in a genetic model of amyotrophic lateral sclerosis. Exp. Neurol. *215*, 368–379.

Pin, J.P., and Duvoisin, R. (1995). Review: Neurotransmitter receptors I. The metabotropic glutamate receptors: Structure and functions. Neuropharmacology *34*, 1–26.

Pischalnikova, A. V., and Sokolova, O.S. (2009). The domain and conformational organization in potassium voltage-gated ion channels. J. Neuroimmune Pharmacol. *4*, 71–82.

Puls, I., Jonnakuty, C., LaMonte, B.H., Holzbaur, E.L.F., Tokito, M., Mann, E., Floeter, M.K., Bidus, K., Drayna, D., Oh, S.J., et al. (2003). Mutant dynactin in motor neuron disease. Nat. Genet. *33*, 455–456.

Ralph, G.S., Radcliffe, P. a, Day, D.M., Carthy, J.M., Leroux, M. a, Lee, D.C.P., Wong, L.-F., Bilsland, L.G., Greensmith, L., Kingsman, S.M., et al. (2005). Silencing mutant SOD1 using RNAi protects against neurodegeneration and extends survival in an ALS model. Nat. Med. *11*, 429–433.

Ramesh, T., Lyon, A.N., Pineda, R.H., Wang, C., Janssen, P.M.L., Canan, B.D., Burghes, A.H.M., and Beattie, C.E. (2010). A genetic model of amyotrophic lateral sclerosis in zebrafish displays phenotypic hallmarks of motoneuron disease. Dis. Model. Mech. *3*, 652–662.

Ramesh, T.M., Shaw, P.J., and McDearmid, J. (2014). A zebrafish model exemplifies the long preclinical period of motor neuron disease. J. Neurol. Neurosurg. Psychiatry *85*, 1288–1289.

Rembach, A., Turner, B.J., Bruce, S., Cheah, I.K., Scott, R.L., Lopes, E.C., Zagami, C.J., Beart, P.M., Cheung, N.S., Langford, S.J., et al. (2004). Antisense peptide nucleic acid targeting GluR3 delays disease onset and progression in

the SOD1 G93A mouse model of familial ALS. J. Neurosci. Res. *77*, 573–582.

Ren, C., Hu, X., Li, X., and Zhou, Q. (2016). Ultra-trace graphene oxide in a water environment triggers Parkinson's disease-like symptoms and metabolic disturbance in zebrafish larvae. Biomaterials *93*, 83–94.

Renart, J., and Martinez, J.L. (1996). Dot Blot Learn more about Dot Blot IMMUNOBLOTTING TECHNIQUES Principles of Molecular Techniques Principles of Molecular Techniques. ScienceDirect *1st Editio*, 579.

Renaud, L., Picher-Martel, V., Codron, P., and Julien, J.-P. (2019). Key role of UBQLN2 in pathogenesis of amyotrophic lateral sclerosis and frontotemporal dementia. Acta Neuropathol. Commun. *7*, 1–11.

Renton, A.E., Majounie, E., Waite, A., Simón-Sánchez, J., Rollinson, S., Gibbs, J.R., Schymick, J.C., Laaksovirta, H., van Swieten, J.C., Myllykangas, L., et al. (2011). A hexanucleotide repeat expansion in C9ORF72 is the cause of chromosome 9p21-linked ALS-FTD. Neuron *72*, 257–268.

Renton, A.E., Majounie, E., Waite, A., Simón-sánchez, J., Rollinson, S., Gibbs, J.R., Schymick, J.C., Laaksovirta, H., Swieten, J.C. Van, Kaganovich, A., et al. (2012). A hexanucleotide repeat expansion in C9ORF72 is the cause of chromosome 9p21-linked ALS-FTD Alan. NIH Public Access *72*, 257–268.

Riancho, J., Ruiz-Soto, M., Berciano, M.T., Berciano, J., and Lafarga, M. (2015). Neuroprotective Effect of Bexarotene in the SOD1G93A Mouse Model of Amyotrophic Lateral Sclerosis. Front. Cell. Neurosci. *9*, 1–17.

Richard Bickerton ; et al (2012). Europe PMC Funders Group. *4*, 90–98.

Rihel, J., Prober, D.A., Arvanites, A., Lam, K., Jang, S., Haggarty, S.J., Kokel, D., Rubin, L.L., Peterson, T., and Schier, A.F. (2010). Zebrafish Behavioral Profiling Links Drugs to Biological Targets and Rest/Wake Regulation. NIH Public Access *327*, 348–351.

Rinaldi, F., Motti, D., Ferraiuolo, L., and Kaspar, B.K. (2017). High content analysis in amyotrophic lateral sclerosis. Mol. Cell. Neurosci. *80*, 180–191.

Ripps, M.E., Huntleyt, G.W., Hoft, P.R., Morrisontt, J.H., and Gordont, J.W. (1995). Transgenic mice expressing an altered murine superoxide dismutase gene provide an animal model of amyotrophic lateral sclerosis. Genetics *92*, 689–693.

Ritossa, F. (1996). Discovery of the heat shock response. Cell Stress Chaperones *1*, 97–98.

Robinson, M.B., Tidwell, J.L., Gould, T., Taylor, A.R., Newbern, J.M., Graves, J., Tytell, M., and Milligan, C.E. (2005). Extracellular heat shock protein 70: A critical component for motoneuron survival. J. Neurosci. *25*, 9735–9745.

Rohde, G., Kermer, P., Reed, J.C., Bähr, M., and Weishaupt, J.H. (2008). Neuron-specific overexpression of the co-chaperone Bcl-2-associated athanogene-1 in superoxide dismutase 1G93A-transgenic mice. Neuroscience *157*, 844–849.

Rose, C.R., Ziemens, D., Untiet, V., and Fahlke, C. (2018). Molecular and cellular physiology of sodium-dependent glutamate transporters. Brain Res. Bull. *136*, 3–16.

Rosen et al. (1993). Mutations in Cu / Zn superoxide dismutase gene are associated. 326, 59–62.

Roser, A.E., Tönges, L., and Lingor, P. (2017). Modulation of microglial activity by rho-kinase (rock) inhibition as therapeutic strategy in parkinson's disease and amyotrophic lateral sclerosis. Front. Aging Neurosci. *9*, 1–8.

Rothstein, J.D. (2017). Edaravone: A new drug approved for ALS. Cell *171*, 725.

Saberi, S., Stauffer, J.E., Jiang, J., Garcia, S.D., Amy, E., Schulte, D., Ohkubo, T., Schloffman, C.L., Maldonado, M., Baughn, M., et al. (2018). Sense-encoded poly-GR dipeptide repeat proteins correlate to neurodegeneration and uniquely co-localize with TDP-43 in dendrites of repeat expanded C9orf72 amyotrophic lateral sclerosis. Acta Neuropathol *135*, 459–474.

Saccon, R.A., Bunton-Stasyshyn, R.K.A., Fisher, E.M.C., and Fratta, P. (2013). Is SOD1 loss of function involved in amyotrophic lateral sclerosis? Brain *136*, 2342–2358.

Santa-Cruz, L.D., Guerrero-Castillo, S., Uribe-Carvajal, S., and Tapia, R. (2016). Mitochondrial Dysfunction during the Early Stages of Excitotoxic Spinal Motor Neuron Degeneration in Vivo. ACS Chem. Neurosci. *7*, 886–896.

Schipper, L.J., Raaphorst, J., Aronica, E., Baas, F., de Haan, R., de Visser, M., and Troost, D. (2016). Prevalence of brain and spinal cord inclusions, including dipeptide repeat proteins, in patients with the C9ORF72 hexanucleotide repeat expansion: a systematic neuropathological review. Neuropathol. Appl. Neurobiol. *42*, 547–560.

Schlesinger (2011). Heat-shock protein 70. Acta Virol. *55*, 189–194.

Scott, S., Kranz, J.E., Cole, J., Lincecum, J.M., Thompson, K., Kelly, N., Bostrom, A., Theodoss, J., Al-Nakhala, B.M., Vieira, F.G., et al. (2008). Design, power, and interpretation of studies in the standard murine model of ALS. Amyotroph. Lateral Scler. *9*, 4–15.

Scull, C.E., Zhang, Y., Tower, N., Rasmussen, L., Padmalayam, I., Hunter, R., Zhai, L., Bostwick, R., and Schneider, D.A. (2019). Discovery of novel inhibitors of ribosome biogenesis by innovative high throughput screening strategies. Biochem. J. *476*, 2209–2219.

Selvaraj, B.T., Livesey, M.R., Zhao, C., Gregory, J.M., James, O.T., Cleary, E.M., Chouhan, A.K., Gane, A.B., Perkins, E.M., Dando, O., et al. (2018). C9ORF72 repeat expansion causes vulnerability of motor neurons to Ca2+-permeable AMPA receptor-mediated excitotoxicity. Nat. Commun. *9*, 1–14.

Seminary, E.R., Sison, S.L., and Ebert, A.D. (2018). Modeling protein aggregation and the heat shock response in ALS iPSC-derived motor neurons. Front. Neurosci. *12*, 1–15.

Sen, I., Nalini, A., Joshi, N.B., and Joshi, P.G. (2005). Cerebrospinal fluid from amyotrophic lateral sclerosis patients preferentially elevates intracellular calcium and toxicity in motor neurons via AMPA/kainate receptor. J. Neurol. Sci. *235*, 45–54.

Seredenina, T., Nayernia, Z., Sorce, S., Maghzal, G.J., Filippova, A., Ling, S.C., Basset, O., Plastre, O., Daali, Y., Rushing, E.J., et al. (2016). Evaluation of NADPH oxidases as drug targets in a mouse model of familial amyotrophic lateral sclerosis. Free Radic. Biol. Med. *97*, 95–108.

Shaw, M.P.. et al (2018). Stable transgenic C9orf72 zebrafish model key aspects of the ALS/FTD phenotype and reveal novel pathological features. Acta Neuropathol. Commun. *6*, 1–16.

Shi, Y., Hung, S.-T., Rocha, G., Lin, S., Linares, G.R., Staats, K.A., Seah, C., Wang, Y., Chickering, M., Lai, J., et al. (2019). Identification and therapeutic rescue of autophagosome and glutamate receptor defects in C9ORF72 and sporadic ALS neurons. JCI Insight *4*, 1–21.

Smith, B.N., Ticozzi, N., Fallini, C., Gkazi, A.S., Topp, S., Kenna, K.P., Scotter, E.L., Kost, J., Keagle, P., Miller, J.W., et al. (2014). Exome-wide rare variant analysis identifies TUBA4A mutations associated with familial ALS. Neuron *84*, 324–331.

Smith, R.A., Bennett, C.F., Cleveland, D.W., Smith, R.A., Miller, T.M., Yamanaka, K., Monia, B.P., Condon, T.P., Hung, G., Lobsiger, C.S., et al. (2006). Antisense oligonucleotide therapy for neurodegenerative disease Find the latest version : Antisense oligonucleotide therapy for neurodegenerative disease. J Clin Invest. *116*, 2290–2296.

Smith, R.G., Siklos, L., Alexianu, M.E., Engelhardt, J.I., Mosier, D.R., Colom, L., Mohamed, A.H., and Appel, S.H. (1996). Autoimmunity and ALS. S40–S46.

Song, L., Chen, L., Zhang, X., Li, J., and Le, W. (2014). Resveratrol ameliorates motor neuron degeneration and improves survival in SOD1G93A mouse model of amyotrophic lateral sclerosis. Biomed Res. Int. *2014*, 1–10.

Spalloni, A., Albo, F., Ferrari, F., Mercuri, N., Bernardi, G., Zona, C., and Longone, P. (2004). Cu/Zn-superoxide dismutase (GLY93???ALA) mutation alters AMPA receptor subunit expression and function and potentiates kainate-mediated toxicity in motor neurons in culture. Neurobiol. Dis. *15*, 340–350.

Sreedharan, J., Blair, I.P., Tripathi, V.B., Hu, X., Vance, C., Rogelj, B., Ackerley, S., Durnall, J.C., Williams, K.L., Buratti, E., et al. (2008). TDP-43 Mutations in Familial and Sporadic Amyotrophic Lateral Sclerosis. Science. *319*, 1668–1672.

Strong, M.J., Volkening, K., Hammond, R., Yang, W., Strong, W., Leystra-Lantz, C., and Shoesmith, C. (2007). TDP43 is a human low molecular weight neurofilament (hNFL) mRNA-binding protein. Mol. Cell. Neurosci. *35*, 320–327.

Sun, Y., Dong, Z., Jin, T., Ang, K.H., Huang, M., Haston, K.M., Peng, J., Zhong, T.P., Finkbeiner, S., Weiss, W.A., et al. (2013). Imaging-based chemical screening reveals activity-dependent neural differentiation of pluripotent stem

cells. Elife *2013*, 1–23.

Swaminathan, A., Bouffard, M., Liao, M., Ryan, S., Callister, J.B., Pickering-Brown, S.M., Armstrong, G.A.B., and Drapeau, P. (2018). Expression of C9orf72-related dipeptides impairs motor function in a vertebrate model. Hum. Mol. Genet. *0*, 1–9.

Swinnen, B., Bento-Abreu, A., Gendron, T.F., Boeynaems, S., Bogaert, E., Nuyts, R., Timmers, M., Scheveneels, W., Hersmus, N., Wang, J., et al. (2018). A zebrafish model for C9orf72 ALS reveals RNA toxicity as a pathogenic mechanism. Acta Neuropathol. *135*, 427–443.

Şxahin, A., Held, A., Bredvik, K., Major, P., Achilli, T.M., Kerson, A.G., Wharton, K., Stilwell, G., and Reenan, R. (2017). Human SOD1 ALS mutations in a Drosophila knock-in model cause severe phenotypes and reveal dosage-sensitive gain- and loss-of-function components. Genetics *205*, 707–723.

Tarasiuk, J., Kułakowska, A., Drozdowski, W., Kornhuber, J., and Lewczuk, P. (2012). CSF markers in amyotrophic lateral sclerosis. J. Neural Transm. *119*, 747–757.

Taylor, J.P., Jr, R.H.B., and Cleveland, D.W. (2016). Decoding ALS: From Genes to Mechanism. Nature. Author Manuscr. *539*, 197–206.

Tazerart, S., Viemari, J.C., Darbon, P., Vinay, L., and Brocard, F. (2007). Contribution of persistent sodium current to locomotor pattern generation in neonatal rats. J. Neurophysiol. *98*, 613–628.

Teyssou, E., Takeda, T., Lebon, V., Boillée, S., Doukouré, B., Bataillon, G., Sazdovitch, V., Cazeneuve, C., Meininger, V., Leguern, E., et al. (2013). Mutations in SQSTM1 encoding p62 in amyotrophic lateral sclerosis: Genetics and neuropathology. Acta Neuropathol. *125*, 511–522.

Tripathi, V.B., Baskaran, P., Shaw, C.E., and Guthrie, S. (2014). Tar DNA-binding protein-43 (TDP-43) regulates axon growth in vitro and in vivo. Neurobiol. Dis. *65*, 25–34.

Tsang, C.K., Liu, Yuan, Thomas, Janice, Zhang Yanjie, and Z., and Steven (2014). Superoxide dismutase 1 acts as a nuclear transcription factor to regulate oxidative stress resistance. Nat. Commun. *5*, 1–26.

Tsuburaya, N., Homma, K., Higuchi, T., Balia, A., Yamakoshi, H., Shibata, N., Nakamura, S., Nakagawa, H., Ikeda, S.I., Umezawa, N., et al. (2018). A small-molecule inhibitor of SOD1-Derlin-1 interaction ameliorates pathology in an ALS mouse model. Nat. Commun. *9*, 1–12.

Turner, B.J., and Talbot, K. (2008). Transgenics, toxicity and therapeutics in rodent models of mutant SOD1-mediated familial ALS. Prog. Neurobiol. *85*, 94–134.

Turner, M.R., and Kiernan, M.C. (2012). Does interneuronal dysfunction contribute to neurodegeneration in amyotrophic lateral sclerosis? Amyotroph. Lateral Scler. *13*, 245–250.

Ugolino, J., Ji, Y.J., Conchina, K., Chu, J., Nirujogi, R.S., Pandey, A., Brady, N.R., Hamacher-brady, A., and Wang, J. (2016). Loss of C9orf72 Enhances Autophagic Activity via Deregulated mTOR and TFEB Signaling. PLOS Genet. *12*, 1–26.

Valentine, J.S., and Hart, P.J. (2003). Misfolded CuZnSOD and amyotrophic lateral sclerosis. Proc. Natl. Acad. Sci. *100*, 3617–3622.

Van, L., Bosch, D., Vandenberghe, W., Klaassen, H., Houtte, E. Van, and Robberecht, W. (2000). Ca -permeable AMPA receptors and selective vulnerability of motor neurons. J. Neurol. Sci. *180*, 29–34.

Vance, C., Lehmann, R., Broihier, H.T., Moore, L.A., Lehmann, R., Lehmann, R., Davey, J., Nielsen, O., Varshavsky, A., Hamon, Y., et al. (2009). Mutations in FUS, an RNA processing protein, cause familial amyotrophic lateral sclerosis type 6. Science. *323*, 1208–1211.

Venken and Bellen (2014). Chemical Mutagens, Transposons, and Transgenes to Interrogate Gene Function in Drosophila melanogaster. Elsevier *68*, 15–28.

Vermeiren, Y., Janssens, J., Van Dam, D., and De Deyn, P.P. (2018). Serotonergic dysfunction in amyotrophic lateral sclerosis and Parkinson's disease: Similar mechanisms, dissimilar outcomes. Front. Neurosci. *12*, 1–9.

Voigt, A., Herholz, D., Fiesel, F.C., Kaur, K., Müller, D., Karsten, P., Weber, S.S., Kahle, P.J., Marquardt, T., and Schulz, J.B. (2010). TDP-43-mediated neuron loss In Vivo requires RNA-binding activity. PLoS One *5*, 1–12.

Vucic, S., Lin, C.S.Y., Cheah, B.C., Murray, J., Menon, P., Krishnan, A. V., and Kiernan, M.C. (2013). Riluzole exerts central and peripheral modulating effects in amyotrophic lateral sclerosis. Brain *136*, 1361–1370.

Wager, T.T., Hou, X., Verhoest, P.R., and Villalobos, A. (2010). Moving beyond rules: The development of a central nervous system multiparameter optimization (CNS MPO) approach to enable alignment of druglike properties. ACS Chem. Neurosci. *1*, 435–449.

Wainger, B.J., Kiskinis, E., Mellin, C., Wiskow, O., Steve, S.W., Berry, J.D., Jr, R.H.B., Cudkowicz, M.E., and Bean, B.P. (2014). Intrinsic membrane hyperexcitability of ALS patient-derived motor neurons. Cell Rep. *7*, 1–11.

Walker, C., Herranz-Martin, S., Karyka, E., Liao, C., Lewis, K., Elsayed, W., Lukashchuk, V., Chiang, S.C., Ray, S., Mulcahy, P.J., et al. (2017). C9orf72 expansion disrupts ATM-mediated chromosomal break repair. Nat. Neurosci. *20*, 1225–1235.

Wang, H., and Hegde, M.L. (2019). New mechanisms of dna repair defects in fused in sarcoma–associated neurodegeneration: Stage set for dna repair-based therapeutics? J. Exp. Neurosci. *13*, 4–8.

Wang, T.H., Wang, S.Y., Wang, X.D., Jiang, H.Q., Yang, Y.Q., Wang, Y., Cheng, J.L., Zhang, C.T., Liang, W.W., and Feng, H.L. (2018). Fisetin Exerts Antioxidant and Neuroprotective Effects in Multiple Mutant hSOD1 Models of

Amyotrophic Lateral Sclerosis by Activating ERK. Neuroscience *379*, 152–166.

Waszkielewicz, A.M.M., Gunia, A., Szkaradek, N., S?oczy?ska, K., Krupi?ska, S., Marona, H., Soczyska, K., Krupiska, S., and Marona, H. (2013). Ion Channels as Drug Targets in Central Nervous System Disorders. Curr. Med. Chem. *20*, 1241–1285.

Wegorzewska, I., Bell, S., Cairns, N.J., Miller, T.M., and Baloh, R.H. (2009). TDP-43 mutant transgenic mice develop features of ALS and frontotemporal lobar degeneration. Proc. Natl. Acad. Sci. *106*, 18809–18814.

Westergard, T., McAvoy, K., Russell, K., Wen, X., Pang, Y., Morris, B., Pasinelli, P., Trotti, D., and Haeusler, A. (2019). Repeat-associated non-AUG translation in C9orf72-ALS/FTD is driven by neuronal excitation and stress. EMBO Mol. Med. *11*, 1-14.

Whitley, E., and Ball, J. (2002). Statistics review 4: Sample size calculations. Crit. Care *6*, 335–341.

Wokke, J. (1996). Riluzole. Lancet *348*, 795–799.

Wong, P.C., Pardo, C.A., Borchelt, D.R., Lee, M.K., Copeland, N.G., Jenkins, N.A., Sisodia, S.S., Cleveland, D.W., and Price, D.L. (1995). An adverse property of a familial ALS-linked SOD1 mutation causes motor neuron disease characterized by vacuolar degeneration of mitochondria. Neuron *14*, 1105–1116.

Xiong, X., Luo, S., Wu, B., and Wang, J. (2017). Comparative Developmental Toxicity and Stress Protein Responses of Dimethyl Sulfoxide to Rare Minnow and Zebrafish Embryos/Larvae. Zebrafish *14*, 60–68.

Xu, W., and Xu, J. (2018). C9orf72 Dipeptide Repeats Cause Selective Neurodegeneration and Cell-Autonomous Excitotoxicity in Drosophila Glutamatergic Neurons . J. Neurosci. *38*, 7741–7752.

Zhang, X.D. (2011). Illustration of SSMD, z score, SSMD*, z* score, and t statistic for hit selection in RNAi high-throughput screens. J. Biomol. Screen. *16*, 775–785.

Zhang, K., Christopher J. Donnelly, A.R.H., Grima, J.C., Machamer, J.B., Steinwald, P., Daley, E.L., Miller, S.J., M., K., Cunningham, Vidensky, S., et al. (2015). The C9ORF72 repeat expansion disrupts nucleocytoplasmic transport. Nature *525*, 56–61.

Zhang, W., Yu, G., Zhang, Y., Tang, F., Lv, J., Tian, G., Zhang, Y., Liu, J., Mi, J., and Zhang, J. (2019). Quantitative Dot Blot (QDB) as a universal platform for absolute quantification of tissue biomarkers. Anal. Biochem. *576*, 42–47.

Zhao, M., Kim, J.R., Bruggen, R. van, and Park, J. (2018). RNA-binding proteins in amyotrophic lateral sclerosis. Mol. Cells *41*, 818–829.

Zhao, Z., Fu, J., Li, S., and Li, Z. (2019). Neuroprotective Effects of Genistein in a SOD1-G93A Transgenic Mouse Model of Amyotrophic Lateral Sclerosis. J. Neuroimmune Pharmacol. *14*, 688–696.

Zhu, S., and Gouaux, E. (2016). Structure and symmetry inform gating principles of ionotropic glutamate receptors. Neuropharmacology *112*, 11–15.

Zou, S., Lan, Y., Wang, H., Zhang, B., and Sun, Y. (2019). The potential roles of aquaporin 4 in amyotrophic lateral sclerosis. Neurol. Sci. *40*, 1541–1549.

Zu, T., Liu, Y., Banez-Coronel, M., Reid, T., Pletnikova, O., Lewis, J., Miller, T.M., Harms, M.B., Falchook, A.E., Subramony, S.H., et al. (2013). RAN proteins and RNA foci from antisense transcripts in C9ORF72 ALS and frontotemporal dementia. Proc. Natl. Acad. Sci. *110*, E4968–E4977.

van Zundert, B., and Brown, R.H. (2017). Silencing strategies for therapy of SOD1-mediated ALS. Neurosci. Lett. *636*, 32–39.

Appendix

Table 1-1: SSMD value for the hits at β value < -0.5 and < -1.0 in the duplicate screens of the LifeArc library. 214 inhibitors of neuronal stress were identified in the *sod1*G93Ros10 zebrafish. Red is < -0.5, green is < -1.0. Compounds were identified with stronger and weaker effects in reducing neuronal stress in the *sod1*G93Ros10 zebrafish model. Some hits had β values comparable to the positive control, riluzole.

LifeArc plates	Rows/ Columns	Object ID from MRCT sheet	SSMD 1st screen	SSMD as an average of DMSO	SSMD as an average of Riluzole	SSMD 2nd screen	SSMD as an average of DMSO	SSMD as an average of Riluzole	SSMD mean of duplicate screen	SSMD SD of duplicate screen
442	I019	MRT00005242	-3.37	0.13	-4.80	-2.07	0.31	-4.47	-2.72	0.92
442	I013	MRT00010424	-3.29	0.13	-4.80	-2.72	0.31	-4.47	-3.00	0.40
442	F005	MRT00201154	-2.88	0.11	-1.83	-6.94	0.01	-5.83	-4.91	2.88
442	K009	MRT00003363	-1.46	0.29	-2.92	-1.80	0.41	-2.78	-1.63	0.25
442	J006	MRT00201428	-1.38	0.13	-4.80	-0.61	0.31	-4.47	-0.99	0.55
442	O013	MRT00023687	-1.34	0.48	-1.91	-2.75	0.15	-4.25	-2.05	1.00
442	A013	MRT00028435	-0.88	0.54	-2.38	-0.86	-0.55	-5.33	-0.87	0.01
442	C019	MRT00203352	-0.78	0.11	-2.06	-1.47	0.24	-3.39	-1.13	0.49
442	J005	MRT00201144	-0.71	0.13	-4.80	-0.83	0.31	-4.47	-0.77	0.08
442	B012	MRT00201470	-0.61	0.54	-2.38	-0.81	-0.55	-5.33	-0.71	0.15
442	M019	MRT00203349	-0.57	0.59	-1.68	-0.92	-0.29	-2.33	-0.75	0.24
442	D020	MRT00004250	-0.53	0.11	-2.06	-0.50	0.24	-3.39	-0.52	0.02
443	B008	MRT00055139	-2.70	0.44	-2.95	-1.20	-0.01	-4.40	-1.95	1.06
443	D021	MRT00201582	-3.09	0.44	-3.25	-2.45	0.37	-5.04	-2.77	0.45
443	F015	MRT00201606	-1.66	0.08	-1.21	-0.80	0.70	-4.25	-1.23	0.61
443	I019	MRT00201738	-1.43	0.45	-2.90	-1.23	0.70	-4.25	-1.33	0.14
443	J022	MRT00201527	-1.36	0.45	-2.90	-0.53	-0.18	-4.07	-0.94	0.58
443	A015	MRT00201699	-1.32	0.44	-2.95	-0.71	-0.01	-4.40	-1.02	0.43
443	K010	MRT00201553	-1.31	0.45	-2.90	-1.68	-0.18	-4.07	-1.50	0.26
443	A013	MRT00201598	-1.31	0.44	-2.95	-1.05	-0.01	-4.40	-1.18	0.18

443	K018	MRT00201502	-1.18	0.45	-2.90	-0.84	0.41	-3.68	-1.01	0.23
443	H021	MRT00201563	-0.88	1.10	-1.76	-0.70	0.55	-3.24	-0.79	0.13
443	G008	MRT00201644	-0.80	0.08	-1.21	-0.90	0.70	-4.25	-0.85	0.07
443	K009	MRT00057174	-0.71	0.45	-2.90	-0.62	-0.18	-4.07	-0.67	0.07
443	E010	MRT00201596	-0.55	0.44	-3.25	-0.79	0.12	-2.71	-0.67	0.17
443	G020	MRT00201741	-0.53	1.10	-1.76	-0.71	0.55	-3.24	-0.62	0.13
443	P016	MRT00201623	-0.79	0.41	-1.70	-0.72	0.37	-5.04	-0.76	0.05
444	F011	MRT00200878	-2.77	0.25	-1.47	-2.82	-0.13	-3.83	-2.80	0.04
444	A05	MRT00200777	-1.88	0.25	-2.41	-1.35	-0.11	-3.92	-1.61	0.37
444	C006	MRT00200712	-0.77	0.25	-2.41	-0.61	0.37	-5.04	-0.69	0.11
444	K011	MRT00200762	-1.81	0.51	-3.30	-1.51	-0.01	-4.47	-1.66	0.21
444	M003	MRT00200759	-1.68	0.14	-1.74	-1.49	-0.19	-4.38	-1.58	0.13
444	H007	MRT00200867	-1.37	0.67	-2.34	-0.54	0.85	-5.43	-0.96	0.59
444	L007	MRT00200870	-1.12	0.51	-3.30	-0.86	-0.19	-4.38	-0.99	0.18
444	C003	MRT00200763	-0.95	0.25	-2.41	-0.65	-0.50	-3.57	-0.80	0.21
444	O003	MRT00200770	-0.90	0.14	-1.74	-0.65	0.11	-3.01	-0.77	0.18
444	H020	MRT00200730	-0.72	0.67	-2.34	-1.77	0.85	-5.43	-1.25	0.74
444	A015	MRT00200815	-0.69	0.25	-2.41	-5.42	-0.11	-3.92	-3.06	3.34
444	I018	MRT00201081	-0.66	0.67	-2.34	-0.65	0.85	-5.43	-0.66	0.01
444	N018	MRT00200707	-1.13	0.37	-5.04	-1.07	0.11	-3.01	-1.10	0.04
444	L006	MRT00200919	-0.60	0.51	-3.30	-0.66	-0.01	-4.47	-0.63	0.04
445	M013	MRT00201059	-1.56	0.07	-1.19	-0.88	0.08	-5.73	-1.22	0.49
445	L016	MRT00203486	-1.41	0.07	-1.19	-2.82	0.14	-7.50	-2.11	1.00
445	A013	MRT00201020	-0.98	0.48	-2.01	-1.67	-0.15	-3.90	-1.32	0.49
445	D019	MRT00203440	-0.96	0.26	-2.25	-0.65	-0.12	-4.94	-0.81	0.22
445	H018	MRT00203501	-0.86	0.06	-1.28	-0.69	-0.02	-3.72	-0.78	0.12

445	C011	MRT00200754	-0.61	0.26	-2.25	-1.42	-0.12	-4.94	-1.01	0.57
445	B005	MRT00203524	-2.98	0.37	-5.04	-0.62	-0.15	-3.90	-1.80	1.67
446	N012	MRT00202123	-3.32	0.14	-3.97	-1.09	-0.34	-6.44	-2.20	1.57
446	F004	MRT00201744	-1.91	0.26	-4.35	-3.71	0.25	-3.77	-2.81	1.28
446	B006	MRT00202284	-1.65	0.06	-5.00	-1.57	-0.21	-5.94	-1.61	0.05
446	O012	MRT00203317	-1.53	0.14	-3.97	-1.49	-0.34	-6.44	-1.51	0.03
446	A006	MRT00203277	-1.31	0.26	-4.35	-1.24	0.42	-4.73	-1.27	0.05
446	A009	MRT00203592	-1.22	0.06	-5.00	-0.60	0.42	-4.73	-0.91	0.43
446	P014	MRT00202461	-0.98	0.42	-4.73	-1.65	0.26	-4.35	-1.32	0.48
446	H016	MRT00040664	-0.97	0.01	-5.11	-0.78	-0.03	-5.97	-0.88	0.13
446	E010	MRT00203316	-0.85	0.19	-3.19	-1.62	0.25	-3.77	-1.23	0.54
446	M009	MRT00203603	-0.83	0.25	-6.08	-0.63	-0.24	-5.82	-0.73	0.14
446	D003	MRT00203393	-0.80	0.19	-3.19	-1.74	-0.21	-5.94	-1.27	0.66
446	I022	MRT00203307	-0.63	0.01	-5.11	-0.56	-0.15	-6.52	-0.60	0.05
446	N021	MRT00203378	-0.60	0.14	-3.97	-1.95	-0.34	-6.44	-1.27	0.95
446	G022	MRT00203295	-1.07	0.21	-5.65	-0.81	0.37	-5.04	-0.94	0.18
446	K010	MRT00203281	-3.06	0.37	-5.04	-2.88	-0.15	-6.52	-2.97	0.12
446	O004	MRT00203275	-0.94	0.47	-3.78	-2.21	-0.34	-6.44	-1.58	0.90
447	L019	MRT00203098	-3.51	0.38	-7.55	-0.61	0.58	-4.82	-2.06	2.06
447	L015	MRT00202665	-1.90	0.38	-7.55	-1.71	0.58	-4.82	-1.81	0.13
447	B019	MRT00202973	-1.56	0.40	-3.00	-0.62	0.30	-3.33	-1.09	0.66
447	E014	MRT00132708	-1.56	0.05	-4.83	-0.69	0.31	-4.04	-1.12	0.61
447	K010	MRT00202005	-1.46	0.16	-3.39	-1.18	0.58	-4.82	-1.32	0.19
447	H012	MRT00201937	-1.36	0.42	-3.71	-0.59	0.23	-6.66	-0.97	0.54
447	E022	MRT00202868	-1.21	0.05	-4.83	-0.94	0.31	-4.04	-1.08	0.19

447	C010	MRT00202518	-1.18	0.40	-3.00	-1.72	0.30	-3.33	-1.45	0.38
447	B021	MRT00201895	-0.92	0.40	-3.00	-1.64	0.30	-3.33	-1.28	0.51
447	C007	MRT00202554	-0.77	0.40	-3.00	-1.16	0.30	-3.33	-0.97	0.28
447	B018	MRT00201916	-0.69	0.40	-3.00	-0.68	0.30	-3.33	-0.69	0.01
447	P013	MRT00203002	-0.62	0.35	-5.05	-0.84	-0.14	-6.08	-0.73	0.16
447	H014	MRT00201929	-0.60	0.42	-3.71	-0.54	0.23	-6.66	-0.57	0.04
447	K006	MRT00202581	-0.54	0.16	-3.39	-0.66	0.58	-4.82	-0.60	0.09
447	M015	MRT00201890	-0.52	0.47	-3.78	-6.35	0.19	-3.81	-3.43	4.12
447	A021	MRT00202685	-2.14	0.37	-4.05	-2.76	0.47	-3.78	-2.45	0.44
447	K004	MRT00202006	-1.35	0.47	-3.78	-3.36	0.58	-4.82	-2.35	1.42
447	P019	MRT00203073	-1.27	0.35	-5.05	-0.72	0.02	-1.97	-0.99	0.39
448	H018	MRT00202356	-1.34	0.36	-5.53	-0.60	0.54	-3.53	-0.97	0.52
448	B008	MRT00202499	-1.22	-0.26	-6.14	-2.00	-0.09	-4.01	-1.61	0.55
448	K010	MRT00202938	-1.07	0.54	-3.80	-1.71	-0.31	-4.99	-1.39	0.45
448	P016	MRT00202655	-1.05	0.10	-4.26	-0.79	-0.01	-5.39	-0.92	0.18
448	P014	MRT00203018	-0.98	0.10	-4.26	-2.29	-0.01	-5.39	-1.64	0.92
448	L015	MRT00184783	-0.85	0.54	-3.80	-0.86	0.22	-4.83	-0.85	0.01
448	N015	MRT00202375	-0.77	0.45	-3.63	-0.54	0.22	-4.83	-0.65	0.16
448	H014	MRT00202517	-0.71	0.36	-5.53	-1.14	0.54	-3.53	-0.92	0.30
448	I007	MRT00201967	-0.70	0.36	-5.53	-1.48	0.54	-3.53	-1.09	0.55
448	K016	MRT00203117	-0.69	0.54	-3.80	-0.78	-0.31	-4.99	-0.74	0.06
448	F008	MRT00202537	-0.62	0.08	-2.88	-1.33	-0.53	-7.23	-0.97	0.50
448	M005	MRT00201921	-0.57	0.30	-1.29	-0.93	0.22	-4.83	-0.75	0.26
448	D003	MRT00202724	-0.55	-0.06	-4.75	-0.66	-0.09	-4.01	-0.61	0.08
448	H022	MRT00202678	-0.51	0.36	-5.53	-0.70	0.54	-3.53	-0.61	0.13

448	E021	MRT00202679	-1.59	0.08	-2.88	-1.35	0.47	-3.78	-1.47	0.17
448	G008	MRT00201898	-0.78	0.08	-2.88	-1.43	0.47	-3.78	-1.10	0.46
449	J012	MRT00202735	-1.84	0.14	-5.29	-0.81	0.50	-5.48	-1.33	0.73
449	P013	MRT00202893	-1.80	0.55	-4.28	-0.99	0.05	-3.02	-1.39	0.57
449	K019	MRT00202464	-1.62	-0.11	-5.22	-0.89	-0.19	-5.44	-1.26	0.51
449	A003	MRT00202245	-1.43	0.58	-3.59	-2.20	0.55	-4.28	-1.82	0.54
449	B004	MRT00202654	-1.27	0.58	-3.59	-1.57	0.00	-6.54	-1.42	0.21
449	D010	MRT00202188	-1.06	0.27	-6.96	-0.82	0.13	-9.14	-0.94	0.17
449	B021	MRT00202261	-1.02	0.58	-3.59	-1.07	0.00	-6.54	-1.05	0.04
449	F022	MRT00201973	-0.79	0.00	-3.63	-1.71	-0.23	-3.50	-1.25	0.65
449	I007	MRT00202200	-0.65	0.14	-5.29	-1.50	0.50	-5.48	-1.07	0.60
449	M009	MRT00202995	-0.65	0.31	-6.33	-1.40	-0.19	-5.44	-1.02	0.53
449	F013	MRT00202765	-0.61	0.00	-3.63	-1.39	0.13	-9.14	-1.00	0.55
449	E003	MRT00203068	-0.52	0.27	-6.96	-1.69	0.13	-9.14	-1.10	0.83
449	A021	MRT00201998	-0.51	0.58	-3.59	-1.05	0.00	-6.54	-0.78	0.38
449	D009	MRT00203014	-0.51	0.27	-6.96	-0.55	0.13	-9.14	-0.53	0.03
449	G009	MRT00202901	-0.60	0.47	-3.78	-0.65	-0.23	-3.50	-0.63	0.04
449	I003	MRT00202248	-1.04	0.14	-5.29	-0.55	0.47	-3.78	-0.79	0.35
449	L008	MRT00201859	-1.67	0.02	-1.97	-0.96	-0.19	-5.44	-1.32	0.50
450	F014	MRT00202041	-5.92	0.21	-4.64	-2.24	-0.04	-5.54	-4.08	2.60
450	E005	MRT00202601	-2.96	0.52	-3.80	-2.70	0.06	-5.10	-2.83	0.19
450	N018	MRT00202928	-2.20	0.78	-4.49	-2.26	0.45	-3.04	-2.23	0.04
450	G003	MRT00202662	-2.19	0.21	-4.64	-1.44	-0.04	-5.54	-1.81	0.53
450	P018	MRT00202994	-2.07	0.29	-5.04	-0.51	0.42	-1.43	-1.29	1.10
450	F010	MRT00202800	-1.97	0.21	-4.64	-0.68	0.37	-5.04	-1.33	0.91

450	E004	MRT00202253	-1.52	0.52	-3.80	-3.71	0.06	-5.10	-2.62	1.55
450	B006	MRT00136583	-1.52	-0.23	-4.52	-1.10	0.16	-4.26	-1.31	0.29
450	H017	MRT00202281	-1.41	0.33	-5.41	-3.20	0.54	-5.17	-2.30	1.27
450	H007	MRT00202788	-1.36	0.33	-5.41	-1.43	0.54	-5.17	-1.39	0.05
450	M013	MRT00202475	-1.16	0.78	-4.49	-0.82	0.45	-3.04	-0.99	0.24
450	F003	MRT00202774	-1.13	0.21	-4.64	-0.68	-0.04	-5.54	-0.91	0.32
450	C019	MRT00129245	-0.96	0.52	-3.80	-1.42	0.06	-5.10	-1.19	0.33
450	M012	MRT00202387	-0.90	0.78	-4.49	-0.93	0.45	-3.04	-0.91	0.02
450	N010	MRT00202572	-0.70	0.78	-4.49	-0.54	0.45	-3.04	-0.62	0.12
450	I020	MRT00202934	-0.56	0.33	-5.41	-0.53	0.54	-5.17	-0.54	0.03
451	G016	MRT00201846	-7.53	1.04	-5.50	-0.61	0.18	-3.54	-4.07	4.90
451	E018	MRT00202279	-6.75	0.47	-9.88	-0.92	0.48	-4.11	-3.83	4.12
451	H006	MRT00203197	-2.31	1.04	-5.50	-0.62	0.18	-3.54	-1.47	1.20
451	B020	MRT00203231	-2.06	0.38	-4.48	-0.63	0.22	-4.96	-1.34	1.01
451	E016	MRT00144530	-1.90	0.47	-9.88	-2.08	0.48	-4.11	-1.99	0.13
451	B016	MRT00203222	-1.87	0.38	-4.48	-0.69	0.22	-4.96	-1.28	0.84
451	E010	MRT00203082	-1.85	0.47	-9.88	-0.57	0.48	-4.11	-1.21	0.90
451	M014	MRT00203139	-1.64	0.14	-4.37	-0.52	0.38	-2.94	-1.08	0.79
451	L004	MRT00203176	-1.20	-0.42	-3.78	-0.64	-0.05	-4.60	-0.92	0.39
451	D018	MRT00203218	-1.16	0.47	-9.88	-0.66	0.48	-4.11	-0.91	0.35
451	I016	MRT00201840	-0.97	0.61	-5.79	-1.73	0.03	-5.10	-1.35	0.54
451	B021	MRT00202869	-0.70	0.38	-4.48	-0.53	0.22	-4.96	-0.61	0.12
451	E003	MRT00200699	-0.69	0.47	-9.88	-0.75	0.48	-4.11	-0.72	0.04
451	B012	MRT00203224	-0.59	0.38	-4.48	-2.89	0.22	-4.96	-1.74	1.63
451	O010	MRT00202484	-0.51	0.26	-4.95	-0.55	0.38	-2.94	-0.53	0.03

451	N008	MRT00203173	-5.24	0.14	-4.37	-0.79	0.38	-2.94	-3.02	3.15
451	E022	MRT00202567	-0.67	1.04	-5.50	-1.08	0.48	-4.11	-0.87	0.29
452	B006	MRT00201306	-4.24	0.95	-2.45	-0.54	-0.27	-4.21	-2.39	2.62
452	I021	MRT00203254	-3.14	-0.09	-5.18	-0.55	0.43	-2.47	-1.85	1.83
452	G014	MRT00201313	-2.12	-0.33	-2.97	-0.51	-0.05	-3.94	-1.32	1.14
452	D015	MRT00201271	-1.86	0.04	-3.71	-0.54	-0.22	-5.38	-1.20	0.94
452	C011	MRT00203269	-1.67	0.04	-3.71	-0.71	-0.22	-5.38	-1.19	0.68
452	I005	MRT00203248	-1.52	-0.09	-5.18	-0.77	0.43	-2.47	-1.15	0.53
452	G005	MRT00203268	-1.36	-0.33	-2.97	-1.12	-0.05	-3.94	-1.24	0.17
452	P006	MRT00201156	-1.23	-0.01	-3.48	-0.57	0.39	-2.35	-0.90	0.47
452	I009	MRT00203252	-1.00	-0.09	-5.18	-1.77	0.43	-2.47	-1.39	0.55
452	P009	MRT00201383	-0.84	-0.01	-3.48	-0.56	0.39	-2.35	-0.70	0.20
452	G004	MRT00201233	-0.70	-0.33	-2.97	-2.22	-0.05	-3.94	-1.46	1.08
452	M016	MRT00201197	-0.90	0.25	-1.75	-1.90	-0.31	-3.66	-1.40	0.71
464	B022	MRT00213757	-2.57	0.39	-5.38	-0.86	0.78	-4.70	-1.72	1.21
464	O019	MRT00215307	-2.39	0.30	-2.52	-5.64	0.06	-2.00	-4.02	2.30
464	E004	MRT00215326	-2.12	-0.07	-6.11	-0.92	0.37	-5.42	-1.52	0.85
464	J018	MRT00213789	-1.82	0.52	-2.69	-0.53	0.22	-2.42	-1.17	0.91
464	C009	MRT00215254	-1.60	0.39	-5.38	-1.02	0.78	-4.70	-1.31	0.41
464	N020	MRT00213806	-1.31	0.54	-2.09	-0.72	0.11	-4.68	-1.01	0.42
464	I004	MRT00215344	-1.20	0.59	-3.60	-0.51	0.44	-2.41	-0.86	0.49
464	D007	MRT00209870	-1.14	-0.07	-6.11	-2.77	0.37	-5.42	-1.96	1.15
464	G006	MRT00215335	-1.03	0.52	-4.96	-1.39	0.36	-5.53	-1.21	0.26
464	K007	MRT00209832	-1.02	0.52	-2.69	-1.64	0.22	-2.42	-1.33	0.44
464	D009	MRT00215383	-0.95	-0.07	-6.11	-1.51	0.37	-5.42	-1.23	0.40

464	H007	MRT00215395	-0.77	0.59	-3.60	-0.61	0.44	-2.41	-0.69	0.11
464	K006	MRT00215353	-0.73	0.52	-2.69	-0.55	0.22	-2.42	-0.64	0.13
464	M016	MRT00215364	-0.71	0.54	-2.09	-1.19	0.11	-4.68	-0.95	0.34
464	E013	MRT00215261	-0.69	-0.07	-6.11	-0.56	0.37	-5.42	-0.62	0.09
464	C021	MRT00209842	-0.62	-0.07	-6.11	-1.07	0.37	-5.42	-0.85	0.32
464	N004	MRT00213799	-0.60	0.54	-2.09	-0.64	0.11	-4.68	-0.62	0.03
464	B011	MRT00215376	-0.56	0.39	-5.38	-0.64	0.78	-4.70	-0.60	0.06
464	F016	MRT00213771	-0.55	0.52	-4.96	-2.76	0.36	-5.53	-1.66	1.56
464	K012	MRT00215356	-1.83	0.52	-2.69	-0.56	0.25	-1.75	-1.20	0.89
464	N022	MRT00213807	-0.73	0.54	-2.09	-0.75	0.25	-1.75	-0.74	0.02
465	G007	MRT00215461	-3.07	0.15	-2.90	-2.00	0.37	-1.60	-2.54	0.76
465	I005	MRT00215469	-1.67	0.15	-2.90	-1.49	-0.02	-5.47	-1.58	0.13
465	H021	MRT00209949	-1.41	0.15	-2.90	-0.81	-0.02	-5.47	-1.11	0.43
465	A017	MRT00215439	-1.31	0.35	-4.53	-0.56	0.60	-2.72	-0.93	0.53
465	A008	MRT00213883	-1.25	0.35	-4.53	-0.52	0.60	-2.72	-0.88	0.51
465	H008	MRT00214041	-1.02	0.15	-2.90	-0.92	-0.02	-5.47	-0.97	0.07
465	J015	MRT00215539	-0.98	0.24	-3.26	-0.56	-0.15	-1.42	-0.77	0.29
465	E011	MRT00215453	-0.81	0.04	-2.64	-0.59	0.37	-1.60	-0.70	0.16
465	H011	MRT00215528	-0.80	0.15	-2.90	-1.25	-0.02	-5.47	-1.02	0.32
465	P009	MRT00215562	-0.76	0.33	-3.51	-3.59	-0.60	-3.34	-2.17	2.00
465	N017	MRT00215557	-0.73	0.33	-3.51	-0.59	0.45	-2.20	-0.66	0.10
465	L016	MRT00214061	-0.70	-0.39	-4.41	-0.61	0.45	-2.20	-0.65	0.06
465	G003	MRT00215459	-0.99	0.15	-2.90	-0.70	0.37	-1.60	-0.84	0.21
466	L019	MRT00215688	-4.29	0.73	-1.59	-0.64	0.34	-1.62	-2.46	2.58
466	E010	MRT00214171	-3.79	0.17	-3.79	-4.57	0.25	-1.75	-4.18	0.55

466	P012	MRT00214366	-3.39	0.18	-3.27	-2.26	-0.42	-3.84	-2.83	0.79
466	H022	MRT00214333	-2.64	0.80	-3.54	-4.20	0.33	-2.38	-3.42	1.10
466	H010	MRT00209993	-2.13	0.80	-3.54	-3.53	0.33	-2.38	-2.83	0.99
466	M018	MRT00214215	-1.74	-0.23	-3.77	-0.58	0.34	-1.62	-1.16	0.82
466	L018	MRT00214351	-1.31	0.73	-1.59	-2.49	0.25	-1.75	-1.90	0.83
466	K016	MRT00214204	-1.26	0.73	-1.59	-0.95	0.34	-1.62	-1.11	0.22
466	D010	MRT00214310	-1.18	0.17	-3.79	-0.61	-0.45	-6.28	-0.89	0.40
466	A005	MRT00209968	-1.16	-0.04	-2.99	-0.72	0.18	-3.27	-0.94	0.31
466	F018	MRT00214323	-1.10	0.43	-2.50	-0.65	0.33	-2.38	-0.87	0.32
466	C008	MRT00214160	-1.09	-0.04	-2.99	-0.73	-0.10	-3.52	-0.91	0.25
466	N007	MRT00215691	-0.99	-0.23	-3.77	-1.18	0.25	-1.75	-1.09	0.14
466	L020	MRT00209997	-0.92	0.73	-1.59	-0.82	0.34	-1.62	-0.87	0.07
466	F016	MRT00214322	-0.88	0.43	-2.50	-0.94	0.33	-2.38	-0.91	0.04
466	G004	MRT00214178	-0.85	0.43	-2.50	-1.24	0.33	-2.38	-1.05	0.27
466	M009	MRT00215623	-0.82	-0.23	-3.77	-0.56	0.34	-1.62	-0.69	0.18
466	P008	MRT00214364	-0.80	0.18	-3.27	-0.82	-0.42	-3.84	-0.81	0.02
466	F020	MRT00214324	-0.70	0.43	-2.50	-0.57	0.33	-2.38	-0.64	0.09
466	F017	MRT00215660	-0.52	0.43	-2.50	-1.13	0.33	-2.38	-0.83	0.43